Comparative anatomy of the diploic vessels in hominids : implications for the evolutionary history of human cranial blood circulation

Jiaming Hui

Sorbonne Université

Ecole doctorale 227

Sciences de la Nature et de l'Homme : évolution et écologie

UMR 7194 / Equipe PaléoFED

Comparative anatomy of the diploic vessels in hominids: Implications for the evolutionary history of human cranial blood circulation

Par Jiaming HUI

Thèse de doctorat de Sciences de l'évolution

Dirigée par Antoine BALZEAU

Co-encadrée par Xiujie WU

Présentée et soutenue publiquement le 03 Octobre 2024

Devant un jury composé de :

Jean-Jacques HUBLIN	Professeur	Président du jury
José BRAGA	Professeur	Rapporteur
María MARTINÓN-TORRES	Professeure	Rapportrice
Amélie BEAUDET	Chaire de professeure junior	Examinatrice
Aurélien MOUNIER	Chargé de recherche	Examinateur
Xiujie WU	Directrice de recherche	Co-encadrante de thèse
Antoine BALZEAU	Directeur de recherche	Directeur de thèse

Acknowledgement

Life is an odd lake, towards which I throw a pebble but see nothing changes on the surface. When I grow impatient after a long wait, ripples suddenly emerge and rush back to me. Ten years ago, when I was an undergraduate preparing for the upcoming exam about Neanderthals, what surrounded me was the hot and humid summer in Canton as well as my anxiety about my future. I didn't know one day I would sit in a laboratory by the Seine with a Neanderthal skull in my hands.

I appreciate my supervisor Prof Antoine BALZEAU and my co-encadrante Prof Xiujie WU. With their help and the funding from the 'Sorbonne University & China Scholarship Council collaborative programme', I got the chance to pursue a PhD degree in Paris. Absolutely, the three years of PhD study was not a relaxing journey, but Prof BALZEAU helped me choose the path that I was adept at and guided me through the mist and dark. Thanks to his encouragement, patience, and expertise, I explored the mystery of evolution with a fruitful harvest. Prof WU gave me solid backing in the last three years. She never hesitated to give me a hand when I encountered difficulties. She was always keen on looking for future opportunities for my career. It was my great fortune to work with them, which would be a precious memory of my life.

I want to give my sincere thanks to Prof Jean-Jacques HUBLIN, Aurélien MOUNIER, Amélie BEAUDET, Dominique GRIMAUD-HERVÉ, Sophie BERLAND, Jean-Jacques BAHAIN, Wu LIU, Patricia WILS, for their advice, comments, and encouragements. I also want to thank Prof Bernhard ZIPFEL, John HAWKS, Patrick SEMAL, Frederick GRINE, Josephine JOORDENS, Eduard POP, and the administrators from the MNHN collection department, for providing me with access to the CT scanning images.

As a foreigner wandering in a country thousands of miles away from the motherland, I have to face loneliness, an old friend of mine. In the first few months, I felt like a satellite lost in the deep universe. Thanks to the company of my family and friends, I am back to the Earth. I treasure the days I spent with Yuping REN in the valley of the Alps and along the Mediterranean coastline. We were clouds, floating from mountains to the sea. I treasure the strolling in the purple sunset in Mont Saint-Michel with Liupeng WANG and Liang TANG. Sunshine colored our eyes. I treasure the dinner under a cherry blossom with Chao WU, Sunbin HUANG, and Liqiong YANG. A spring in Paris never arrives late.

Now, I finished the thesis and threw another pebble towards the lake. Who knows what we will see in the future?

Table of Contents

Abstract

Hominidae are featured with large and energy-consuming brains, which necessitates effective vascular networks providing metabolic support. The diploic venous system is important to cranial blood circulation, since it facilitates the exchanges between extra- and intra-cranial blood. The diploic venous system also transports cerebrospinal fluid and may regulate brain temperature. Considering the physiological significance of the diploic venous system, it may have been involved in brain evolution. However, the anatomy and evolution of the diploic venous system remain unknown in most Hominidae members, hindering us from verifying its relationship with brain evolution. Moreover, as the morphology of cranial inner structures can potentially function as taxonomic signals, it is meaningful to estimate the significance of the diploic venous system in taxonomic analyses, of which the precondition is mapping the characteristics in each taxon.

This study investigated extant great apes, extant humans, and *Homo* fossils from the Early, Middle, and Late Pleistocene. The diploic venous systems of most fossil specimens were unexplored in previous studies. Many of them are critical to understanding the evolutionary history of humans. This study developed a new protocol for identifying, reconstructing, and analyzing the diploic venous system. With high-resolution Micro-CT images, this study non-invasively detected and digitally reconstructed the macro-and microscopic structures of diploe, which was a chronic difficulty for traditional dissections. As soft tissues of vessels were not preserved, the bony diploic channels were used as proxies of the venous network. Through qualitative inspections, this study described their distribution and drainage pathways, as well as their spatial interactions with endocasts and bone thickness. Through quantitative methods, including the intensity scale, fractal analysis, and relative volume analysis, this study evaluated their degrees of complexity, sizes, and general intensity levels.

This study presents the diploic venous system in extinct hominins, and it discovered

non-documented structures in great apes and corrected the classic description of extant humans. The results showed that chimpanzees and gorillas had less developed diploic venous systems than hominins. A highly developed system was not an autapomorphy of *Homo sapiens*, which was different from previous understanding, instead, it emerged in hominins since the Early Pleistocene and was widely shared among the genus *Homo*. The taxonomic differences in the diploic venous drainage patterns between hominids mainly appeared in the sphenoid greater wing, asterional region, paranasal sinuses, and parietal foramina. Brain size did not determine the intensity of the diploic venous network, as small-brained hominin species also had dense and large diploic venous networks comparable to those of large-brained taxa. Brain shape could affect diploic vessels, as the compression from pronounced brain gyri corresponded to the areas with evident thinning in cranial bones, which were usually bypassed by diploic vessels. As brain shape varied among hominids, it contributed to the taxonomic differences in diploic vessel distribution. Additionally, the structures of the diploic venous system could facilitate heat exchange, but no clear evidence indicated that it had a key role in brain thermoregulation. Finally, the diploic venous system might have co-evolved with other vascular networks and paranasal sinuses.

In conclusion, this work is the first comprehensive comparison of the diploic venous systems among great apes, fossil hominins, and extant humans. The findings contribute to our knowledge of the diploic venous system, preliminarily mapping its general evolutionary trajectory in human lineage. This study also sheds light on the evolutionary history of human brains, revealing the spatial interaction between vessels, cranial bones, and brains. The taxonomic differences manifesting in this study suggest that the diploic venous system has potential application values in future taxonomic and phylogenetic discussions, especially in distinguishing *H. neanderthalensis* and *H. sapiens*.

Keywords: Brain, vascularization, evolution, imaging methodologies, fossil, hominins

Résumé étendu en français

Contexte :

Les hominidés (terme qui regroupe les hominines, soient les humains fossiles et les humains actuels, ainsi que nos plus proches cousins actuels, dont les chimpanzés et les gorilles) sont dotés d'un cerveau volumineux et énergivore, ce qui nécessite des réseaux vasculaires efficaces dans la tête pour assurer le soutien métabolique. Le système veineux diploïque qui traverse les os du crâne est important pour la circulation sanguine dans la tête, car il facilite les échanges sanguins entre les réseaux vasculaires extracrâniens et intracrâniens. Pour de nombreux vaisseaux intracrâniens, comme les sinus duraux, le système veineux diploïque sert également de voie collatérale en cas de thrombose. Par ailleurs, le système veineux diploïque participe au transport du liquide cérébrospinal et peut réguler la température du cerveau. Compte tenu de l'importance physiologique du système veineux diploïque, il pourrait avoir été impliqué dans l'évolution du cerveau, comme l'ont fait de nombreux autres vaisseaux crâniens.

En outre, de nombreuses études ont montré que la morphologie des structures internes du crâne peut potentiellement servir de signaux taxonomiques. De nombreux vaisseaux crâniens ont montré des variations inter-espèces chez les hominidés, et donc le système veineux diploïque hautement intégré à eux peut également avoir de telles implications taxonomiques. Les vaisseaux diploïques préservés peuvent revêtir une importance particulière pour identifier les affinités des spécimens fossiles lorsque la surface externe est sérieusement endommagée par les processus taphonomiques. Afin d'estimer les valeurs d'application du système veineux diploïque dans les analyses taxonomiques ou phylogénétiques, la condition préalable est de cartographier les caractéristiques dans chaque taxon d'hominidés.

Cependant, les connaissances sur l'anatomie et l'évolution du système veineux diploïque sont rares. L’inspection des vaisseaux diploïques pose un problème méthodologique chronique. La dissection traditionnelle est invasive et peut perdre des informations sur les voies de drainages de dimensions microscopique. La radiographie et la tomographie médicale ont été utilisés dans certaines études, mais leurs résolutions d'image ne sont pas suffisantes pour détecter les petites branches vasculaires. Certains ont suggéré que les grands singes semblaient avoir un système veineux diploïque

beaucoup moins développé que les humains actuels, mais le résultat a été conclu à partir d'un échantillon plutôt limité. Même si leurs systèmes sont effectivement moins développés, on peut se demander si leurs systèmes sont simplement des versions réduites de vaisseaux humains existants, ou s'ils possèdent des caractéristiques uniques ? Et pour la plupart des espèces d'hominines fossiles, leurs systèmes veineux diploïques restent inexplorés. La polarité évolutive du système veineux diploïque est encore floue. Même les connaissances actuelles sur les humains actuels, au sein de la littérature médicale, sont également largement contestées et nécessitent une vérification à partir de données plus empiriques. Ainsi, la trajectoire évolutive du système veineux diploïque chez les hominidés reste inconnue, ce qui nous empêche de vérifier sa relation avec le cerveau au cours de l'évolution et sa signification dans les discussions taxonomiques.

Méthodes et matériel :

Cette étude a porté sur les crânes secs de chimpanzés, de gorilles et d'humains actuels, ainsi que sur 18 hominines fossiles du Pléistocène inférieur, moyen et supérieur d'Europe, d'Asie de l'Est et d'Afrique d'espèces variées. Les systèmes veineux diploïques de la plupart des spécimens fossiles étaient inexplorés dans les études précédentes. La plupart des spécimens étudiés sont essentiels à la compréhension de l'histoire évolutive de l'humanité.

Cette étude a développé un nouveau protocole pour identifier, reconstruire et analyser le système veineux diploïque. À l'aide de données de numérisation Micro-CT à haute résolution et le logiciel 3D Slicer cette étude a détecté de manière non invasive et reconstruit numériquement les canaux diploïques de tailles variables, qui sont les coquilles osseuses des vaisseaux diploïques préservés dans les fossiles et les crânes secs. Les tissus mous des vaisseaux n'étant pas préservés, les canaux diploïques osseux ont été utilisés comme proxy du réseau veineux.

Grâce à des inspections qualitatives, cette étude a fourni des informations détaillées sur la distribution et les voies de drainage du système veineux diploïque, notamment leur anastomose avec d'autres réseaux vasculaires et sinus paranasaux. La répartition des vaisseaux diploïques a été comparée à la carte des couleurs de l'épaisseur de la voûte crânienne ainsi qu'à la forme des surfaces endocrâniennes et ectocrâniennes. Grâce à

des méthodes quantitatives, notamment l'échelle d'évaluation de l'intensité, l'analyse fractale et l'analyse du volume relatif, cette étude a évalué les degrés de complexité, les tailles et les niveaux d'intensité générale des systèmes veineux diploïques.

Résultats et discussion :

Cette étude a permis de découvrir le système veineux diploïque chez des spécimens fossiles de plusieurs espèces humaines, dont beaucoup n'avaient jamais été observés auparavant pour toutes ces caractéristiques internes. L'étude a également révélé des structures non documentées chez les grands singes et a affiné et corrigé les descriptions classiques des humains actuels. Les résultats ont montré que le système veineux diploïque des grands singes est beaucoup moins développé que celui des hominines. Un système très développé n'est pour autant pas une autapomorphie de *Homo sapiens*. Un système très développé serait apparu au moins au Pléistocène inférieur, d'après les données dont nous disposons, et semble être partagé par les différentes espèces du genre *Homo* étudiée dans le cadre de ce travail. Le système veineux diploïque du genre *Homo* n'a pas évolué continuellement pour devenir plus développé au cours de l'évolution humaine. De même, la grande variabilité morphologique est une caractéristique constante partagée par les hominines.

Les différences taxonomiques entre les hominidés apparaissent principalement dans les schémas de drainage entourant les sinus paranasaux, l'astérion, les foramina pariétal et l'os sphénoïde. Les chimpanzés possèdent des vaisseaux diploïques sphénoïdes hautement connectifs, qui pourraient servir de tige de vaisseaux méningés et de raccourci entre les sinus paranasaux et les fosses crâniennes moyennes et postérieures. *H. neanderthalensis* avait un modèle de drainage spécial dans la région de l'astérion, à la jonction entre les os pariétaux, temporaux et occipital. Alors que les vaisseaux diploïques pariétaux étaient presque toujours connectés au sinus transverse-sigmoïde chez d'autres hominidés, ils étaient généralement isolés chez *H. neanderthalensis*. De plus, les foramens pariétaux avec leur anastomose avec les vaisseaux diploïques apparaissaient fréquemment chez d'autres hominidés, mais ils étaient rares chez *H. neanderthalensis*. Enfin, la connexion constante entre le sinus frontal et les vaisseaux diploïques apparait comme aléatoire au sein de notre échantillon pour *H. sapiens*, ce qui peut être attribué à la grande variabilité de la taille du sinus frontal chez *H. sapiens*.

La taille du cerveau ne déterminerait pas l'intensité du système veineux diploïque, puisque les espèces d'*Homo* à petit cerveau (par exemple, *Homo naledi*) possédaient un système veineux diploïque développé de manière comparable à celui des espèces à grand cerveau. Cependant, la forme du cerveau pourrait affecter la distribution des vaisseaux diploïques. La compression due aux gyri cérébraux prononcés et aux granulations arachnoïdiennes implique souvent un amincissement évident des os crâniens dans les zones correspondantes. Lorsque l'épaisseur d'une zone était inférieure à un certain seuil, les vaisseaux diploïques avaient tendance à contourner la zone. Les connexions entre les vaisseaux diploïques et les autres réseaux vasculaires sont également affectées dans ces zones minces. Les hominidés présentant des variations inter-espèces dans la forme de leur cerveau, cela a contribué aux différences taxonomiques dans la distribution des vaisseaux diploïques.

Un emplacement commun d'amincissement évident partagé par les hominidés se trouve dans la partie latéro-inférieure de l'os frontal, sous la ligne temporale. La zone mince est comprimée de manière intracrânienne par le gyrus frontal inférieur. Les vaisseaux diploïques environnants contournent cette mince zone et ne courent que le long de ses bords. Et par rapport aux chimpanzés, cette zone d'amincissement évident est plus prononcée et étendue chez les hominines, ce qui signifie également une zone plus grande que les vaisseaux diploïques doivent contourner. La compression du gyrus précentral contribue à l'amincissement de la partie antéro-supérieure de l'os pariétal, que l'on retrouve chez *H. heidelbergensis* (par exemple Kabwe 1) et chez les *H. erectus* asiatiques. Mais l'amincissement est plus prononcé chez *H. neanderthalensis* et *H. sapiens*, réduisant les vaisseaux diploïques dans ces zones. Un autre amincissement évident de l'os pariétal est apparu dans sa partie inférieure, qui était comprimée par le lobule pariétal inférieur prononcé et les gyri temporaux. Il est visible systématiquement chez les *H. sapiens* actuels et fossiles. Les vaisseaux diploïques de la moitié inférieure de l'os pariétal ont dû contourner cette zone mince.

Enfin, la compression du lobe occipital sur la voute crânienne apparait prédominante au sein de l'échantillon d'hominidés, mais l'effet d'amincissement provoqué par la compression montre des variations interspécifiques. Un amincissement évident et un manque de vaisseaux diploïques ont pu être constatés en permanence chez les chimpanzés et *H. sapiens*. La fosse suprainiaque chez *H. neanderthalensis* diminue

l'épaisseur diploïque, elle n'a pas produit d'amincissement évident ni affecté les vaisseaux diploïques.

Cette étude a également révélé que les nombreuses entrées et sorties du système veineux diploïque pouvaient faciliter l'échange de chaleur entre l'espace extracrânien et intracrânien, mais aucune preuve claire n'a été apportée quant au rôle clé du système veineux diploïque dans la thermorégulation du cerveau. Les données ne suggèrent pas non plus que les capacités de thermorégulation du système veineux diploïque ont conditionné l'évolution des cerveaux au sein des hominines. Enfin, le système veineux diploïque pourrait avoir coévolué avec les sinus paranasaux et les réseaux vasculaires qui lui sont reliés. La morphologie et les voies de drainage des vaisseaux diploïques dans les os frontal et sphénoïde sont peut-être une adaptation à l'évolution des sinus paranasaux. Les schémas de drainage dans la région astérienne sont liés à la localisation spatiale des sinus transverse et sigmoïde. Les vaisseaux diploïques occipitaux développés chez les hominines sont adaptés aux exigences élevées du drainage extracrânien du sang veineux dans le plexus veineux des vertébrés, qui est induit par la bipédie.

Conclusion et perspective :

Ce travail est la première comparaison complète entre les grands singes, les hominines fossiles et les humains actuels dans le domaine de l'étude du système veineux diploïque. Les résultats contribuent à notre connaissance de l'anatomie et de l'évolution du système veineux diploïque, en traçant de manière préliminaire la trajectoire évolutive générale du système chez les hominidés. Cette étude a également mis en lumière l'histoire évolutive du cerveau humain, en révélant l'interaction spatiale entre les vaisseaux, les os crâniens et les cerveaux. Les différences taxonomiques qui se manifestent dans cette étude suggèrent que le système veineux diploïque a des valeurs d'application potentielles dans les discussions taxonomiques et phylogénétiques futures, notamment en distinguant *H. neanderthalensis* et *H. sapiens*.

Comme une grande partie de cette étude est basée sur une analyse qualitative, on s'attend à voir davantage de données quantitatives dans les études suivantes fournissant des informations plus riches. En particulier, l'analyse fractale et l'analyse du volume relatif testées dans cette étude ont manifesté leurs valeurs d'application. Des travaux

futurs sont également nécessaires pour développer des algorithmes plus avancés automatisant l'identification et la segmentation des canaux diploïques et des structures taphonomiques. De plus, étant donné que les trois couches de l'os crânien ne sont pas d'épaisseur égale, des recherches futures devraient étudier l'interaction spatiale entre les vaisseaux diploïques et chaque couche. Enfin, sur la base de cette étude, les recherches futures devraient étudier davantage de primates non humains et d'espèces fossiles du Pliocène supérieur et du Pléistocène inférieur. Cela complétera la carte de la trajectoire évolutive des vaisseaux diploïques chez les hominidés.

Mots clés : cerveau, vascularisation, évolution, Micro-CT, imagerie, fossile, homininés

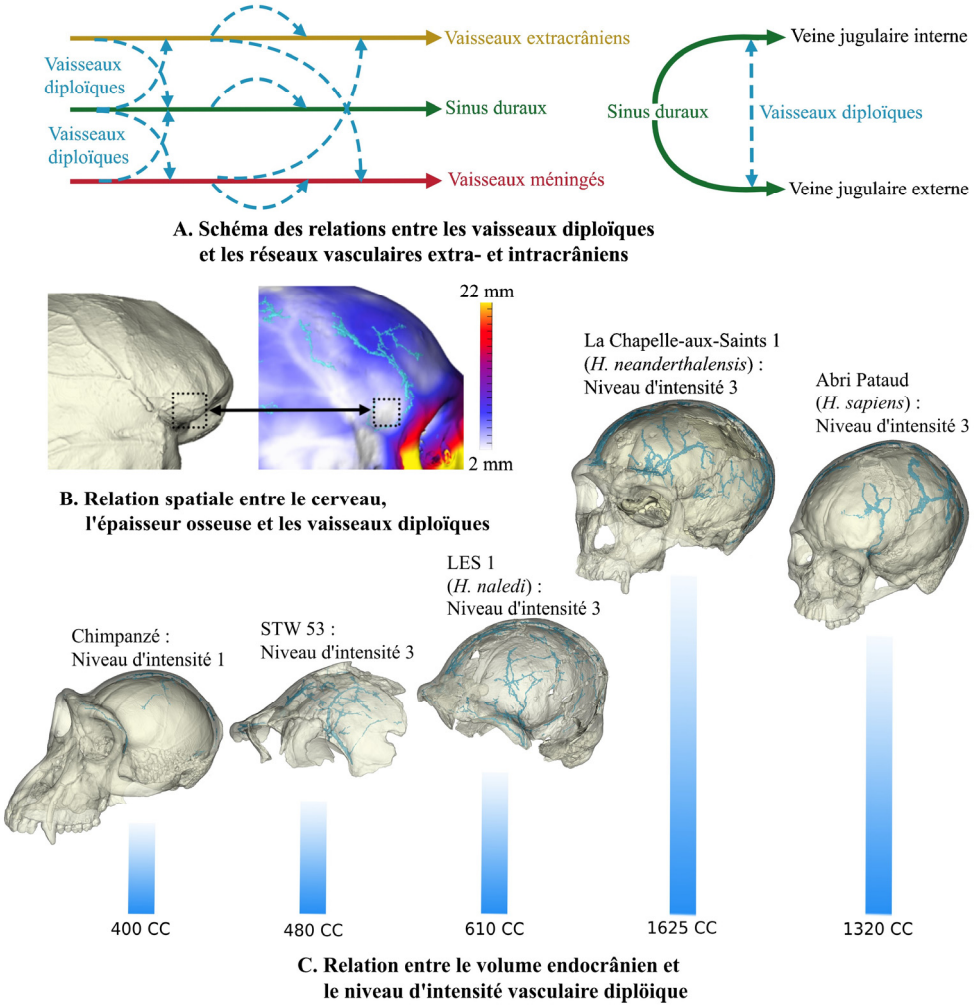

Résumé graphique

1. Introduction

1.1 The significance of the diploic venous system

For humans and other vertebrate animals, the circulatory system is the cornerstone of life, maintaining the metabolic and immune processes. Without the support and adaptation of the circulatory system, the evolution of vertebrate animals could not have been possible. Among all vertebrates, hominids (here defined as the members of Hominidae) are featured with their large brains and high intelligence, which have high metabolic demands (Aiello & Dean, 1990; Boyer & Harrington, 2018; Falk, 1990; Roth & Dicke, 2012). Hominids therefore need a developed circulatory network in the head with an effective mechanism facilitating the exchange of extracranial and intracranial blood. Arterial blood needs to enter the cranium and supply the energy-consuming brain with oxygen and nutrients (Lang, 1983; Schmidt & Thews, 1989). Meanwhile, venous blood needs to exit the cranium and remove waste (Aiello & Dean, 1990; Cheng & Haorah, 2019; Lang, 1983). In both cases, blood has to penetrate the cranium, which is a thick and hard barrier between extracranial and intracranial vascular layers.

In this respect, the diploic venous system plays an important role in bridging the vascular layers. The diploic vessels (DVs) are enclosed in bony diploic channels (DCs), extending inside the diploe. Many orifices in the cranial bones function as the inlets and outlets of DVs. By anastomosing with the DVs through these orifices, extracranial and intracranial vessels make their drainage effectively pass through the cranial bone. In addition, the diploic venous system may transport cerebrospinal fluid, regulate brain temperature, and function as collateral pathways for dural sinuses (Cabanac & Brinnel, 1985; Falk, 1990; Tsutsumi et al., 2015). Considering the involvement of DVs in brain physiology, DVs may have been involved in brain evolution, like other head vascular networks might have done (Aiello & Dean, 1990; Falk, 1986; Saban, 1995; Schwartz et al., 2002a). For these reasons, if we want to understand the evolutionary history of our featured brains, which is a core issue concerned with human evolution, it is

necessary to explore the anatomy and evolution of DVs in extant and extinct hominids.

As an internal structure of cranial bones, the diploic venous system also has potential utility in taxonomy and phylogeny. Many internal structures (e.g., semicircular channels, diploe of suprainiac fossa) have manifested morphological differences among hominid taxa, and have been applied in estimating the taxonomic statuses of fossil specimens (Li et al., 2017; Wu et al., 2014; Y. Zhang & Li, 2023). Especially, utilizing internal structures becomes more critical when the external cranial surface cannot provide enough evolutionary information. Many findings revealed the intra-species variations in hominid meningeal vessels, emissary vessels, and dural sinuses (Braga, 1995; Bruner & Sherkat, 2008; Píšová et al., 2017; Saban, 1995). As the diploic venous system is highly integrated with them, it may also show differences among hominid taxa, and if so, it may contribute to future taxonomic or phylogenetic discussions. Furthermore, because the bony channels of diploic venous system are hard tissues protected by inner and outer tables, sometimes they can be well preserved in fossils when the external surface is seriously damaged by the taphonomic process. This further increases the application value of the diploic venous system in fossil studies.

Finally, it is also worth mentioning that the study of evolutionary history aims at understanding all aspects of a creature. However, constrained by the preservation condition of fossil materials, the study of human evolution is biased towards the musculoskeletal system and nervous systems. We have scarce knowledge about the appearance of vascular networks in extinct hominid species. Considering this, reconstructing and presenting the diploic venous system of these extinct creatures will contribute to a more comprehensive understanding of them and satisfy our scientific curiosity.

1.2 Research questions and objectives

Despite the significance of the diploic venous system in the field of anatomy and paleoanthropology, there are only a few studies on this system. This is mainly attributed to the difficulties in inspecting the diploe with traditional dissection methods, which damage the crania and cannot be applied to precious fossil specimens. Although projectional X-ray and clinical CT are devoid of invading cranial bones, their resolutions are not high enough to reveal details of diploic structures.

As a result, although anatomists have correctly described the general picture of the human circulatory system in the 17th century, they did not notice the existence of DVs until the 19th century (Breschet, 1829; Hershkovitz et al., 1999; Kilgour, 1961). Since the discovery of the diploic venous system in extant humans, the classic descriptions published in anatomical books have been criticized for poor accuracy (Hershkovitz et al., 1999). As for non-human primates, only scarce studies have provided clues about the diploic venous system in a small sample of great apes, without detailed morphological and physiological information (A. J. E. Cave, 1994; Hershkovitz et al., 1999). Similarly, only several Middle and Late Pleistocene hominin fossils have been analyzed ('hominin' is defined as the human lineage derived from the chimpanzee-human last common ancestor, including all extinct and extant species), and constrained by preservation statuses and imaging resolutions, their diploic venous networks were not completely reconstructed (Rangel de Lázaro et al., 2016, 2018). In short, two centuries after the discovery of the diploic venous system, the knowledge about this system remains at the infancy stage.

The deficiency and uncertainty of empirical data hinder us from mapping the evolutionary trajectory of the diploic venous system, and thus we cannot verify whether its morphology is a potential taxonomic signal distinguishing hominid fossils. Some have pointed out that great apes (including chimpanzees, gorillas, and orangutans) seemed to have a much less developed diploic venous system than humans, though the

result was concluded from a rather limited sample size (Hershkovitz et al., 1999; Kunz & Iliadis, 2007). If the diploic venous system of extant apes is close to the primitive status in fossil apes (including the chimpanzee–human last common ancestor), a question would be raised: did the diploic venous system evolve to be more developed during the course of human evolution? Also, for the hominid species with less developed diploic venous systems, are their diploic venous systems merely scaled-down versions of extant human vessels, or do they have unique characteristics?

Without enough empirical data, it is also difficult to verify the important hypotheses on the relationship between the brain and the diploic venous system. An ongoing date in the field of paleoanthropology is about the possible correlation between cranial vessels and encephalization. In this regard, many tests have been done in meningeal vessels and emissary vessels (Braga & Boesch, 1997; Bruner et al., 2006; Falk, 1990; Saban, 1995), but it is unknown whether a larger-brained species tends to possess a more developed diploic venous system than those with smaller brains. Furthermore, it is hypothesized that the diploic venous system together with the emissary vessels drain cool blood to counteract the thermal loads generated by large brains (Falk, 1990). However, from the limited evidence, it remains unclear whether the anatomical structure of the diploic venous system is suited to thermoregulatory demands, and to what extent can the diploic venous system contribute to cooling down a brain.

In addition, some have pointed out the possible co-variation between the diploic venous system and cranial bones, especially the bone thickness (Rangel de Lázaro et al., 2020). And some have pointed out that cranial bone thickness can interact with endocranial morphology (Albessard-Ball, 2018; Balzeau, 2013). Therefore, there is a possible spatial interaction between the brain, the diploic venous system, and the cranial bone thickness, which is awaiting to be tested.

Considering the constraints concerned with imaging methods, high-resolution Micro-

CT scanning should be applied, apart from traditional dissections and clinical CT scanning. The new imaging method can non-invasively detect the microscopic and macroscopic structures of diploe, which paves the way for reconstructing a more complete picture of the diploic venous network.

To explore the research questions discussed above, it is necessary to include more great ape specimens, which allows identifying the differences between human and non-human primates as well as the evolutionary polarity. A comparative study is also necessary for hominin species from each period of the Pleistocene, which conditions the reconstruction of the evolutionary history and interspecies variations among human lineage. What is more, a comparison between the species with various brain sizes and shapes can contribute to understanding the relationship between the brain and the diploic venous system. In this case, a comparison between *H. sapiens* and *H. neanderthalensis* is especially important. It would be interesting to estimate whether these two groups with comparable brain sizes possess comparably developed diploic venous systems, and whether their differences in the system result from their distinct brain shapes and thermoregulatory demands.

Additionally, there is a special methodological question for analyzing diploic venous systems in fossil specimens. As the diploic venous system of fossil crania is sometimes incomplete, comparing their absolute sizes (e.g., lumen diameter, branch length, volume) with those of extant specimens may generate distorted results. For this reason, it is necessary to induce a new method for the quantitative evaluation of fossil diploic venous systems. One candidate is calculating the relative volume of the diploic venous system, which means the ratio of diploic channel volume to bone volume. Another candidate is fractal analysis, a method of calculating the fractal dimension of a network. The fractal dimension is an indicator of the degree of complexity. A complex network tends to have a high fractal dimension (Di Ieva, 2016; Mandelbrot, 1982). The fractal analysis has been applied in evaluating retinal arteries and middle meningeal vessels

(Bruner et al., 2006; Masters, 2004), but its usefulness for diploic venous systems is unclear.

In this context, this study first aims to describe the diploic venous system in various extant and fossil hominid species. Based on the description, this study aims to map the evolutionary trend and test the taxonomic significance of diploic venous systems. Secondly, this study aims to explore the mechanism behind the variation and evolution of diploic venous systems, with special attention paid to the interaction between the brain, cranial bone, and diploic venous systems. Finally, this study aims to test the usefulness of new quantitative methods (relative volume and fractal analysis) in evaluating the size and complexity of fossil diploic channels, which would benefit future studies.

1.3 Thesis configuration

The thesis is composed of nine chapters, including this current introduction (Chapter 1).

Chapter 2 defines terminologies and details the current anatomical and evolutionary knowledge about the diploic venous system and its associated vessels and sinuses.

Chapter 3 lists the extant and fossil specimens used in this study, introducing their background information about preservation conditions, curation institute, geological location, and dating.

Chapter 4 details the protocols of CT scanning and 3D reconstruction, as well as the qualitative and quantitative methods for estimating the drainage, distribution, and intensity of diploic venous systems.

Chapter 5 is the result of detailed and comparative observations of the diploic vascular drainage pathways among hominid specimens, showing the characteristics of each taxon.

Chapter 6 is the result showing the intensity levels, fractal dimensions, and relative sizes of diploic venous systems in each taxon.

Chapter 7 is the result of the comparison between the endocranial morphology and the distribution patterns of bone thickness and diploic venous system, revealing the interaction between these three structures.

Chapter 8 is the discussion section. It first verifies and corrects the classic descriptions from anatomical books, discussing the usefulness and limits of the methods tested in this study. It then maps the general evolutionary trajectory of the diploic venous system,

with special attention to the unique features of each taxon that may have application value in taxonomic or phylogenetic analyses. Finally, this chapter considers the mechanism behind the inter-species variation in the diploic venous system, discussing the possible influence from other vascular structures, brain morphology, bone thickness, and thermoregulatory demands.

In the end, Chapter 9 concludes the main contributions and limits of this study, pointing out the remained questions for future studies.

The thesis includes some figures and text from my published papers (Hui & Balzeau, 2023b, 2023a), which are open-access under the 'Creative commons attribution license'. Besides, some parts of the thesis are in preparation for submission to journals and conferences.

2. Current knowledge and terminological considerations

2.1 Diploic venous system

The diploic vessels (DVs, Figure 2.1) are valveless vessels with a single endothelial layer (García-González et al., 2009). They are enclosed in the diploic channels (DCs), the bony shells of DVs, running between the inner and outer tables of the cranial bones (García-González et al., 2009; Rangel de Lázaro et al., 2020). The DCs are usually taken as the proxy of the DVs in dry skulls and fossils. The classic description in anatomical books claims that the DVs are located in the frontal, parietal, and occipital bones (Breschet, 1829; Hershkovitz et al., 1999; Schünke et al., 2016). The DVs can be detected in fetuses (Hershkovitz et al., 1999), and they progressively develop following the growth of cranial size and thickness (Rangel de Lázaro et al., 2020). Among adults, the characteristics of DVs no longer show associations with ages (Hershkovitz et al., 1999).

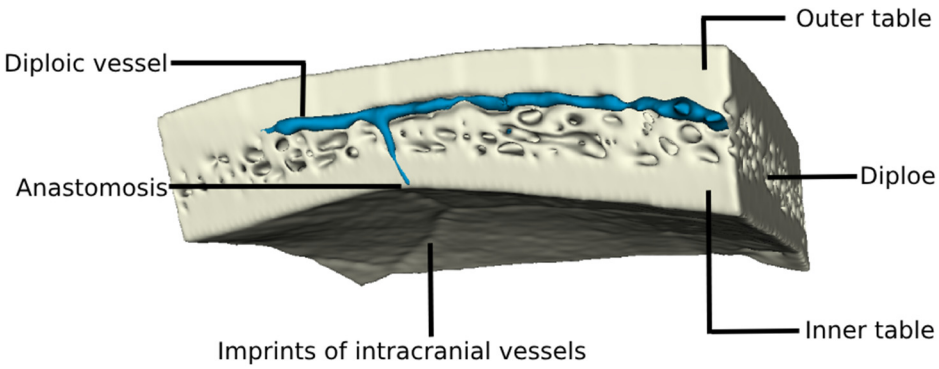

Figure 2.1 The layers of a cranial bone and the location of diploic vessels.

Breschet (1829) first sorted the DVs in extant humans into four main sections (Figure 2.2)—the frontal diploic vessel (FDV), anterior temporal diploic vessel (ATDV), posterior temporal diploic vessel (PTDV), and occipital diploic vessel (ODV). This categorisation is widely used in anatomy to date. Tsutsumi et al. (2013) further developed a new classification comprising the frontoorbital route (FO), pteriofrontparietal route (PFP), occipitoparietal route (OP), and occipitocervical route

(OC). The division of each branch in the latter classification method is analogous to that of the Breschet's, but what is different is that the FO could be subsequently divided into OFO (the orbital part of the frontoorbital route) and PFO (the pterional part of the frontoorbital route).

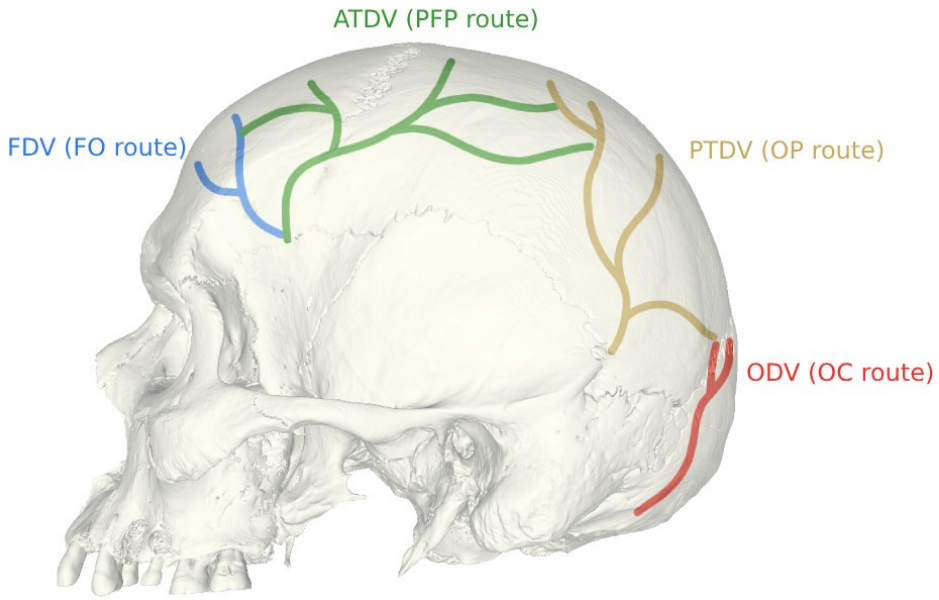

Figure 2.2 The classifications of diploic venous networks established by Breschet (1829) and Tsutsumi et al. (2013). FDV, frontal diploic vessel; ATDV, anterior temporal diploic vessel; PTDV, posterior temporal diploic vessel; ODV, occipital diploic vessel; FO, frontoorbital route; PFP, pteriofrontparietal route; OP, occipitoparietal route; OC, occipitocervical route.

A detailed categorisation like this may help us better understand the composition of the diploic venous system, but it may not be generally applicable (Hershkovitz et al., 1999). There is a simpler classification with broad application value sorting the vessels more straightforwardly into the frontal, parietal, and occipital parts, and this approach has been applied in many anthropological studies (Eisová et al., 2022; Hershkovitz et al., 1999; Lachkar et al., 2019; Rangel de Lázaro et al., 2020).

With Breschet (1829) classification method, García-González et al. (2009) detailed the drainage of the DVs in extant humans. According to their findings, the FDV and ATDV connected to the sphenoparietal sinus and superior sagittal sinus. The PTDV received

tributaries from the ODV and connected to the superior sagittal, transverse, and sigmoid sinuses. Similarly, Tsutsumi et al. (2013) also found the PFP (equivalent to the ATDV) connected to the superior sagittal sinus, and PFP merged with the FO (equivalent to the FDV) at the pterion, communicating with the sphenoparietal sinus and the middle meningeal vessels. Besides, they found the OP (equivalent to the PTDV) linked the posterior part of the superior sagittal sinus with the transverse and sigmoid sinuses, which was in accord with García-González's description.

In Tsutsumi's findings, however, the FO (equivalent to the FDV) did not drain into the superior sagittal sinus but into the superficial vein. The OC (equivalent to the ODV) did not course into the OP but is occasionally contiguous with the superior sagittal sinus, and it emptied extra-cranially into the suboccipital venous channels. Hershkovitz et al. (1999) neither found any anastomosis between the frontal DVs and the superior sagittal sinus, but the anastomosis of DVs with the superior ophthalmic vein, meningeal vessels, and sphenoparietal sinus were documented. Using the simpler classification method, Hershkovitz et al. (1999) did not divide the DV branches in the parietal bone. In their research, the parietal DVs as a whole might connect to the meningeal vessels, sphenoparietal sinus, parietal foramen, mastoid foramen, transverse sinus, sigmoid sinus, or straight sinus. At the individual level, the connection between these vascular networks and parietal DVs could vary with the distribution pattern of DVs (e.g., spider, serpentine, and bonsai patterns).

Generally, previous researchers have highlighted the possibilities of how the DVs can be connected to the other vascular systems, but they were far from reaching a consensus on the morphology and drainage, given the inconsistency in their findings. This could be attributed to the diverse methods they applied (e.g., traditional dissection, X-ray, or MRI), which reveal different levels of details, but another explanation could be the high variability in the diploic venous system.

In addition to extant humans, Hershkovitz et al. (1999) analyzed the diploic venous systems of seven great ape crania (chimpanzees, gorillas, and orangutans), suggesting that great apes have much simpler and smaller DVs than extant humans. Cave (1994) analyzed five gorilla crania and described the connection between the ectocranial foramina and diploe. Still, none of these studies provided us with detailed descriptions of the DVs of non-human primates.

As for fossil hominin species, two pioneering studies attempted to reconstruct the DVs for Kabwe 1 and three *H. neanderthalensis* crania (Rangel de Lázaro et al., 2016, 2018), stating that *H. neanderthalensis* has much less developed diploic venous systems than extant humans in terms of complexity and absolute volume. Still, constrained by taphonomical damages and imaging resolution, the reconstruction for these fossil specimens seems to be incomplete. And there is no complete information about the drainage pathways of their DVs. Moreover, the limited sample size is not enough to confirm taxonomic differences or an evolutionary trend.

2.2 Associated structures

2.2.1 Emissary vessels

Concluding from most studies (Braga, 1995; Braga & Boesch, 1997; Hedjoudje et al., 2019; Jelev & Malinova, 2020; Lang, 1983), the emissary vessels are usually taken as those housed in emissary channels (i.e., cranial foramina) bridging the extra-and intracranial vessels (Figure 2.3). The emissary vessels differ from DVs in morphology and physiology. A DV courses along the diploe, where it has ramifications and long extensions. The DVs frequently anastomose with each other and form a large network. In comparison, an emissary vessel pierces through the cranial bone, with only a short section passing through the diploe. An emissary vessel usually has no ramifications in the diploe, and it is usually isolated from other emissary vessels. As a result, through the large diploic venous network, the drainage from an extra-/intracranial vessel connected with a DV can be transported far from the connecting point. Through the short emissary vessel, the drainage from an extra-/intracranial vessel can only penetrate the bone and reach the adjacent vessels on the opposite side of the cranial wall.

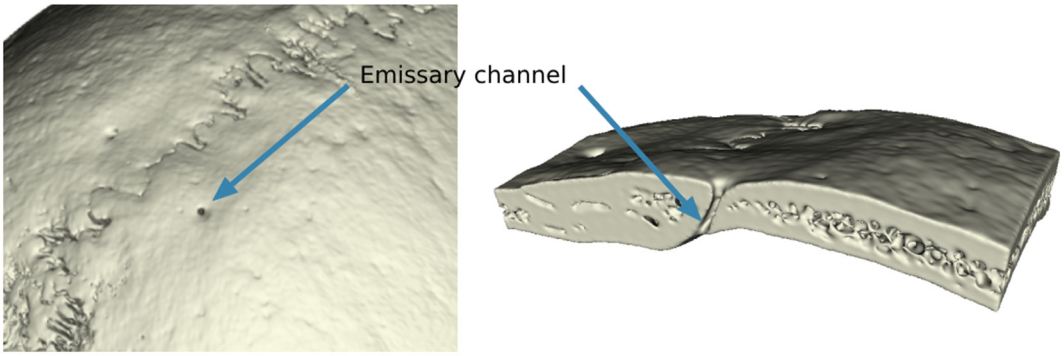

Figure 2.3 The orifices of emissary channels on the ectocranial surface (left) and the dissection of the emissary channel (right).

Some expanded the definition of emissary vessels. For instance, petrosquamous sinus was occasionally considered as emissary vessels (Marsot-Dupuch et al., 2001; Pekcevik & Pekcevik, 2013; Zhao et al., 2014), for this intracranial vessel extends extracranially and thus bridges the intra-and extracranial networks. However, the expanded definition

is problematic. As almost all cranial vessels have branches extending intra-or extracranially, following the expanded definition, they all can be classified as emissary vessels. Considering this, the narrow sense of the terminology ‘emissary vessels’, as detailed above, is more feasible. Only the short vascular branches inside the emissary channels should be called emissary vessels, while the intra-and extracranial vessels connected with them should not be included in this category.

It is unclear how many emissary vessels a hominid cranium possesses, as the number is large and most are microscopic vessels difficult to inspect (Bruner & Eisova, 2024). Nevertheless, the emissary vessels housed in large foramina have been frequently described. In the parietal bones, the parietal foramina are in the parasagittal area, and the embedded emissary vessels link extracranial vessels with the superior sagittal sinus (Al-Shuaili et al., 2024; Cabanac & Brinnel, 1985; De Souza Ferreira et al., 2021). The mastoid foramina are in the petromastoid part of the temporal bone, housing emissary vessels linking the sigmoid sinus and extracranial vessels (Falk, 1990; Louis et al., 2009). In the occipital bone, several foramina are along the superior nuchal line and midline, linking extracranial vessels with superior sagittal sinus, transverse sinus, or other sinuses (Hedjoudje et al., 2019; Jelev & Malinova, 2020; Louis et al., 2009). DVs may anastomose with these parietal, mastoid, and occipital emissary vessels (García-González et al., 2009; Hershkovitz et al., 1999; Jelev & Malinova, 2020). In addition, many large emissary foramina are located in the skull base (e.g., condyle foramen, retroarticular foramen), through which blood from the intracranial space exits the head.

It is hypothesized that the thermal capability of emissary vessels may condition the increase of brain volume during human evolution (Falk, 1990). If so, a large brain with high thermal loads is expected to possess highly developed emissary vessels. Still, this hypothesis is controversial because the small diameter of emissary vessels may not considerably cool down a brain (Brengelmann, 1990). Moreover, the current findings from fossil records cannot sufficiently evidence the hypothesis (Braga & Boesch, 1997).

2.2.2 Extracranial vessels

Overview

The extracranial vascular networks that may connect with DVs are mainly composed of the ophthalmic, periorbital, superficial temporal, deep temporal, occipital, and posterior auricular vessels. They supply the scalp, muscle, eye, bone, and other tissues. The arteries derive from either the internal or external carotid artery. The veins derive from either the internal or external jugular vein. These extracranial vessels leave scarce impressions on the skull. However, knowledge from anatomical records can help determine approximately the original location of vessels in dry skulls. Additionally, the emissary foramina connected with these vessels are preserved on the bone, which are the inlets/outlets of blood drainage. They provide information about how these vessels communicate with the diploic venous system. The anatomical studies on the extracranial vessels in great apes and hominin fossils are scarce. The descriptions below are mainly concluded from anatomical records of extant humans.

Ophthalmic vessels

As a branch of the internal carotid artery, the ophthalmic artery extends from the subdural space of the sphenoid bone to the orbit (Hayreh, 2006; Schünke et al., 2016). The ophthalmic artery gives off many branches, including the supraorbital, ethmoid, and supratrochlear arteries. The ophthalmic artery in extant humans may occasionally give off a branch supplying the meninges, while in great apes the incidence is higher (Falk, 1993; Lang, 1983). The human ophthalmic artery occasionally does not connect to the internal carotid artery, instead, it derives from the meningeal artery (Hayreh, 2006).

The superior ophthalmic vein (Figure 2.4) connects to the supraorbital and angular veins (Cheung & McNab, 2003; Gausas, 2004). Different from what was known previously, the superior ophthalmic vein has valves keeping the blood draining posteriorly, as revealed by new research (J. Zhang & Stringer, 2010) The drainage

finally courses into the cavernous sinus through the superior orbital fissure (Hayreh, 2006). In comparison, the inferior ophthalmic vein is valveless. (Cheung & McNab, 2003; J. Zhang & Stringer, 2010). The inferior ophthalmic vein derives from the venous plexus and finally joins the superior ophthalmic vein (J. Zhang & Stringer, 2010). The middle and medial ophthalmic veins are absent in most individuals, and so are the collateral veins (Cheung & McNab, 2003; Hayreh, 2006). But when they appear, they can communicate the superior and inferior venous networks (Hayreh, 2006).

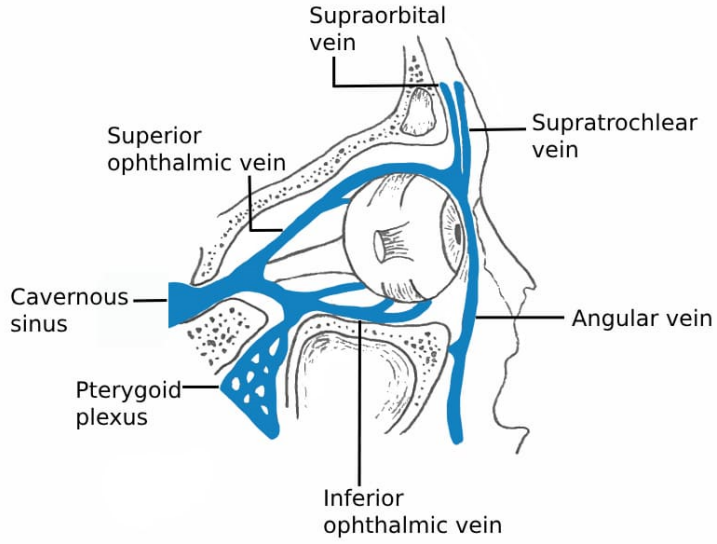

Figure 2.4 The venous network surrounding the eye.

Periorbital vessels

Surrounding the orbit are rich vessels supporting the forehead, eyelid, eye, nasal region, and infraorbital region (Cong et al., 2017; Cotofana et al., 2017; Schünke et al., 2016). Among them, the vessels consistently coursing over and adjacent to the neurocranium are the supraorbital vessels and supratrochlear vessels (Cong et al., 2017; Edizer et al., 2009; Erdogmus & Govsa, 2007).

The supraorbital artery derives from the ophthalmic artery, connecting to the supratrochlear, superficial temporal, and angular arteries, as well as the superior orbital arcade (Edizer et al., 2009; Erdogmus & Govsa, 2007; Liao et al., 2022; Motomura et al., 2003). The trunk of the supraorbital artery usually penetrates the supraorbital

foramen or notch, and then when ascending in the forehead region it divides into a superficial branch inside the subcutaneous and muscle layers and a deep branch between the periosteum and the muscle (Chrcanovic et al., 2011; Erdogmus & Govsa, 2007; Kato & Outi, 1962). The supraorbital vein derives from the superior ophthalmic and angular veins, with anastomosis with the supratrochlear veins and superficial temporal vessels (Delgove et al., 1991; J. Zhang & Stringer, 2010). The pathway of the supraorbital vein differs from the supraorbital artery. The vein enters the supraorbital foramen/notch and gives off a long and transverse branch running along the supraorbital rim (Erdogmus & Govsa, 2007; Kato & Outi, 1962; J. Zhang & Stringer, 2010).

Like the supraorbital artery, the supratrochlear artery originates from the ophthalmic artery and divides into a superficial branch in the subcutaneous layer and a deep branch between the muscle and bone (Edizer et al., 2009; Liao et al., 2022). The supratrochlear artery runs superiorly in the forehead, adjacent to the midline (Schünke et al., 2016). The artery connects to the supraorbital, angular, and superficial temporal arteries, as well as the superior orbital arcade (Erdogmus & Govsa, 2007; Gausas, 2004; Kato & Outi, 1962; Motomura et al., 2003). The supratrochlear vein shares a similar pathway with the supratrochlear artery, but the vein derives from the angular vein rather than from the orbit (Schünke et al., 2016; Zhang & Stringer, 2010).

These periorbital vessels usually do not leave impressions on the external surface of the bone. A study of 556 dry skulls shows that 27% of the skulls present grooves on the frontal squama, which are assumed to be the vascular impressions left by the supraorbital vessels (Schunk & Maruyama, 1960). However, these grooves also match the matches the drainage pathway of the superficial temporal vessels.

Superficial temporal vessels

The superficial temporal vessels support the parotid gland, scalp, and face (Lang, 1983), located inside the subcutaneous tissues and above the muscles or aponeuroses (Ellis &

Mahadevan, 2014; Imanishi et al., 2002). In the upper cranium, the superficial temporal vessels are remarkably close to the bones (Figure 2.5), as the muscle and aponeurosis are rather thin in these areas (Ellis & Mahadevan, 2014; K.-L. Lee et al., 2019).

Originating from the external carotid artery, the superficial temporal artery courses superiorly towards the zygomatic arch, where it usually divides into two branches—the frontal and parietal branches (Marano et al., 1985; Pinar & Govsa, 2006). The frontal branch extends anterosuperiorly and enters the upper facial area, while the parietal branch extends posterosuperiorly and enters the parietal and occipital areas (Ellis & Mahadevan, 2014). The frontal branch connects to the supraorbital, supratrochlear, and occasionally zygomatico-orbital arteries, while the parietal branch connects to the posterior auricular and occipital arteries (Edizer et al., 2009; Pinar & Govsa, 2006).

The superficial temporal vein is a branch of the retromandibular vein, which is a tributary of both the internal and external jugular veins (Rao et al., 2018). Like the superficial temporal artery, the vein usually gives off the frontal and parietal branches at the zygomatic arch, and these two venous branches follow the coursing directions of the arterial branches, connecting to the periorbital vessels, posterior auricular vessels, and occipital veins (Delgove et al., 1991). The trunks of the superficial temporal vein are adjacent and parallel to the superficial temporal artery, but the frontal and parietal branches of the vein are distant from those arterial branches and cover a larger drainage area than the arterial branches do (Imanishi et al., 2002; H.-J. Lee et al., 2018).

The superficial temporal artery and vein are rarely discussed in the studies of evolution. This is because they usually do not leave impressions on the fossil bones. However, in the upper frontal and upper parietal bones, numerous foramina link the extracranial vessels, diploe, and intracranial space. Considering the superficial temporal artery and vein are the only extracranial vessels coursing there, it is almost certain that these foramina connect to the superficial temporal artery or vein. Finally, it is worth noting

that when the soft tissue is not preserved, it is unknown whether the foramina is connected to the artery or vein. It is better to use the collective name ‘superficial temporal vessels’ than ‘superficial temporal artery’ or ‘superficial temporal vein’ in this study.

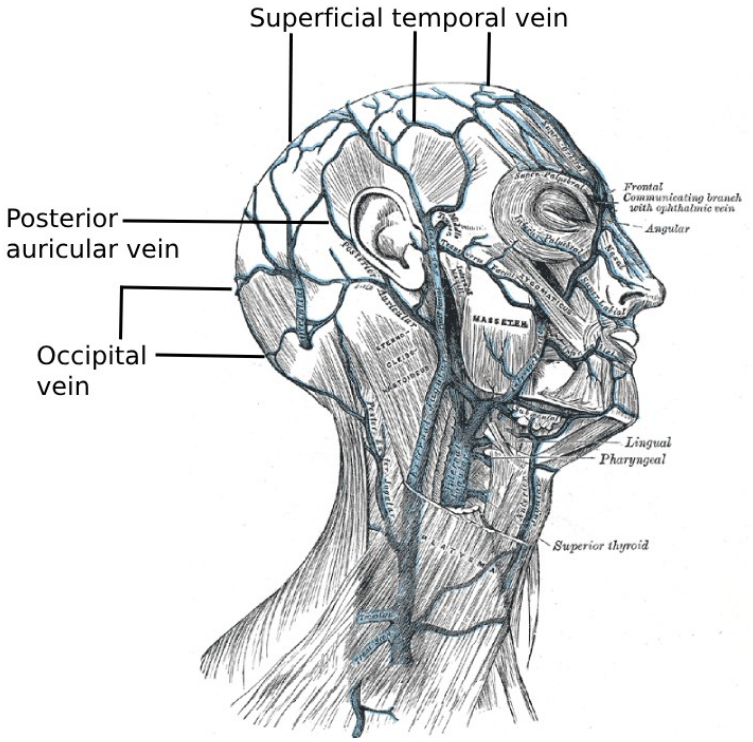

Figure 2.5 The superficial temporal vein (the illustration was drawn by Henry Vandyke Carter and published by Henry Gray (1918) in *Anatomy of the Human Body*).

Deep temporal vessels

The deep temporal artery and vein are inside the temporal fossa, coursing between the muscles and bones (Zhou et al., 2023). The deep temporal artery derives from the maxillary artery, a branch of the external carotid artery (Lang, 1983). When the deep temporal artery ascends in the pterional region, it divides into the anterior and posterior branches (Zhou et al., 2023). The drainage of the deep temporal artery is unclear, but its connection with the superficial temporal vessels has been noted (Casanova et al., 1986).

Likewise, the deep temporal vein courses between the bone and muscle (Davison &

Kaplan, 2005). The branching pattern of the deep temporal vein is variable—it always runs towards the facial region and sometimes gives off branches extending posteriorly (McKinnon et al., 2022). The drainage of the vein is unclear. However, Tsutsumi et al.(2022) have recently noticed that DVs connect to the vessels of the temporal muscle in the pterional region. Interestingly, the deep temporal vein is in this region and is adjacent to the muscle and bone. Thus, DVs possibly connect to the deep temporal vein.

Posterior auricular vessels and occipital vessels

The posterior auricular and occipital vessels support the inferoposterior part of the head (Figure 2.5). The posterior auricular artery originates usually from the external carotid artery (Gómez Díaz & Cruz Sánchez, 2016; Zümre et al., 2005). The trunk of the posterior auricular artery courses in the subcutaneous layer, between the ear and mastoid process, giving off branches entering the ear and the occipital bone (Gómez Díaz & Cruz Sánchez, 2016; Schünke et al., 2016). The posterior auricular vein is close to the accompanied artery (Ellis & Mahadevan, 2014; Schünke et al., 2016). The vein communicates with the mastoid emissary vessels and unites with the retromandibular vein before joining the external jugular vein (Lang, 1983; Prakash et al., 2006).

The occipital artery usually originates from the external carotid artery (Guo et al., 2019; Ostrowski et al., 2023). The trunk of the occipital artery can be divided into three segments—the digastric, suboccipital, and occipital segments (Keser et al., 2018). The inferior part of the digastric segment is in the neck, while the superior part is adjacent to the cranial bone (Alvernia et al., 2006). Close to the mastoid notch, there are grooves for the occipital arteries (Alvernia et al., 2006; Ostrowski et al., 2023). The digastric segment gives off branches extending into the muscle or extending into the jugular or styloid foramen before entering the posterior fossa (Alvernia et al., 2006). The suboccipital segment gives off a deeper branch coursing above the suboccipital triangle and a superficial branch between the splenius capitis and semispinalis capitis (Alvernia et al., 2006). Finally, the occipital segment has many branches over the occipital area

(Keser et al., 2018; Pinar & Govsa, 2006; Schünke et al., 2016).

Like the occipital artery, the occipital vein extends from the neck to the occipital bone (Schünke et al., 2016). There is no clear division of the vein in published research, but it is clear that the occipital vein is widespread over the occipital area, where it connects to the emissary vessels and superficial temporal vessels (Delgove et al., 1991; Ellis & Mahadevan, 2014; Schünke et al., 2016). The inferior part of the occipital vein connects to the mastoid foramen and joins the external jugular vein or suboccipital venous plexus (Pekcevik & Pekcevik, 2013), and the latter is connected to the vertebrate venous plexus.

2.2.3 Meningeal vessels

Overview

The meningeal vessels are embedded between the cranial bones and dura mater (Chmielewski et al., 2013; Sant'Anna et al., 2021), leaving many imprints on the inner wall of the cranium (Figure 2.6). As the pathways of these arteries and veins are very close and parallel, it remains controversial whether the imprints are left by meningeal arteries, veins, or both (Bruner & Sherkat, 2008; Falk, 1993). For this reason, it is better to name them 'imprints of meningeal vessels'.

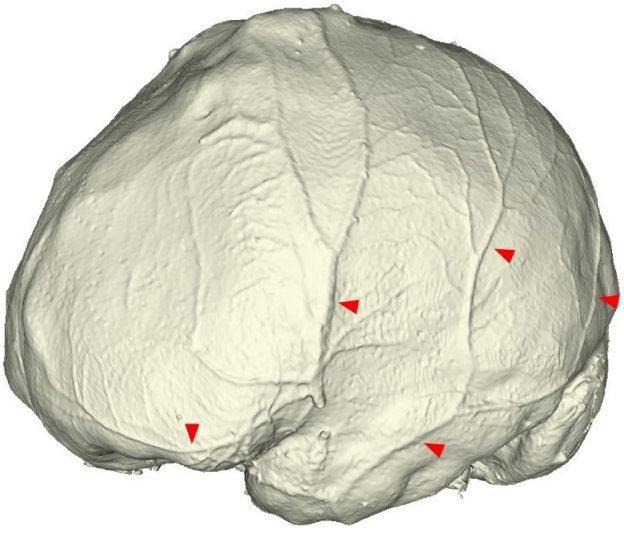

Figure 2.6 The imprints of meningeal vessels (marked in red) on an extant human endocast.

So far, there are no standard terminologies or classifications of meningeal vessels. Based on the description provided by many previous studies (Bruner & Sherkat, 2008; Falk, 1993; Saban, 1995; Sant'Anna et al., 2021; Seker et al., 2010), the meningeal vessels frequently described and discussed in the field of human evolution can be divided as the anterior meningeal vessels (AMV), orbital meningeal vessels (OMV), and middle meningeal vessels (MMV). In addition, in the posterior cranial fossa of the skull base, there are posterior meningeal vessels. However, they are tiny and difficult to inspect in fossils and dry skulls (Schwartz et al., 2002a; Seker et al., 2010), and they are of limited importance for the small size of their territory.

Anterior meningeal vessels

The anterior meningeal vessels are on the most anterior part of the anterior fossa (Sant'Anna et al., 2021; Seker et al., 2010). The anterior meningeal vessels derive from the anterior ethmoidal vessels (Figure 2.7), extending from the ethmoid bone to the area surrounding the frontal crest (Sant'Anna et al., 2021; Seker et al., 2010). The drainage of the anterior meningeal vessels is not clear. It is unknown whether the vessels connect to the adjacent frontal sinus and DVs.

Orbital meningeal vessels

The orbital meningeal vessels stem from the orbit (Figure 2.7), and thus they are sometimes taken as a recurrent branch of the ophthalmic vessels (Falk, 1993; Kubo, 2022). The orbital meningeal vessels usually connect to the orbit through the superior orbital fissure in extant humans, and through the cranio-orbital foramen in non-human primates (Bruner & Sherkat, 2008; Kubo, 2022). The orbital meningeal vessels are highly developed in great apes. They usually occupy the frontal area and frequently extend into the parietal (Falk, 1993). The orbital meningeal vessels occupy the territory originally belonging to the middle meningeal vessels, when the latter is absent in some ape individuals (Bruner & Sherkat, 2008; Falk, 1993).

In contrast, the orbital meningeal vessels in extant humans are much less developed. They are usually limited in the anterior fossa and rarely extend into the parietal (Bonasia et al., 2020; Kubo, 2022). In the early-established and widely-applied classification (Adachi's system) of meningeal vessels, the orbital meningeal vessels are even ignored (Adachi, 1928). Interestingly, a recent investigation has noticed the developed orbital meningeal vessels in many *H. erectus* specimens (Kubo, 2022), stating that the incidence of the orbital meningeal vessels reaching the parietal area is around 16%, which is higher than that of extant humans but lower than great apes. Finally, so far there are no reports about whether the orbital meningeal vessels are connected with the DVs. It is also unclear whether the variation of the territory of orbital meningeal vessels can influence the drainage or distribution of DVs.

Middle meningeal vessels

The middle meningeal vessels are branches of the maxillary vessels (Figure 2.7), usually stemming from the foramen spinosum in the skull base. For some ape individuals with no foramen spinosum, the middle meningeal vessels instead stem from the foramen ovale or petrosphenoid fissure (Falk, 1993). The middle meningeal vessels are variable among great apes. In gorillas, orangutans, and chimpanzees, the middle meningeal vessels are sometimes absent and replaced by the orbital meningeal vessels (Bruner & Sherkat, 2008; Falk, 1993). In bonobos, the middle meningeal vessels are always present (Falk, 1993). Also, the territory of middle meningeal vessels is variable. The least developed type only occupies the lower part of the middle cranial fossa, while the most developed can occupy the majority of the endocranial surface (Falk, 1993). The middle meningeal vessels in chimpanzees usually have dominance over the orbital meningeal vessels, while in orangutans the orbital meningeal vessels are usually the dominant (Falk, 1993).

In comparison, the middle meningeal vessels in extant humans are constantly present

and have dominance over other meningeal vessels (Bruner & Sherkat, 2008; Seker et al., 2010). Close to the foramen spinosum, the middle meningeal vessels in hominins usually divide into two branches (Aiello & Dean, 1990). The anterior branch mainly supplies the frontal and the anterior part of the parietal, while the posterior branch mainly supplies the temporal, occipital, and posterior parts of the parietal (Aiello & Dean, 1990; Bruner & Sherkat, 2008). In extant humans and *H. neanderthalensis*, the anterior branch is the most developed (Bruner & Sherkat, 2008). In *H. erectus*, the anterior branch is comparably or less developed than the posterior (Schwartz et al., 2002a).

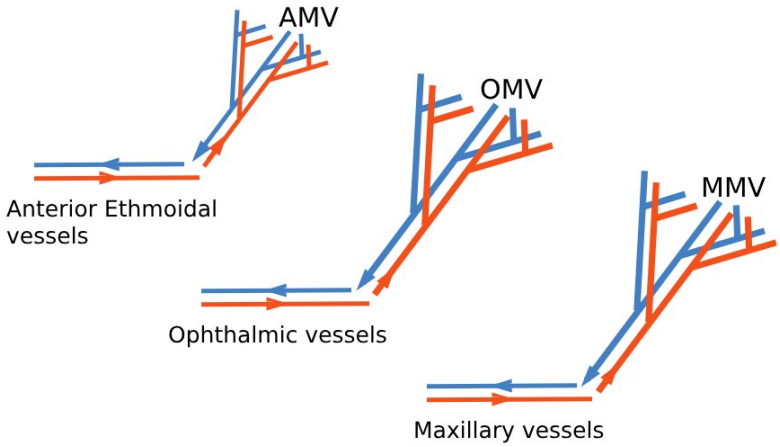

Figure 2.7 The origins of anterior meningeal vessels (AMV), orbital meningeal vessels (OMV), and middle meningeal vessels (MMV). The venous routes are blue, and the arterial are red.

Some hypothesized that the intensity degree of middle meningeal vessels is positively correlated with brain size (Saban, 1995). However, some chimpanzee middle meningeal vessels are highly reticulated, while large-brained *H. neanderthalensis* has simpler middle meningeal vessels than that of *H. sapiens* (Bruner & Sherkat, 2008; Schwartz et al., 2002a). In addition, the anastomosis between middle meningeal vessels and DVs has been documented in studies (Rangel de Lázaro et al., 2016; Tsutsumi et al., 2013), which emphasize that the pterional area is the place where the anastomosis usually present. Still, the possible presence of the anastomosis in other areas is poorly explored.

2.2.4 Dural sinuses

Overview

The dural sinuses are embedded between the periosteal and meningeal layers of the dural mater (Schünke et al., 2016). The dural sinuses collect venous blood from the brain cortex and then empty blood extracranially (Betts et al., 2022; Kılıç & Akakın, 2007). The dural sinuses also connect with the arachnoid granulations (Figure 2.8), transporting cerebrospinal fluid (Duncan, 2003; Upton & Weller, 1985). Because the dural sinuses are valveless (Uddin et al., 2006), the drainage flow is associated with body postures (Batson, 1944; Falk, 1990). Many dural sinuses leave imprints on the endocranial surface, providing us with an opportunity to inspect them in fossil and dry skulls. Some studies have documented the evolution of the sinuses in hominins (Peña-Melián et al., 2011; Rosas et al., 2008, 2014; Schwartz et al., 2002a). However, the connection between the dural sinuses and the diploic venous system is so far unclear in fossil hominins (García-González et al., 2009; Hershkovitz et al., 1999; Tsutsumi et al., 2013).

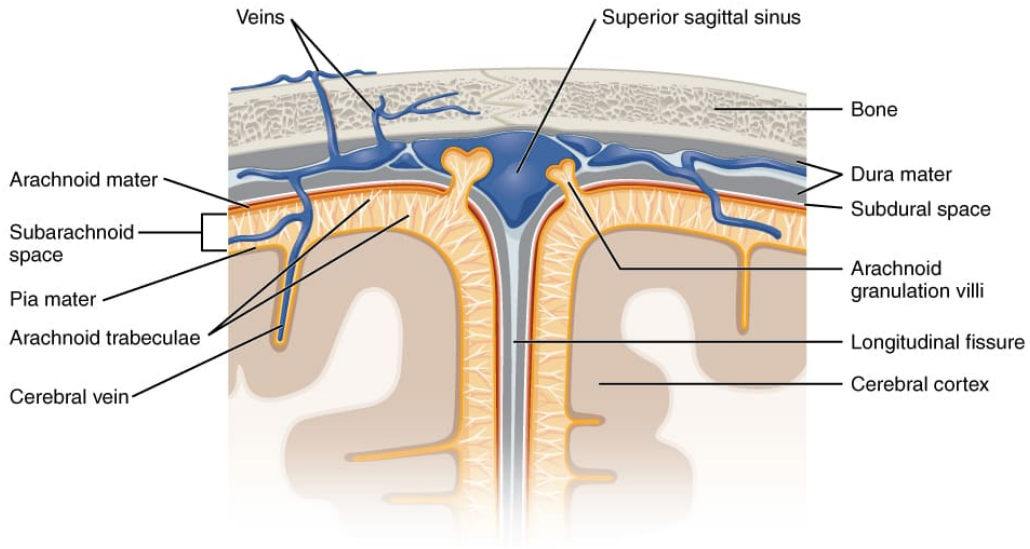

Figure 2.8 The arachnoid granulations communicate the subarachnoid space with the superior sagittal sinus. The figure is from Betts et al.(2022), which is published on Openstax.

Superior sagittal sinus

The superior sagittal sinus is the main stem of the dural sinus network (Figure 2.9). Its

main function is collecting venous blood from the superficial cortical veins (Juskys et al., 2022; Lang, 1983). It also receives cerebrospinal fluid from arachnoid granulations (Upton & Weller, 1985). Like other dural sinuses, the superior sagittal sinus has no valves regulating the direction of blood flow (Uddin et al., 2006). The connection between DVs and superior sagittal sinus has been documented in extant humans (García-González et al., 2009; Hershkovitz et al., 1999; Tsutsumi et al., 2013). Furthermore, the connection also emerges in non-primate mammals, including dogs, aardvarks, tree shrews, and moles (Miller et al., 1979; Thewissen, 1989).

The superior sagittal sinus starts from the foramen cecum (Patchana et al., 2019), then it courses along the middle-sagittal plane of the cranium and stops at the confluence of sinuses (Lang, 1983; Samadian et al., 2011). The superior sagittal sinus has a wide lumen size (Juskys et al., 2022), however, the majority of its imprint on the cranial bones is shallow and unclear, with only the part in the occipital bone clearly presented. For this reason, the superior sagittal sinus is not detailly described in fossil records, and its evolutionary trajectory has not been fully discussed (Schwartz et al., 2002a).

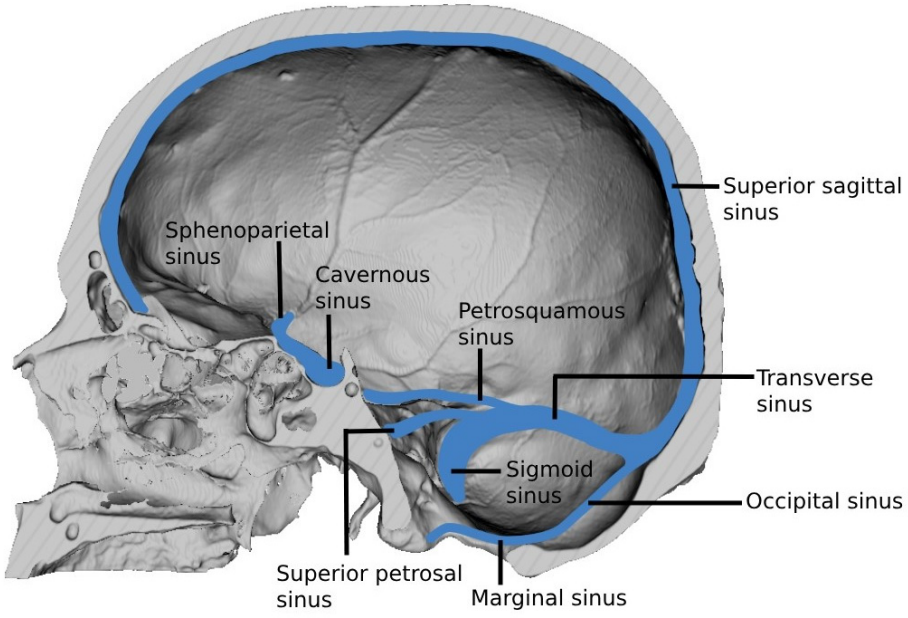

Figure 2.9 The major dural sinuses in a human head.

Cavernous and intercavernous sinuses

The cavernous sinus is located in the central area of the sphenoid bone and functions as a center of the venous network in the skull base (Figure 2.9). Many veins and dural sinuses connect to the cavernous sinus, including the sphenoparietal sinus, superior & inferior ophthalmic veins, superior & inferior petrosal sinus, and many cerebral veins (Cheung & McNab, 2003; Hayreh, 2006; Lang, 1983; Tubbs et al., 2007). There are a pair of cavernous sinuses on the lateral sides of the body of the sphenoid bone (Aiello & Dean, 1990; Lang, 1983). The gap between them is narrow, where intercavernous sinuses bridge the cavernous sinuses on the two sides (Lang, 1983). The morphology and drainage of the cavernous and intercavernous sinuses have not been detailly documented in fossils. Their connections with the DVs are also unclear.

Sphenoparietal sinus

The sphenoparietal sinus is also called the 'Breschet sinus' (Ruız et al., 2004). It courses along the lesser wing (Ruız et al., 2004; Tubbs et al., 2007). In most cases, the sphenoparietal sinus is anastomosed with the meningeal vessels in the pterional region (Figure 2.9), and it connects to the cavernous sinus close to the ophthalmic nerve (Tubbs et al., 2007). It is also noticed that some cerebral veins of the frontal lobe and ophthalmic veins may drain into the sphenoparietal sinus (Lang, 1983). The connection between the sphenoparietal sinus and DVs is documented in a few studies on extant humans, and it is reported to appear in the pterional region (García-González et al., 2009; Hershkovitz et al., 1999). In addition, the imprint of the sinus is found in many hominin fossils (Schwartz et al., 2002a), but there is no detailed description of its evolution.

Petrosquamous sinus

The petrosquamous sinus is in the middle fossa (Figure 2.9), coursing along the petrosquamous suture (Lang, 1983). The posterior end of the petrosquamous sinus is anastomosed with the transverse-sigmoid sinuses, and the anterior end is with the stem

of middle meningeal vessels (Butler, 1957; San Millán Ruíz et al., 2006). For this reason, the petrosquamous sinus could be taken as a branch of the middle meningeal vessels, like in an early study of *H. neanderthalensis* (Heim, 1976). The petrosquamous sinus bridges the transverse-sigmoid sinus and middle meningeal vessels, allowing the drainage in the transverse-sigmoid sinus to transfer to the external jugular system (San Millán Ruíz et al., 2006). Some notice the frequent communication between petrosquamous sinus and extracranial vessels in extant humans (Zhao et al., 2014). The connection between the sinus and DVs is also documented in extant humans, but the presence is not consistent (García-González et al., 2009).

Compared with most dural sinuses, the petrosquamous sinus is relatively narrow and not consistently presented. Many early studies suggested that the petrosquamous sinus was a fetal remnant and was rather rare in adult humans (Chell, 1991; Marsot-Dupuch et al., 2001). Nevertheless, some found the sinus frequently in adult humans (San Millán Ruíz et al., 2006). In addition, the sinus has been found in *H. habilis*, *H. erectus*, and *H. neanderthalensis* (Balzeau & Pagano, 2022; Schwartz et al., 2002a). In particular, *H. neanderthalensis* seems to have a high incidence of the sinus (Rosas et al., 2014).

Transverse and sigmoid sinuses

When the superior sagittal sinus arrives in the confluence of sinuses (Figure 2.9), it splits into several sinuses, and the majority continues into the transverse sinus in most hominids (Falk, 1986, 1990; Peña-Melián et al., 2011; Singh et al., 2004). In addition to receiving the drainage from the superior sagittal sinus, the transverse sinus also absorbs cerebrospinal fluid from arachnoid granulations (Duncan, 2003; Leach et al., 1996). The anastomosis between the transverse sinus and DVs has been documented in many studies on extant humans (García-González et al., 2009; Hershkovitz et al., 1999; Tsutsumi et al., 2013).

Beginning from the confluence of sinuses, the transverse sinus courses laterally along

the superior nuchal line, entering the asterional region, where the transverse sinus continues into the sigmoid sinus (Lang, 1983; Schünke et al., 2016). The sigmoid sinus then course horizontally, adjacent to the mastoid and petrous parts of the temporal bone, and finally joins the internal jugular vein through the jugular foramen (Falk, 1990; Falk & Conroy, 1983; Schünke et al., 2016). Because the transverse sinus and sigmoid sinus are a continuum and there is no clear boundary between them, it is reasonable and convenient to take them as a whole in anatomical studies.

The transverse-sigmoid sinuses usually appear in pairs, and there is a noticeable asymmetry in fossil and extant humans (Peña-Melián et al., 2011; Rosas et al., 2008; Schwartz et al., 2002a). In extant humans, the majority of the drainage from the superior sagittal sinus preferentially runs into the right transverse-sigmoid sinuses, which is more pronounced than the left one (Schwartz et al., 2002a; Smith, 1907). In extinct *Homo* species, both the left dominance type and right dominance type are common in fossil records (Peña-Melián et al., 2011; Rosas et al., 2008).

Occipital and marginal sinus

The occipital sinus begins at the confluence of sinuses (Figure 2.9), where it receives drainage from the superior sagittal sinus (Betts et al., 2022; Lang, 1983). Then the occipital sinus courses anteriorly along the midline, reaching the posterior edge of the foramen magnum and finally splitting into two branches surrounding the foramen magnum (Falk & Conroy, 1983; Kobayashi et al., 2006). The two branches are called marginal sinus. The drainage from the occipital and marginal empties into the vertebral venous plexus (Batson, 1944; Falk, 1990). Occasionally, the occipital sinus shows variations in extant humans. Starting from the confluence of sinuses, the occipital sinus may split into two branches without coursing along the midline, and they finally join the transverse-sigmoid sinus (Shin et al., 2017; Tubbs et al., 2011). In this case, the occipital sinus is called ‘oblique occipital sinus’.

The occipital and marginal sinus is in small size in extant great apes, extant humans, and most fossil *Homo* species (Falk, 1990). Especially, the occipital sinus is the smallest dural sinus among extant humans (Tubbs et al., 2011). However, through fossil records, Falk and Conroy (1983) revealed that the robust australopithecines and *A. afarensis* have an enlarged occipital and marginal sinus.

2.2.5 Frontal and ethmoid sinuses

The frontal sinus is a cavity located in the supraorbital area (Figure 2.10), extending towards the ethmoid bone and nasal cavity (Lang, 1983). The frontal sinus is lined by mucoperiosteum, and the mucus produced by the latter is drained into the nasal cavity (Daniels et al., 2003; Lang, 1983). Among primates, only chimpanzees, bonobos, gorillas, and hominins have ethmoidally-derived frontal sinuses (Balzeau et al., 2021; A. J. Cave & Haines, 1940). The frontal sinus morphology is different in each taxon, and thus it has potential in phylogenetics (Balzeau et al., 2022).

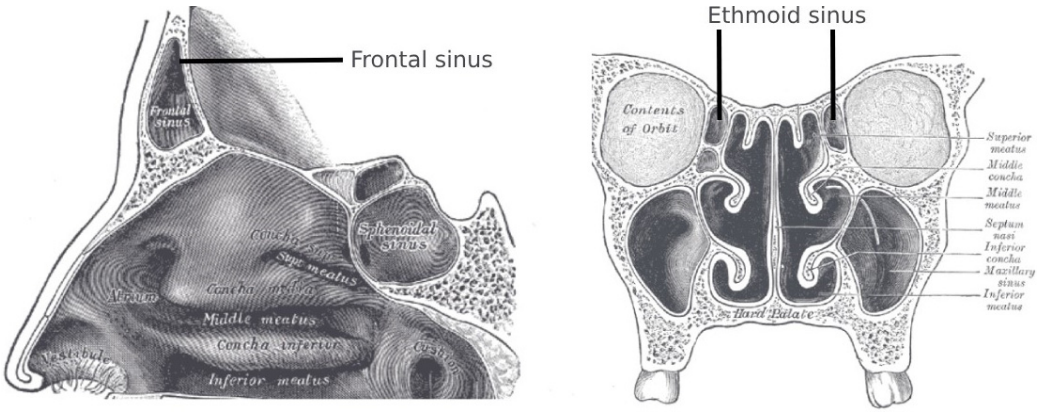

Figure 2.10 The frontal and ethmoid sinuses in extant humans (the illustration was drawn by Henry Vandyke Carter and published by Henry Gray (1918) in *Anatomy of the Human Body*).

The size of the chimpanzee frontal sinus is usually large and positively correlated with the cranial size (Balzeau et al., 2021, 2022). The chimpanzee frontal sinus is directly connected with the ethmoid sinuses, and it is difficult to find a clear boundary between them (Balzeau et al., 2021). In chimpanzees, the drainage from the frontal sinus first courses into the middle ethmoid sinus before entering the nasal cavity (House et al.,

1966). Cave & Haines (1940) argued that the frontal sinus as well as other paranasal sinuses of chimpanzees are the most primitive among all great apes.

The evolution of ethmoid sinuses in hominins is unclear, as these structures are rarely preserved in fossils. However, the frontal sinus has been described in many fossils. Unlike chimpanzees, the frontal sinus in hominin fossils is not significantly correlated with endocranial size, but in the species including and after *Homo erectus,* it seems related to the frontal lobe morphology (Balzeau et al., 2022). In extent humans, the frontal sinus is usually larger in male individuals but its morphology is highly variable among populations (Tatlisumak et al., 2008). The drainage of the frontal sinus in extant humans no longer courses into the ethmoid sinus, but instead runs into the frontal ostium, ethmoid infundibulum, and finally the nasal cavity (Daniels et al., 2003; Kountakis et al., 2016; Lang, 1983).

Interestingly, Lang (1983) noted that DVs in extant humans may sometimes connect to the frontal sinus mucoperiosteum. However, we do not know the incidence of the connection in extant humans and whether it appears in great apes and fossil hominins. Furthermore, given that the ethmoid sinuses are closely connected with the frontal sinus, it is necessary to ask if the DVs connect to the ethmoid sinuses as well.

3. Materials

3.1 Extant specimens

3.1.1 Extant great apes

The chimpanzee (*Pan troglodytes*) and gorilla (*Gorilla gorilla*) cranial specimens are from the French national museum of natural history (Muséum national d'Histoire naturelle, Paris), and they were mainly collected by the museum in the last century (Table 3.1). The dry skull specimens of great apes used in this study are selected strictly following the criteria: 1) the cranium should be from mature individuals; 2) the cranium should be complete or near complete, with diploic structures clear to inspect through Micro-CT; 3) there should be no obvious pathological signs found on the cranial bones. Also, the left and right hemispheres of a cranium are sometimes different in vascular distribution and drainage pathways. Given this asymmetry, this current study follows the usual protocols of previous studies on great ape and human vascular systems (Eisová et al., 2022; Falk, 1993; García-González et al., 2009; Tsutsumi et al., 2022), and virtually divides every cranium into two hemicrania. Each hemicranium is inspected and analysed separately. In total, from the collections of Muséum national d'Histoire naturelle, 18 chimpanzee crania are selected. This includes 7 female crania, 7 male crania, and 4 crania with unknown sex. Besides, 11 gorilla crania are selected, including 7 female crania and 4 male crania. The sex information was from the collection records of Muséum national d'Histoire naturelle.

3.1.2 Extant humans

The cranial specimens of extant *H. sapiens* are curated in Muséum national d'Histoire naturelle (Table 3.1). All these dry skulls are from European adult individuals, collected from France, Hungary, Moldova, Romania, and Russia. The selection criteria of extant human specimens are the same as those of extant apes. Also, each human cranium is virtually divided into two hemicrania for the reasons detailed above in the ape section.

In total, 28 individuals are selected for this study, including 8 from France, 1 from Hungary, 2 from Moldova, 13 from Romania, and 4 from Russia. The sex and age information of the specimens is unknown, but this does not impede the following analyses, as sex and age have an insignificant influence on adult humans' diploic venous system (Eisová et al., 2022).

Table 3.1 The inventory of specimens

Specimens	**Geological period**	**Taxon**	**CT resolution (voxel size)**	**Material source**
KNM-ER 1805	Early Pleistocene	*H. habilis?*	0.084 mm	KNM&MPEA
StW 53	Early Pleistocene	*H. habilis?*	0.082 mm	UW
Tighennif 4	Middle Pleistocene	*H. erectus?*	0.069 mm	MNHN
Trinil 2	Middle Pleistocene	*H. erectus*	0.048 mm	NBC
Hexian	Middle Pleistocene	*H. erectus*	0.16 mm	IVPP
Kabwe 1	Middle Pleistocene	*H. heidelbergensis?*	0.127 mm	NHM
Florisbad	Middle Pleistocene	*H. heidelbergensis?*	0.125 mm	NMSA
LES 1	Middle Pleistocene	*H. naledi*	0.097 mm	UW
Maba 1	Middle Pleistocene	Unclear	0.053 mm	IVPP
La Quina H5	Late Pleistocene	*H. neanderthalensis*	0.109 mm	MNHN
La Chapelle-aux-Saints 1	Late Pleistocene	*H. neanderthalensis*	0.123 mm	MNHN
La Ferrassie 1	Late Pleistocene	*H. neanderthalensis*	0.132 mm	MNHN
Spy 1	Late Pleistocene	*H. neanderthalensis*	0.095 mm	RBINS
Spy 10	Late Pleistocene	*H. neanderthalensis*	0.095 mm	RBINS
Cro-Magnon 1	Late Pleistocene	*H. sapiens*	0.115 mm	MNHN
Cro-Magnon 2	Late Pleistocene	*H. sapiens*	0.110 mm	MNHN
Cro-Magnon 3	Late Pleistocene	*H. sapiens*	0.110 mm	MNHN
Abri Pataud 1	Late Pleistocene	*H. sapiens*	0.110 mm	MNHN
Extant *H. sapiens*	Holocene	*H. sapiens*	0.111-0.132 mm	MNHN
Extant *P. troglodytes*	Holocene	*P. troglodytes*	0.105-0.121 mm	MNHN
Extant *G. gorilla*	Holocene	*G. gorilla*	0.125-0.164mm	MNHN

* KNM: National Museums of Kenya; MPEA: Max Planck Institute for Evolutionary Anthropology; UW: University of Johannesburg; MNHN: Muséum national d'Histoire naturelle (France); NBC: Naturalis Biodiversity Center (Netherlands); IVPP: Institute of Vertebrate Paleontology and Paleoanthroplogy (China); NHM: Natural History Museum (London); NMSA: National Museum of South Africa; RBINS: Royal Belgian Institute of Natural Sciences.

3.2 Hominin fossils

Compared with collecting extant materials, collecting a large sample of hominin fossils is more challenging. This is because well-preserved fossil hominin crania are rare. Through the 'The Human Fossil Record' data archive (https://human-fossil-record.org/) and the databases of institutions, this current study searches for specimens with a relatively well-preserved diploe. Many fossils with their diploic structures damaged seriously cannot be included in this study, though their surfaces are well-preserved. Secondly, the small diameter of diploic venous channels makes this study rely on Micro-CT scanning, which is not accessible for many fossils. This further prevented some fossils from being included here.

Despite these difficulties, this study still has managed to collect a sample of 18 hominin fossil crania (Table 3.1), which are provided by nine institutions worldwide. In terms of chronology, the ages of these fossil crania range from 1.9 Ma to 20 ka, covering the entire period from the emergence of early *Homo* to the expansion of *H. sapiens* populations. Moreover, these cranial fossils are from Europe, East Asia, and Africa (Figure 3.1). This may contribute to our understanding of the diversity of hominin populations from different regions. Besides, all fossils belong to adult individuals. This helps avoid the interference from ontogenetic processes. Both hemicrania of each fossil are carefully examined. However, limited by preservation statuses, one side of a fossil may be incomplete. The archaeological, taxonomical, and chronological background information, as well as the preservation details, are listed below.

3.2.1 Early Pleistocene hominins

KNM-ER 1805 (1.88-1.90 Ma)

The cranial fossil of KNM-ER 1805 is from the Koobi Fora site in Northern Kenya (Schwartz et al., 2002c), and it belongs to the National Museums of Kenya. The specimen has been dated back to 1.88-1.90 Ma (Feibel et al., 1989). Although many researchers classified the specimen as *Homo habilis* (Kimbel et al., 1984; Wood, 1992),

some argued that the specimen should be assigned to *H. erectus*, *H. ergaster*, or even a group outside the genus *Homo* (Grine et al., 1996; Prat, 2002; Rightmire, 1993).

The neurocranium of KNM-ER 1805 is generally complete, while the facial area is seriously damaged. The ecto-and endo-cranial surfaces of the neurocranium are modestly eroded, with many vascular imprints and foramina clearly manifested. The diploic layer of the cranial bone is filled in by sediments, which makes the majority of the diploic structures unidentifiable. The preserved diploic channels are mainly in the posterior half of the cranium.

StW 53 (1.78-1.49 Ma)

The specimen StW 53 is a fragmental cranial fossil discovered in the member 5 of the Sterkfontein site, South Africa (Curnoe & Tobias, 2006). The specimen is curated at the University of the Witwatersrand, Johannesburg. In the latest paleomagnetic study, the specimen has been dated back to 1.78 -1.49 Ma (Herries & Shaw, 2011). Although StW 53 was first identified as *H. habilis* when discovered (Hughes & Tobias, 1977), its taxonomical status remains under debate in the following decades. While Curnoe & Tobias (2006) reconfirmed StW 53 as a member of *H. habilis* with new morphological evidence, a few studies argued that StW 53 should align with *Australopithecus africanus* (Clarke, 2008; Ferguson, 1989; Williams et al., 2012). Moreover, Curnoe (2010) later reallocated StW 53 to a new species: *Homo gautengensis*.

A large area of the neurocranium of StW 53 is missing. Still, given its old date, its preservation condition is considered relatively complete and precious, and that is a reason why StW 53 has been taken as a rather critical fossil representing early hominins in South Africa (Curnoe & Tobias, 2006). In detail, the frontal bone retains the right supraorbital ridge and anterior half of the frontal squama. The diploe of the frontal bone is generally well-preserved. The right parietal and temporal bones are preserved, but the diploe of them is largely mineralised. Only two fragments of the parietal bone retain

their diploic structures. As for the occipital bone, the area below the lambdoid is preserved and its diploic layer is slightly damaged.

3.2.2 Middle Pleistocene hominins

Tighennif 4 (700 ka)

The Tighennif 4 specimen is also known as 'Ternifine 4', discovered from the Tighennif site in Algeria. The specimen is curated in Muséum national d'Histoire naturelle, France. Paleomagnetic and paleontological analyses gave the site an age of around 700 ka (Geraads et al., 1986). When first discovered, Tighennif human remains were assigned to a new taxon: *Atlanthropus mauritanicus*, but this taxon was rarely used (Schwartz et al., 2002c). Instead, some studies tend to use the name '*Homo mauritanicus*' (Hublin, 2001; Stringer, 2003), and some more prefer to allocate the fossil to *Homo erectus* (Geraads et al., 1986; Geraads, 2016; Rightmire, 1990; Schwartz et al., 2002c). Furthermore, Bermúdez De Castro et al.(2007) suggested that Tighennif human remains could belong to a subspecies of *Homo ergaster*.

Tighennif 4 specimen is a near-complete parietal bone. The sutures, ectocranial surface, and endocranial surface are rather well-preserved. The imprints of vessels and foramina are clear to inspect. A few breaks made by the taphonomic process interrupt the diploic layer, but the impact is very limited. Most diploic structures are almost intact.

Trinil 2 (early Middle Pleistocene)

Trinil 2 cranium is the holotype of *H. erectus*, discovered from the sediments of the Solo River at Trinil, Indonesia. Now the human remains from Trinil are curated in the Naturalis Biodiversity Center, Netherlands. The stratigraphic and chronological background of Trinil human remains is unclear. Although many studies have attempted to precisely date the fossils, all their results finally got involved in debates (Schwartz et al., 2002c), and some raised the possibility that the fossils may come from different stratigraphic layers (Bartsiokas & Day, 1993; L. Hilgen et al., 2023; Pop et al., 2023).

However, it is widely accepted to give Trinil 2 an early Middle Pleistocene age (Schwartz et al., 2002c).

Trinil 2 retains its upper half of the cranium, with the facial area and skull base missing. The ectocranial and endocranial surfaces are eroded modestly, with the majority of vascular imprints visible. The diploe has been filled in by sediments, which make most diploic structures of parietal and occipital bones blurry and unidentifiable.

Hexian (412±25 ka)

The fossil specimen widely known as 'Hexian' is labelled as PA830, which is a very well-preserved cranium discovered in Longtan Cave, Hexian County, China (Cui & Wu, 2015). Hexian specimen is now curated in the Institute of Vertebrate Paleontology and Paleoanthropology, Chinese Academy of Sciences. The chronological studies on this cranium have inconsistent conclusions, but the commonly accepted result from the newest ESR and U-series analyses shows that the Hexian specimen has an age of 412 ±25 ka (Liu et al., 2017, 2022; S. Xing et al., 2014). Based on the gross morphology of the cranium, Hexian is clearly classified as *Homo erectus* (Cui & Wu, 2015; Durband et al., 2005). Interestingly, some morphological traits of the Hexian labyrinth are close to those of *Homo neanderthalensis* (Wu et al., 2014).

The neurocranium of Hexian is almost complete, except that the skull base is missing and the pterional regions on both sides are slightly damaged. The diploe of the neurocranium is slightly mineralised, and most diploic structures remain identifiable. The ectocranial and endocranial surfaces are eroded during the taphonomy process, but the imprints of a few vessels (especially the meningeal vessels and dural sinuses) and foramina are left.

Kabwe 1 (299±25 ka)

Kabwe 1 is also known as 'Broken Hill 1'. The specimen was excavated from a mine

in Broken Hill (now Kabwe), Zambia (Woodward, 1921), and now is curated in the Natural History Museum in London. While earlier chronological studies based on fauna data suggested Kabwe 1 had an age of about 500 ka (Millard, 2008), a recent direct dating gave Kabwe 1 an age of 299±25 ka (Grün et al., 2020). Kabwe 1 was first assigned to *Homo rhodesiensis* when discovered (Woodward, 1921). However, the classification was done in the very early age of paleoanthropology, and it was not based on adequate comparative analyses (Trinkaus, 2009). Now Kabwe 1 is frequently assigned to *Homo heidelbergensis*, or at least considered as a potential *H. heidelbergensis* (Balzeau et al., 2017; Buck & Stringer, 2014; Godinho & O'Higgins, 2017, 2018).

Kabwe 1 is well-known as 'one of the best-preserved' hominin skulls (Grün et al., 2020). The cranium is almost complete, except for the lower and right parts of the skull. Also, the vascular grooves and foramina on the external and internal surfaces are visible. The diploe of the frontal and occipital bones is not damaged, but some areas of the diploe inside parietal bones show modest taphonomical alteration, which makes many diploic structures unidentifiable.

Florisbad (259±35 ka)

The specimen Florisbad is a partial cranium discovered at the Florisbad Spring, South Africa. The fossil is curated in the National Museum of South Africa. The latest chronological study on the fossil gave it an age of 259±35 ka (Grün et al., 1996). Still, the age has been questioned for the problematic stratigraphic background (Berger & Hawks, 2023). The taxonomy of the Florisbad specimen is so far unclear. While many assigned it to 'early *H. sapiens*' (Berger & Hawks, 2023; Hublin et al., 2017), some studies noted its morphological affinities with *H. heidelbergensis* and *H. neanderthalensis* (Bruner & Lombard, 2020). Especially, the cranial morphology shares definite similarities with Kabwe 1 (Rightmire, 1978), and the meningeal vascular system is more archaic than those in *H. neanderthalensis* and *H. sapiens* (Bruner &

Lombard, 2020).

The neurocranium of Florisbad retains its frontal and parietal bones. The left supraorbital ridge of the frontal bone is missing, and the frontal squama is slightly damaged by animals. The parietal bones are fragmental and only the upper half is preserved. Although the ectocranial and endocranial surfaces of the rest bones are generally well-preserved, the majority of the diploe is damaged. A study raised the possibility that Florisbad individual had suffered from haematological or metabolic disorders (Curnoe & Brink, 2010), and the diseases might have thickened and destructed the diploic layer. However, the study was not based on high-definition CT scanning (voxel size was 0.625 mm), and thus the diploic structures were not presented clearly. The latest high-definition Micro-CT scanning used in my study, as detailed in the Methods section, shows that most damage in the diploe is taphonomical (fossilization breaks, erosion, and sediments).

LES 1 (241-335 ka)

The cranial specimen LES 1 is from the Lesedi Chamber of Rising Star Cave, South Africa. Now the specimen is housed at the University of the Witwatersrand, Johannesburg. Chronological studies have confirmed the Middle Pleistocene age of the hominin remains from Rising Star Cave (Dirks et al., 2017; Hawks et al., 2017), and the recent U-Th test of the flowstone from the cave further constrained the age range to 241-335 ka (Robbins et al., 2021). LES 1 is assigned to *Homo naledi*, and it is possibly a male individual (de Ruiter et al., 2019).

The specimen LES 1 is a partial skull. The frontal, left parietal, and left temporal bones are relatively well-preserved, with some small areas missing. The left sphenoid, right parietal, and occipital bones are damaged largely, and the skull base is all missing. The ectocranial and endocranial surfaces have been eroded but many foramina and vascular imprints remain visible. The diploe of these rest bones is relatively well-preserved, with

slight taphonomic destructions.

Maba 1 (230±5 ka)

The Maba 1 specimen is a partial cranium excavated at the Maba site, China. The age of the specimen is uncertain. The first chronological study with the Uranium series test gave it an age of 129-135 ka (Yuan et al., 1986), while the faunal assemblage indicated the possibility of the late Middle Pleistocene (Wu et al., 2011). The latest dating shows that the Maba site should be at least 230±5 ka and may be older than 278 ± 4ka (Shen et al., 2014). In any case, it is widely accepted that Maba 1 has an age of around 300-130 ka (Liu et al., 2022; Wu & Bruner, 2016). The evolutionary status of Maba 1 is even more controversial. Woo & Pen (1959), as well as X. Wu (1988), have revealed the affinities of Maba 1 to Asian *H. erectus* and *H. neanderthalensis* in terms of gross morphology. The study on endocast also pointed out the similarities between Maba 1 and *H. heidelbergensis*, *H. neanderthalensis*, and *H. sapiens* (Wu & Bruner, 2016).

The specimen Maba 1 retains its upper half of the neurocranium. The left orbit of the frontal bone is missing and so is the majority of the squamous part. The missing part has been reconstructed artificially. The left pterional region is missing while the right is partially preserved. The parietal bones retain their upper halves and the occipital bone is missing. The diploe of these rest bones is slightly damaged by taphonomical breaks and sediments, but most diploic cavities are clear to see with Micro-CT scanning.

3.2.3 Late Pleistocene hominins

La Quina H5 (55-63 ka)

La Quina H5 cranium was discovered in La Quina Cave, France. The layer where La Quina H5 came from corresponds to the Mousterian layers dated back to 55-63 ka (Frouin et al., 2017). La Quina H5 possibly belong to an adult female (L'Engle Williams et al., 2022), and is recognized as a 'classic' *H. neanderthalensis* (Schwartz et al., 2002b).

The neurocranium of La Quina H5 is nearly complete, with the skull base damaged taphonomically. The ectocranial surface, endocranial surface and diploe are interrupted by clean taphonomic breaks, but the structures of vessels and foramina are generally well-preserved.

La Chapelle-aux-Saints 1 (47±3 ka or 56±4 ka)

La Chapelle-aux-Saints 1 cranium was excavated from the Bouffia Bonneval Cave at the La Chapelle-aux-Saints village, France. La Chapelle-aux-Saints 1 belongs to a male individual, and it is considered a 'classic' *H. neanderthalensis* in Western Europe (Schwartz et al., 2002b). Now the cranium is curated in Muséum national d'Histoire naturelle. An ESR analysis gave it an age of 56±4 ka or 47±3 ka (Grün & Stringer, 1991).

The neurocranium of La Chapelle-aux-Saints 1 is near complete, with a large portion of the left parietal bone missing. Besides, all other cranial bones have small sections missing and are restored by artificial materials. The ectocranial and endocranial surfaces are slightly eroded, with most foramina and vascular grooves preserved. The diploe is slightly interrupted by taphonomical breaks, but most diploic structures are almost intact.

La Ferrassie 1 (32-52 ka)

La Ferrassie 1 cranium was discovered from the La Ferrassie rock shelter, France. Now the cranium is curated in Muséum national d'Histoire naturelle. La Ferrasie 1 is taken as an example of 'classic' *H. neanderthalensis* in Western Europe (Schwartz et al., 2002b). A recent chronological study showed that La Ferrassie 1 individual had an age of 44.9-44.1 ka (Guérin et al., 2023).

The restored cranium of La Ferrassie 1 is nearly complete, but most areas of the

neurocranium were actually in fragments when discovered. The gaps between the fragments are filled in by artificial materials. These taphonomic breaks interrupted the vascular imprints on the bone surface and diploe. Main branches of the endocranial vessels and diploic venous system remain visible, especially in the right side.

Spy 1 (40.6-44.2ka)

The cranium of Spy 1 was excavated from the Spy Cave, Belgium. Now it is curated in the Royal Belgian Institute of Natural Sciences. The human remains from Spy Cave may represent the last *H. neanderthalensis* population surviving in Northwest Europe, even though its chronological background is controversial (Devièse et al., 2021). While some earlier tests gave Spy Neanderthals an age of around 23.88 ka, a recent study with a more efficient method of removing contamination dated the Spy population back to 44.2-40.6 ka (Devièse et al., 2021; Semal et al., 2009).

Spy 1 cranium retains its frontal, zygomatic, parietal, temporal, and occipital bones. A large proportion of the lateral sides of the cranium is missing and replaced by artificial materials. The ectocranial and endocranial surfaces of the preserved bones are slightly eroded, with most vascular imprints and foramina visible. The diploe of the bones is interrupted by clean fossilization breaks, but most remaining diploic structures are clear and identifiable.

SPY 10 (40.6-44.2 ka)

Spy 10 cranium is sometimes labelled as ‘Spy 2’ in some studies. The chronological background of Spy 10 is the same as that of Spy 1, and they both are curated by the Royal Belgian Institute of Natural Sciences.

The preservation condition of Spy 10 is comparable to that of Spy 1. Spy 10 cranium retains its frontal, parietal, temporal, and occipital bones. The middle part of the frontal bone, the pterional regions of both sides, as well as the lower half of the occipital bone,

are largely damaged taphonomically and replaced by artificial materials. The ectocranial and endocranial surfaces and diploic structures are well-preserved, despite the fossilization breaks.

Cro-Magnon 1 (<28 ka)

Cro-Magnon 1 cranium is from the Cro-Magnon rock shelter in France, and now it is curated in Muséum national d'Histoire naturelle, France. Cro-Magnon human remains are one of the first fossils recognized as *Homo sapiens* (Balzeau et al., 2013), and Cro-Magnon 1 individual is further recognized as an adult male (Schwartz et al., 2002b). While an earlier study dated Cro-Magnon human remains back to around 30 ka (Movius, 1969), a recent test suggested that its age was younger than expected and should not be older than 28 ka (Henry-Gambier, 2002).

Cro-Magnon 1 cranium is almost complete. Most anatomical features on the surfaces and in the diploe are rather well-preserved. Although a large circular area with damage is present in the frontal bone, this area is possibly caused by pathological conditions instead of taphonomical erosion.

Cro-Magnon 2 (<28 ka)

Cro-Magnon 2 is an adult female cranium curated in Muséum national d'Histoire naturelle. The chronological background of Cro-Magnon 2 is the same as that of Cro-Magnon 1, but the former is not preserved as perfectly as the latter. Cro-Magnon 2 cranium retains much of its face and the neurocranium. The right part of the frontal squama is damaged. Much of the sphenoid, right parietal, and occipital bones are missing. The surface and diploe of the preserved bones are damaged slightly, with most diploic structures, foramina, and vascular imprints clear to inspect.

Cro-Magnon 3 (<28 ka)

Cro-Magnon 3 is an adult male cranium curated in Muséum national d'Histoire naturelle.

Its chronological background is the same as that of Cro-Magnon 1 and Cro-Magnon 2. Cro-Magnon 3 cranium retains its upper half, with the face and skull base largely missing. The ectocranial surface and diploe of the cranium are generally well preserved, while the endocranial surface is damaged taphonomically and covered by artificial materials.

Abri Pataud 1 (around 22 ka)

Abri Pataud 1 was discovered from the level 2 of the Abri Pataud site, France (Schwartz et al., 2002b). The level 2 of the site belongs to the Final Gravettian culture and is recently dated back to around 22ka (Douka et al., 2020). Abri Pataud 1 is curated in Muséum national d'Histoire naturelle. The fossil is assigned to *Homo sapiens* and described as a young adult female (Schwartz et al., 2002b).

The Abri Pataud 1 cranium is near-complete, especially the ectocranial surface of the cranium is almost intact. The paracoronal and pterional regions of the endocranial surface are slightly damaged. This has a limited impact on the inspection of the diploic and meningeal vessels in such areas, but the majority of vascular networks of the cranium are well-preserved.

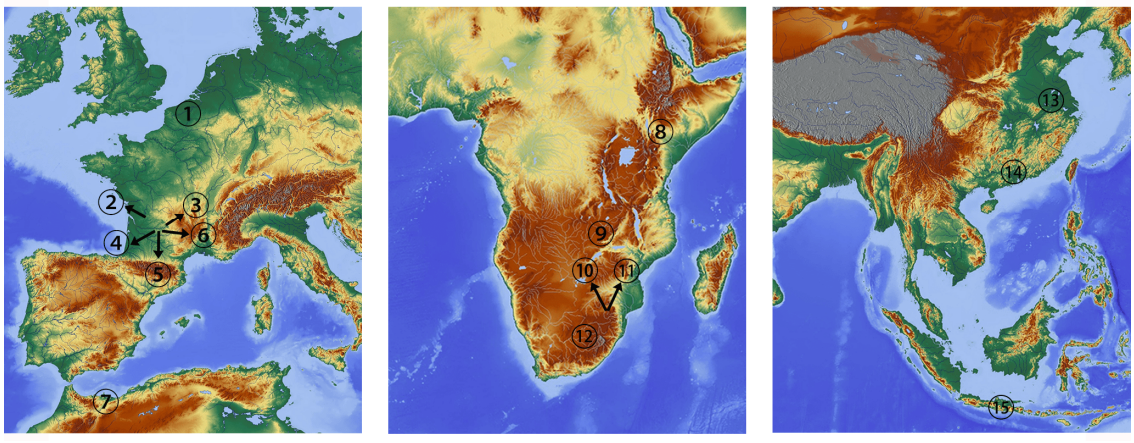

Figure 3.1 The localities of fossils included in this study. 1 to 7 in Europe and Northern Africa: Spy, La Quina, La Chapelle-aux-saints, La Ferrassie, Abri Pataud, Cro-Magnon, Tighennif; 8 to 12 in Eastern and Southern Africa: Koobi Fora, Kabwe, Rising Star cave, Sterkfontein, Florisbad; 13 to 15 in Asia: Hexian, Maba, Trinil.

4. Methods

4.1 Imaging data and 3D reconstruction

4.1.1 Micro-CT scanning and data preprocessing

In dry skulls and fossils, the diploic vessels as soft tissues were not preserved. Thus, their bony shells—diploic channels (DCs)—are used as a proxy. DCs were hidden behind the cortical bones and were usually narrow in width. Considering this, the analyses in this study were based on high-resolution Micro-CT data. The Micro-CT scanning of extant dry skulls was conducted in Muséum national d'Histoire naturelle, with the platform GE phoenix v|tome|x L240. The Micro-CT data of hominin fossils were provided by their host institutions with various scanning platforms, including GE phoenix v|tome|x L240, GE v|tome|x m300&180, RX Solutions EasyTom 150, METRIS X-TEK HMX ST 225, and CT450-TY-ICT.

The scanning resolution varied among the specimens, but the voxel size was always isometric and set below 0.16 m in each specimen, with most being smaller than 0.11 mm (see Table 3.1 in the Materials section). A smaller voxel size brings to the tomographic images a higher resolution and more details. Compared with the clinical CT data used in previous studies, the resolutions of the tomographic images used in this study were much improved, making it possible to observe microscopic structures in the cranium (Figure 4.1). Given the diameters of DCs were reported to be usually over 0.5 mm (Hershkovitz et al., 1999; Rangel de Lázaro et al., 2016, 2020), the small voxel sizes in this study were viable to detect the detailed morphology of DCs. Absolutely, they were also effective for observing some larger structures such as the arachnoid granulations, brain gyri, and meningeal vascular imprints. Furthermore, the application of Micro-CT data is especially important for fossil specimens, as the high resolution makes it much easier to distinguish biological structures from sediments and taphonomic structures (Figure 4.1).

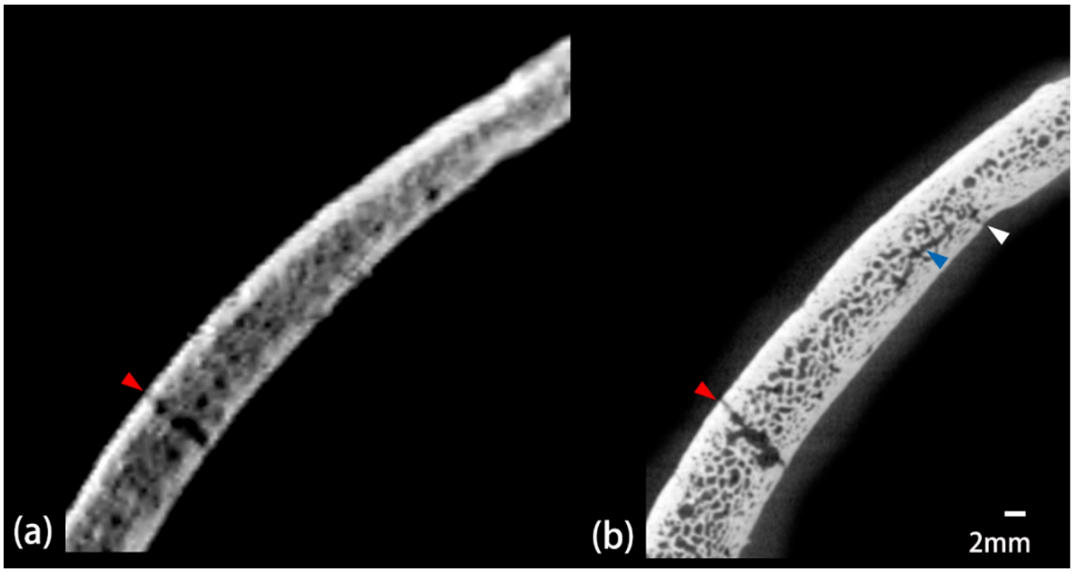

Figure 4.1 The clinical CT image (a) and Micro-CT image (b) of the same area of La Chapelle-aux-Saints 1 specimen. The voxel size of the former stands at 0.4 mm, while that of the latter stands at 0.123 mm. The taphonomic break (marked in red) is easier to identify via a Micro-CT image. The DC (blue) and draining orifices (white) are only identifiable via Micro-CT. The figure is from Hui & Balzeau (2023b).

The Micro-CT data first need to be pre-processed before visual inspections and 3D modelling. The protocol has been published in my paper (Hui & Balzeau, 2023b). In detail, the Micro-CT data were first loaded into ImageJ v1.53t (Schneider et al., 2012) as image sequences. The software could automatically adjust the window and level values of images, clarifying the boundary and contrast between the bone tissues and background (as well as air-filled diploic cavities, see Figure 4.2). Following this, these 16-bit images were then changed into 8-bit. This step decreased the data sizes by half to enhance the computer processing speed in the following analyses but did not change their voxel sizes.

4.1.2 Acquisition of 3D models and CVT colormaps

The 2D tomographic images processed by ImageJ could be directly used in visual inspections, but merely inspecting 2D images could only provide partial information about the anatomy of DCs. In order to observe the DCs from more perspectives, it was necessary to construct the 3D models of the cranium and DCs. To understand the

interaction between DC, bone, and brain, it was additionally necessary to construct the 3D models of endocasts, along with the colormaps of cranial vault thickness (CVT).

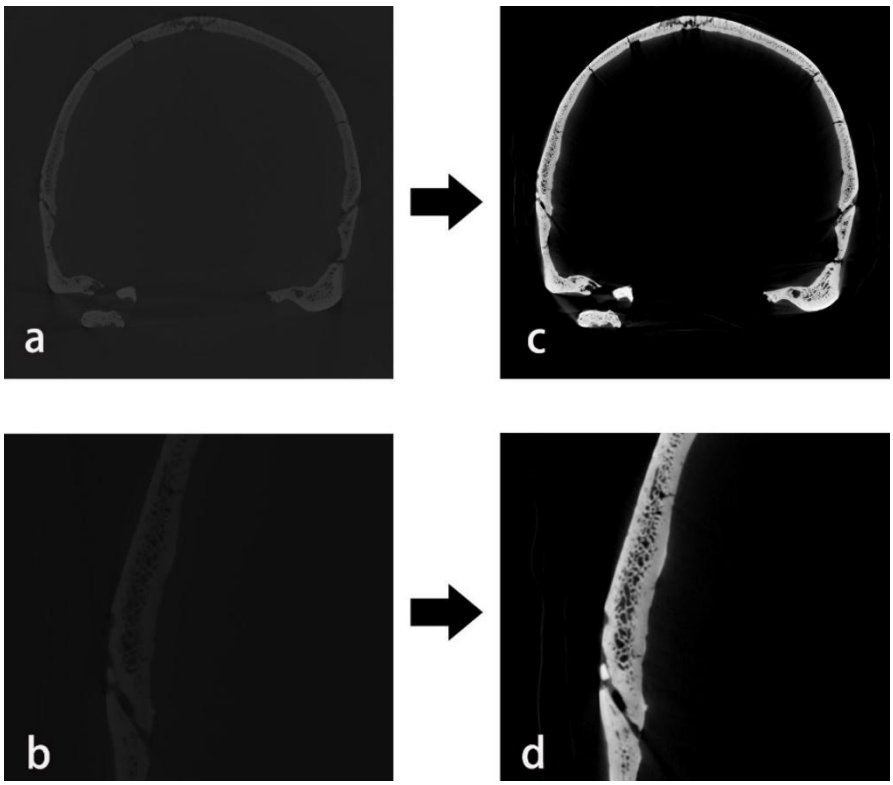

Figure 4.2 Processing Micro-CT image stacks in ImageJ. The original images have a low contrast between the object and the background (a), and the diploe is difficult to observe even in the close-up (b). After the process, we can see a strong contrast (c) with the boundary of the diploic structures clearly defined (d).

To construct the 3D cranial models (Figure 4.3), the Micro-CT images processed by ImageJ were loaded into 3D Slicer v4.13 (Fedorov et al., 2012). Following the protocol described in my published paper (Hui & Balzeau, 2023b), the cranial bone tissues were segmented with the 'Threshold' function. In detail, the highest value (i.e., grey value) of the threshold range was set as 255, while the lowest value depends on the intensity of bone tissues—this aimed to let the threshold range cover the most bone tissue and the least diploic cavities. The voxels of bone tissues were thus segmented from the CT image stacks, and 3D Slicer could automatically display the 3D models. The 3D cranial model generated in this manner replicated not just the surface of the original cranium

but also its diploe.

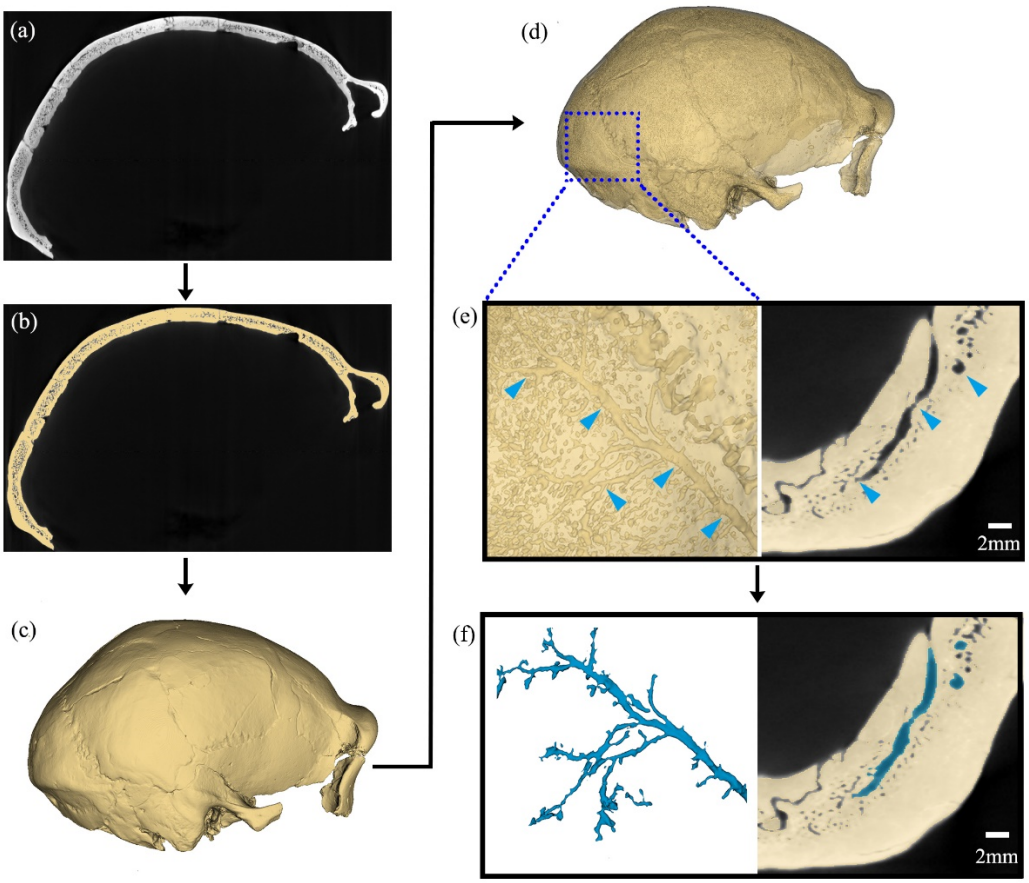

Figure 4.3 The segmentation of cranial bone and DC. The 2D image stacks (a) were loaded in 3D Slicer, where the 'Threshold' function segments the bones and excludes diploic cavities (b). The segmented voxels are automatically displayed as a 3D model (c), which can be rendered transparent (d). DCs could be located in the transparent model and 2D images (e). Finally, the 3D model of DC branches was constructed with the 'FloodFilling' and 'Paint' functions. The figure is from Hui & Balzeau (2023b).

The identification of DCs also followed the published protocol (Hui & Balzeau, 2023b). By setting the opacity level to 50%, the cranial model would be displayed transparently and thus the embedded diploic structures were rendered visible (Figure 4.3). Among numerous diploic cavities, some were in the shape of blood vessels and anastomosed with other vessels or sinuses. These diploic cavities were identified as DCs. The position where a DC attaches to a non-vascular-like structure was identified as the terminal point of this DC branch. Some DC branches, especially those in fossil specimens, have similar grey levels with bone tissues in CT images. This is due to their

extremely narrow diameters, short lengths, or taphonomic alterations. These DCs can hardly be excluded when using the 'Threshold' function, which makes their voxels segmented together with bone tissues. As a result, these DCs were not displayed as empty cavities and thus not visible in transparent 3D cranial models. To find these DCs, this study applied the commonly used manner of radiological interpretation in clinical medicine. This means inspecting 2D tomographic images slice by slice in 3D Slicer, from the coronal, sagittal and axial views. To ensure all identifiable DCs in a cranium were found, over 1800 tomographic images of each cranium need to be inspected carefully. Moreover, this inspection process was repeated three times to avoid omissions.

The method of modelling DCs has also been described in my published paper (Hui & Balzeau, 2023b). In detail, after locating a DC branch, the 'FloodFilling' function was then used to segment its voxels. After choosing a random voxel of the DC as the starting point, 'FloodFilling' would calculate the grey values of voxels surrounding the starting points. All the connected voxels sharing similar values with the point would then be segmented automatically. Because the DCs were air-filled, their voxels usually share similarly low grey values, which were in marked contrast with intense bone tissues. This way, 'FloodFilling' could segment DCs and exclude bone tissues (Figure 4.3). Noise might be generated through this process, and it could be cleaned manually or semi-automatically with the 'island' function. These automatic functions accelerated the speed of segmentation, but they could not be applied to all DCs. The voxels of some DC branches were variable or similar to surrounding bone tissues. These DCs had to be segmented manually with the 'Paint' function, which made the segmentation of DCs a time-consuming process. Finally, the models of DC networks were displayed automatically in 3D Slicer.

The endocast models of extant apes and humans were generated through the 'WrapSolidify' function in 3D Slicer. The function could automatically detect the

largest cavity inside a cranial model—for hominids, the largest is absolutely the endocast—and automatically finish the segmentation. As for fossil specimens, many of these crania were incomplete, which prevented the 'WrapSolidify' function from identifying the endocast cavity. For this reason, the endocast models of hominin fossils were segmented manually. In detail, the cranial model in 3D Slicer would be converted into STL format and then loaded into Agisoft Metashape v1.8.3 (Agisoft LLC., https://www.agisoft.com/), where the ectocranial surface and diploic structures were all erased manually. The endocranial surface left became the model of the endocast. These two methods of endocast modelling were both based on high-resolution Micro-CT data and they both precisely segmented the endocranial surfaces. This ensured that the models produced by the two methods were equally precise. The only noticeable difference between them was the processing speed, as the automatic method could facilitate the segmentation process.

The CVT colormaps were generated by following the widely applied protocol in previous studies (Balzeau et al., 2017; Balzeau & Charlier, 2016; Beaudet et al., 2022; Hui & Balzeau, 2023a). The 3D models of crania and endocasts were loaded in Avizo v9.0. The 'SurfaceDistance' function in Avizo could automatically calculate the distance between the ectocranial surface and endocast. For neurocranium, the surface distance is equal to bone thickness. Finally, the surface distance values of every local area were translated into colors according to the color scale. The range of the color scale could be adjusted according to research needs (detailed below in 4.2.6). The colormaps were displayed on the ectocranial surface.

4.2 Qualitative and quantitative analyses

4.2.1 Vascular drainage pattern

The drainage pattern means the pathway of a vessel and its connections with other vessels. In other words, to document the DC drainage pattern, it is critical to investigate

how DCs course inside the cranium, as well as how the DCs anastomose with which vessels or sinuses.

In this study, the investigation of the drainage pattern relied on visually inspecting crania through transparent 3D models and 2D tomographic images. The protocols for inspecting cranial models and tomographic images have been detailed above, with which the DCs were identified and located. By tracing the coursing of DCs, this study detected not only their pathways but also their inlets and outlets. Usually, the inlets/outlets were foramina connected with vascular imprints and paranasal sinuses. By locating these foramina and identifying the connected imprints and sinuses, we would know which vessels or sinuses were anastomosed with DCs.

4.2.2 Intensity level

The effectiveness of a vascular system is closely related to its morphology, especially the size and branching pattern. A highly developed vascular network should have large diameters, long lengths and many ramifications, facilitating the transport of a large volume of drainage across various regions and offering alternative pathways for circulation (Coyle & Heistad, 1991; Hui & Balzeau, 2023b; Jain, 1988; Schmidt & Thews, 1989). In this study, to evaluate how developed were the DC networks in great apes, hominin fossils, and extant humans, an intensity scale modified from the one used in a previous study (Hershkovitz et al., 1999) was established (Figure 4.4). A diploic venous system with a high intensity level should have large and complex DCs. The details are listed below:

Level 1: The diploic venous network is the least developed. The DC branches are sparse and scattered in the cranium, with scarce ramifications, very narrow diameters (usually smaller than 1.0 mm), and short lengths (usually shorter than 3.0 cm).

Level 2: The diploic venous network is moderately developed. Rich DCs can be found

in at most one cranial bone, while those in other bones are sparse. The diameters of most DC main branches range from 1.0 to 1.5 mm, and the lengths are mostly shorter than 5.0 cm. They give off several secondary branches but most secondary branches do not anastomose with each other.

Level 3: The diploic venous network is highly developed. The DCs are widely spread over the entire neurocranium (excluding the temporal squama). The main branches are mostly wider than 1.5 mm and longer than 5.0 cm, with several extremely long DC branches (>10.0 cm) running across a whole cranial bone. The main branches also give off many complex secondary branches that frequently anastomose with each other.

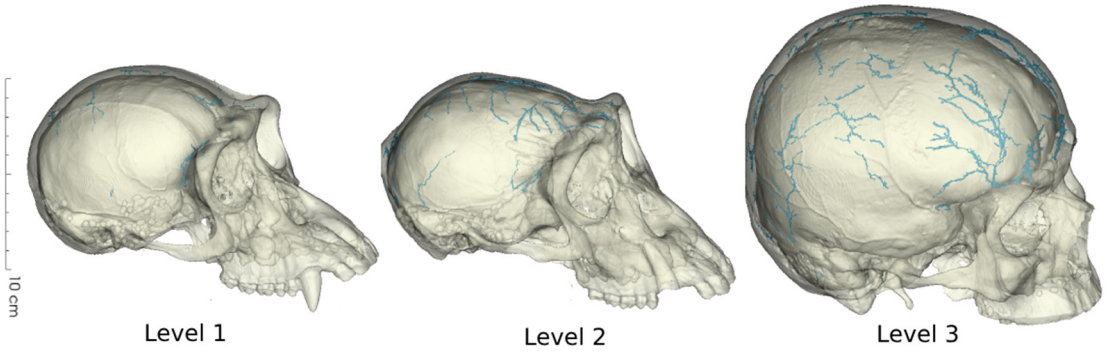

Figure 4.4 Examples of the intensity levels

The scale was applied to all specimens in this study. For fossil specimens, many DC branches were filled in by sediments or damaged taphonomically. Many DCs were thus not clear enough to identify in the transparent models of fossil crania. For this reason, simply inspecting their transparent cranial model would not be reliable. Before evaluating fossil specimens, it was necessary to find and model all the DCs.

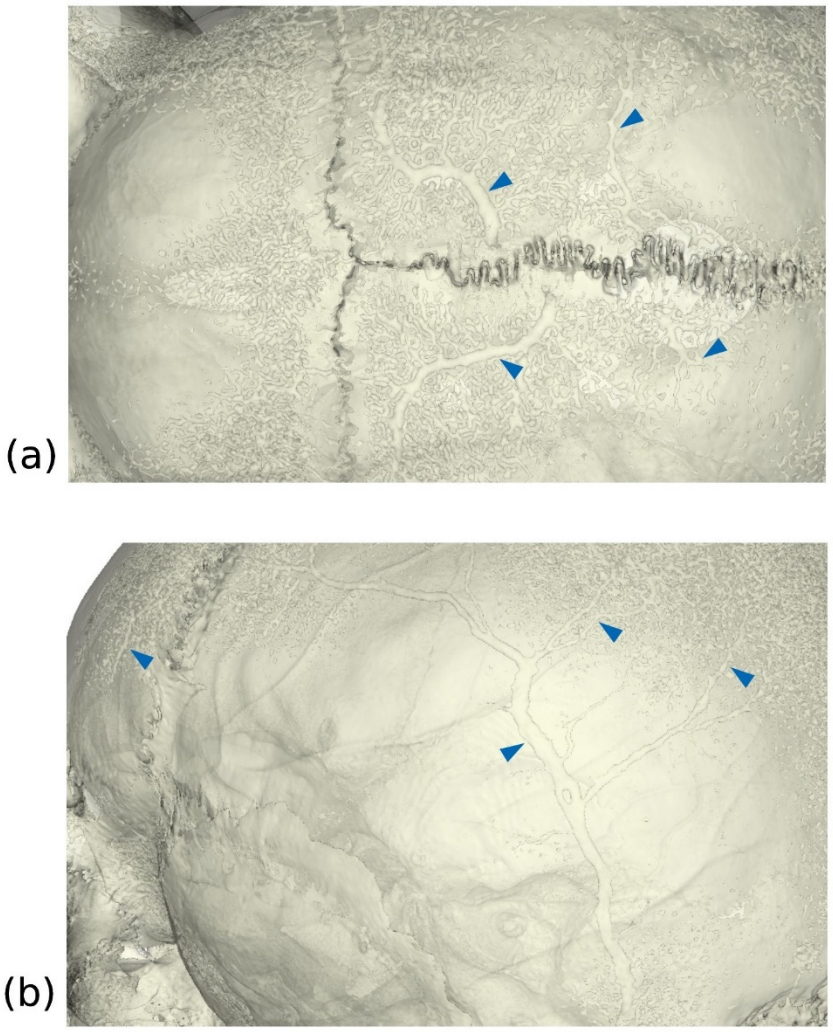

Figure 4.5 In transparent models of extant dry skulls of chimpanzees (a) and humans, the DCs (marked in blue) are clear and identifiable.

In comparison, the preservation statuses of dry skulls of extant great apes and humans were much better. The diploic structures were not altered nor damaged by the taphonomic process, and thus the majority of their DC network was clear and visible in the transparent cranial models (Figure 4.5). Although a few extremely narrow and short DCs were not displayed in 3D models, and some small sections of diploe were too complex to identify the embedded DCs, these minor branches and areas were not significant enough to change the grading results. For these reasons, the evaluation of extant specimens was conducted via visually inspecting transparent cranial models, without the necessity of constructing the 3D models of DCs. This was important

because constructing DC models was an extremely time-consuming process, even though a semi-automatic workflow has been used in this study. Under the current technical conditions in the fields of paleoanthropology and virtual anthropology, it was not possible to fully automate the workflow to significantly increase processing speed. It was thus infeasible to model numerous DCs of every individual in a large sample of extant great apes and humans. Furthermore, the transparent cranial models of extant humans and apes precisely displayed the contour of DCs, without distorting their sizes. In the following analyses (as detailed below), this study created DC models for 10 extant human and chimpanzee crania. In each cranium, most DC models could fit closely in the empty DC cavities of transparent cranial models, and there was no noticeable difference in size between the two. In general, using transparent cranial models did not change the grading results but it could accelerate the process speed.

4.2.3 Fractal analysis

Apart from the intensity level scale based on qualitative inspections, there were so far no other methods used in previous studies quantifying the degree of complexity of the diploic venous system. As mentioned in the Introduction, fractal analysis was a candidate with potential application values. Here, this current study tested whether a fractal analysis could be applied for DCs, especially for those in fossils. Five *H. neanderthalensis* and four fossil *H. sapiens* with relatively complete diploic venous networks were selected for the test.

The protocol of fractal analysis has been published in my paper (Hui & Balzeau, 2023b) and is retold below: The first step of fractal analysis was converting the 3D models of the diploic venous network into 2D patterns (Figure 4.6). This was because main DC branches were limited by bone thickness, only extending along the thin diploë, which resembles a curved 2D surface. Using the "Screenshot" function in 3D Slicer, this study captured close-up and orthographic views of each part of the DC model, with photographing areas smaller than 2 cm^2 each time. The screenshots must overlap, so

that AutoStitch (Brown & Lowe, 2007) and Adobe Photoshop v2017 (Adobe Inc., San Jose, CA) automatically recognized the corresponding features in the overlapping areas to align and merge these pictures, creating a complete 2D pattern of the entire DC network. In ImageJ v1.53t (Schneider et al., 2012), the pattern was then converted into a binary image. In some spherical areas, such as the parietal eminence, the conversion enlarged the distance between branches, but the branches were not deformed and the degree of complexity was unaffected. Finally, the fractal dimensions of the binary 2D pattern were calculated using the box-counting method with the plugin BoneJ v2 (Domander et al., 2021) in ImageJ. For lineal 2D patterns, their fractal dimensions vary from 1.0 to 2.0.

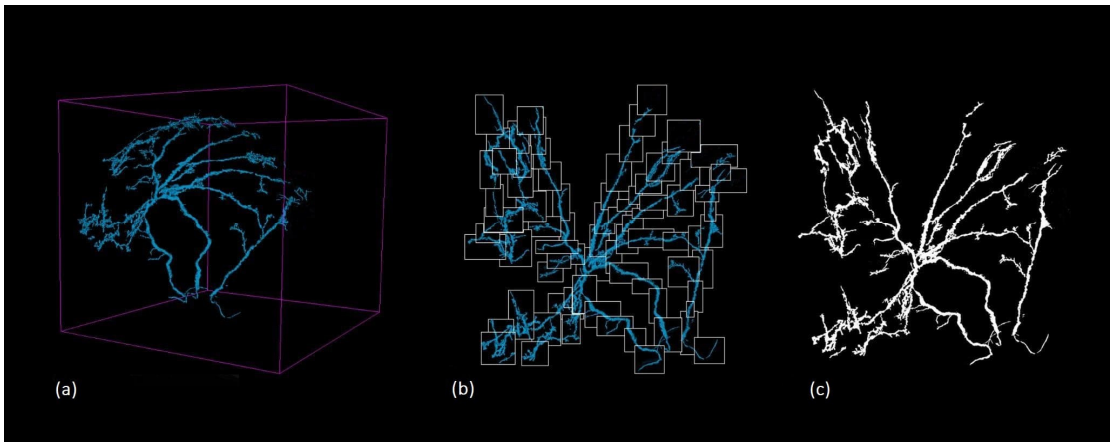

Figure 4.6 The conversion from a 3D model of DCs to a binary pattern. The figure is from my published paper (Hui & Balzeau, 2023b).

Also, as stated in my published paper (Hui & Balzeau, 2023b): Fractal analyses were merely conducted on complete DC branches, excluding incomplete branches affected by taphonomic processes. According to fractal geometry principles, the fractal dimension of a complete branch within a self-similar structure is equivalent to that of the entire shape (Di Ieva, 2016; Mandelbrot, 1982). Human vascular networks were considered self-similar (Bruner et al., 2006; Masters, 2004), suggesting that even seriously damaged bones could be included in the fractal analysis if at least one intact DC branch remained. Still, as biological structures, DC networks did not have perfect

self-similarity. Thus, while the fractal dimension of selected DC branches should approximate that of the overall network, they might not be identical.

4.2.4 Relative volume index

Because comparing the absolute volume of DVs among incomplete fossils may lead to biased results, this current study instead tested the application of the relative volume analysis. Thus, this study induced the DC volume index and tested it in a selection of five chimpanzees, five extant humans, five *H. neanderthalensis*, four fossil *H. sapiens*, StW 53 specimen, and one *H. naledi* specimen (LES 1). As stated in my published paper (Hui & Balzeau, 2023b), the formula was: DC volume index = (DC volume/Bone tissue volume) *100. The protocol has also been published in my paper (Hui & Balzeau, 2023b), and is retold below: First, the “Scissors” function in 3D Slicer was used to remove from the 3D models the areas affected by taphonomic damages that might distort the volume index. Following this, the volumes of the remaining segments of DCs and bone tissues were quantified using the "Segment Statistics" function in 3D Slicer. Furthermore, considering that the index of a largely damaged bone might not accurately reflect that of the original bone, this study excluded any bone from the volume analysis if visual inspection revealed damage to approximately one-third of the bone.

4.2.5 Distribution pattern in parietal bones

The morphology of DCs in the parietal bones shows high diversity, resulting in the formation of distinctive patterns. Based on a large sample of extant humans, Hershkovitz et al. (1999) have identified six types of distribution patterns: spider, serpentine, coronal, thousand lakes, and hybrid (Figure 4.7). Besides, Hershkovitz et al.(1999) noted that there were some individuals with scarce DCs that could not form a featured pattern.

This widely applied classification was used in this current study, in order to test whether these patterns appear in great apes, fossil hominins, and the current sample of extant humans. For the reasons mentioned above, the inspection of distribution patterns in extant apes and humans was based on 3D cranial models, as the patterns were clearly manifested in transparent cranial models. For fossils, their DCs displayed in transparent cranial models were sometimes unclear, and thus the inspection was based on 3D models of DCs.

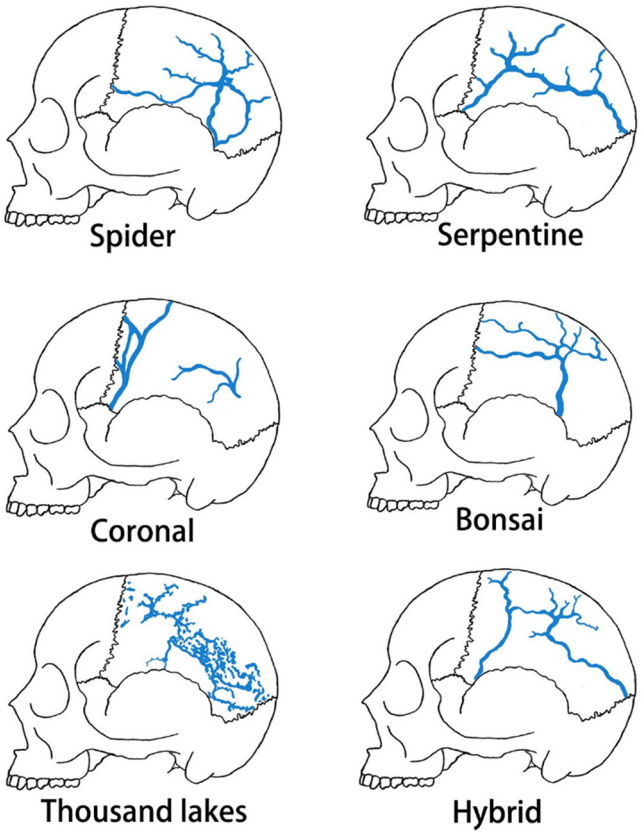

Figure 4.7 The distribution patterns of parietal DCs classified by Hershkovitz et al. (1999). The figure is redrawn from Hershkovitz et al. (1999) and has been published by Hui & Balzeau (2023b).

4.2.6 Spatial relationship between DC, CVT, and brain

To investigate whether bone thickness was influenced by brain morphology and whether bone thickness affected the distribution and morphology of DCs, the precondition was creating CVT colormaps in Avizo following the protocol detailed above. The color shifted from light blue to dark blue and then to red as the thickness

value increased (Figure 4.8). Besides, areas thinner than the lower limit of color scale analysing range were uniformly colored in white, while areas thicker than the upper limits were uniformly yellow. By observing the distribution of colors on the ectocranial surface, it was feasible to know the overall thickness and find the areas of thickening or thinning. Additionally, as the color would shift immediately from red to yellow when local thickness reached the upper limit of the scale range, by adjusting the upper limit value multiple times and observing at which value a particular area would shift from red to yellow, we could know the thickness value of that area.

When making comparisons between individuals, a standard color scale range was applied to all crania. Here, the standard scale was set to range from 2 mm to 22 mm (Figure 4.8). This ensured that most extremely thin and thick areas of neurocranium were included in the analysis range, and meanwhile kept the details of thickness variation distinguishable. The majority of the face was thus out of the analysis range and uniformly colored in yellow. Additionally, this color scale has been used in many previous studies, with the same color sequence and analysis range (Balzeau, 2013; Balzeau et al., 2017; Balzeau & Charlier, 2016; Boman et al., 2016), which benefited the comparison between their results and those in this current study.

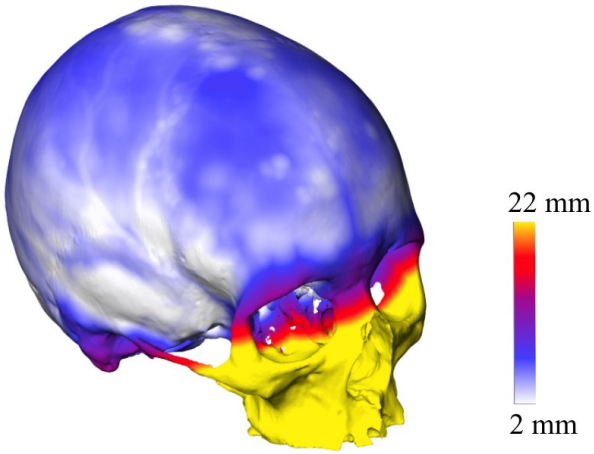

Figure 4.8 The standard color scale used for interindividual comparisons, ranging from 2 mm to 22 mm. The thickness variation was distinguishable in the neurocranium. The lower face, which was not the subject of this study, was excluded from the analysis range and uniformly colored in yellow.

The CVT colormaps were then compared with endocast models (Figure 4.9). This was to investigate whether the thickness variation corresponded to the compression from brain gyri or arachnoid granulations. Also, to investigate whether the distribution and extension of DCs are affected by local thickness variation, the CVT colormaps were compared with DC models. Here, transparent cranial models were not used, as it was necessary to observe whether certain small DCs appear in some particular areas, while these DCs might not be clearly visible in transparent cranial models. Also, constrained by the time-consuming process of DC segmentation, as discussed above, it was infeasible to create DC models of all extant humans and apes. Thus, 10 best preserved dry skulls of this extant sample (5 chimpanzees and 5 extant humans) were selected for the DC segmentation and comparison between DCs and CVT. Similarly, although DC segmentation was conducted for all fossil specimens, only those with well-preserved diploe were selected for the comparison between DCs and CVT. This was to prevent taphonomic damage from distorting the results. In-depth case studies of these selected specimens provided a chance to thoroughly describe the variation in each specimen, which led to the exploration of new phenomena and the clues of the mechanism behind DC variation.

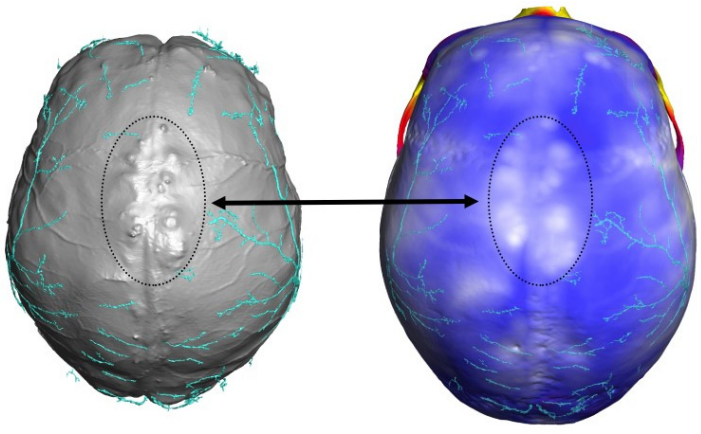

Figure 4.9 An example of the comparison between endocast, DCs, and CVT colormap. The bone thickness variation could correspond to the lack of DC as well as the compression from gyri and arachnoid granulations.

5. Results—The drainage pathway of the diploic venous system

5.1 The drainage pathway of the diploic vessels in chimpanzees

Overview

The distribution and drainage pathway of the DCs and other connected vessels on the left and right sides show asymmetry (Figure 5.1). Therefore, the cranium (tomographic images and 3D models) of each individual was divided into two hemicrania and they were observed and analyzed separately. A total of 36 hemicrania from 18 chimpanzee individuals were included. The specimens were well-preserved. The DCs and the imprints of the meningeal vessels, dural sinuses, and some extracranial vessels were clearly visible, and so were the emissary foramina.

While the emissary channels were widespread over the entire cranium, the DCs in chimpanzees were mainly found in the frontal, sphenoid, parietal, and occipital bones. It was noteworthy that the distribution of DCs is constrained in only a small area of each bone (Figure 5.1). Only in two hemicrania (from the same individual) the DCs in the nasal bones were found. Among these bones, the DC network in the frontal bone was more developed than the others, as it usually possessed the longest and widest DC branches.

Frontal bone

The distribution and morphology of the DCs in the frontal bone exhibited high variability. However, in all specimens, the frontal DCs consistently appeared in the supraorbital torus, the frontal crest, and the boundary between the orbital plate and the frontal squama.

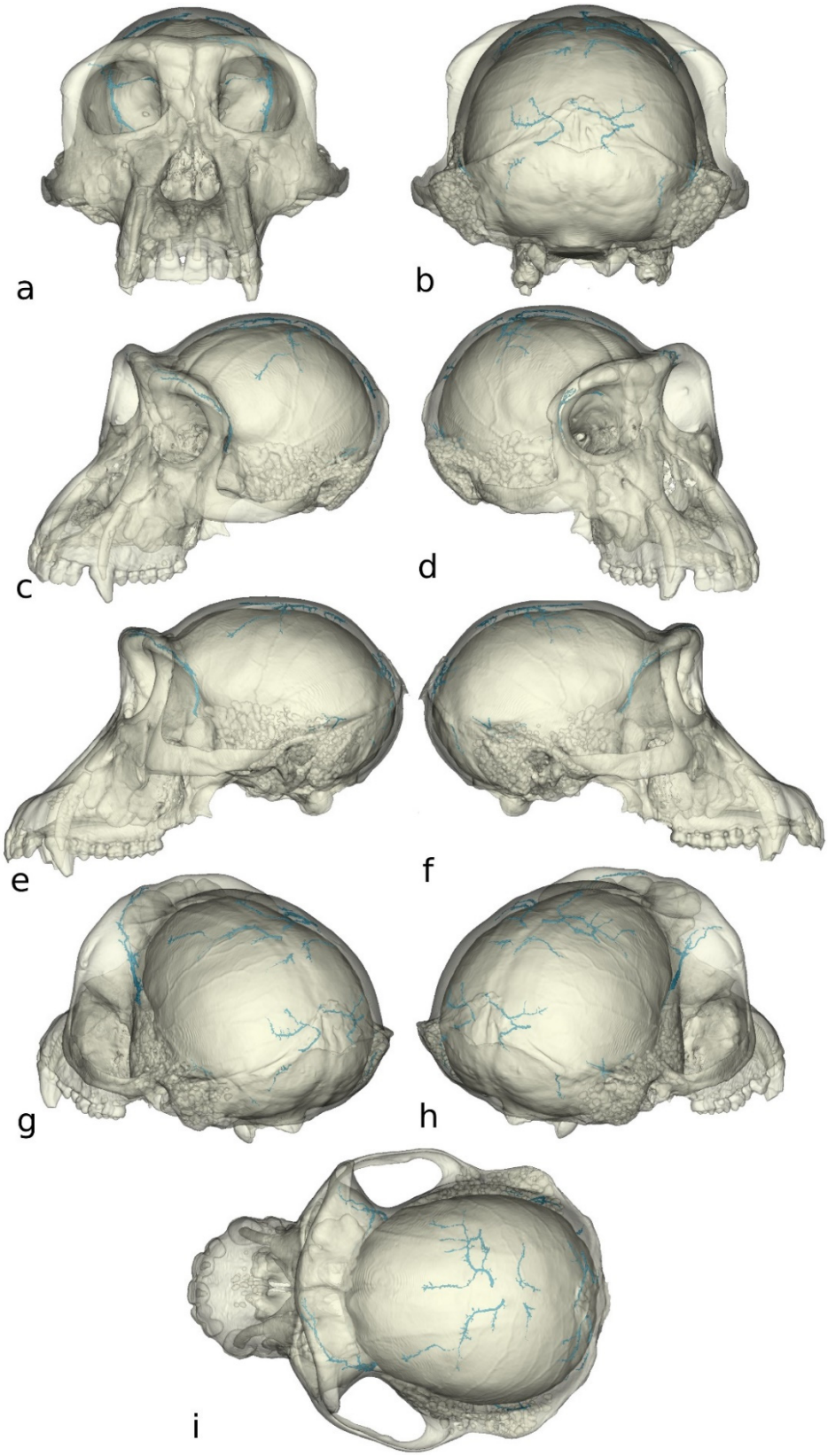

Figure 5.1 The diploic channels (in blue) in a chimpanzee cranium, shown in the anterior (a), posterior (b), anterolateral (c and d), lateral (e and f), posterolateral (g and h), superior (i) views.

In all hemicrania (n=36), the DCs inside the supraorbital area anastomosed with the periorbital vessels and frontal sinus. In very rare cases (5.56%; n=2), the DCs within the supraorbital torus extended into the nasal bone. Within the supraorbital torus and other parts of the orbit, there were also numerous emissary channels of varying sizes. In all hemicrania (n=36), these emissary channels directly linked the frontal sinus to the periorbital vessels or other extracranial vessels. The DCs in the frontal crest had variable sizes, but their drainage patterns were consistent. In all specimens, they anastomosed with the superior sagittal sinus.

The DCs found along the boundary between the orbital plate and frontal squama were long and wide, appearing in pairs on the left and right hemicrania in each individual. They ran continuously from the lateral sides of the frontal sinus, passing by the orbital plate, to the pterional region. In all specimens, these DC branches functioned as a bridge linking together the frontal sinus, sphenoparietal sinus, orbital/periorbital vascular system, and meningeal vessels. As explained in Chapter 2, meningeal vessels could be classified into anterior meningeal vessels (AMVs), orbital meningeal vessels (OMVs), and middle meningeal vessels (MMVs). The AMVs in chimpanzees were small and less variable, frequently connecting to the frontal DCs (in 41.7% of hemicrania specimens, n=15) and frontal sinus (72.2% of hemicrania specimens, n=26). In contrast, the OMVs and MMVs were highly variable and presented many distribution types (Figure 5.2). 5.6% of the hemicrania specimens (n=2) manifested the type-I pattern, in which the OMVs and MMVs were constrained in the frontal and parietal bones respectively. 11.1% of the hemicrania specimens (n=4) manifested the type-II, seeing the OMVs extending from the frontal into the parietal bone and the MMVs constrained in the parietal bone. 11.1% of the hemicrania specimens (n=4) manifested the type-III, with the OMVs limited in the frontal bone and the MMVs extending from the parietal into the frontal bone. 66.7% of the specimens (n=24) had the type-IV, in which OMVs and MMVs both extended between the frontal and parietal bones. Finally, 5.6% of specimens possessing type-V had no MMVs in the parietal bones (n=2) and their parietal bones were

dominated by the OMVs.

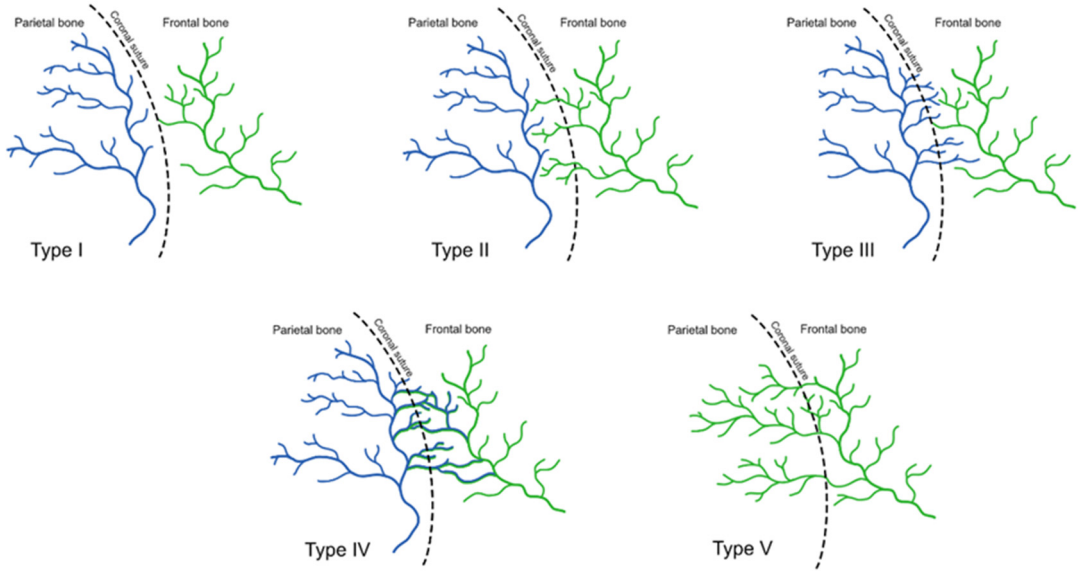

Figure 5.2 The distribution types of the orbital meningeal vessels (OMV) and middle meningeal vessels (MMVs). Type-I: OMVs and MMVs were separated by the coronal suture; Type-II: OMVs were distributed in the frontal and parietal bones while MMVs were constrained in the parietal bone; Type-III: OMVs were constrained in the frontal bone while MMVs extended from the parietal bone to the frontal bone; Type-IV: OMVs and MMVs coexisted in the frontal and parietal bones; Type-V: OMVs dominated the frontal and parietal bones while MMVs were absent.

When the frontal DCs arrived in the pterional region, they always anastomosed with the OMVs, while their anastomosis with the MMVs was not consistent. The hemisphere specimens (n=28) with type-III and type-IV saw their MMVs connecting with the frontal DCs in the pterional region, while in the other specimens, the MMVs were constrained in the parietal area, with no connection with the frontal DCs.

Besides, in 88.9% of the hemicrania (n=32), the frontal DCs circumferentially ran along and connected to the posterior edge of the ethmoid sinus, extending into the sphenoid

bone (the lesser wing and body) and connecting to the intercavernous or cavernous sinus (Figure 5.3). In two individuals of the sample, the extension of the frontal DCs did not stop at the sphenoid bone, but kept extending posteriorly into the clivus of the occipital bone and connected to the basilar plexus.

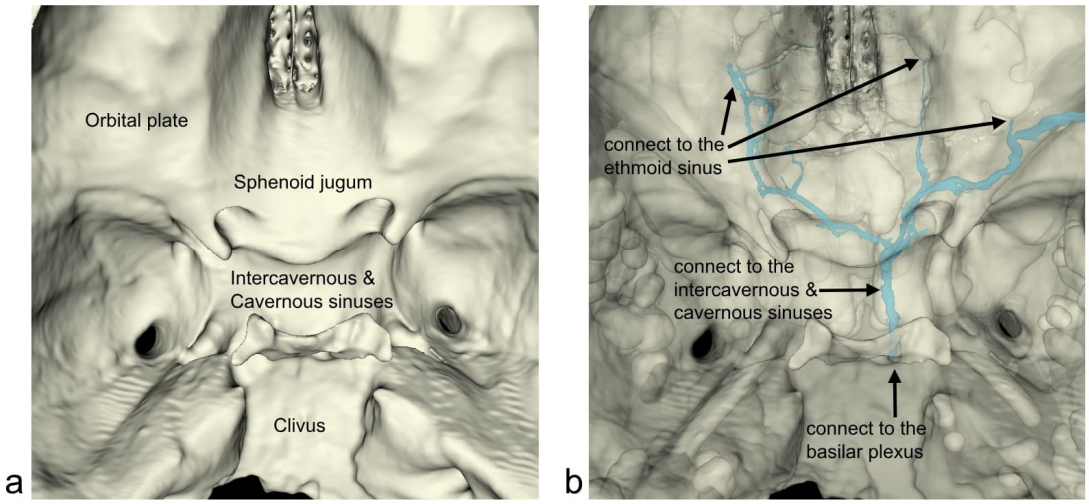

Figure 5.3 The superior view of the skull base in chimpanzees (a). In the transparent view (b), the DCs ran from the frontal bone into the sphenoid bone, connecting to the ethmoid sinus, cavernous/intercavernous sinus, and finally leading to the basilar plexus in the clivus of the occipital bone.

Sphenoid bone

The DCs did not consistently appear in the sphenoid bone in chimpanzees, but the incidence is high. 97.2% of the chimpanzee hemicrania specimens (n=35) housed DCs in the lesser wings and the bodies of the sphenoid bones.

As mentioned above, these DC branches in the lesser wings or bodies of the bones were the extensions of the frontal DCs surrounding the lateral and posterior edges of the ethmoid sinuses, running into the cavernous & intercavernous sinuses (Figure 5.3). In all chimpanzee specimens, the ethmoid sinuses were fused with the frontal sinuses, and there was no obvious boundary splitting them. The blood drainage from the frontal sinus could directly course into the ethmoid sinuses, and then it could enter the sphenoid

bone through the DCs. Thus, these DCs built a direct and short link (like a ‘shortcut’) between the frontal sinus, ethmoid sinus, and cavernous/intercavernous sinus.

Another interesting finding was the DC branches found in the greater wings of the sphenoid bones in chimpanzees (Figure 5.4). These DCs in the greater wings appeared in 25.0% of the hemicrania specimens (n=9). Each greater wing on one side only possessed one such DC branch, which was long and wide, with scarce ramifications. It ran between the pterional region and the centre of the middle cranial fossa. In the pterional region, the DC branch was connected with the MMVs, sphenoparietal sinus, and extracranial vessels. In the centre of the middle cranial fossa, the branch was connected with the carotid canal, carotid groove, pterygoid fossa, foramen lacerum, or a foramen close to the foramen ovale. As a result, the DC branch in the greater wing functioned as a stem of the MMV network. This DC branch – or we may call it ‘stem’ – might transport the venous drainage between the middle cranial fossa and the ramified MMV branches in the upper cranial vault.

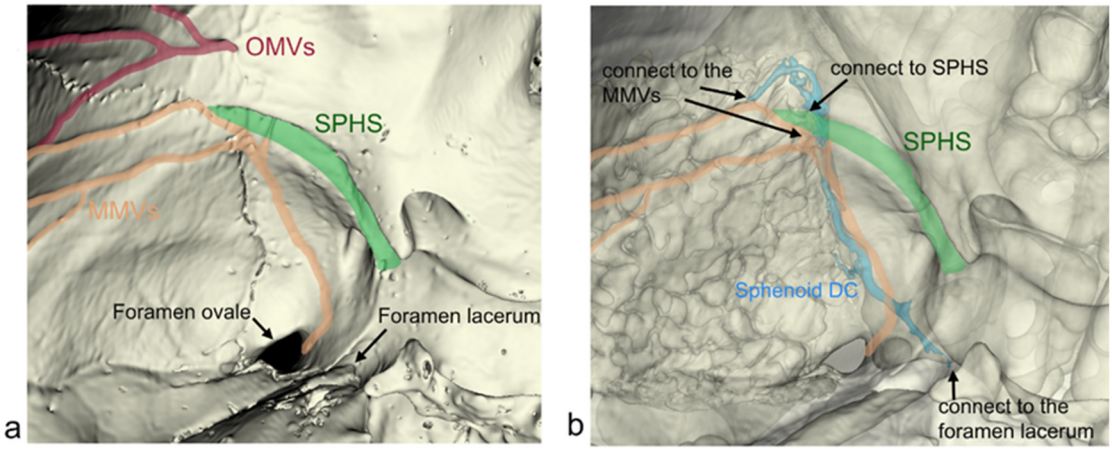

Figure 5.4 The center of the middle cranial fossa is shown in (a). In the transparent view (b), we can see the DC branch hidden in the greater wing. The DC branch functioned as a stem of the MMV network, connecting to the foramen lacerum, sphenoparietal sinus (SPHS) and MMVs.

Parietal bone

The parietal DCs were variable in morphology and distribution. Their distribution patterns were different from any pattern documented previously in human populations (Hershkovitz et al., 1999). The parietal DCs consistently appeared in the parasagittal area, where they extended in the mid-lateral direction. The large branches terminated at the temporal lines while only a few or even no branches appeared below the temporal lines (Figure 5.1). In all specimens, the DCs in the parasagittal area were short and consistently connected with the superior sagittal sinus. In 80.6% of the hemicrania specimens (n=27), the DCs in this area were connected with the OMVs, and 94.4% of hemicrania specimens (n=34) were connected with the MMVs.

Unlike the parietal foramina in humans that usually appeared in pairs, 44.4% of the chimpanzee individuals (n=8) only housed a single parietal foramen, which was located in the sagittal suture or on one side of the cranium (Figure 5.5). The emissary vessels inside these parietal foramina consistently connected to the parietal DCs. The rest of the specimens housed no parietal foramen.

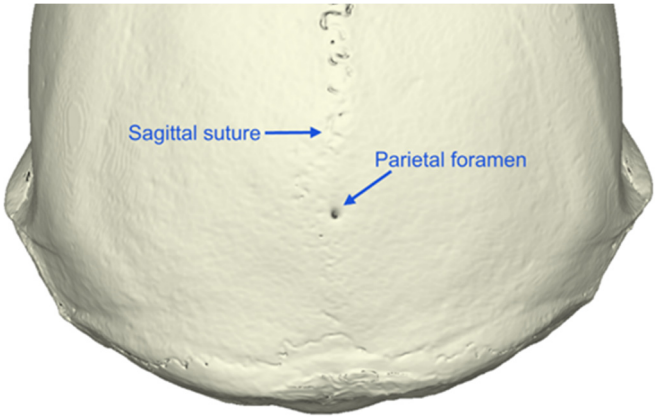

Figure 5.5 The parietal foramen in chimpanzees appeared alone and it was located in or adjacent to the sagittal suture.

Still, regardless of the parietal foramina, the parietal DCs in all specimens had connections with the extracranial vessels through many microscopic foramina distributed over the bone. Interestingly, in one special case, there was a large foramen

above the right asterion (Figure 5.6). It was the outlet of a long and wide channel bridging the extracranial vessels and petrosquamous sinus. This special channel had not been documented in previous studies on great apes. In addition, the adjacent mastoid emissary channels were consistently found in all specimens and they had no anastomosis with the DCs.

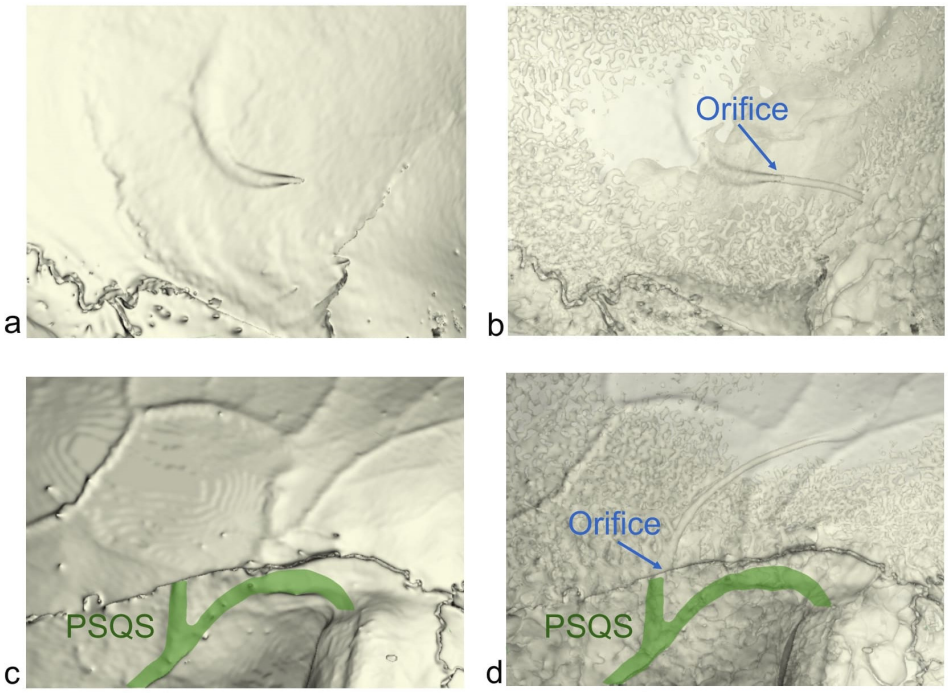

Figure 5.6 The channel linking the extracranial vessels and petrosquamous sinus (PSQS). The extracranial orifice is shown in (a) and (b). The intracranial outlet connected with is shown in (c) and (d).

The asterional region of chimpanzees manifested five types of connection patterns (Figure 5.7). 41.7% of the hemisphere specimens (n=15) showed the pattern A, in which the parietal DCs simultaneously connected to the transverse-sigmoid sinus and petrosquamous sinus, with the occipital DCs approaching the asterion and connecting to the transverse-sigmoid sinus. 44.4% of the hemisphere specimens (n=16) showed the pattern B, which was similar to pattern A, but the occipital DCs did not enter the asterional area. 2.8% of the specimens (n=1) showed the pattern C, in which the connection in the region only concerned the transverse-sigmoid sinus and parietal DCs. 5.6% of the specimens (n=2) showed the pattern D, in which the parietal DCs in the

region connected to the petrosquamous sinus solely while the occipital DCs connected to the transverse-sigmoid sinus. Finally, in the pattern E (5.6%; n=2), the parietal DCs had no direct connection with the transverse-sigmoid and petrosquamous sinuses, while the occipital DCs connected to the transverse-sigmoid sinus solely. Interestingly, the pattern F and G (occipital DCs connected with transverse-sigmoid sinus, while parietal DCs connected to transverse-sigmoid sinus or superior petrosal sinus) appeared in fossil hominins and extant humans, but they did not appear in this chimpanzee sample.

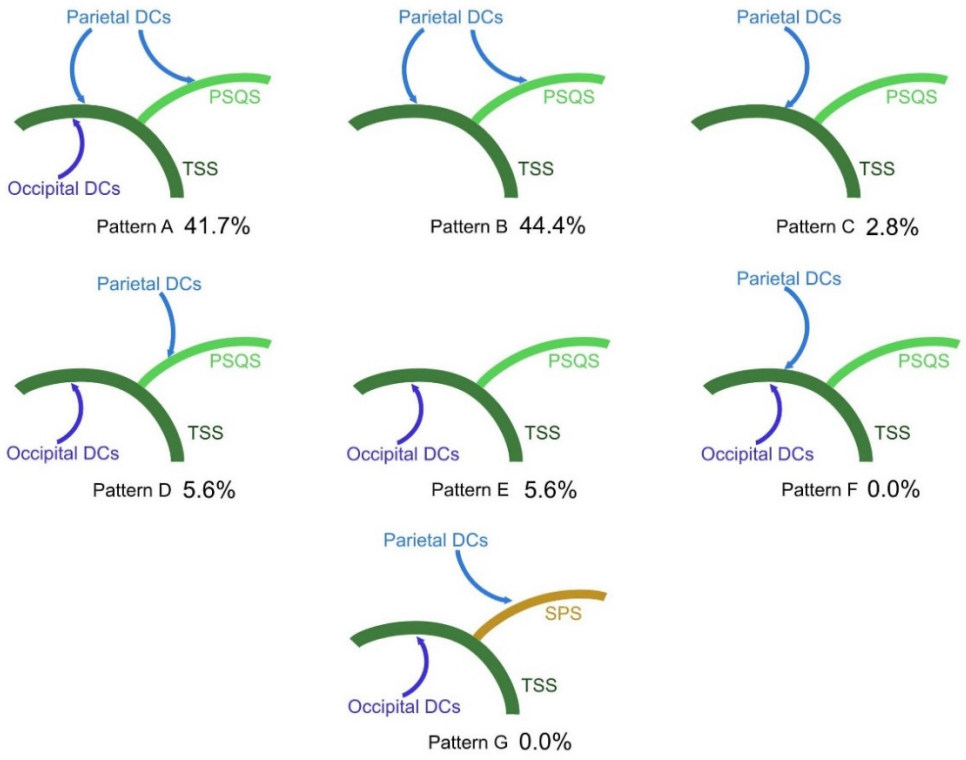

Figure 5.7 The connection pattern of the DCs and dural sinuses surrounding the asterion in chimpanzees. Pattern A: the parietal DCs connect to both transverse-sigmoid sinus (TSS) and petrosquamous sinus (PSQS), and the occipital DCs connect to TSS; Pattern B: the parietal DCs connect to TSS and PSQS, while the occipital DCs are absent in the asterional region; Pattern C: the parietal DCs connect to TSS while the occipital DCs are absent in the asterional region; Pattern D: the parietal DCs connect to the PSQS and the occipital DCs connect to TSS; Pattern E: parietal DCs do not connect to dural sinuses in this region while the occipital DCs connect to TSS; Pattern F: parietal and occipital DCs connect to the TSS; Pattern G: parietal DCs connect to the SPS, and the occipital DCs connect to the TSS.

Occipital bone

The diploic layer of the occipital bone was more complex than those of the parietal and frontal bones. Many diploic cavities displayed long and curved shapes somewhat similar to vessels, but it could not be confirmed if they were the real DCs housing the diploic veins. Still, there were many foramina and identifiable DCs showing us the drainage pathways in this bone.

The occipital DCs were mainly found along the midline and nuchal crest and in the asterional region. These occipital DCs could extend across the lambdoid suture, anastomosing with parietal DCs. Apart from the connection between the occipital DCs and transverse-sigmoid sinus inside the asterional region, as described above, the transverse-sigmoid sinus of 91.7% of the hemicrania specimens (n=33) also had anastomosis with the occipital DCs located close to the midline. In addition, the occipital DCs in all specimens possessed connections with the superior sagittal sinus and extracranial vessels (occipital vessels) along the midline, and 83.3% of the hemicrania specimens (n=30) showed connections between the occipital DCs and occipital sinus.

Comparison with gorillas

In the preliminary analysis of the gorilla sample (including 22 hemicrania from 11 individuals), the diploic venous system of gorillas was similar to that of chimpanzees (Figure 5.8). The DCs in gorilla crania were sparse and did not form any distribution pattern recorded in the Hershkovitz's system (Hershkovitz et al., 1999). Gorilla DCs had consistent connections with the frontal sinus, periorbital/ophthalmic vessels, meningeal vessels, superior sagittal sinus, and transverse-sigmoid sinus. However, unlike chimpanzees, they did not show a shortcut pathway between the ethmoid sinus and cavernous/intercavernous sinus. The imprint of petrosquamous sinus in gorillas did not consistently appear in all specimens, neither was its connection with the DCs.

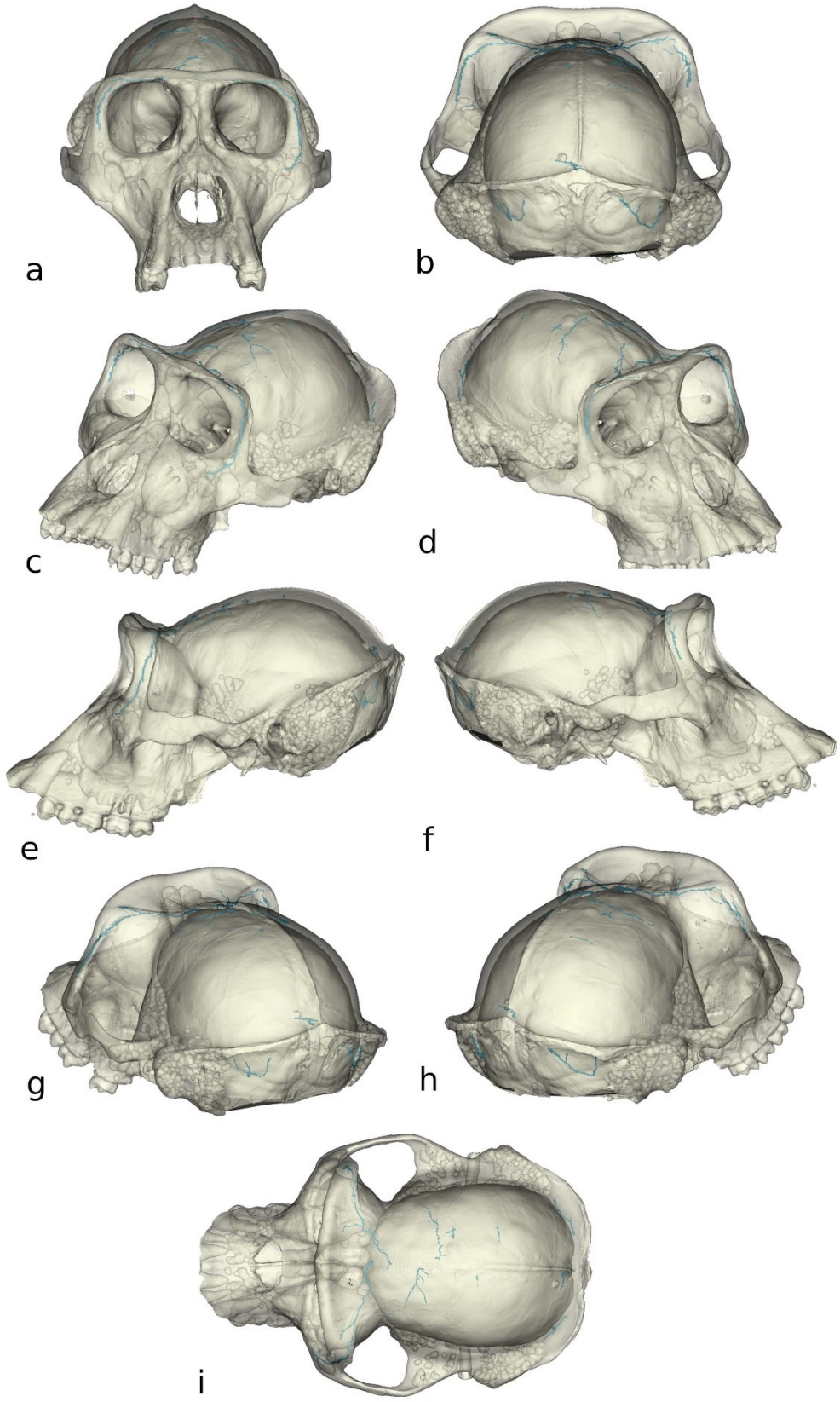

Figure 5.8 The diploic channels (in blue) in a gorilla cranium, shown in the anterior (a), posterior (b), anterolateral (c and d), lateral (e and f), posterolateral (g and h), superior (i) views.

5.2 The drainage pathway of the diploic vessels in extant humans

Overview

Like the chimpanzees, as the distribution and drainage pathways of extant *H. sapiens* DCs on the left and right sides showed asymmetry, the cranium (tomographic images and 3D models) of each individual was divided into two hemicrania and they were observed and analysed separately. A total of 56 hemicrania from 28 extant human individuals were included in this study. The specimens were adult dry skulls collected from Europe, including France (16 hemicrania, 28.6%), Hungary (2 hemicrania, 3.6%), Moldova (4 hemicrania, 7.1%), Romania (26 hemicrania, 46.4%), and Russia (8 hemicrania, 14.3%). All crania were well preserved, with some of them almost intact.

In general, the DC networks in these extant *H. sapiens* had wide diameters, long lengths, and numerous ramifications (Figure 5.9). The DCs in extant *H. sapiens* were widespread in the neurocranium. The DC network in each bone usually extended across the sutures and anastomosed with the DCs in adjacent bones. The DC networks in the frontal and parietal bones were usually comparably developed. They were larger and more complex than that in the occipital bone, while those in the sphenoid and temporal bones were the least developed, with rather short and narrow branches.

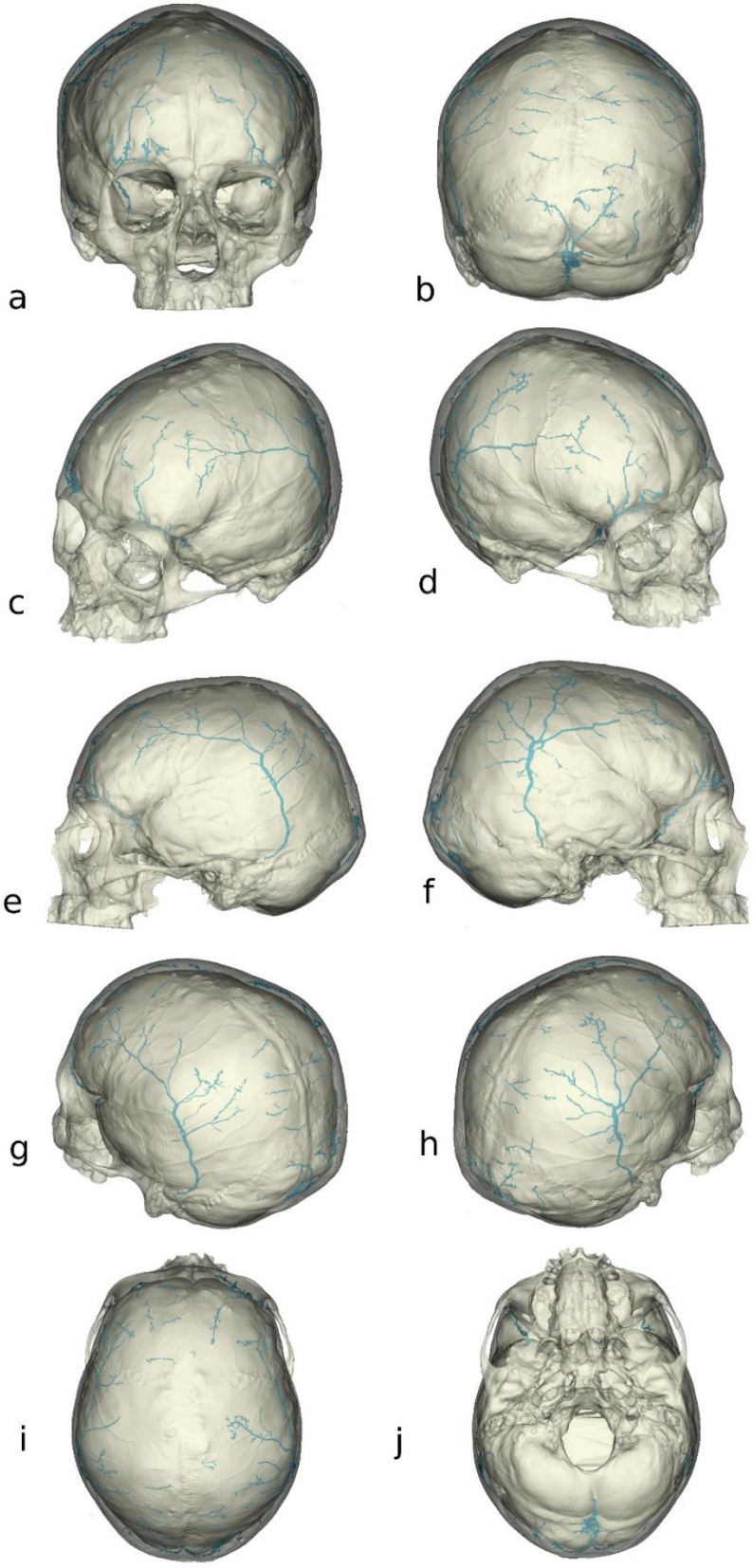

Figure 5.9 The diploic channels (in blue) in an extant human cranium, shown in the anterior (a), posterior (b), anterolateral (c and d), lateral (e and f), posterolateral (g and h), superior (i), and inferior (j) views.

Frontal bone

In extant *H. sapiens* specimens, the morphology of the frontal DC network was variable but the DC branches could always be found in the frontal squama, supraorbital ridge, pterional region, and orbital plate. The main DC branches always appeared bilaterally in the frontal squama (Figure 5.9). They extended externally to communicate with extracranial vessels (including at least the superficial temporal vessels) through microscopic foramina. They also extended internally to communicate with the superior sagittal sinus and meningeal vessels. In this sample of extant *H. sapiens*, the configuration of meningeal vessels was less diverse than that of great ape specimens. Here, the MMVs derived from the cranial base always dominated the frontal area and connected to the frontal DCs (Figure 5.10). The OMVs, as branches of the ophthalmic vessels, appeared and connected to the frontal DCs in 83.9% (n=47) of hemicrania specimens. Moreover, when the OMVs appeared, they only occupied the orbital plate and its surrounding areas. Besides, the AMVs derived from the ethmoid vessels were limited in a very small area located at the lower part of the frontal crest (Figure 5.11). Although the AMVs had constant links with the frontal sinus, they only connected to the frontal DCs in 46.4% (n=26) of hemicrania specimens.

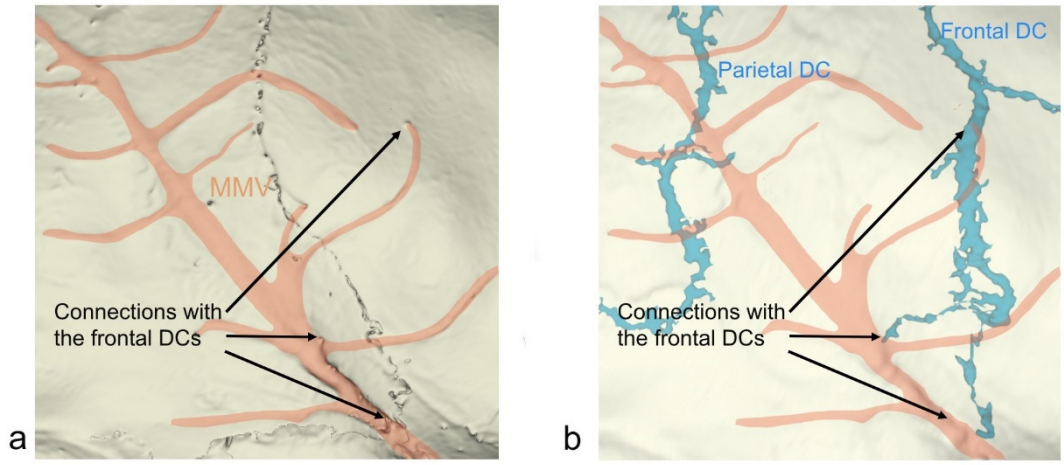

Figure 5.10 The anastomosis between MMV and frontal and parietal DCs.

The main DC branches always extended from the frontal squama to the supraorbital ridge, where they had constant connections with the periorbital and/or ophthalmic

vessels. A large number of emissary channels bridged the frontal sinus with the periorbital and ophthalmic vessels directly. Similarly, the link between the frontal DCs and frontal sinus in the supraorbital ridge was frequent but not constant, with the incidence reaching 91.7% (n=51). Still, compared with the emissary channels connected with the frontal sinus, the DCs connected with the frontal sinus were fewer and narrower.

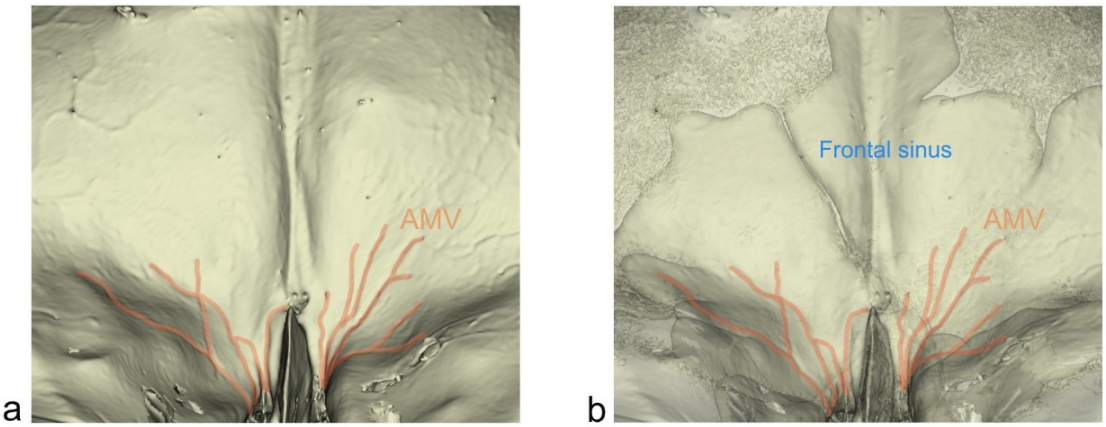

Figure 5.11 The spatial location of frontal sinus and AMVs.

In the orbital plate and pterional region, the frontal DCs always connected to the sphenoparietal sinus and the stem of MMVs. Also, when OMV appeared (in 83.9% of hemicrania specimens, as mentioned above), the frontal DCs located in or close to the orbital plate connected to its stem or branches. Still, the DCs rarely (in 12.5% of hemicrania specimens, n=7) semi-encircled the orbital plate like those observed in chimpanzees. Furthermore, the DCs in the orbital plate did not connect to the ethmoid sinus, let alone establish a shortcut between the ethmoid sinus and the cavernous/intercavernous sinus.

Sphenoid bone

DC branches could be found in the sphenoid bones of all hemicrania specimens (Figure 5.12), and they always appeared in the lesser wing and the upper part of the greater wing. The DCs in the lesser wing were actually the extensions of the frontal DCs, showing short lengths and always connecting to the sphenoparietal sinus. The DCs in

the greater wing area were also short in length. They connected intracranially to the sphenoparietal sinus and the stem of MMV, while also extending extracranially through the large foramina and connecting to the vessels supporting the temporalis muscle (including at least the deep temporal vessels). In other words, unlike the pattern in chimpanzees, the DCs in the greater wing of extant humans could not function as stems of MMV to connect the skull base. Here, the DCs in the greater wings of extant humans could only function as bridges communicating extracranial and intracranial space.

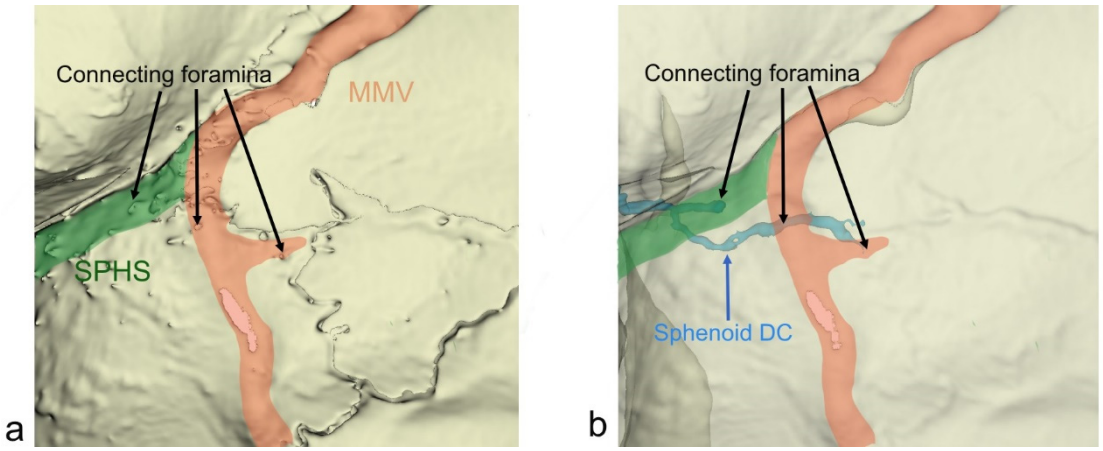

Figure 5.12 The sphenoid DCs in extant humans connect with the middle meningeal vessels (MMVs) and sphenoparietal sinus (SPHS).

Parietal bone

The distribution pattern of parietal DCs was variable. 16.1% (n=9) of hemicrania manifested the bonsai pattern; 14.3% (n=8) manifested the serpentine patten; 12.5% (n=7) manifested the spider pattern; 3.6% (n=2) manifested the coronal pattern; 3.6% (n=2) manifested the thousand-lakes pattern; 21.4% (n=12) manifested the hybrid pattern. Besides, 28.6% (n=16) of hemicrania showed distribution patterns not recorded in Hershkovitz's (1999) classification system.

The distribution pattern did not affect how a DC network in a hemicranium connected to other vascular networks. Along the superior edge of the parietal bone (i.e., the parasagittal area) in each hemicranium, the DC branches extended mid-laterally and

showed many connections with the superior sagittal sinus. 67.9% (n=38) of hemicrania had the parietal foramina connected with the DCs in the parasagittal area. The absence of parietal foramina in the rest specimens did not stop the communication between the DCs and extracranial vessels, as there were many microscopic foramina across the external surface functioning as the outlets of the DCs. Also, the imprints of MMVs were widespread across the internal surface of the parietal bone, and they had constant connections with the DCs in all specimens.

In the asterional area, the asterion landmark was usually located at the same level as the transverse-sigmoid sinus (83.9%; n=47). In a few cases (14.3%; n=8), the asterion was inferior to the transverse-sigmoid sinus. In only one hemicranium specimen, the asterion was at the upper edge of the transverse-sigmoid sinus. The DCs surrounding the asterion manifested a variable and complex drainage pattern. Here, this current study used the same classification that had been applied to the great ape specimens (Figure 5.13). The result showed that the pattern A was the most frequent (46.4%; n=26), in which the parietal DCs connected to the petrosquamous sinus and the transverse-sigmoid sinus simultaneously, while the occipital DC connected to the transverse-sigmoid sinus solely. 21.4% (n=12) of hemicrania manifested the pattern B, in which parietal DCs connected the petrosquamous sinus and transverse-sigmoid sinus, while the occipital DCs did not connect the transverse-sigmoid sinus near the asterion. The pattern C was the least frequent (7.1%; n=4), with the parietal DCs connected to the transverse-sigmoid sinus while the occipital DCs did not appear in the asterional area. The pattern F accounted for 25.0% (n=14) of the sample, in which the parietal and occipital DCs only connected the transverse-sigmoid sinus. Finally, the pattern D, E, and G were not manifested in the sample.

It was apparent that the anastomosis between the parietal DCs and transverse-sigmoid sinus was constant in the sample of extant humans. The inspection also revealed that the parietal DC branches connected with the transverse-sigmoid sinus were always

larger than those connected with the petrosquamous sinus. Besides, it is interesting to note that the special channel linking the petrosquamous sinus directly to extracranial space, which was found in only one chimpanzee hemicranium, turned out to be more frequent in extant human specimens with an occurrence rate of 10.7% (n=6).

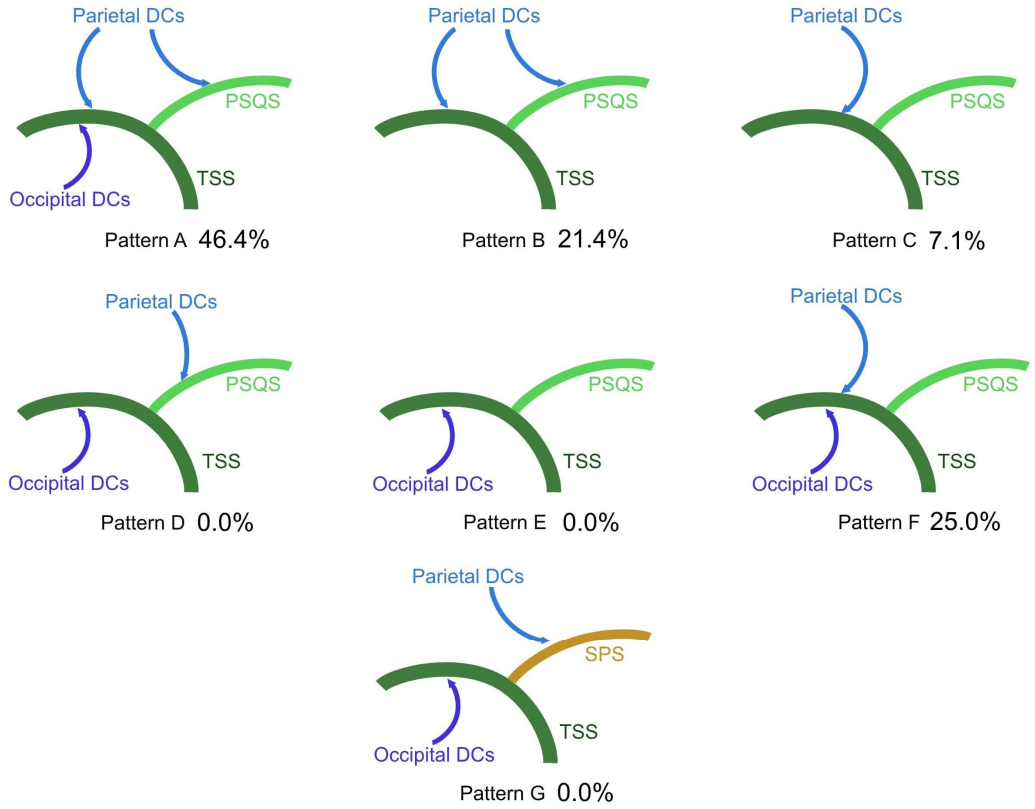

Figure 5.13 The connection pattern of the DCs and dural sinuses surrounding the asterion in extant *H. sapiens*. Pattern A: the parietal DCs connect to both transverse-sigmoid sinus (TSS) and petrosquamous sinus (PSQS), and the occipital DCs connect to TSS; Pattern B: the parietal DCs connect to TSS and PSQS, while the occipital DCs are absent in the asterional region; Pattern C: the parietal DCs connect to TSS while the occipital DCs are absent in the asterional region; Pattern D: the parietal DCs connect to the PSQS and the occipital DCs connect to TSS; Pattern E: parietal DCs do not connect to dural sinuses in this region while the occipital DCs connect to TSS; Pattern F: parietal and occipital DCs connect to the TSS; Pattern G: parietal DCs connect to the SPS, and the occipital DC connect to the TSS.

Temporal bone

The temporal DCs have been found in 89.3% (n=50) of hemicrania specimens. Although the temporal bone was large, the temporal DCs were rather small and narrow when compared with the DCs in the calvaria. As there was almost no visible diploe in the squamous part, there were no DCs found in this part. As for the petrous, tympanic, and mastoid parts, most space was occupied by the mastoid cells and inner ear, and thus the DCs were limited in a small region. The drainage pathway of temporal DCs was simple, as they had few ramifications and only connected to the mastoid emissary vessels. In addition, although the mastoid emissary vessels were close to the parietal and occipital DCs in the asterional area, they rarely had any connection. Only 3.6% (n=2) of hemicrania specimens manifested connections between the parietal DCs and mastoid emissary vessel, and only 7.1% (n=4) manifested connections between the occipital DCs and mastoid emissary vessel.

Occipital bone

Like the pattern observed in the great apes, the diploic structures along the midline of occipital bone were complex in extant *H. sapiens*, where many cavities showed vascular-like shapes. It was uncertain to tell if all of them were DCs by simply judging from the shape. Still, the inspection of the location of foramina (i.e., the inlets/outlets of DCs) showed the drainage pattern and location of the DCs.

In extant humans, the occipital DCs in all specimens constantly drained into the superior sagittal sinus through many foramina located along the midline. Outside the asterional area, there were always connections between the transverse-sigmoid sinus and occipital DCs. In 57.1% (n=32) of hemicrania specimens, MMVs extended from the parietal bone into the upper part of the occipital bone, connecting to the occipital DCs. In the base of the occipital bone, 80.4% (n=45) of hemicrania specimens had DCs connected to the occipital sinus. Finally, the occipital vessels always connected to the DCs through many large foramina on the external surface of the bone.

5.3 The drainage pathway of the diploic vessels in hominin fossils

5.3.1 Early Pleistocene hominins

KNM-ER 1805

The diploe of the neurocranium was damaged during the taphonomic process, with many diploic structures filled with sediments and thus rendered unidentifiable (Figure 5.14). In the frontal bone, only one short DC branch could be identified. It was close to the midline and possibly anastomosed with the superior sagittal sinus or meningeal vessels. The parietal bone retained several DC branches, which were found anastomosed with the MMV. Finally, in the occipital bone, several DC branches were located at the juncture of the midline and superior nuchal line. Their drainage pathways were unclear due to the taphonomic damage.

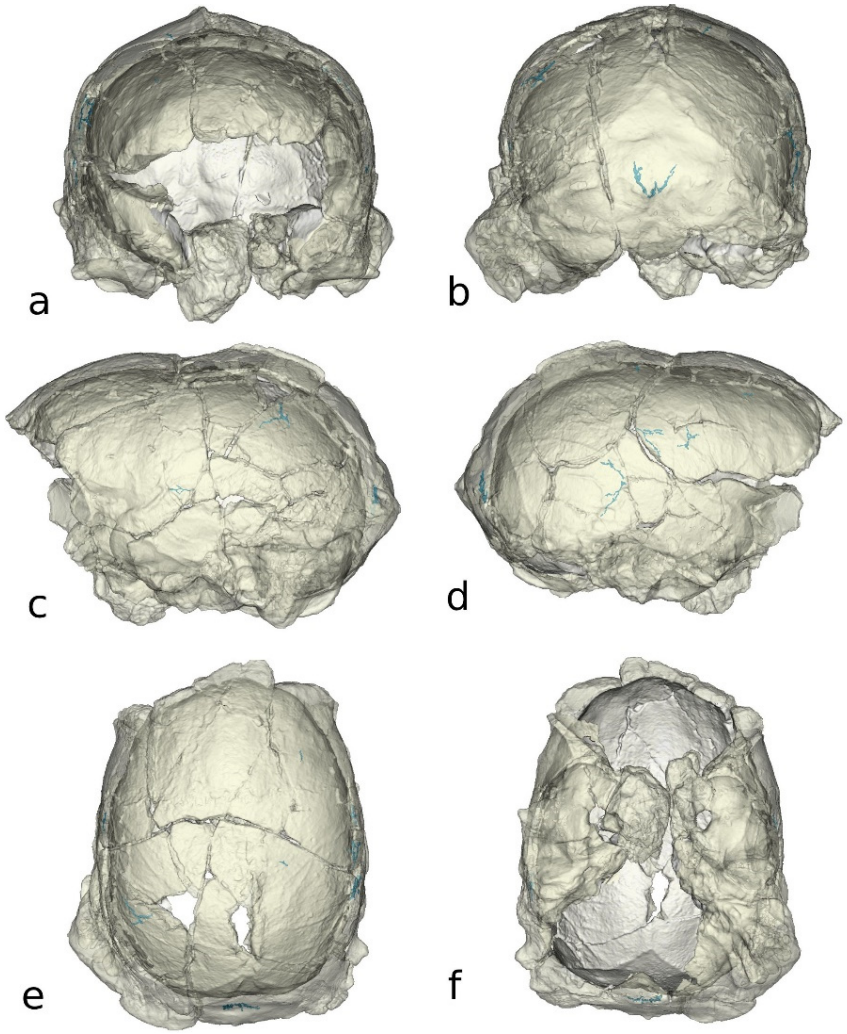

Figure 5.14 The diploic channels (in blue) in KNM-ER 1805, shown in the anterior (a), posterior (b), lateral (c and d), superior (e) and inferior (f) views.

StW 53

The StW 53 cranium has split into several fragments. Among them, the pieces labelled 53a and 53e possessed well-preserved diploic layers, allowing reconstructing the diploic venous system in the frontal, left parietal (posterior part), and occipital (middle part) bones. In the general view, the DC network in the preserved diploe manifested long and wide branches with a large number of ramifications and anastomosis (Figure 5.15 and 5.16).

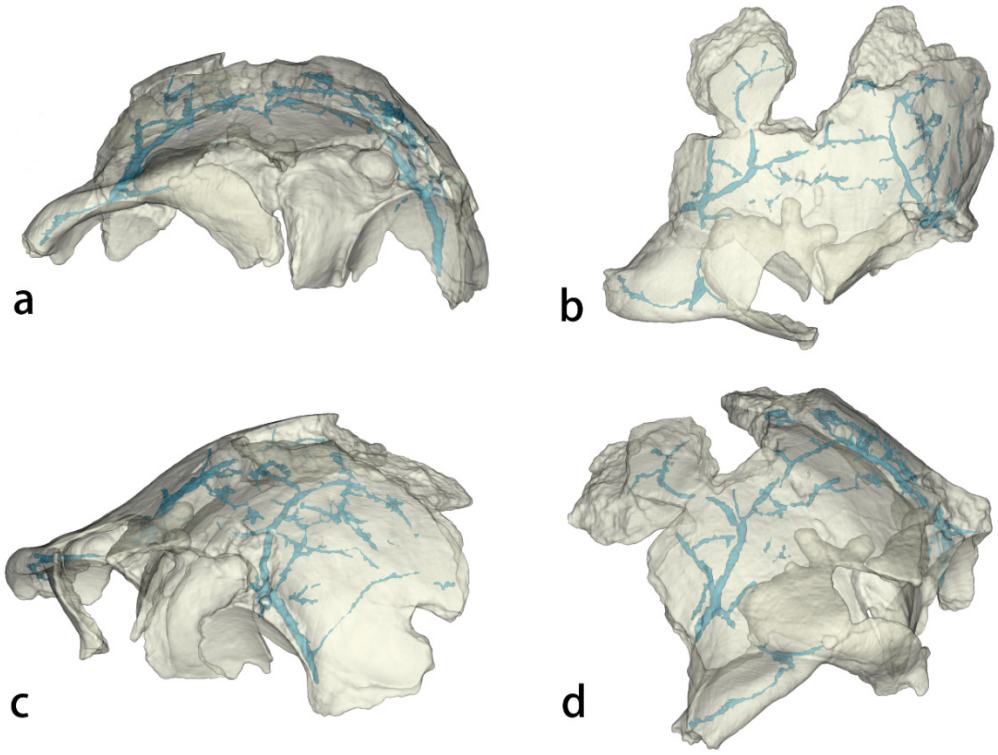

Figure 5.15 The diploic channels (in blue) in the StW 53a fossil, shown in the anterior (a), superior (b), and anterolateral (c and d) views.

The DC network in the frontal bone (53a) was generally symmetric (Figure 5.15). A pair of main DC branches coursed in the anteroposterior direction, from the supraorbital torus to the squama, and ramify mediolaterally. In the supraorbital torus, the thin DC branch on the right side ran along the orbit, connecting to the periorbital vessels. In the frontal squama, the DCs connected to the extracranial vessels (including at least the superficial temporal vessels), frontal sinus, superior sagittal sinus, and meningeal

vessels. The DCs also descended across the temporal line, showing a tendency to run into the pterional region, where they might anastomose with the stem of the meningeal vessels. Still, constrained by the preservation, it was unavailable to confirm the anastomosis and to observe whether the anastomosis was with the OMV or the MMV.

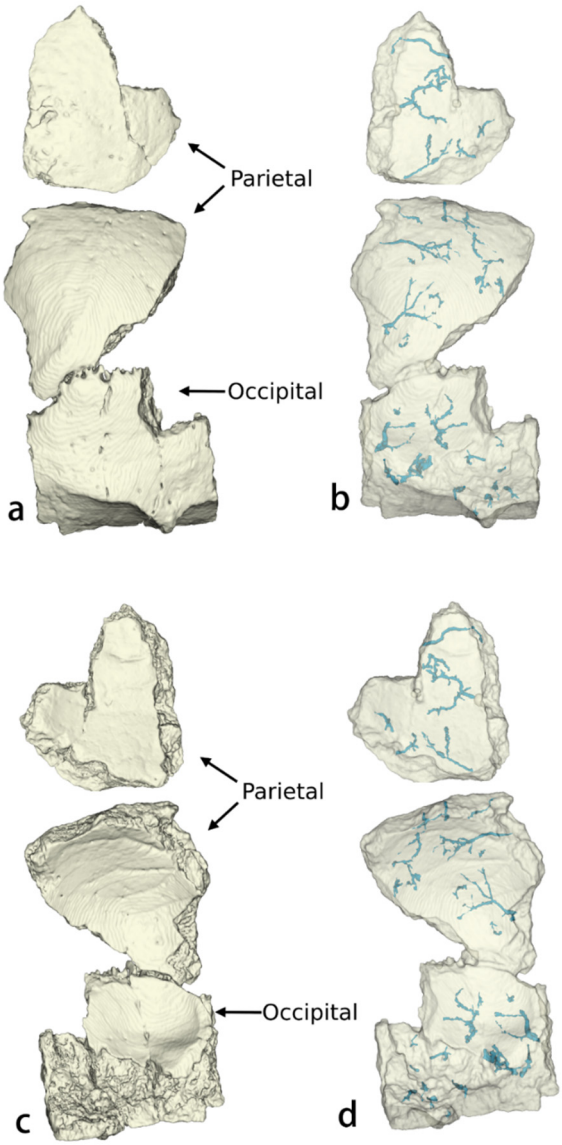

Figure 5.16 The diploic channels (in blue) in the StW 53e fossil, shown in the outer (a and b) and inner views (c and d). The parietal bone of the fossil has split into two.

In the parietal bone (in 53e,), the DCs extended multi-directionally and ramified frequently (Figure 5.16). On the outer surface, although the parietal foramen was not found, the DCs communicated with the extracranial vessels through many microscopic foramina. On the inner surface, many microscopic foramina were distributed along the

imprint of the MMV, connecting with the DCs.

The fragment 53e also preserved the middle part of the occipital bone, in which most DC branches were found above the nuchal line. On the outer surface, the occipital DCs possessed many outlets along the nuchal line and occipital protuberance, through which the DCs connected to the occipital vessels. On the inner surface, there were also several microscopic foramina functioning as the inlets/outlets of the DCs. However, it was unclear which vessels they connected to, as no vascular imprint was found on the inner surface.

5.3.2 Middle Pleistocene hominins

Tighennif 4

The right parietal bone of Tighennif 4 was almost complete (Figure 5.17). Few fracture lines caused by the taphonomic process broke up the bone, but they did not considerably change the morphology of the diploic layer or the vessel imprints on surfaces. In general, the parietal DC network had long and wide branches with many ramifications, reaching most areas of the parietal bone.

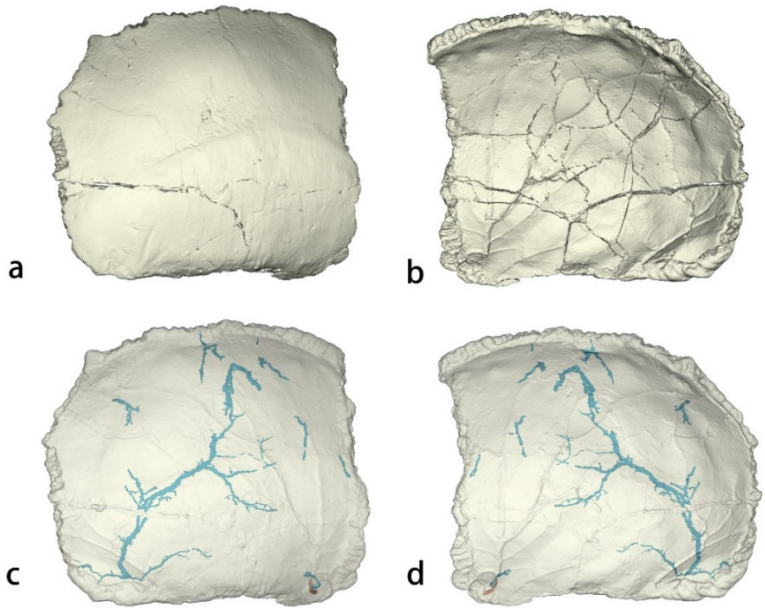

Figure 5.17 The outer (a) and inner (b) surfaces of the parietal bone of Tighennif 4. The DCs (in blue) and the bony channel of the stem of MMV (in red) are displayed in c and d.

In the anterior part of the parietal bone, a relatively short DC branch connected to a bony channel posterior to the pterion, inside which the stem of the anterior branch of MMV coursed. Most large DC branches were distributed in the middle part of the bone, where these DCs had multiple links with the superior sagittal sinus and the anterior and posterior branches of MMV. Especially, in the middle part of the parietal bone, there was a very long branch running through the entire bone, descending from the sagittal suture to the squamosal suture. Finally, the stem of this long branch exited the diploe and entered the transverse-sigmoid sinus in the asterional region, where the asterion landmark was at the lower edge of the groove of the transverse-sigmoid sinus.

In addition, the outer surface of the parietal bone displayed many microscopic foramina, which linked the extracranial vessels (possibly the superficial temporal vessels) and DCs. Still, there was no parietal foramen found in this specimen.

Trinil 2

Although the surfaces of the Trinil 2 cranium were well-preserved, there was serious damage to the diploic layer. A large amount of sediment has entered the diploic cavities, causing numerous DCs to be indiscernible in Micro-CT images. Nevertheless, abundant foramina were preserved on the inner and outer surfaces of the cranial bones (Figure 5.18). The remaining DCs were mainly found in the frontal bone, with a few discovered in the parietal and occipital bones (Figure 5.19). With the foramina and remaining DCs, it was feasible to harvest crucial information about the drainage pathway of the DC system and its connections with other anatomical structures.

In the supraorbital torus, the DCs ran anteriorly into the frontal sinus, periorbital vessels, and superficial temporal vessels. The DC branch in the middle supraorbital torus was an extension of the DCs from the frontal squama, where the DCs were long, complex, and coursing in the anteroposterior direction. Most long DC branches in the squama

were displayed along the frontal crest. The DCs in the frontal squama anastomosed with the superior sagittal sinus, meningeal vessels, and extracranial vessels (including at least the superficial temporal vessels). The anastomosis between the stem of MMVs and frontal DCs was found in the pterional areas.

In the parietal bones, the remaining DCs were found in the anterior and inferior parts of the bones, showing a few connections with the superior sagittal sinus and MMV. Besides, a large number of foramina were distributed in the imprint of MMV, extending towards the diploe. This indicated the abundant connections between the parietal DCs and MMV, even though most parietal DCs could not be reconstructed in the damaged diploic layer. Also constrained by the preservation condition, the parietal foramen was not detectable. The asterional areas were largely damaged and the asterion could not be located precisely as the sutures were fused. However, on the right asterional region, there was a noticeably large foramen in the imprint of the transverse-sigmoid sinus, which was a possible connecting point with the parietal DCs (Figure 5.18).

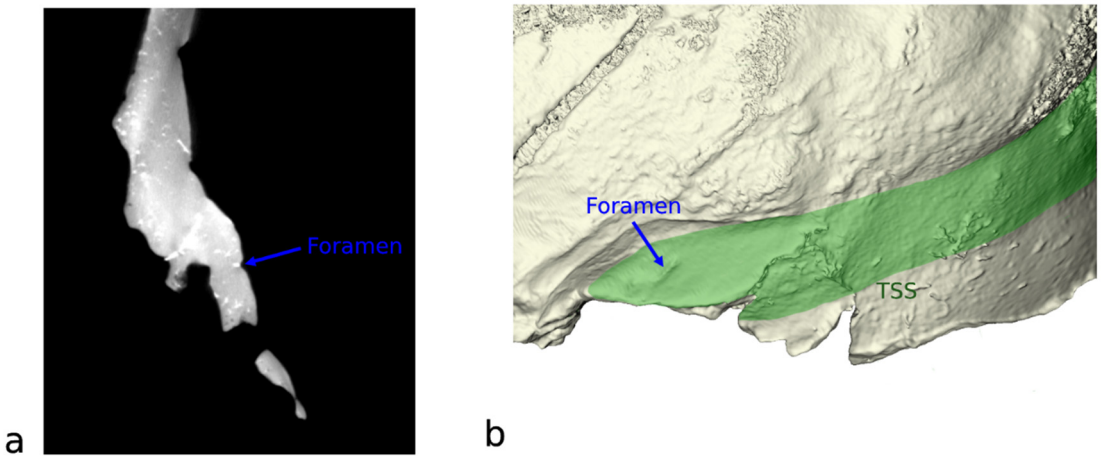

Figure 5.18 The right asterional region of Trinil 2 cranium, The foramen located in the transverse-sigmoid sinus (TSS, colored in green) imprint was a possible outlet of the parietal DCs, shown in the tomographic image (a) and 3D model (b).

The imprints of the transverse-sigmoid sinus and superior sagittal sinus possessed many foramina close to the midline of the occipital bone. These foramina possibly dignified the connections between the occipital DCs and these dural sinuses. Besides, several

foramina were discovered on the outer surface of the occipital bone. Especially, a pair of large foramina (possibly the mastoid foramina) was located inferoposterior to the asterion, linking the occipital DCs with the occipital vessels.

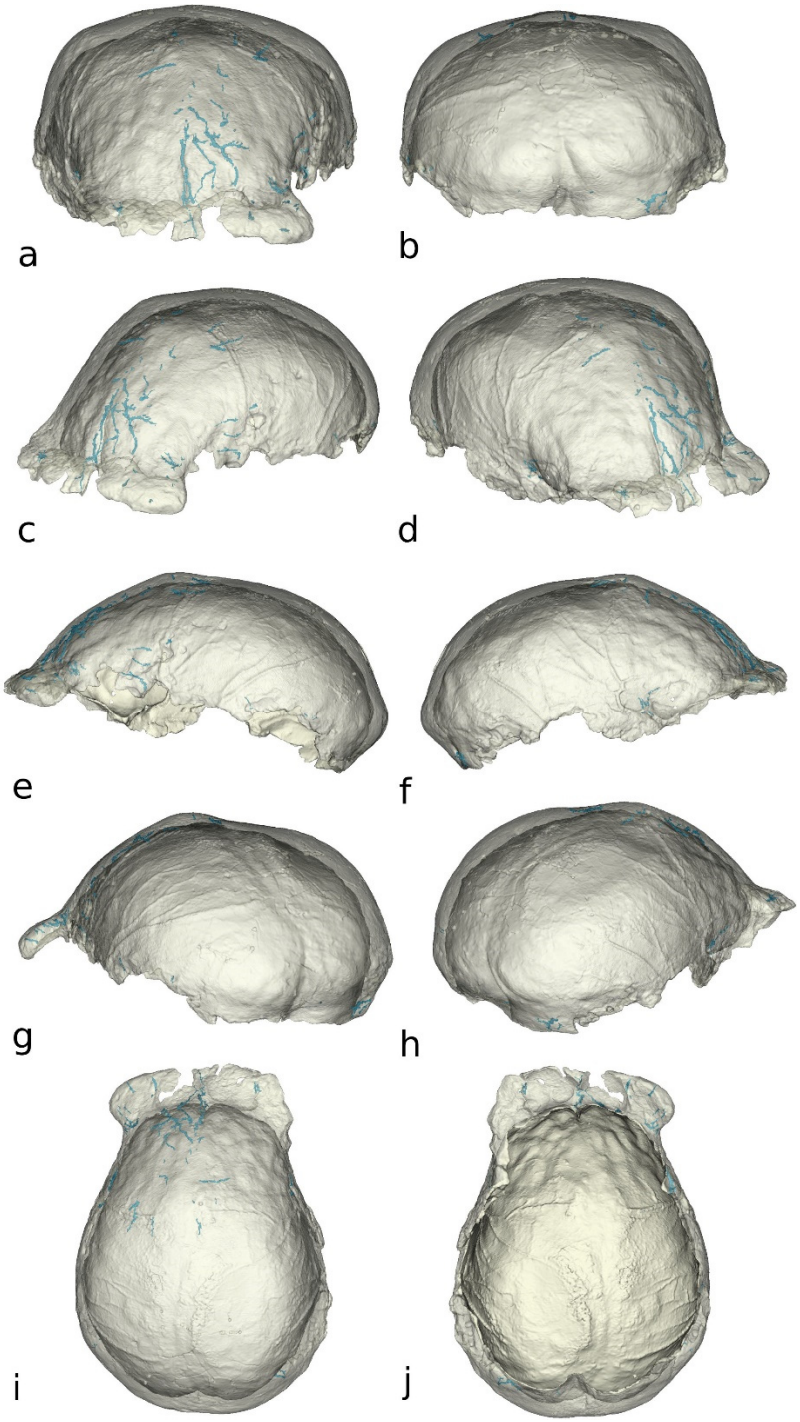

Figure 5.19 The diploic channels (in blue) in Trinil 2, shown in the anterior (a), posterior (b), anterolateral (c and d), lateral (e and f), posterolateral (g and h), superior (i), and inferior (j) views.

Hexian

The Hexian cranium was generally well-preserved. Within the diploic layer, there were fracture lines formed during the taphonomic process, which interrupted some DC branches. However, for qualitative observation, there was no significant impact. DCs were mainly found in the frontal, parietal, and occipital bones, with a small portion present in the sphenoid bone (Figure 5.21). Among these, the frontal bone exhibited the highest density of DCs, and the parietal DCs likewise formed a relatively complex and developed network.

In the supraorbital torus, the pair of main DC branches passed medial-laterally along the posterior edge of the torus. They ramified anteriorly and superiorly, anastomosing with the periorbital vessels, superficial temporal vessels, and frontal sinus. The DCs in the supraorbital torus also extended into the frontal squama and pterional region.

In the frontal squama, there were many short DC branches distributed along the frontal crest, connected with the superior sagittal sinus and AMV. The relatively longer DC branches were found in the lateral parts of the frontal squama, coursing in the anteroposterior direction. These long branches connected to the meningeal vessels and extended into the pterional region of the sphenoid bone, where a DC branch seemed connected with the stem of the MMV.

In the parietal bones, the anterior two-thirds of the parasagittal area displayed a very thin or even no diploic layer (Figure 5.20). The region with absent diploe was generally symmetric, and the diploe gradually thinned and finally disappeared when approaching the sagittal suture. Considering this, the absence of the diploe might not result from the taphonomic process. If so, the extension of the DCs and their connection with other vessels might have never taken place in this area. This was a rare trait among all the fossil and extant specimens in this study. In the Hexian cranium, the connections between the parietal DCs and superior sagittal sinus could only be found in the posterior

one-third of the parasagittal area, where the DCs coursed in the medial-lateral direction and anastomosed with the left parietal foramen. The connection of the DCs with the MMV could be found in the lateral parts of the parietal bones, where the DCs coursed in diverse directions and a pair of long branches descended towards the asterion.

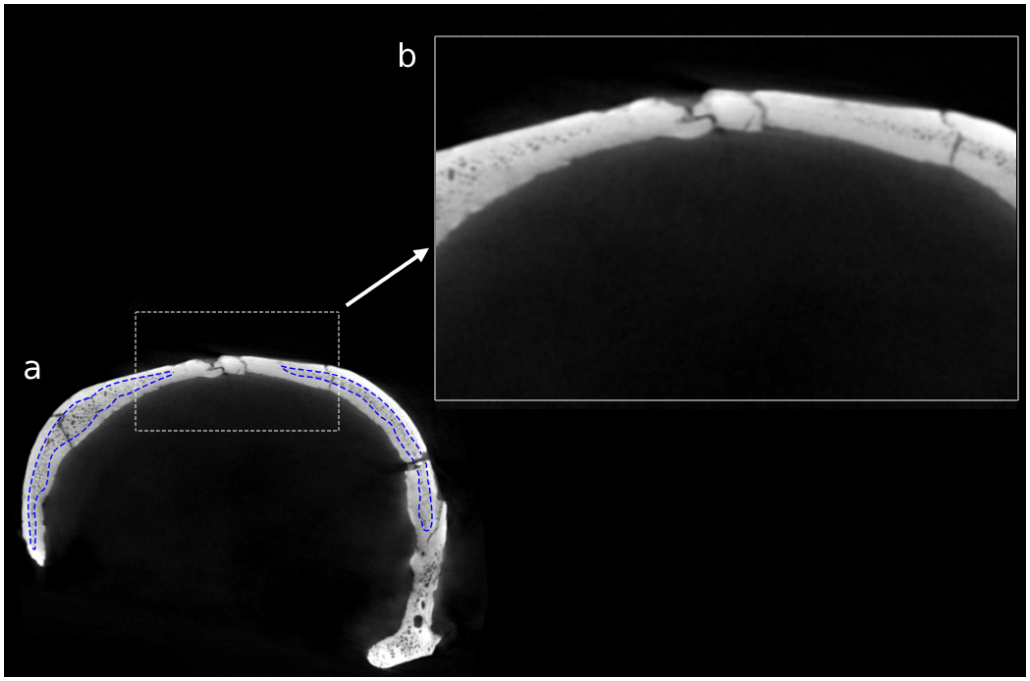

Figure 5.20 The diploic layer (blue dashed lines) was shown in the coronal section of the Hexian skull (a). The close-up (b) shows the diploe gradually thins when approaching the sagittal suture until it disappears.

In the right asterional area, the mastoid emissary channel was preserved and connected to the transverse-sigmoid sinus. In the better-preserved left asterional area (Figure 5.22), it was noticeable that the long parietal DC branch anastomosed with the petrosquamous sinus, anterior to the asterion. The transverse-sigmoid sinus receiving a tributary from the petrosquamous sinus was located inferior to the asterion, with no direct connection with the parietal DC. Instead, the transverse-sigmoid sinus was connected with a branch of the occipital DC, posterior to the asterion. The drainage pattern of the left asterional area was classified as pattern D.

The other part of the occipital DC network was located along the midline, coursing in

the superoinferior direction. These branches anastomosed extracranially with the occipital vessels, and intracranially with the superior sagittal sinus.

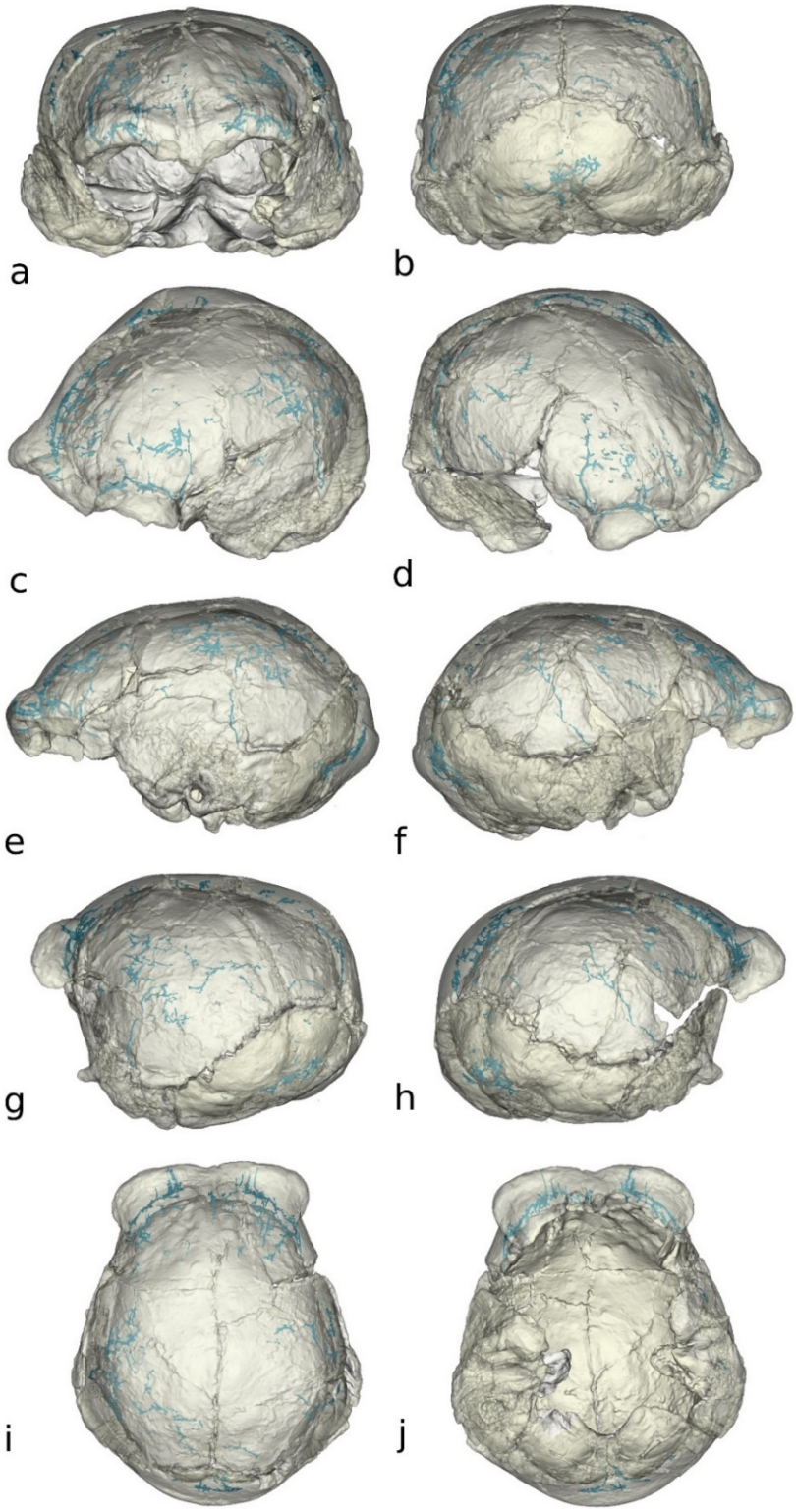

Figure 5.21 The diploic channels (in blue) in the Hexian cranium, shown in the anterior (a), posterior (b), anterolateral (c and d), lateral (e and f), posterolateral (g and h), superior (i), and inferior (j) views.

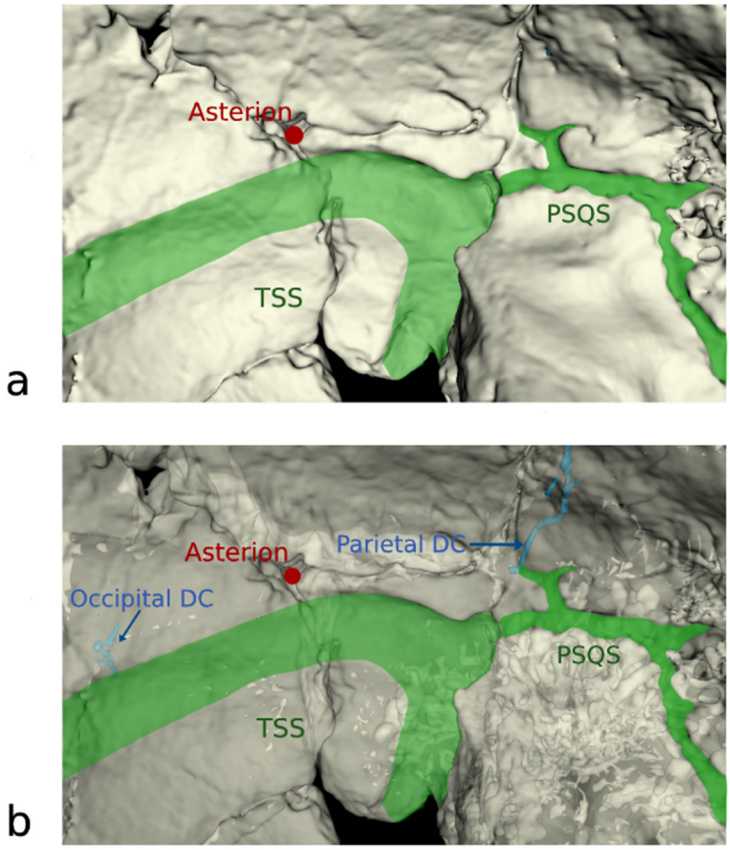

Figure 5.22 The drainage pattern surrounding the asterion is shown in the opaque (a) and transparent (b) views.

Kabwe 1

Although the outer and inner surfaces of the Kabwe 1 cranium were well-preserved, the diploic structures were considerably affected by the taphonomic process. All over the cranium, there were many parts of the diploic layer filled with sediments. As a result, the DC branches inside these parts, if there were any, could not be identified through Micro-CT. However, the visible branches in other intact parts could provide us with rich information through a qualitative way about the drainage pathways. The DCs were only found in the frontal, parietal, and occipital bones (Figure 5.23). Among them, the parietal bones seemed to possess the most abundant DC branches, even though much of their diploic layer was damaged and many branches were incomplete.

In the frontal bone, most DC branches extended in the anteroposterior direction. The DCs in the supraorbital torus anastomosed with the periorbital vessels and gave off branches extending into the frontal sinus. Likewise, many emissary channels bridged the periorbital vessels and frontal sinus directly, without passing through DCs. While most DC branches in the supraorbital torus were short, which was not a consequence of preservation, there was a long branch on the right side running into the frontal squama and pterional region, where most long branches were located.

The DCs in the frontal squama and pterional region did not display anastomosis with the extracranial vessels, which might result from the preservation condition of the outer table. Still, these DCs in the frontal squama showed clear connections with the meningeal vessels and superior sagittal sinus. As for the pterional region, it was noticeable that the DCs descend along the lateral margin of the orbital plates, entering the sphenoparietal sinus. Also, the stem of MMV courses in a short bony channel inside the pterional region, where it receives tributaries from the frontal and parietal DCs. The stem of the OMV coursed through another bony channel in the pterional region, but the stem neither connected to the frontal DCs nor the parietal DCs.

Along the sagittal suture, there were many short parietal DC branches extending in the medial-lateral direction. They were connected with the superior sagittal sinus and one of them connected to the parietal foramen on the left side. Because of the preservation, it was unknown whether there were other foramina bridging the DCs and extracranial vessels. Besides these small branches, the main parietal DC branches were distributed in the lateral and inferior parts of the bones. They coursed in the anteroposterior direction and gave off many shorter branches coursing in the superoinferior direction. These DCs in the lateral and inferior parts anastomosed intracranially with the MMV. Among them, one branch descended to the left asterion region, connecting to the transverse-sigmoid sinus.

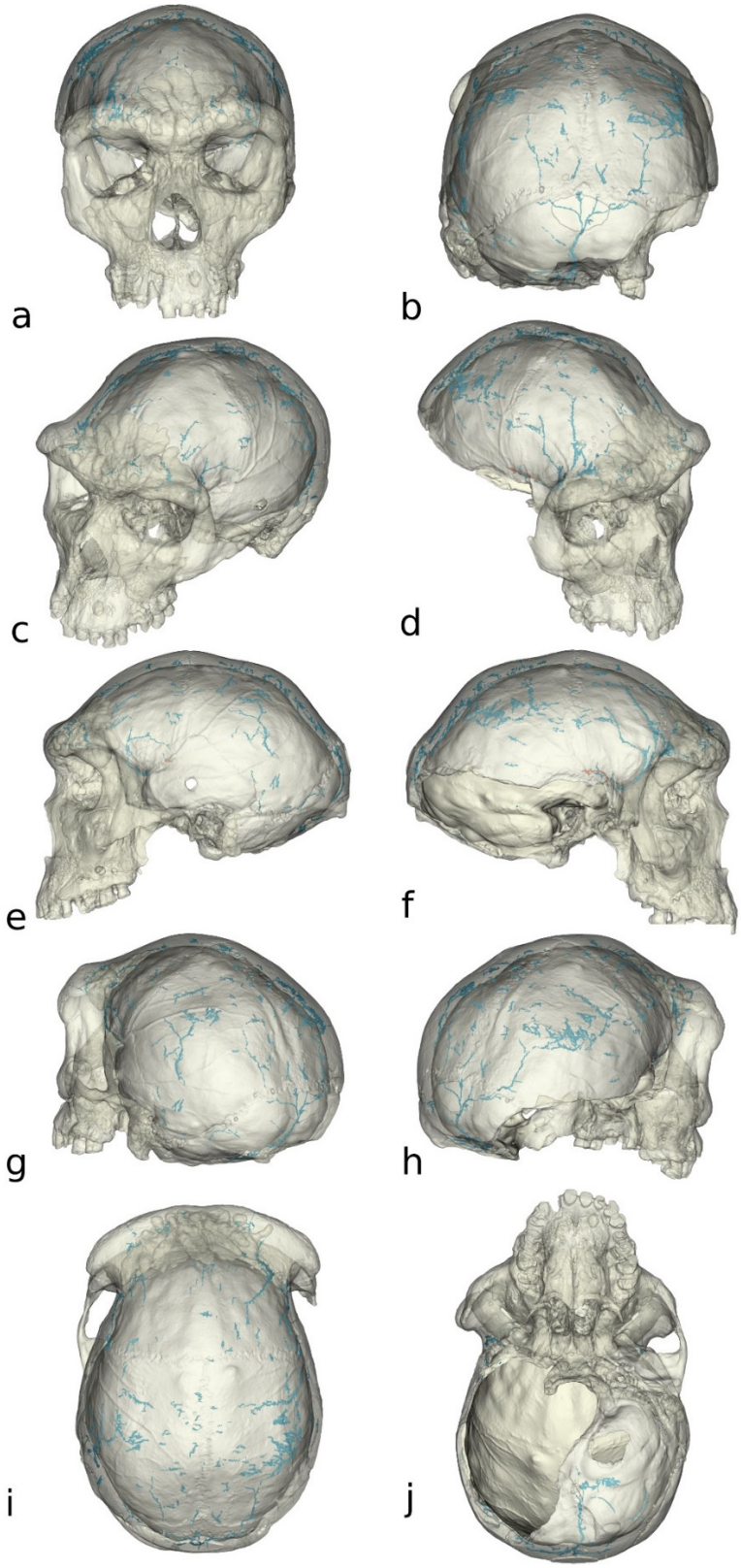

Figure 5.23 The diploic channels (in blue) in the Kabwe 1 cranium, shown in the anterior (a), posterior (b), anterolateral (c and d), lateral (e and f), posterolateral (g and h), superior (i), and inferior (j) views.

The left asterion was preserved well and covered by the transverse-sigmoid sinus (Figure 5.24). The petrosquamous sinus was found close to the asterion and connected with the transverse-sigmoid sinus, but there was no detectable anastomosis between the petrosquamous sinus and DCs. The connecting point between the transverse-sigmoid sinus and parietal DCs was at the suture, anterior to the asterion, while the connecting point between the transverse-sigmoid sinus and mastoid emissary vessel was at the temporal bone, anteroinferior to the asterion. The transverse-sigmoid sinus also developed a small branch posterior to the asterion, anastomosing with one occipital DC branch located along the lower lambdoid suture. The drainage pattern in the asterional area was classified as the pattern F.

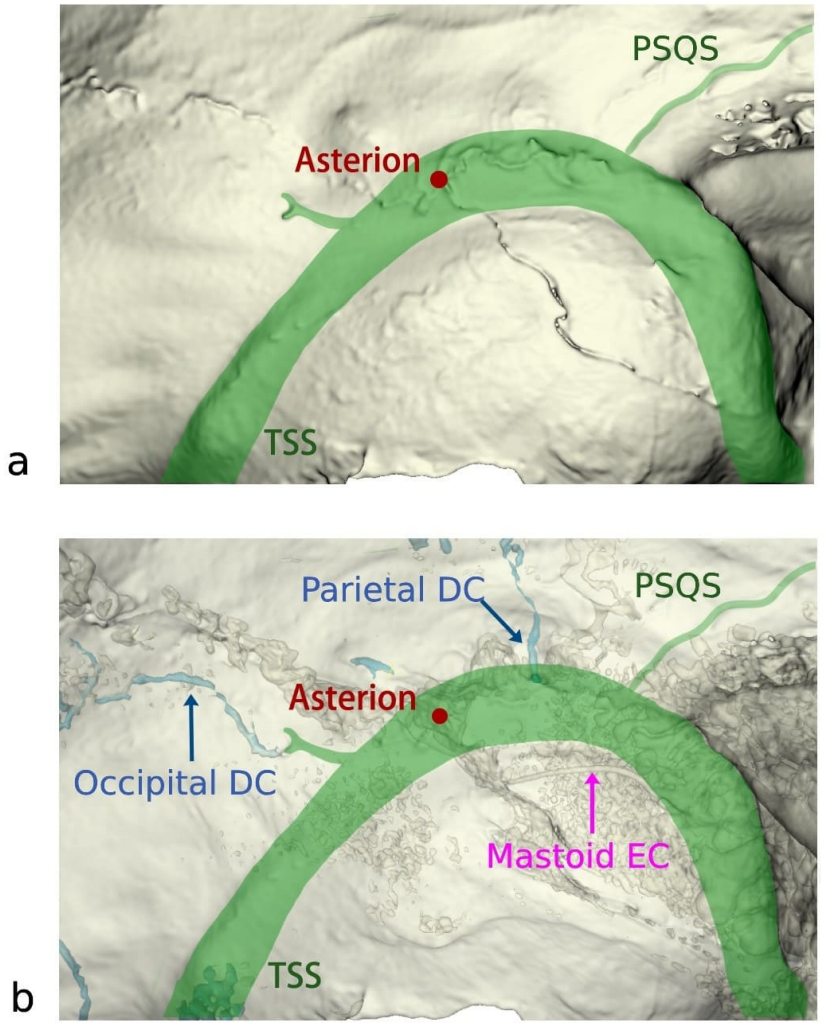

Figure 5.24 The drainage pattern surrounding the asterion is shown in the opaque (a) and transparent (b) views.

Other occipital DCs were distributed along the sagittal plane, with a single branch extending into the cerebral fossa. These branches connected intracranially with the superior sagittal sinus and extracranially with the occipital vessels. The superior part of the occipital DCs extended across the suture and fused with the parietal DCs, and the latter was fused with the frontal DCs. Thus, the frontal, parietal, and occipital DCs formed a long and direct drainage way running through the entire cranium.

Florisbad

The diploe of the incomplete Florisbad cranium had been filled by sediments. Most DCs were thus rendered unidentifiable. Still, several frontal and parietal DC branches were detected (Figure 5.25).

A DC branch coursed along the supraorbital torus, anastomosing with the extracranial vessels (periorbital or superficial temporal vessels) through a large foramen on the external surface. Due to the taphonomical damage, no complete DC branches were found surrounding the frontal sinus. However, a short channel linked the diploe with the frontal sinus (Figure 5.26), indicating that the DC network in Florisbad should have a connection with the sinus. In addition, many emissary venous channels were found in the torus, bridging the frontal sinus and periorbital vessels (Figure 5.26).

Incomplete DC branches were found in the frontal squama. The branch adjacent to the frontal crest extended to a large foramen which might be the connecting point between the DC network and the superior sagittal sinus. The DCs near the temporal line were adjacent to the meningeal vessels, but no connections were found between them. Incomplete DC branches were also found in the parietal bones. They seemed to anastomose with the posterior branch of MMV.

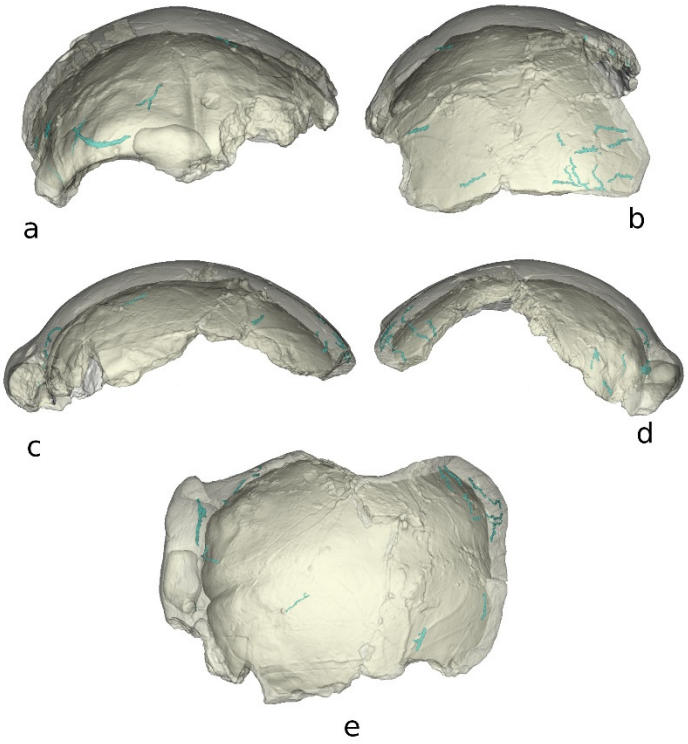

Figure 5.25 The diploic channels of Florisbad, shown in the anterior (a), posterior (b), lateral (c and d), and superior (e) views.

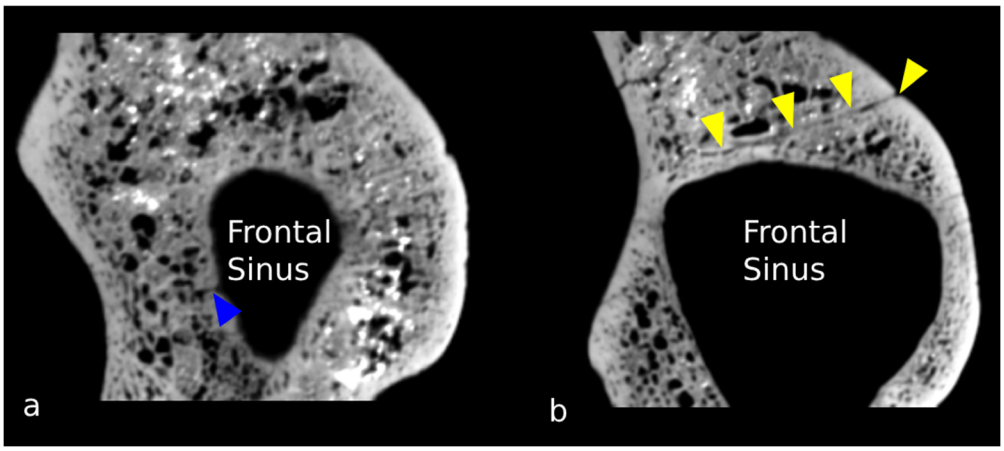

Figure 5.26 The sagittal section of the supraorbital torus. The short channel (a, blue arrow) links the frontal sinus and the diploe, and an emissary channel is marked by yellow arrows (b).

LES 1

The diploic layer, frontal sinus, and most other internal structures of the remained part of the specimen were well-preserved. The imprints of the meningeal vessels were

obscure, with a few main branches identifiable. Generally, the DC network in the cranium displayed a high degree of symmetry and was highly developed (Figure 5.28). Most DCs were found in the frontal, parietal and occipital bones, with few branches detected in the sphenoid bone. Among them, the frontal and parietal bones held the most abundant branches.

In the frontal bone, the supraorbital torus housed two pairs of long DC branches running in the medial-lateral direction, along the anterior and posterior borders of the ridge. The DCs in the supraorbital torus connected to the AMV, periorbital vessels, frontal sinus, and possibly superficial temporal vessels. Also, these DCs extended into the frontal squama, the pterional region of the sphenoid bone, and possibly the left orbital plate, in which a microscopic foramen linked the DCs with the ophthalmic vessels.

The DCs in the frontal squama are concentrated at the lateral sides, where the main DC branches coursed in the anteroposterior direction and ramified medially and laterally. These DCs connected to the extracranial vessels (including at least the superficial temporal vessels), superior sagittal sinus, and meningeal vessels. Still, because of the damage in the optical plates, it could not be confirmed if these meningeal vessels in the frontal squama were the OMV or MMV. Together with the DCs of the supraorbital torus, the DCs from the squama extended into the pterional region, where the DCs entered the stem of MMV and extracranial vessels.

In the parietal bones, the DCs were generally evenly distributed. Long branches coursed and ramified in many directions and seemed connected with the frontal DCs. The outer surface of the parietal bones manifested many microscopic foramina linking the DCs and extracranial vessels. There was no parietal foramen along the sagittal suture, but this might result from the taphonomic damage in the posterior part of the bones. On the inner surface, many foramina linked the DCs with the MMV and superior sagittal sinus. Especially, there were foramina, close and superior to the asterion, linking the

descending DC branches with the transverse-sigmoid sinus and petrosquamous sinus (Figure 5.27). The imprint of the transverse-sigmoid sinus overlapped the asterion. The connecting points of the transverse-sigmoid sinus with the petrosquamous sinus and mastoid foramen were anterior to the asterion, while its connecting point with the occipital DCs was located posterior to the asterion. The drainage pattern in the asterional region was classified as pattern A.

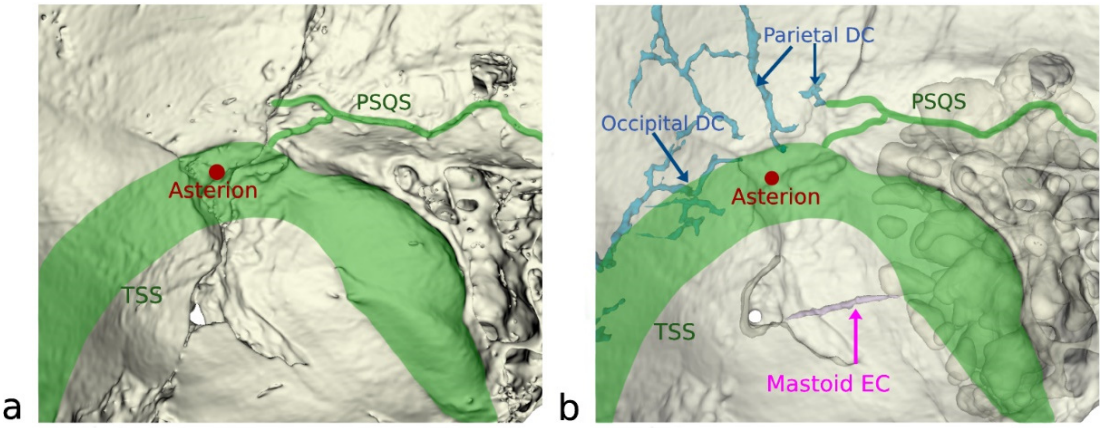

Figure 5.27 The drainage pattern surrounding the asterion is shown in the opaque (a) and transparent (b) views.

The occipital DC network was not complete because of the taphonomic damage. The remained occipital DCs on the left side anastomosed with the parietal DCs and extracranially with the occipital vessels. As the DCs in the frontal, parietal, and occipital bones were connected, the cranium displayed a long and direct drainage way running through the entire cranium.

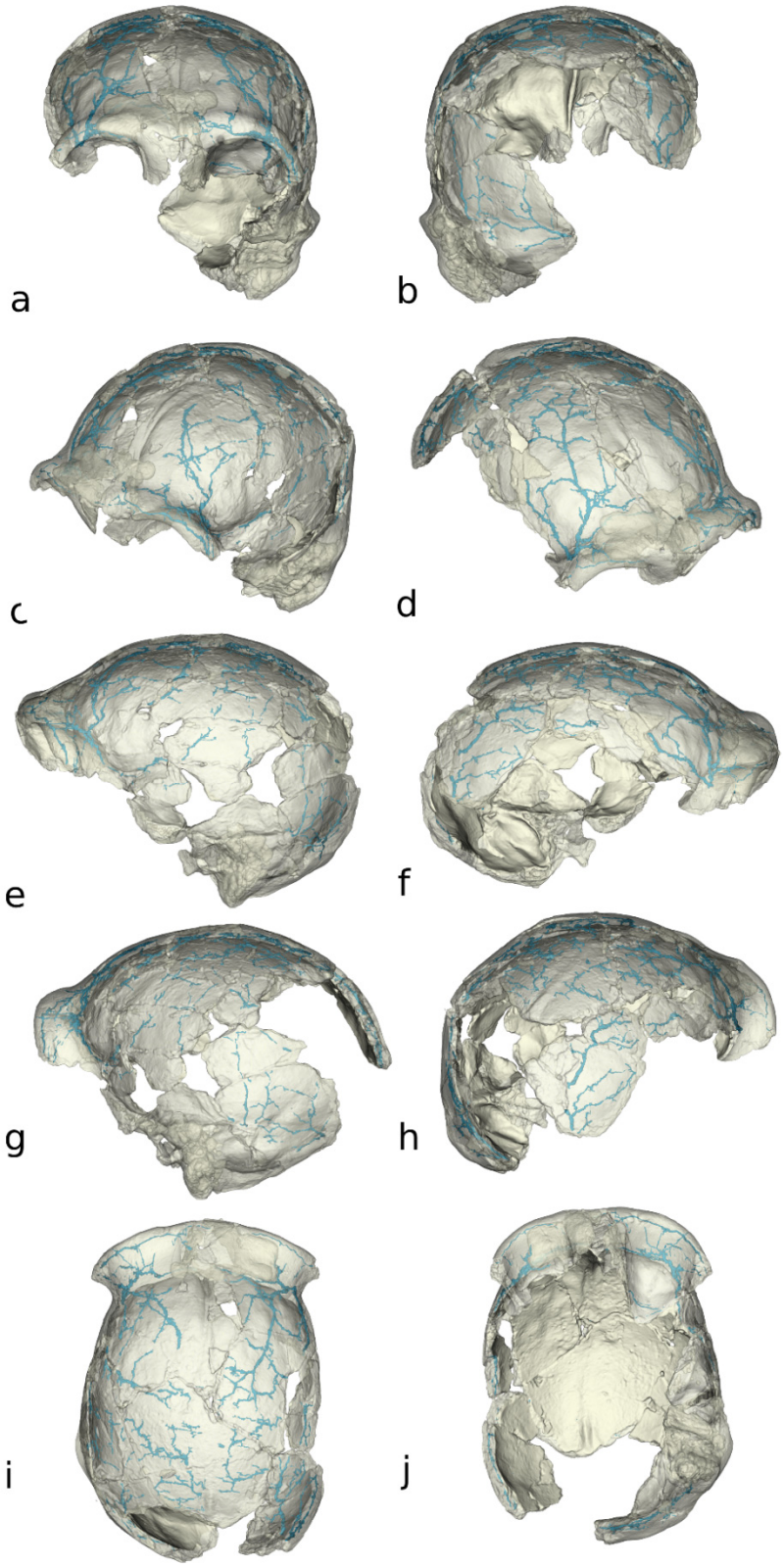

Figure 5.28 The diploic channels (in blue) in the LES 1 cranium, shown in the anterior (a), posterior (b), anterolateral (c and d), lateral (e and f), posterolateral (g and h), superior (i), and inferior (j) views.

Maba 1

The diploic layer of the Maba 1 specimen was generally well-preserved. A few diploic cavities in the frontal and parietal bones were filled with sediments or damaged by the fracture lines caused by taphonomic processes. This led to minor discontinuities in some DC branches in 3D reconstruction. Still, it did not have a significant impact on the qualitative analysis of the DC distribution and drainage pattern. As shown in Figure 5.29, the DCs of the Maba 1 specimen were mainly found in the frontal and parietal bones, while some short and narrow branches were housed in the zygomatic and sphenoid bones.

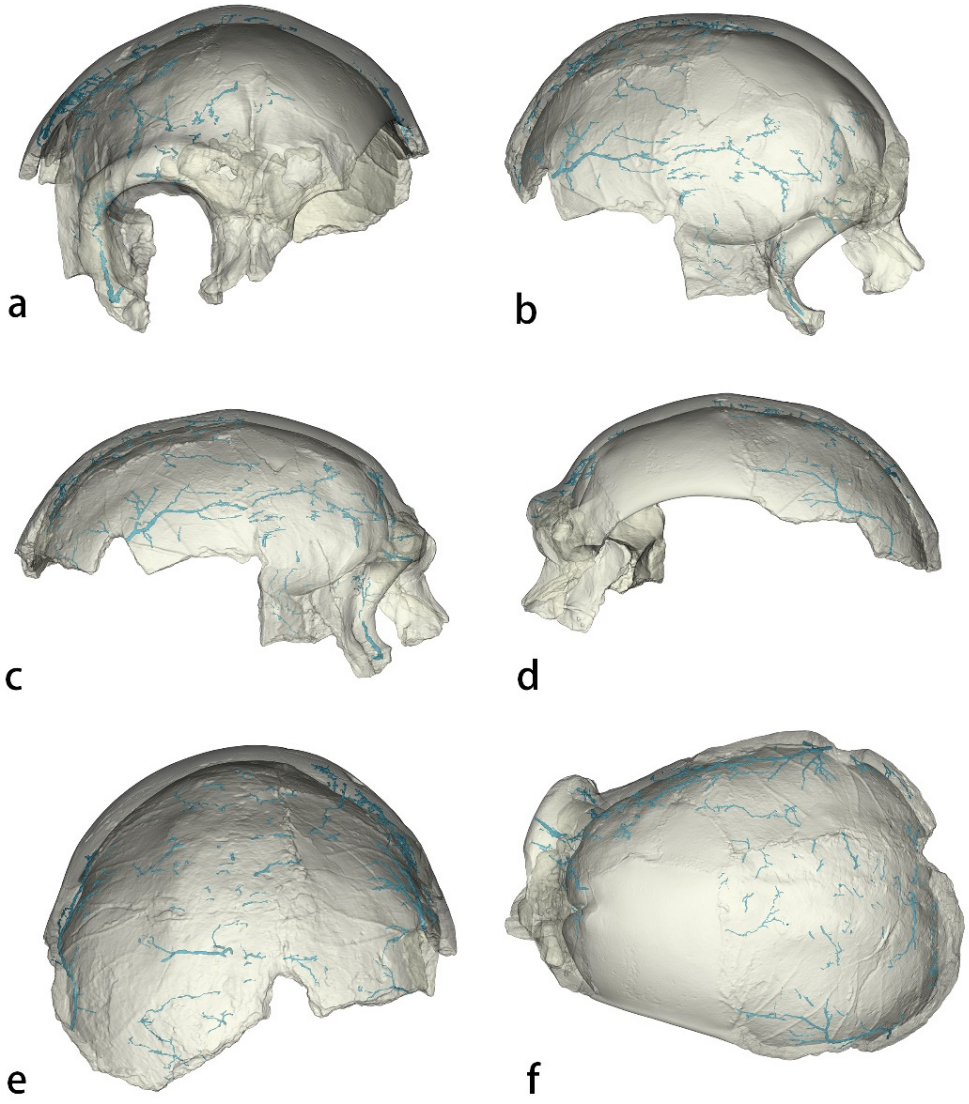

Figure 5.29 The diploic channels (in blue) in the Maba 1 cranium, shown in the anterior (a), anterolateral (b), lateral (c and d), posterior (e), and superior (f) views.

The frontal DCs mainly coursed in the anteroposterior direction, extending from the frontal squama to the supraorbital torus. One branch in the right supraorbital torus extended inferiorly into the zygomatic bone and finally entered the orbital vascular system through a foramen at the inferolateral side of the orbit. Besides, all the DC branches in the supraorbital torus extended extracranially into the periorbital vessels. Some of these branches in the supraorbital torus also extended intracranially into the superior sagittal sinus, frontal sinus, and meningeal vessels. Because of the preservation condition, the origin of these meningeal vessels could not be confirmed, but they seemed to be derived from the stem of MMV. What is more, in the preserved orbit, there was no trace of direct connections between the orbital vascular system and the meningeal branches. Interestingly, there were emissary channels in the frontal crest directly linking the superior sagittal sinus and extracranial vessels (probably the superficial temporal vessel), without connecting to the DCs.

As for the frontal squama, there were many foramina on the extracranial surface linking the DCs and the extracranial vessels (including at least the superficial temporal vessel). On the intracranial surface of the squama, there were multiple foramina linking these DCs with the anterior branch of the MMV. Also, on the right side, several DC branches entered the sphenoid bone, finally extending into the stem of the MMV at the pterional region and into the extracranial surface. The posterior part of the DCs in the squama was continuous with the parietal DCs. As the coronal suture was largely fused, there was no obvious boundary between the two networks

The parietal DCs in the lateral part of the parietal bones were long branches coursing in the anteroposterior direction. On the contrary, the DCs close to the sagittal suture were much shorter and mainly coursed along the coronal plane. On the intracranial surface, many foramina linked the former with the anterior and posterior branches of the MMV, while the latter was mainly connected with the superior sagittal sinus. On

the extracranial surface, many foramina linked both of them with the extracranial vessels (including at least the superficial temporal vessel). Although most of these communicating foramina were microscopic, there was a large parietal foramen (largest diameter = 2.1 mm) on the left side of the parietal bone, adjacent to the sagittal suture (Figure 5.30). The parietal foramen linked the superior sagittal sinus and extracranial vessels, and it was anastomosed with the DCs. The parietal foramen was considered absent in a previous study (Woo & Pen, 1959). This was probably because the outlet of the foramen was covered with sediments (Figure 5.30), and thus it was difficult to identify unless using CT scanning. Also because of the preservation, the right side of the sagittal suture was lost. Thus, it was unknown whether there was another parietal foramen on the other side.

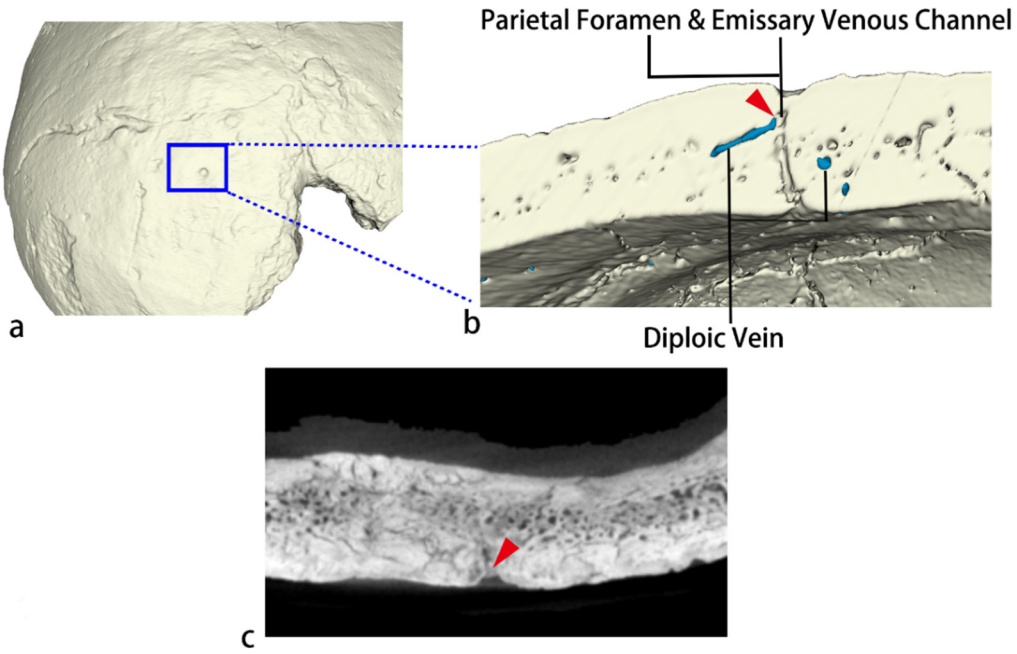

Figure 5.30 The parietal foramen found in the Maba 1 cranium (a). The emissary channel inside the parietal foramen links the extra- and intra-cranium space with the diploic channels (b). The outer part of the foramen is filled with sediments (c, red arrow), which makes it difficult to identify unless using Micro-CT scanning.

The inferior part of the parietal bone and the occipital bone were lost as well, so it was

impossible to detect the ramification and drainage pattern of the skull base. However, the posterior ends of the main parietal DC branches tended to course inferiorly towards the asterional region, like all other Mid-Pleistocene hominin specimens and modern specimens. Considering the parietal and frontal DCs were continuous, the DC network in the Maba 1 specimen formed a direct pathway transporting blood between the facial area and the posterior part of the cranium.

5.3.3 Late Pleistocene hominins

Simple descriptions of the DCs of the Late Pleistocene specimens have been published in my papers (Hui & Balzeau, 2023b, 2023a). Here, this current study reused some data, figures, and findings from these published papers and provided a more comprehensive description with more details.

La Quina H5

The diploe of the specimen was well preserved. The DC network was highly developed, with the parietal bones housing the most DC branches (Figure 5.32).

In the frontal squama, there were two large branches on both sides running in the anteroposterior direction, with the left branch changing into the medial-lateral direction when approaching the supraorbital area. The drainage patterns of the two large branches were the same. The anterior ends of them connected to the frontal sinus and periorbital vessels, while the posterior ends crossed the coronal suture and anastomosed with the parietal DCs. Many small foramina were located on the ectocranial and endocranial surfaces, linking the large frontal DCs with the MMVs and superficial temporal vessels. Many other foramina were detected in the groove for the superior sagittal sinus, connected with the small DC branches scattered in the frontal squama center.

The parietal DC networks on both sides showed the spider pattern, with most branches radiating from the centre of the parietal bone. The whole network had connecting points

scattered in the bone with the MMVs and superficial temporal vessels. The DCs running superiorly connected with the superior sagittal sinus. The DCs approaching the left asterion connected to the petrosquamous sinus, without direct connections with the transverse-sigmoid sinus, which was located inferior to the asterion (Figure 5.31). The right asterional region was damaged and the drainage pattern was unclear. Besides, no parietal foramina appeared in the bones.

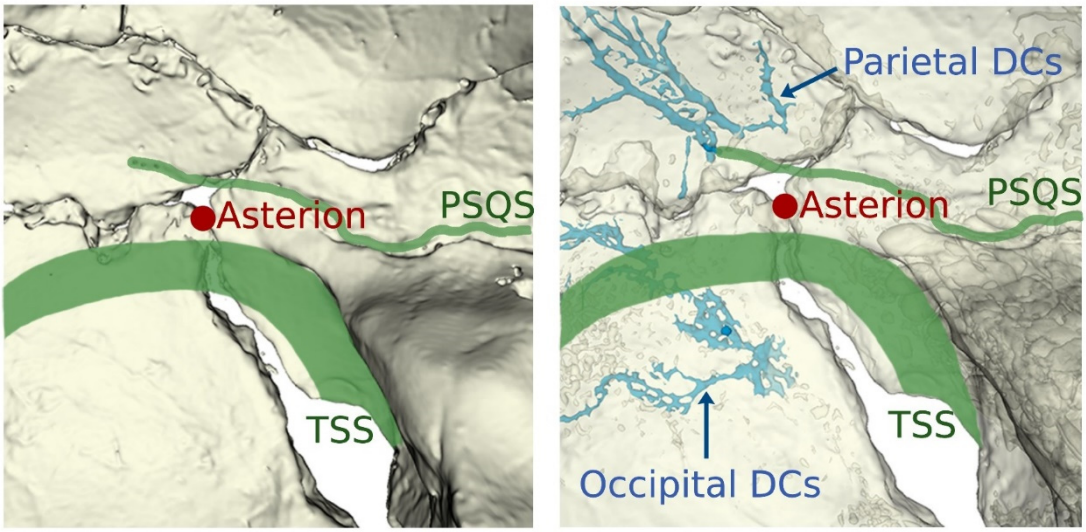

Figure 5.31 The drainage pattern in the asterional region of La Quina H5. The figure is from Hui & Balzeau (2023b).

There were two pairs of DC branches in the occipital bone. The superior pair was in the occipital plane, extending from the midline to the lambdoid suture. They were connected with the superior sagittal sinus, occipital vessel, and MMV. The inferior pair of occipital DCs were located in the nuchal plane, close to the asterion on both sides, extending both extracranially into the occipital vessel and intracranially into the transverse-sigmoid sinus. Thus, the drainage pattern of the left asterional regions was identified as pattern D.

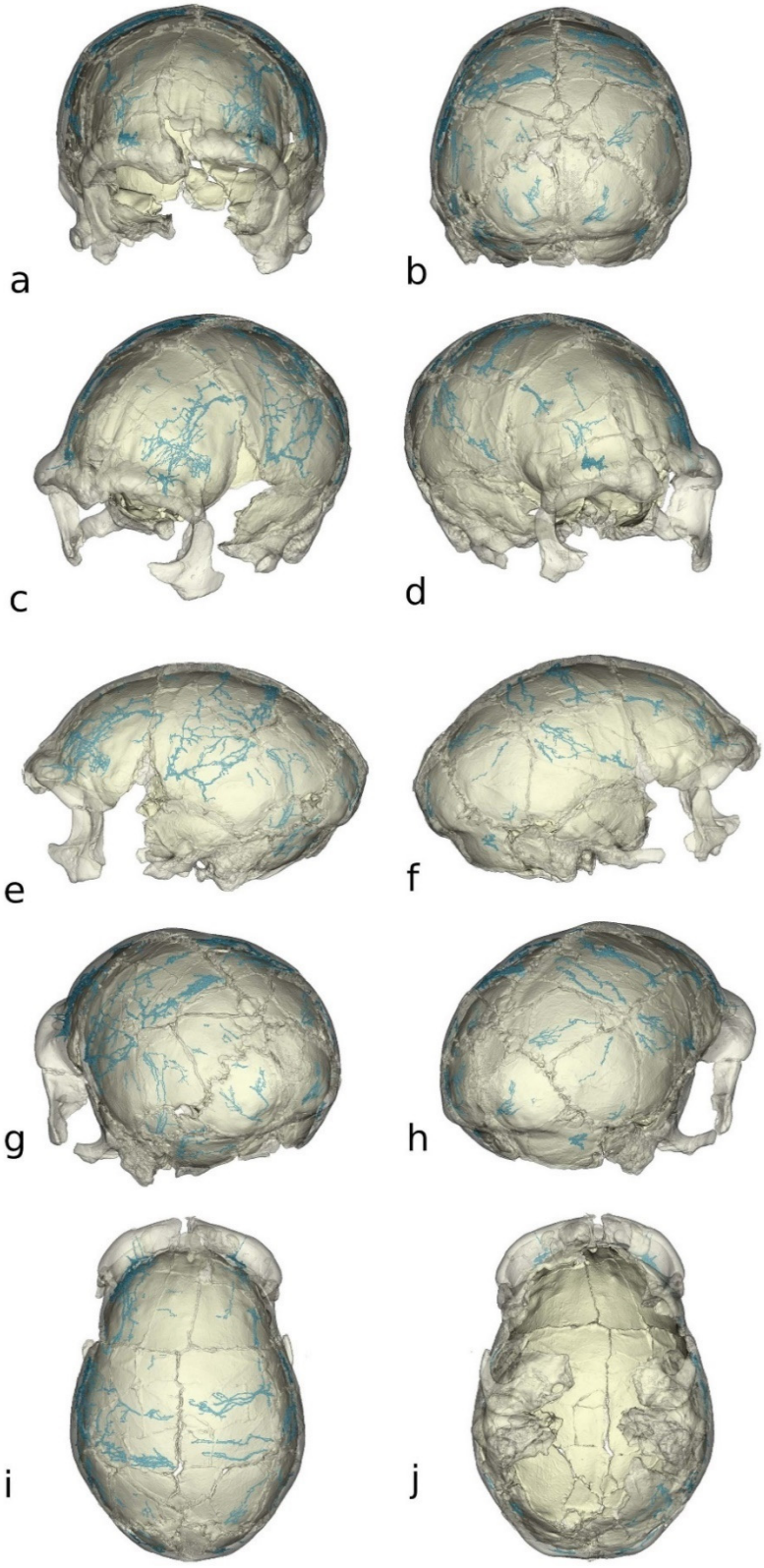

Figure 5.32 The diploic channels (in blue) in the La Quina H5 cranium, shown in the anterior (a), posterior (b), anterolateral (c and d), lateral (e and f), posterolateral (g and h), superior (i), and inferior (j) views.

La Chapelle-aux-Saints 1

The diploic structures of the specimen were very well preserved, despite a large area missing in the left parietal bone. The parietal bones housed the most and largest DC branches (Figure 5.33).

A pair of large DC branches ran across the frontal bone. In the supraorbital area, the DC branches connected with the frontal sinus and periorbital vessels. In the frontal squama, the DC branches connected to AMV, MMV and superficial temporal vessels. The DCs also ramified toward the midline of the squama, approaching but not anastomosing with the superior sagittal sinus. At the posterior edge of the frontal bone, the DCs ran posteriorly across the coronal suture and anastomosed with the parietal DCs. Besides, adjacent to the left pterion, the stem of MMVs entered a bony canal, where it anastomosed with the surrounding DC branches (including the frontal, parietal, and sphenoid DCs).

In the parietal bones, the DCs formed a reticulated network in a pattern similar to the spider type. The superior part of the spider-like network coursed in the mediolateral direction, approaching the sagittal suture and connecting to the superior sagittal sinus. As the anterior section of the sagittal suture was fused, some small DCs ran across the midline and bridged the parietal DC networks of the two hemicrania. In the asterional region on the left side (Figure 5.34), the drainage pathways of DCs formed the pattern D, in which the parietal DCs network connected with the petrosquamous sinus, while the occipital DCs connected to the transverse-sigmoid sinus, which was located inferior to the asterion. The asterional region on the right side was more seriously damaged, and it was only confirmed that the parietal DCs connected with the occipital DCs, and the latter connected to the transverse-sigmoid sinus. Besides, the whole parietal DC network had dense connecting points with the MMV. No parietal foramina appeared in the cranium, but many microscopic foramina bridged the DCs and superficial temporal vessels.

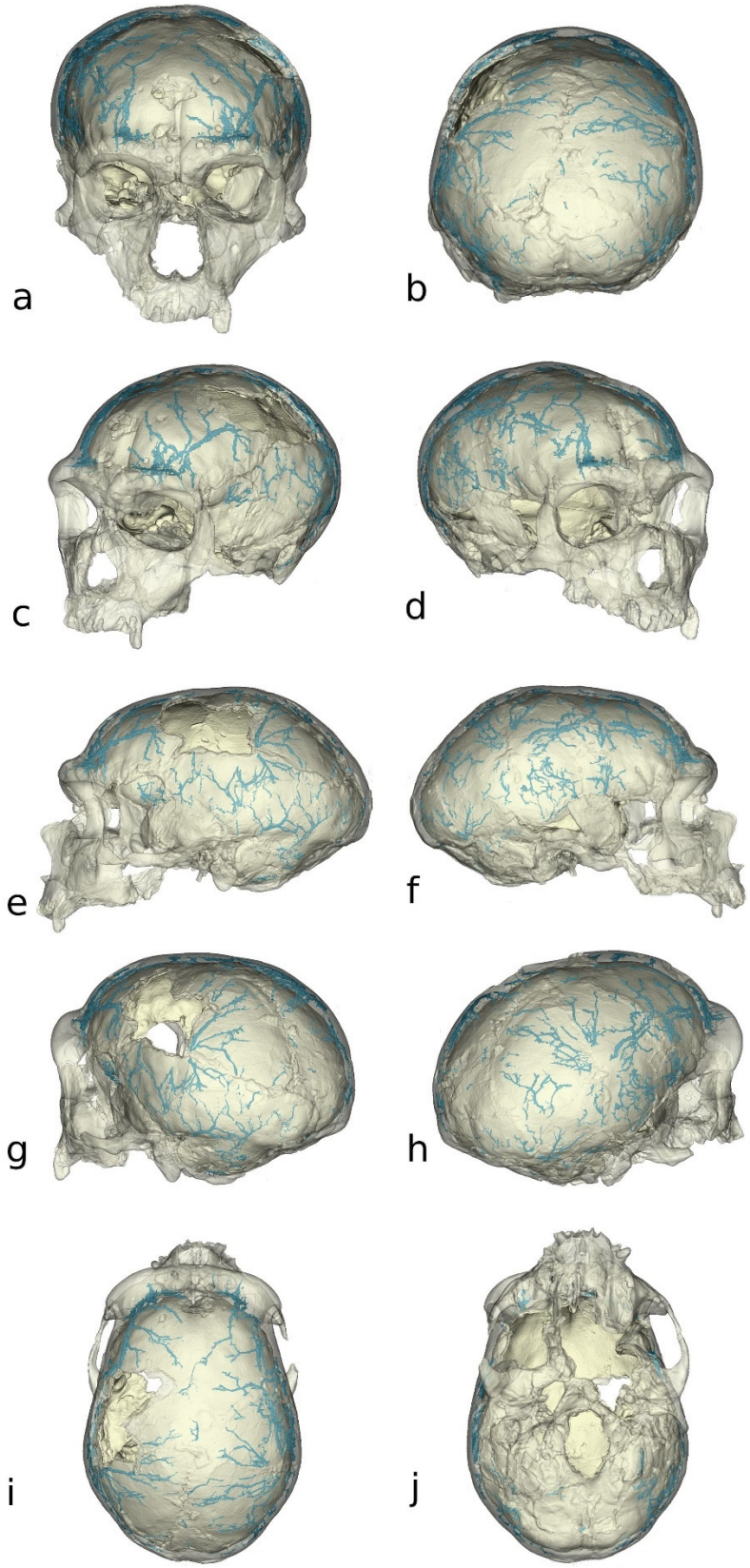

Figure 5.33 The diploic channels (in blue) in the La Chapelle-aux-Saints 1 cranium, shown in the anterior (a), posterior (b), anterolateral (c and d), lateral (e and f), posterolateral (g and h), superior (i), and inferior (j) views.

The occipital DCs could be divided into three main branches. The middle branch was located at the midline of the occipital bone, extending extracranially into the occipital vessel and intracranially into the superior sagittal sinus and the confluence of the sinuses. The two lateral branches extended along the lambdoid suture, from the occipital plane to the mastoid notch, connecting to the MMV, occipital vessel, and transverse-sigmoid sinus.

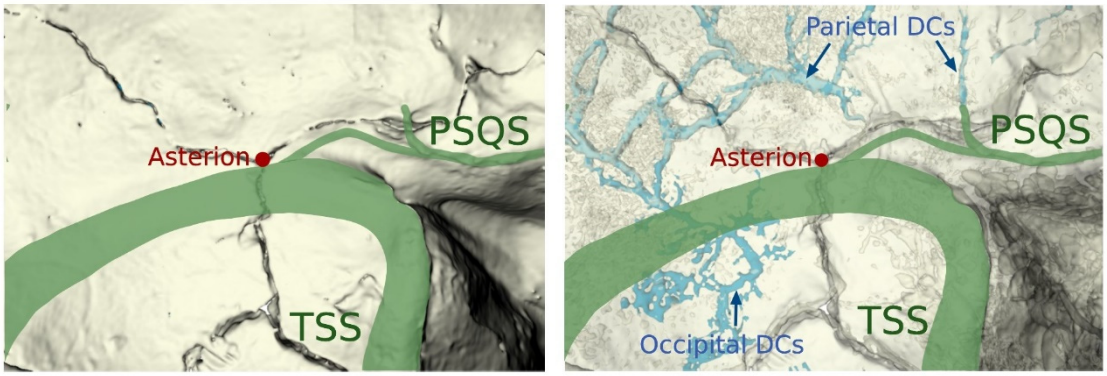

Figure 5.34 The drainage pattern in the asterional region of La Chapelle-aux-Saints 1.

La Ferrassie 1

The specimen was in fragments and many areas of the neurocranium were missing. It was clear that the parietal bones house more DC branches than the frontal and occipital bones (Figure 5.35).

In the frontal bone, there were two large DC branches draining parallel to the temporal lines in the squama. The anterior ends of both branches had connections with the periorbital vessels and superficial temporal vessels, while the posterior end connected to the MMV outside the pterion region. The left branch also connected to the frontal sinus, while the connections on the right side were unclear due to taphonomic damage. Between the two large DC branches, a pair of small DC branches were scattered in the frontal squama centre and connected with the superior sagittal sinus.

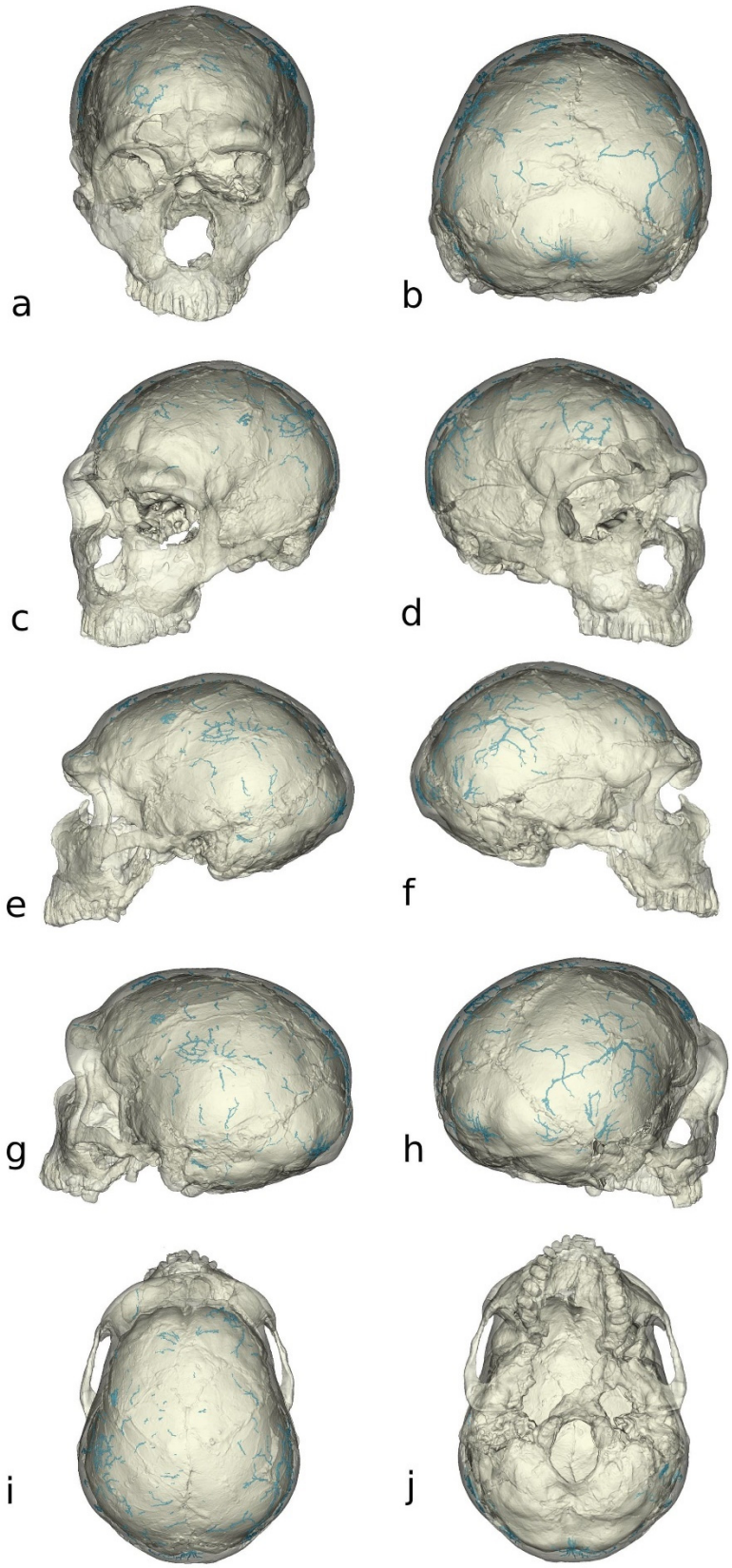

Figure 5.35 The diploic channels (in blue) in the La Ferrassie 1 cranium, shown in the anterior (a), posterior (b), anterolateral (c and d), lateral (e and f), posterolateral (g and h), superior (i), and inferior (j) views.

The preserved part of the left parietal DC network was likely in the spider pattern, while the pattern of the right could not be identified. The superior parts of the parietal DC networks on both sides had many branches ascending in the medial-lateral direction, connecting with the superior sagittal sinus. Another feature that the two sides had in common was that they both had dense connecting points with the MMV and extracranial vessels across the bones, though the parietal foramen was not present in the bones. Additionally, the asterional regions were not complete due to taphonomic damages. It was unclear whether the parietal DCs connect with the transverse-sigmoid sinus and petrosquamous sinus.

The DCs in the occipital plane could be divided into three sections. The middle was a 'tree-like' structure linked with the superior sagittal sinus, occipital vessels, and MMV. The other two parts were close to the asterion, anastomosing with the MMV and occipital vessels. In the nuchal plane, there were also two branches approaching the asterion. They extended extra-cranially into the occipital vessel, and the left one extended intracranially to connect with the transverse-sigmoid sinus.

Spy 1

Many areas of the cranium were not preserved and thus the DC network was not complete. Large areas of the lateral walls were replaced with artificial materials. The parietal bone housed the most DCs compared with the frontal and occipital bones (Figure 5.37).

The frontal DCs mostly ran in the anteroposterior direction. In the supraorbital area, the DCs connected to the frontal sinus and periorbital vessels. In the frontal squama, the DCs were connected with the superior sagittal sinus, superficial temporal vessel, and MMV. Especially, an independent DC branch inferior to the right temporal line seemed to extend to the pterional region, where it might connect with the stem of the MMV.

The DCs in the left parietal bones arose from the asterion, where they developed a large number of branches ascending towards the coronal and sagittal sutures. The distribution pattern was not recorded in the classification established by Hershkovitz et al. (1999). When ascending anteriorly and superiorly, the parietal DCs anastomosed with the superior sagittal sinus and the stem and minor branches of MMV. Besides, many microscopic foramina linked the DCs with the superficial temporal vessels, though the parietal foramen was not present.

In the asterional regions on both sides, it seemed that the parietal DCs connect to the superior petrosal sinus (Figure 5.36). And there seemed no connection between the DCs and the trunk of the transverse-sigmoid sinus. Instead, the transverse-sigmoid sinus was inferior to the asterion and connected with occipital DCs coursing along the lambdoid suture. This drainage pattern classified as 'pattern G' was rather rare (Figures 5.7, 5.13, and 5.36), as the connection between the superior petrosal sinus and parietal DCs did not appear in other fossil and extant specimens. Additionally, the occipital DCs connected to the superior sagittal sinus, and occipital vessel.

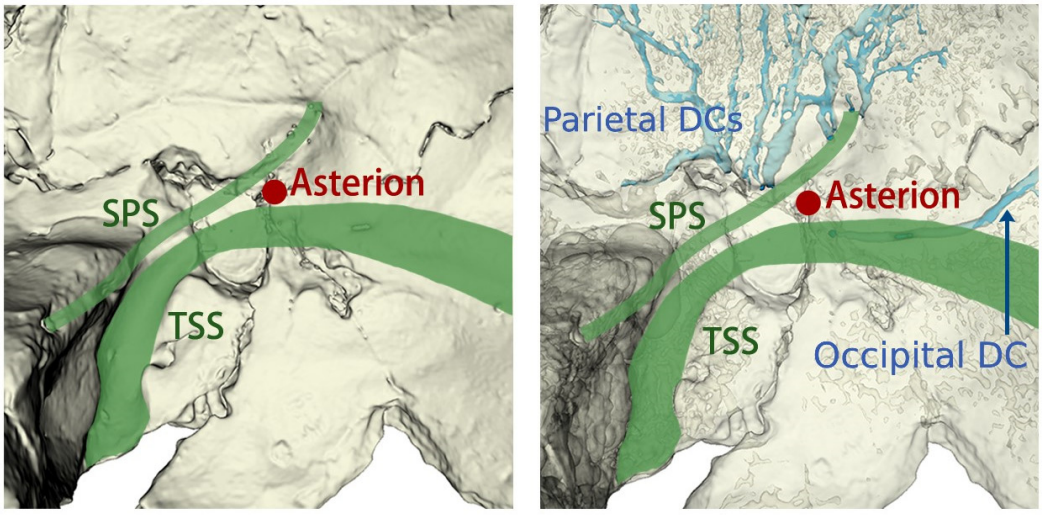

Figure 5.36 The drainage pattern in the asterional region of Spy 1. The figure is from Hui & Balzeau (2023b).

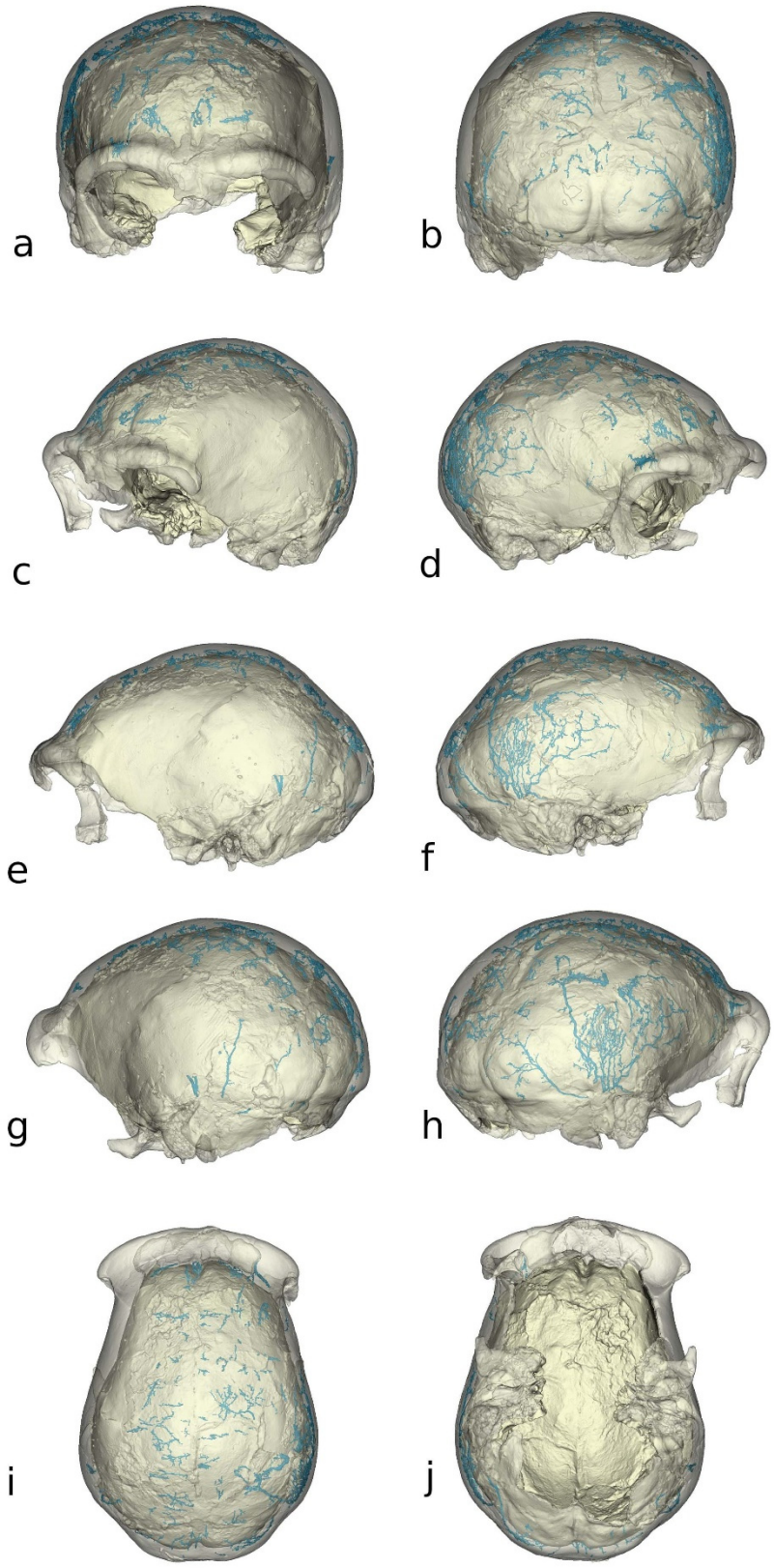

Figure 5.37 The diploic channels (in blue) in the Spy 1 cranium, shown in the anterior (a), posterior (b), anterolateral (c and d), lateral (e and f), posterolateral (g and h), superior (i), and inferior (j) views.

Spy 10

Like the cranium of Spy 1, many large areas in the cranium of Spy 10 were missing and replaced by artificial materials. Most DCs were housed in the frontal and parietal bones (Figure 5.38).

In the frontal bone, many large DC branches were distributed in the supraorbital area and frontal squama, running parallel to the temporal lines. In the supraorbital area, the DCs connected with the frontal sinus and periorbital vessels. In the squama, the DCs connected to the MMV and superficial temporal vessel, and ramified towards the midline, where they had connecting points with the superior sagittal sinus.

The distribution pattern of parietal DCs on the left side was similar to that of Spy 1, which was not recorded in the classification established by Hershkovitz et al. (1999). The distribution pattern of the right side was close to the spider type, but they had more ramifications than the typical mode recorded by Hershkovitz et al., (1999). Across the parietal bones on both sides, the DC network of Spy 10 had dense connecting points with the MMV. The stem of MMV entered a bony canal in the pterional region on the left side and anastomosed with the parietal DCs. Although parietal foramen was not present, many microscopic foramina linked the parietal DCs and superficial temporal vessels. Along the sagittal suture, the superior sagittal sinus had many connecting points with the parietal DCs. In the asterional regions, the drainage pattern was not complete due to taphonomic damages. The asterion landmarks were superior to the transverse-sigmoid sinus. The parietal DCs on the left side anastomosed with a vessel that seemed to be a small branch of the transverse-sigmoid sinus or petrosquamous sinus. Although there was no direct connection between the parietal DCs and the trunk of the transverse-sigmoid sinus, the latter had some minor connections with the DCs in the petromastoid part of the temporal bones on both sides, which were also connected with the emissary channels housed in the mastoid foramina.

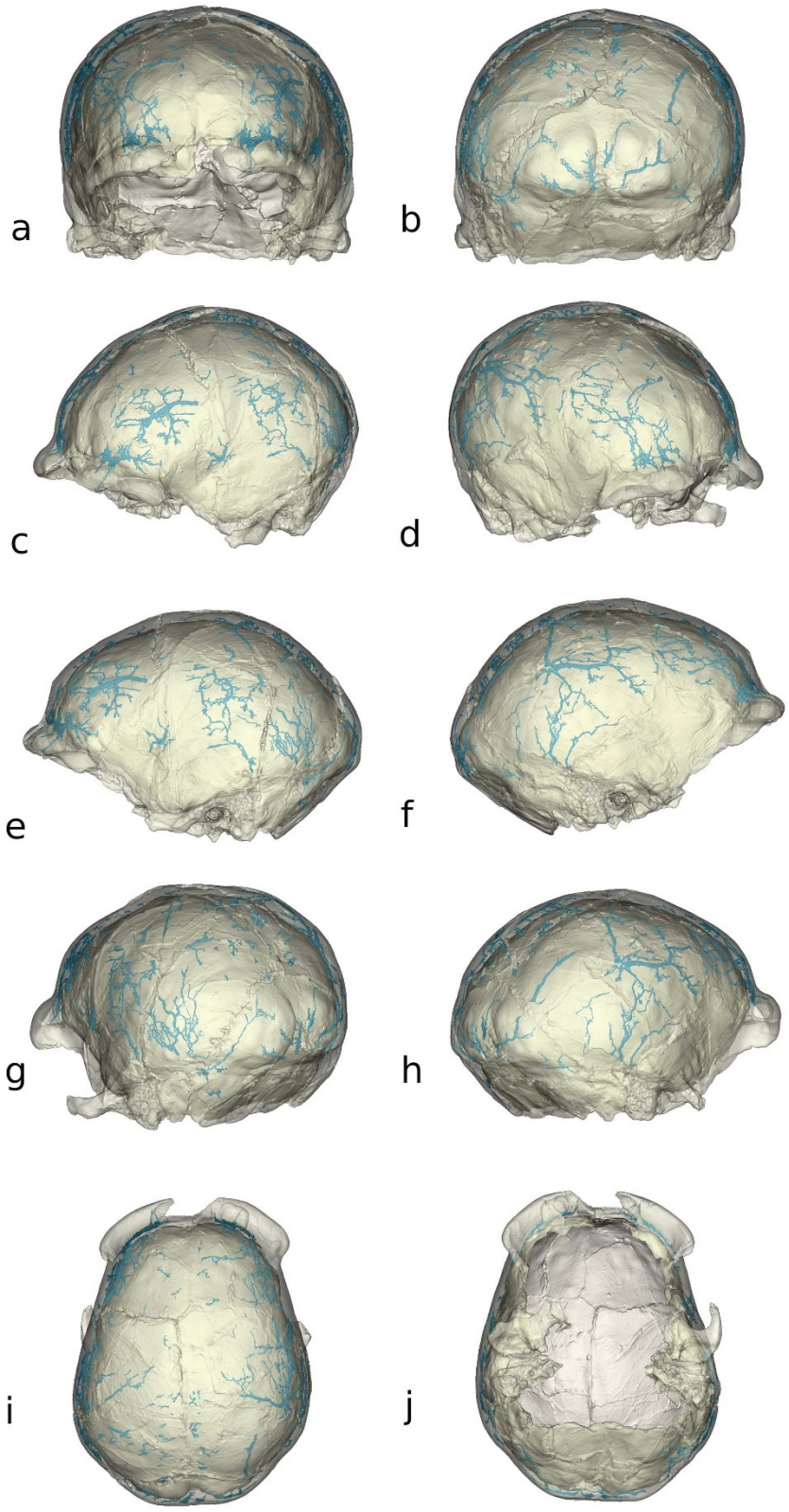

Figure 5.38 The diploic channels (in blue) in the Spy 10 cranium, shown in the anterior (a), posterior (b), anterolateral (c and d), lateral (e and f), posterolateral (g and h), superior (i), and inferior (j) views

In the occipital bone, DC branches were mostly scattered in the occipital plane. There was a pair of DC branches coursing along the lambdoid suture, linked with the MMV and occipital vessel. This pair of branches had no connection with the transverse-sigmoid sinus, though they arrived at the diploe adjacent to the sinus. The other branches in the occipital bone form a 'tree-like' structure radiating from the lower edge of the suprainiac fossa, draining into the superior sagittal sinus and occipital vessel.

Cro-Magnon 1

The neurocranium was nearly complete, despite a pathologically damaged area in the frontal bone. The frontal and parietal bones housed more DCs than other bones (Figure 5.39). The frontal and parietal DCs were comparably developed.

In the frontal bone, most DC branches coursed in the mediolateral direction. The DC branches in the supraorbital area ran around the orbit, extending into the zygomatic bone on the right side, and connecting to the frontal sinus and periorbital vessels on both sides. In the frontal squama, the DC branches approach the coronal suture and the midline of the frontal squama, connecting to the parietal DCs, MMV, superficial temporal vessel, superior sagittal sinus, and arachnoid granulations. Especially, in the pterional region, the stems of MMVs on both sides were embedded in the bony canals, inside which they anastomosed with the frontal and parietal DCs. The sphenoparietal sinus ran along the lesser wings of the sphenoid bone, receiving tributaries from the frontal DCs in the pterional region.

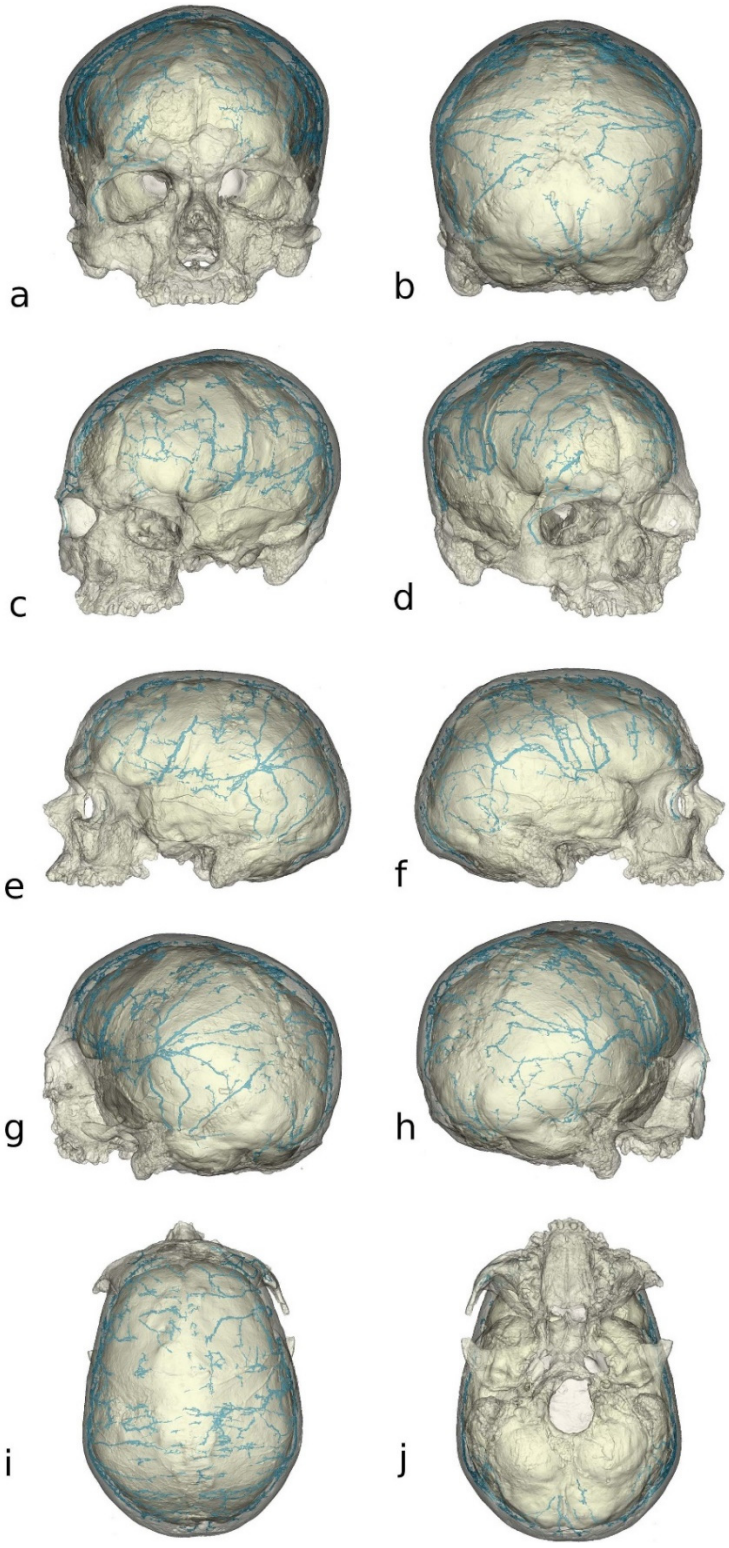

Figure 5.39 The diploic channels (in blue) in the Cro-Magnon 1 cranium, shown in the anterior (a), posterior (b), anterolateral (c and d), lateral (e and f), posterolateral (g and h), superior (i), and inferior (j) views

The parietal DCs on the left side manifested a spider pattern, and the DCs on the right were a hybrid of the spider and serpentine patterns. Along the sagittal suture, the parietal DCs had connections with the superior sagittal sinus, arachnoid granulations, and the left parietal foramen. Across the parietal bones, the DCs had many connecting points with the MMV and superficial temporal vessels. In the asterional regions on both sides, the asterion was at the same level as the transverse-sigmoid sinus. The parietal and occipital DCs directly connected to the trunk of the transverse-sigmoid sinus (pattern F, Figure 5.40). Additionally, the parietal DCs in the asterional regions connected to the occipital DCs on both sides and to the mastoid foramen and occipital vessel (or the posterior auricular vessel) on the left side.

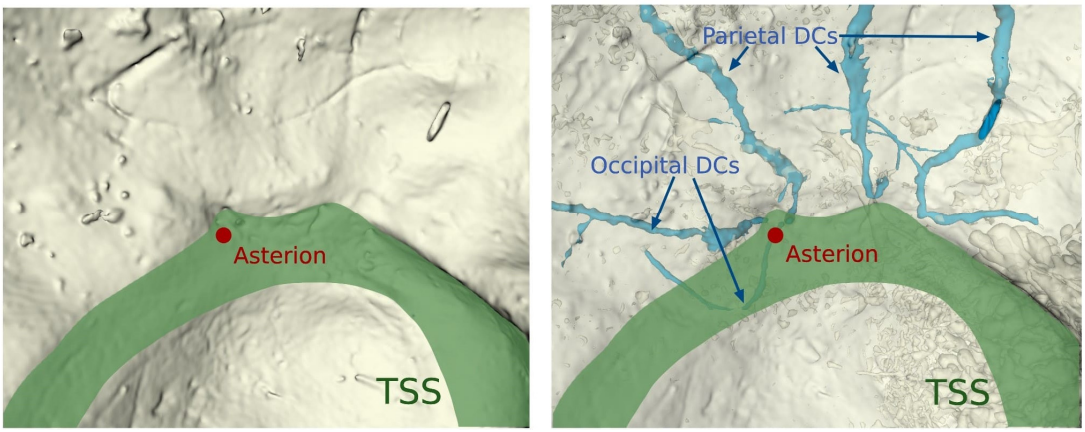

Figure 5.40 The drainage pattern in the asterional region of Cro-Magnon 1.

Outside the asterional regions, the occipital DCs branches arose from the superior nuchal line to the lambda. They had connecting points with the MMV, occipital vessel, superior sagittal sinus, and transverse-sigmoid sinus.

Cro-Magnon 2

The right half of the cranium was seriously damaged, while the left was relatively well preserved. The diploic structures of the remaining bones were clear to inspect. Most DCs were housed in the parietal bones (Figure 5.42).

In the frontal bone, the DC branches on both sides manifested a circle-like pattern,

extending from the supraorbital area to the frontal squama. These branches were connected with the superior sagittal sinus, periorbital vessels, and MMV. Constrained by the preservation condition, the drainage pattern surrounding the pterion was not detectable. But considering that the DC branches on the right side gave off minor arms towards the pterion, it might connect with the stems of MMVs or sphenoparietal sinus in the corresponding area.

In the parietal bones, most DC branches coursed in the superoinferior direction and their distribution patterns on both sides were similar to the coronal pattern. The large DC branches were concentrated in the anterior half of the bones, with some independent branches scattering in the posterior half. The parietal DCs had many connecting points with the MMV, superior sagittal sinus, and extracranial vessels. The parietal foramen appeared on the left side and connected to DCs. The asterional region on the right side was not preserved, while the one on the left side manifested the drainage pattern F, with the transverse-sigmoid sinus connected with parietal and occipital DCs (Figure 5.41). The asterion was covered by the imprint of the transverse-sigmoid sinus.

The occipital bone was not well preserved. The remained DCs were all in the occipital plane. They anastomosed with the MMV, superior sagittal sinus, and occipital vessel.

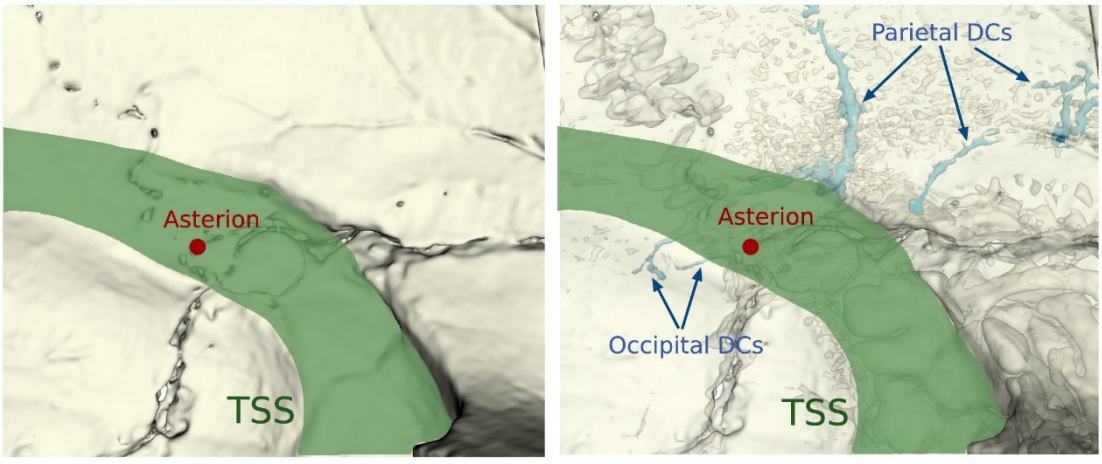

Figure 5.41 The drainage pattern in the asterional region of Cro-Magnon 2.

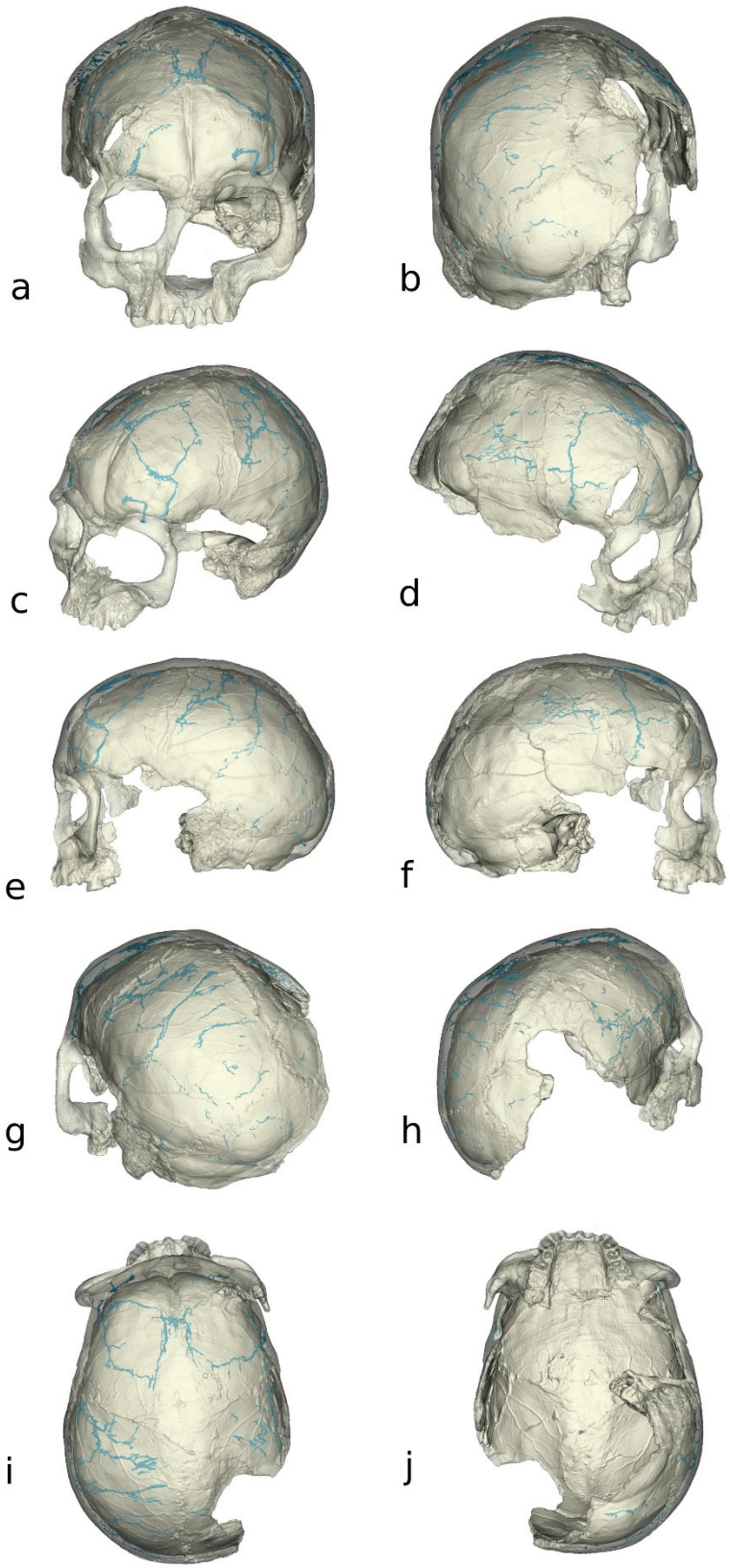

Figure 5.42 The diploic channels (in blue) in the Cro-Magnon 2 cranium, shown in the anterior (a), posterior (b), anterolateral (c and d), lateral (e and f), posterolateral (g and h), superior (i), and inferior (j) views.

Cro-Magnon 3

The upper half of the cranium was generally well preserved, with the diploic structures clear to inspect. Most DCs were housed in the frontal and parietal bones (Figure 5.43). The frontal and parietal DCs were comparably developed.

In the frontal bone, a pair of large DC branches extended from the supraorbital area to the frontal squama. Their anterior ends anastomosed with the periorbital vessels. The trunks of both branches had connecting points with the superficial temporal vessels and MMV in the frontal squama. Also, the right branch developed two arms connected with the superior sagittal sinus and arachnoid granulations when running posteriorly along the midline. There was another pair of small DC branches located near the pterion on both sides, which were posterior to and anastomosing with the large branches described above. The second pair of DCs were directly connected with the stems of MMVs when the latter ran through the bony canal in the frontal bone.

The parietal DC networks on both sides showed the bonsai pattern. Most large DC branches coursed mediolaterally and ramified towards many directions. Along the sagittal suture, the parietal DCs connected to the superior sagittal sinus, but not to the parietal foramina. Across the bones, the parietal DCs had many connections with the MMV and superficial temporal vessels. The asterional regions on both sides were damaged, and there were no detectable connecting points between parietal DCs and transverse-sigmoid sinus. However, given that the right parietal DCs arrived at the area beneath the groove and extended toward the endocranial surface, the DCs were highly possible to anastomose with the transverse-sigmoid sinus. Also, the DCs on both sides gave off short branches entering the occipital bone as well as the ossicle at the lambda, though they had no link with the occipital DCs.

The occipital bone was not well preserved. The remaining DCs were concentrated in the occipital plane, anastomosing with the superior sagittal sinus and occipital vessel.

Besides, there were two small branches coursing parallel to but not anastomosed with the transverse-sigmoid sinus.

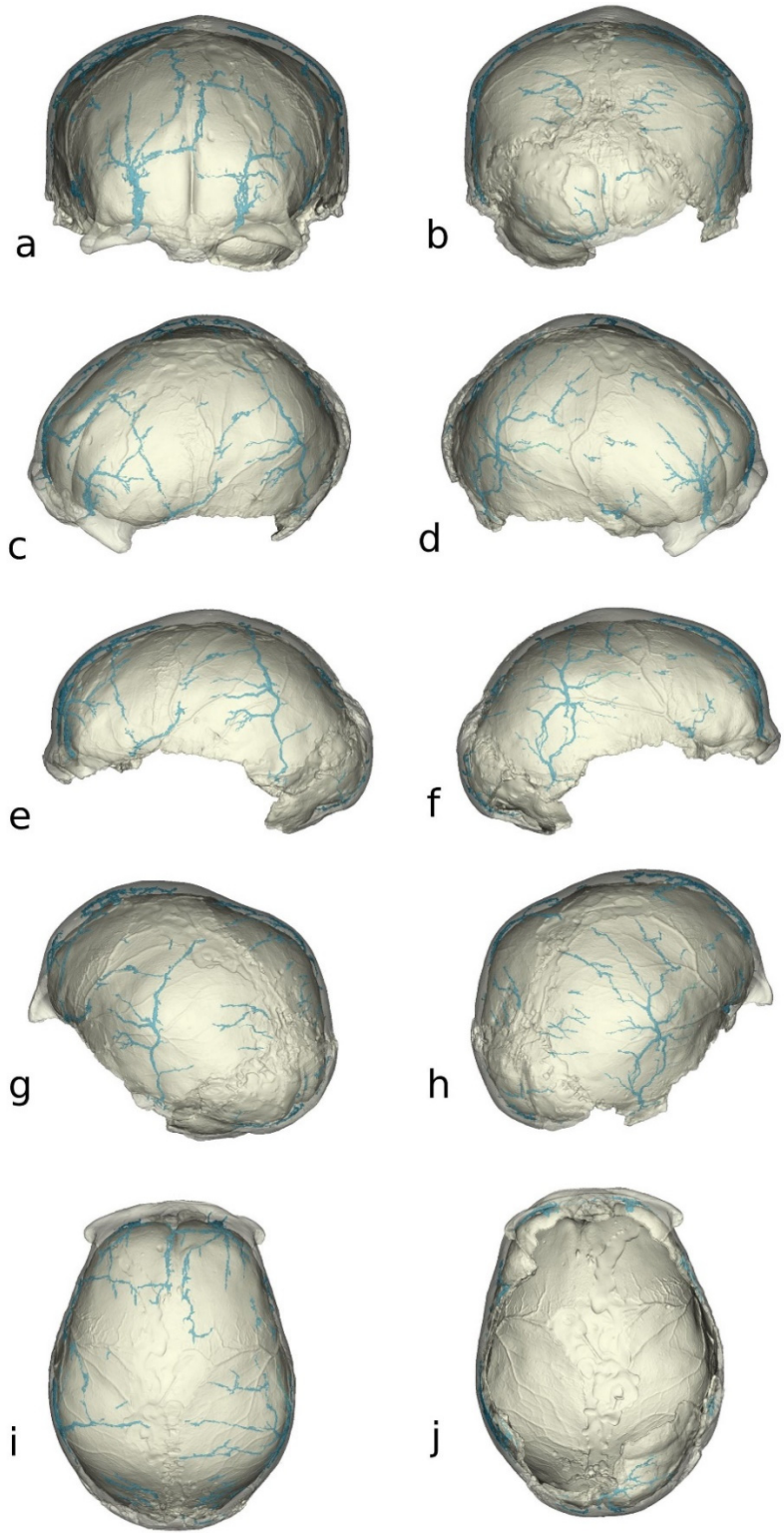

Figure 5.43 The diploic channels (in blue) in the Cro-Magnon 3 cranium, shown in the anterior (a), posterior (b), anterolateral (c and d), lateral (e and f), posterolateral (g and h), superior (i), and inferior (j) views.

Abri Pataud 1

The specimen was near complete, despite the paracoronal and pterional areas being slightly damaged. Most DCs were housed in the frontal and parietal bones (Figure 5.44).

In the frontal bone, a pair of large branches extended from the frontal squama to the orbital plates. In the frontal squama, the large branches had connections with the superior sagittal sinus, superficial temporal vessel, and MMV. In the orbital plates, the branches extended into the lesser wings of the sphenoid bone, where they gave off branches that anastomosed with the sphenoparietal sinus and entered the cavity inside the anterior clinoid process. Besides, in the supraorbital areas, the diploe was rather complex with no diploic structures in the shape of vessels. However, small DC branches should be present here, as there were a large number of foramina, not the emissary channels, in the area linking the diploe with the periorbital vessels and AMV.

The distribution pattern of the parietal DCs on both sides was a hybrid of the coronal and spider patterns. Along the sagittal suture, the parietal DCs had many connecting points with the superior sagittal sinus. Across the parietal bones, the DCs had dense connecting points with the MMV and superficial temporal vessels. In the asterional regions on both sides, the asterion landmark was at the lower edge of the transverse-sigmoid sinus. The parietal DCs drained directly into the trunk of the transverse-sigmoid sinus, while the occipital DCs were not present (Figure 5.45). Thus, the drainage pattern of the asterional regions was classified as pattern C. Finally, although the parietal foramina were present, they had no links with DCs.

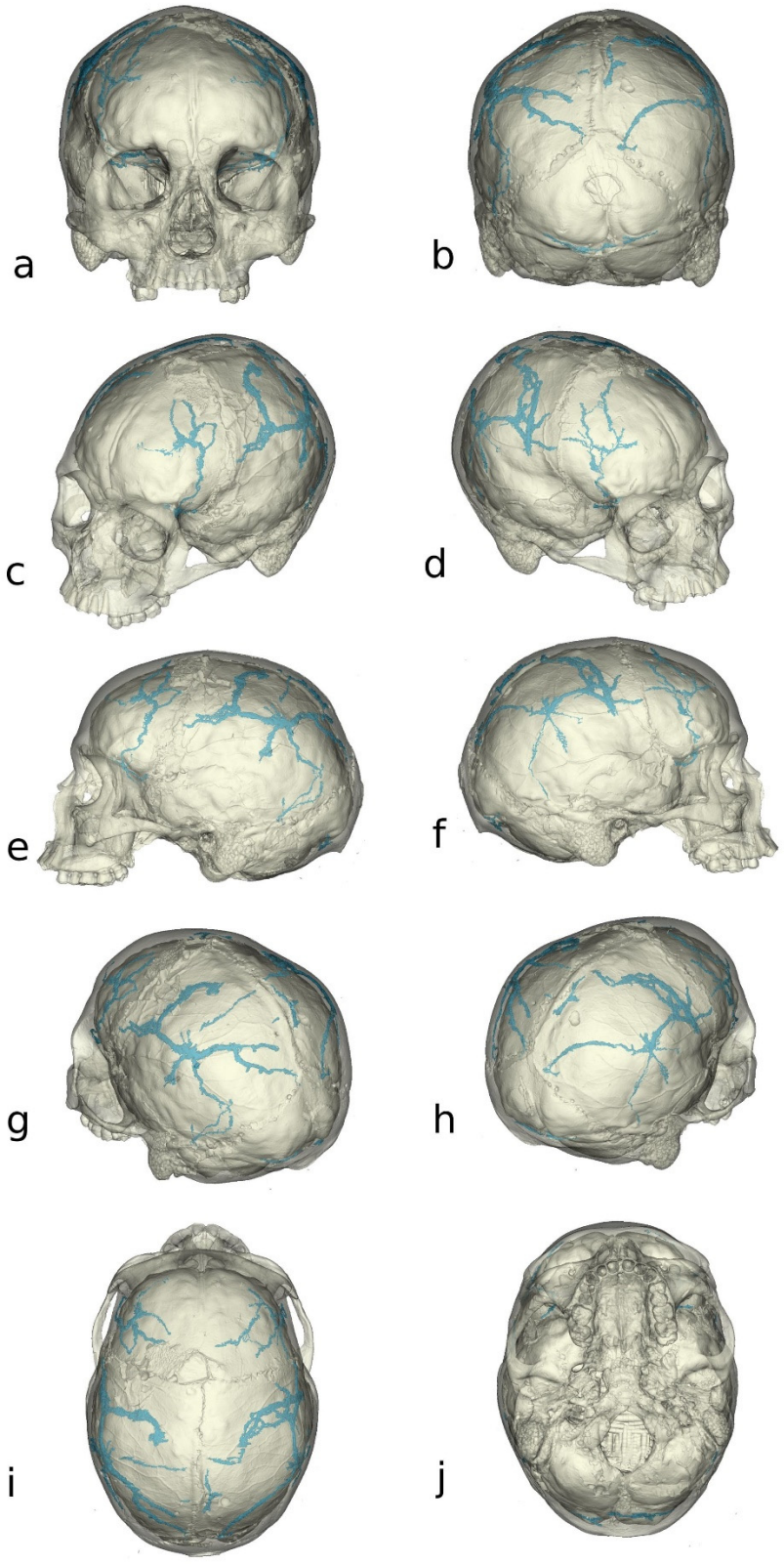

Figure 5.44 The diploic channels (in blue) in the Abri Pataud 1 cranium, shown in the anterior (a), posterior (b), anterolateral (c and d), lateral (e and f), posterolateral (g and h), superior (i), and inferior (j) views.

Like the supraorbital area, the occipital bone has an over-complex diploe along the midline and the diploic structures there were not in a typical shape of vessels. This made it difficult to locate and segment all the occipital DCs. Still, the location of the foramina and the few clearly manifested DCs indicated that the occipital DCs were connected with the superior sagittal sinus, confluence of the sinuses, and occipital vessels.

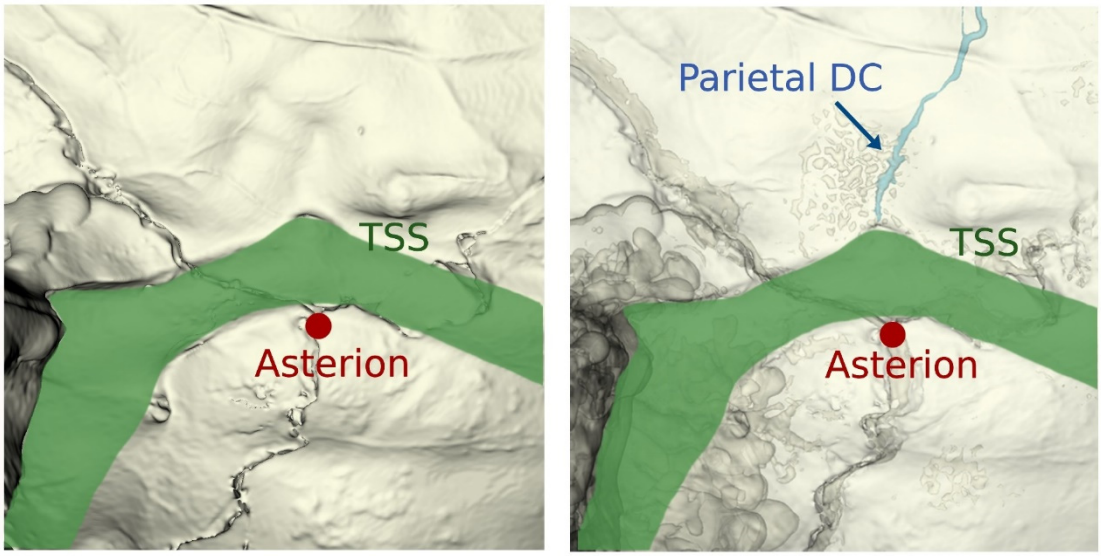

Figure 5.45 The drainage pattern in the asterional region of Abri Pataud 1. The figure is from Hui & Balzeau (2023b).

5.4 Synthesis

From the descriptions of great apes, extant humans, and fossil hominins, it was clear that the diploic venous system kept its high morphological variability across the hominid sample. Still, large similarities in drainage patterns were shared among the sample. When DCs extended towards the extracranial space, they always connected to the periorbital vessels, superficial temporal vessels, and occipital vessels. When DCs extended towards the intracranial space, they always connected with the meningeal vessels, sphenoparietal sinus, superior sagittal sinus, and transverse-sigmoid sinus (Tables 5.1-5.4).

Besides, interspecies variations were also detected in the drainage pathways of DCs. Compared with fossil hominins and extant humans, Chimpanzees had a distinct diploic venous system with smaller DC branches and irrigation territories. However, the chimpanzee diploic venous system was not simply a reduced version of those of hominins. The chimpanzee DCs formed a shortcut between paranasal sinuses and middle and posterior cranial fossae, which was a trait not manifested in the hominin sample. For the latter without the 'shortcut', the drainage from the frontal sinus had to travel through a long route in the frontal squama and temporal fossa, and then through the sphenoparietal sinus, if the drainage needs to enter the cavernous/intercavernous sinus.

Furthermore, the newly discovered DCs in chimpanzee great wings in this study served as a stem of MMVs, which was never found in hominins. Previous studies have noticed one stem of MMV on each hemicranium running on the endocranial surface. Here, this study discovered another stem hidden inside the diploe of the sphenoid bone. Because the newly noticed stem could only be detected through projectional radiography or computed tomography and it did not consistently appear in every specimen, it is understandable why it was undiscovered. In addition, previous studies noticed that the stem of the MMV network could connect with the foramen spinosum, foramen ovale,

or sphenopetrosal fissure. Here, this study showed the newly found stem could connect to even more foramina and canals.

The chimpanzee meningeal networks were different from hominins and this led to their different connection pattern with DCs. The AMVs were always small and simple in chimpanzee and hominin samples, with frequent anastomosis with DCs. The OMVs in chimpanzees dominated the frontal bone and sometimes the parietal bone, consistently anastomosing with the DCs. In hominins, the OMVs were less developed and not consistently connected to the DCs. More than 10% of extant human specimens did not house OMVs. In comparison, the MMVs were occasionally absent in the chimpanzee sample (around 5%) but were always present in hominins and connected to DCs.

Differences in drainage pathways also manifested among hominins. The connection between the frontal sinus and DCs did not consistently appear in fossil and extant *H. sapiens*, while the connection was consistent in the well-preserved specimens of other hominin species and in extant chimpanzees. Besides, the parietal foramina were usually presented in extant humans and usually connected to their parietal DCs. In comparison, more than half of chimpanzee specimens had no parietal foramen, while the rest only had a single parietal foramen along the suture and connecting to the DCs. As for fossil hominins, except those with serious damage in the corresponding area, the presence of parietal foramen was variable. Kabwe 1 (*H. heidelbergensis*), Hexian (*H. erectus*), Maba 1 (unclear taxon), and all fossil *H. sapiens* specimens had at least one parietal foramen and it was connected to the DCs; Tighennif 4 (*H. erectus* or *H. ergaster*), LES 1 (*H. naledi*), and all *H. neanderthalensis* specimens had no parietal foramen.

In addition, the asterional area also displayed variable drainage patterns among hominids. The pattern A and B were the most frequent in chimpanzees. The patterns A, B, and F were the most frequent in extant humans. As for those fossils with well-preserved asterional areas, pattern A was manifested in LES 1; Pattern C was in Abri

Pataud 1; Pattern D was in Hexain, La Quina H5, and La Chapelle-aux-Saints 1; Pattern F was in Kabwe 1, Cro-Magnon 1 and Cro-Magnon 2; Pattern G was in Spy 1. In general, the direct connection between parietal DCs and transverse-sigmoid sinus was a common feature among chimpanzees, extant humans, and most fossil hominins. The isolation between the parietal DCs and transverse-sigmoid sinus only appeared in Hexian *H. erectus* and *H. neanderthalensis* specimens.

Table 5.1 The DC connections with extracranial vessels

	Periorbital/ophthalmic vessels↔DC	**Superficial temporal vessel↔DC**	**Occipital vessel ↔DC**	**Parietal foramen↔DC**
Chimpanzees	100%	100%	100%	44.4%
Extant humans	100%	100%	100%	67.9%
KNM-ER 1805	N/A	N/A	N/A	N/A
StW 53	+	+	+	N/A
Tighennif 4	N/A	+	N/A	—
Trinil 2	+	+	+	N/A
Hexian	+	+	+	+
Kabwe 1	+		+	+
Florisbad	N/A	N/A	N/A	N/A
LES 1	+	+	+	N/A
Maba 1	+	+	N/A	+
La Quina H5	+	+	+	—
La Chapelle-aux-Saints 1	+	+	+	—
La Ferrassie 1	+	+	+	—
Spy 1	+	+	+	—
Spy 10	+	+	+	—
Cro-Magnon 1	+	+	+	+
Cro-Magnon 2	+	+	+	—
Cro-Magnon 3	+	+	+	—
Abri Pataud 1	+	+	+	—

Note: '+', connection manifested; '—', connection not manifested; 'N/A', not detectable for preservation constraints.

Table 5.2 The DC connections with dural sinuses

	Superior sagittal sinus↔DC	Transverse-sigmoid sinus ↔DC	Petrosquamous sinus↔DC	Sphenoparietal sinus↔DC	Asterional pattern
Chimpanzees	100%	100%	91.7%	100%	A, B, C, D, E
Extant humans	100%	100%	67.8%	100%	A, B, C, F
KNM-ER 1805	N/A	N/A	N/A	N/A	N/A
StW 53	+	N/A	N/A	N/A	N/A
Tighennif 4	+	+	N/A	N/A	N/A
Trinil 2	+	+	N/A	N/A	N/A
Hexian	+	+	+	N/A	D
Kabwe 1	+	+	—	+	F
Florisbad	+	N/A	N/A	N/A	N/A
LES 1	+	+	+	N/A	A
Maba 1	+	N/A	N/A	N/A	N/A
La Quina H5	+	+	+	N/A	D
La Chapelle-aux-Saints 1	+	+	+	N/A	D
La Ferrassie 1	+	+	N/A	N/A	N/A
Spy 1	+	+	—	N/A	G
Spy 10	+	+	N/A	N/A	N/A
Cro-Magnon 1	+	+	—	+	F
Cro-Magnon 2	+	+	—	N/A	F
Cro-Magnon 3	+	N/A	N/A	+	N/A
Abri Pataud 1	+	+	—	+	C

Note: '+', connection manifested; '—', connection not manifested; 'N/A', not detectable for preservation constraints.

Table 5.3 The DC connections with paranasal sinuses

	Frontal sinus ↔DC	Ethmoid sinus↔DC	Paranasal sinus↔DC↔Cavernous sinus shortcut
Chimpanzees	100%	88.89%	88.89%
Extant humans	91.7%	—	—
KNM-ER 1805	N/A	N/A	N/A
StW 53	+	N/A	N/A
Tighennif 4	N/A	N/A	N/A
Trinil 2	+	N/A	N/A
Hexian	+	N/A	N/A
Kabwe 1	+	—	—
Florisbad	+	N/A	N/A
LES 1	+	N/A	N/A
Maba 1	+	N/A	N/A
La Quina H5	+	N/A	N/A
La Chapelle-aux-Saints 1	+	N/A	N/A
La Ferrassie 1	+	N/A	N/A
Spy 1	+	N/A	N/A
Spy 10	+	N/A	N/A
Cro-Magnon 1	+	—	—
Cro-Magnon 2	—	N/A	N/A
Cro-Magnon 3	—	N/A	N/A
Abri Pataud 1	—	—	—

Note: '+', connection manifested; '—', connection not manifested; 'N/A', not detectable for preservation constraints.

Table 5.4 The DC connections with meningeal vessels

	DC serves as MMV stem	AMV↔DC	OMV↔DC	MMV↔DC
Chimpanzees	25.0%	41.7%	100%	94.4%
Extant humans	—	46.4%	83.9%	100%
KNM-ER 1805	N/A	N/A	N/A	+
StW 53	N/A	N/A	N/A	+
Tighennif 4	N/A	N/A	N/A	+
Trinil 2	N/A	N/A	N/A	+
Hexian	N/A	+	N/A	+
Kabwe 1	—	—	N/A	+
Florisbad	N/A	N/A	N/A	+
LES 1	N/A	+	N/A	+
Maba 1	N/A	—	N/A	+
La Quina H5	N/A	N/A	N/A	+
La Chapelle-aux-Saints 1	N/A	+	N/A	+
La Ferrassie 1	—	N/A	N/A	+
Spy 1	N/A	N/A	N/A	+
Spy 10	N/A	N/A	N/A	+
Cro-Magnon 1	—	—	—	+
Cro-Magnon 2	N/A	—	N/A	+
Cro-Magnon 3	N/A	N/A	N/A	+
Abri Pataud 1	—	+	—	+

Note: '+', connection manifested; '—', connection not manifested; 'N/A', not detectable for preservation constraints; AMV, anterior meningeal vessels; OMV, orbital meningeal vessels; MMV, middle meningeal vessels.

6. Results—The quantification of DC morphology

6.1 Intensity level

Most chimpanzee specimens showed low intensity levels. 77.8% (14 individuals) of the chimpanzee sample were rated as level 1 (Table 6.1). 16.7% (Three individuals) of the sample were rated as level 2. Only 5.6% (one individual) of the sample reached level 3. Similarly, the intensity levels of gorilla specimens were low. 72.7% (8 individuals) were at the level 1 and 27.3% (3 individuals) reached the level 2.

In contrast, extant human specimens generally had a much more developed diploic venous network. Only 3.6% (one individual) of the extant human sample were rated as level 1. 7.1% (two individuals) of the sample were rated as level 2. 89.3% (25 individuals) of the sample reached level 3.

Among Early Pleistocene hominin specimens, StW 53 was rated as level 3, while the diploic venous network of KNM-ER 1805 was seriously damaged and not possible to be evaluated.

Among Middle Pleistocene hominin specimens, the diploic venous networks of Hexian, Kabwe 1, LES 1, and Maba 1 clearly reached level 3. Besides, Tighennif 4 was a single and well-preserved parietal bone, with other cranial bones missing. The intensity level of its entire cranium was unknown. However, if the DCs in other bones shared a similar degree of size and complexity with those in the preserved parietal bone, the intensity level of the cranium should be level 3. Similarly, the evaluation of Trinil 2 was also constrained by the preservation status. The real intensity level of its DC network of the entire cranium was unknown, but it might not be lower than level 2. Florisbad was more seriously damaged, but the diameter and density of these preserved DC branches indicated its intensity level might be at level 2 or level 3.

Finally, for the Late Pleistocene hominins (*H. neanderthalensis* and *H. sapiens*), the diploic venous networks of all specimens reached level 3.

Table 6.1 The intensity level of diploic channels

	Taxon	**Intensity level**
Extant chimpanzees (18 individuals)	*P. troglodytes*	L1: 77.8%; L2:16.7%; L3: 5.6%
Extant gorillas (11 individuals)	*G. gorilla*	L1: 72.7%; L2: 27.3%
Extant humans (28 individuals)	*H. sapiens*	L1: 3.6%; L2:7.1%; L3: 89.3%
KNM-ER 1805	*H. habilis?*	N/A
StW 53	*H. habilis?*	L3
Hexian	*H. erectus*	L3
Kabwe 1	*H. heidelbergensis?*	L3
LES 1	*H. naledi*	L3
Maba 1	Unclear	L3
Tighennif 4	*H. erectus?*	L3?
Trinil 2	*H. erectus*	L2 or L3
Florisbad	*H. heidelbergensis?*	L2 or L3
La Chapelle-aux-Saints 1	*H.neanderthalensis*	L3
La Ferrassie 1	*H.neanderthalensis*	L3
La Quina H5	*H.neanderthalensis*	L3
Spy 1	*H.neanderthalensis*	L3
Spy 10	*H.neanderthalensis*	L3
Abri Pataud 1	*H.sapiens*	L3
Cro-Magnon 1	*H.sapiens*	L3
Cro-Magnon 2	*H.sapiens*	L3
Cro-Magnon 3	*H.sapiens*	L3

6.2 Fractal analysis

To evaluate the useability of fractal analyses in the study of the diploic venous system, especially the useability for fossil specimens, the analysis was tested in five *H. neanderthalensis* and four fossil *H. sapiens* (Table 6.2). The result is from my published paper (Hui & Balzeau, 2023b).

In detail, the fractal dimensions of the frontal DCs ranged from 1.5 to 1.6 in the *H. neanderthalensis* sample, and from 1.4 to 1.5 in the *H. sapiens* sample. For the parietal DCs, their fractal dimensions ranged from 1.4 to 1.6 in the *H. neanderthalensis* sample, and from 1.4 to 1.5 in the *H. sapiens* sample. For the occipital DCs, their dimensions ranged from 1.4 to 1.5 in *H. neanderthalensis* sample, and from 1.3 to 1.4 in the *H. sapiens* sample.

From this, it is noticeable that *H. neanderthalensis* and fossil *H. sapiens* specimens shared a large overlap in their parietal DC dimension range. *H. neanderthalensis* specimens showed higher dimensions than *H. sapiens* specimens in the frontal and occipital DCs. For each specimen, the dimension of occipital DCs was usually lower than those of frontal and parietal DCs.

Table 6.2 The fractal dimensions of diploic channels

	Taxon	Frontal	Parietal	Occipital
La Chapelle-aux-Saints 1	*H.neanderthalensis*	1.5	1.5	1.5
La Ferrassie 1	*H.neanderthalensis*	N/A	1.4	1.4
La Quina H5	*H.neanderthalensis*	1.6	1.4	1.4
Spy 1	*H.neanderthalensis*	N/A	1.6	1.4
Spy 10	*H.neanderthalensis*	1.5	1.5	1.4
Abri Pataud 1	*H.sapiens*	1.4	1.4	1.4
Cro-Magnon 1	*H.sapiens*	1.5	1.5	1.4
Cro-Magnon 2	*H.sapiens*	1.4	1.4	1.3
Cro-Magnon 3	*H.sapiens*	1.4	1.4	1.4

Note: Bones without any complete DC branches were excluded from the comparison. For the parietal bones, the better-preserved side was selected for comparison.

6.3 Volume index

The analysis of DC volume indices was tested in a larger group, including five chimpanzees, five extant humans, StW 53 specimen, *H. naledi* (LES 1 specimen), *H. neanderthalensis*, and fossil *H. sapiens* specimens (Table 6.3, Figures 6.1-6.3). This allowed a quantitative analysis of the relationship between brain size and DC size. Part of the result is from my published paper (Hui & Balzeau, 2023b). The endocranial volume of fossil specimens was from published data (Aiello & Dean, 1990; Balzeau et al., 2013; Hawks et al., 2017; Schwartz et al., 2002a).

The volume indices (DC volume index = (DC volume/Bone tissue volume) *100) of the frontal DCs ranged from 0.1 to 0.8 in the chimpanzee sample, from 0.6 to 1.2 in the extant human sample, from 0.8 to 2.2 in the *H. neanderthalensis* sample, from 0.7 to 1.6 in the fossil *H. sapiens* sample, and stood at 1.4 and 1.3 for StW 53 and *H. naledi* specimen respectively. The indices of the parietal DCs ranged from 0.1 to 0.4 in chimpanzees, from 0.4 to 1.7 in extant humans, from 0.8 to 2.8 in the *H. neanderthalensis* sample, from 0.8 to 1.9 in the fossil *H. sapiens* sample, and stood at 1.4 for the *H. naledi* specimen. The indices of the occipital DCs ranged from <0.1 to 0.3 in chimpanzees, from 0.2 to 0.6 in extant humans, from 0.3 to 0.8 in the *H. neanderthalensis* sample, and from 0.2 to 0.3 in the fossil *H. sapien*s sample.

In general, chimpanzee indices were much lower than those of hominins. The figures for StW 53 and *H. naledi* specimen fell within the range of Late Pleistocene hominins. *H. neanderthalensis* and *H. sapiens* specimens (including fossils and extant specimens) had a large overlap in the variation range of the indices of the frontal and parietal DCs. In each individual, the frontal and parietal DCs usually had higher indices than occipital DCs. And the highest values of all categories were always found in La Chapelle-aux-Saints 1. Within the sample of *H. neanderthalensis* and *H. sapiens*, the individuals with larger brains tended to have higher DC volume indices (Figure 6.1-6.3). But when including in the comparison the data of chimpanzees and other hominin fossils, the

correlation no longer appeared. Small-brained StW 53 and *H. naledi* had much higher indices than small-brained chimpanzees, and their levels were comparable with *H. neanderthalensis* and *H. sapiens*.

Table 6.3 The diploic channel volume indices

	Taxon	Frontal	Parietal	Occipital
Chimpanzees (n=5)	*P. troglodytes*	0.1-0.8	0.1-0.4	<0.1-0.3
Extant humans (n=5)	*H. sapiens*	0.6-1.2	0.4-1.7	0.2-0.6
StW 53	*H. habilis?*	1.4	N/A	N/A
LES 1	*H. naledi*	1.3	1.4	N/A
La Chapelle-aux-Saints 1	*H.neanderthalensis*	2.2	2.8	0.8
La Ferrassie 1	*H.neanderthalensis*	N/A	0.8	0.3
La Quina H5	*H.neanderthalensis*	0.8	1.4	0.5
Spy 1	*H.neanderthalensis*	N/A	1.3	0.3
Spy 10	*H.neanderthalensis*	1.6	1.1	0.7
Abri Pataud 1	*H.sapiens*	1.0	1.9	0.2
Cro-Magnon 1	*H.sapiens*	1.3	1.4	0.3
Cro-Magnon 2	*H.sapiens*	0.7	0.8	N/A
Cro-Magnon 3	*H.sapiens*	1.6	1.0	N/A

Note: Bones damaged severely were excluded in the comparison, as the remaining fragments might not be sufficient to represent the value of the whole bone. For the parietal bones, the better-preserved side was selected for comparison.

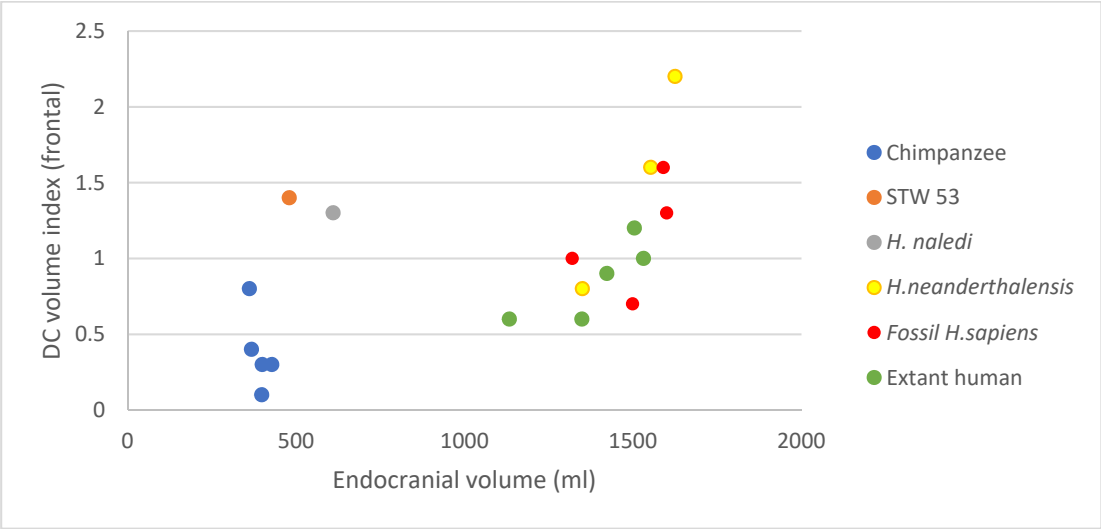

Figure 6.1 The scatter plot of endocranial volume and frontal DC volume index

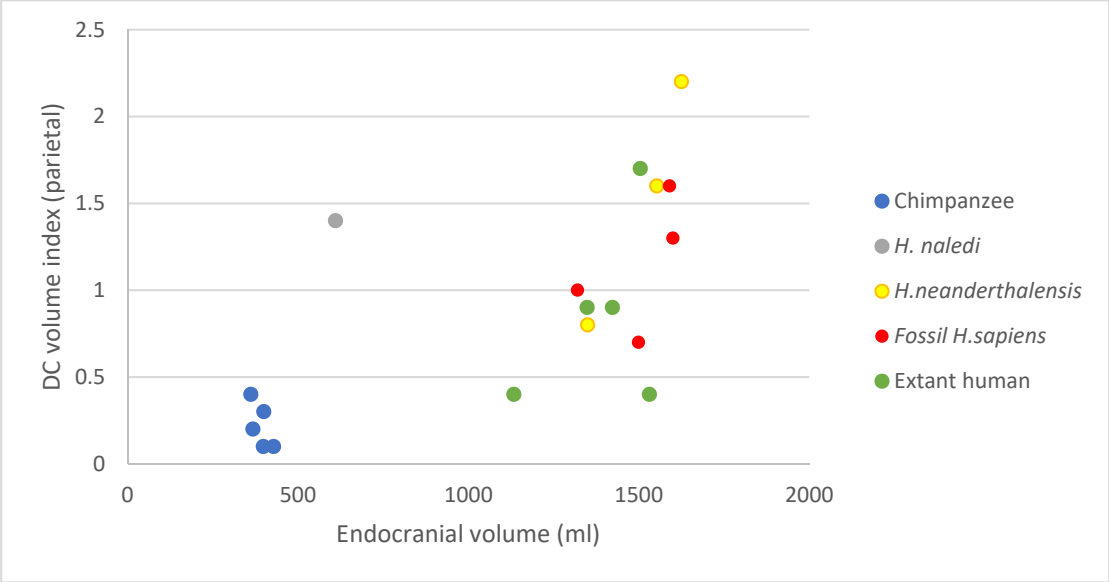

Figure 6.2 The scatter plot of endocranial volume and parietal DC volume index. (For fossil specimens, the better-preserved side was selected for comparison. For extant specimens, the left side was selected)

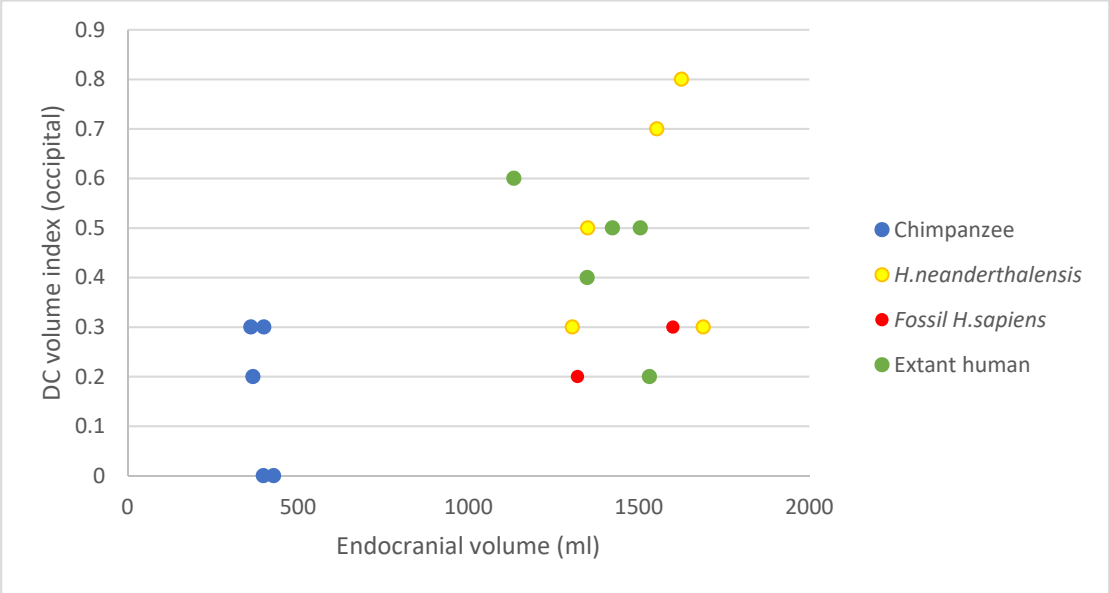

Figure 6.3 The scatter plot of endocranial volume and occipital DC volume index

6.4 Synthesis

From the results, it is clear that chimpanzee and gorilla diploic venous systems were much less developed than those of fossil hominins and extant humans. This result is accordant with the qualitative descriptions in Chapter 5. Among the hominins, the fossil specimens from the Early, Middle, and Late Pleistocene all manifested highly developed diploic venous networks, except for those not well preserved. The intensity of their diploic venous network all reached the level 3, the same level as extant humans. In other words, extant humans and fossil *H. sapiens* did not possess more developed diploic venous systems in terms of intensity level than other hominin specimens.

The fractal analyses and relative volume indices provided detailed comparative information between *H. neanderthalensis* and *H. sapiens* specimens. The diploic venous systems of the two samples were generally comparable in the degree of complexity and size. Some *H. neanderthalensis* specimens even displayed more complex and larger DCs than *H. sapiens* specimens. In addition, it has been noticed that a high degree of DC complexity did not always come with a larger DC size. For instance, the frontal DCs of La Quina H5 manifested the highest fractal dimension, but its volume index was lower than those of most other specimens. Furthermore, it was shown in the scatter plots that the DC index seemed to correlate positively with brain size in *H. neanderthalensis* and *H. sapiens*. However, this possible correlation did not manifest in the chimpanzees and small-brained hominins.

This study highlighted that the fractal analysis and volume index were more informative than the intensity level analysis. However, some frontal and occipital bones of these *H. neanderthalensis* and *H. sapiens* specimens could not be included in the analyses for their preservation, even though the general preservation statuses of these crania were almost the best in this study and in global fossil records. This indicated that fractal and volume index analyses may have a smaller application range than the intensity level analysis.

7. The spatial relationship between bone, brain, and diploic vessels

7.1 The spatial relationship between bone, brain, and diploic vessels in chimpanzees

7.1.1 The case study of chimpanzee specimens

Overview

Five specimens were selected for the following in-depth case study and interindividual comparison. They were selected for their almost intact preservation status and for their variable thickness and degree of DC development, which allowed exploring more variations within a limited sample size. They were labelled as ZM-1947-151 (male), ZM-1959-35 (male), ZM-1974-72 (female), ZM-1982-02 (unknown sex), and ZM-1987-004 (female).

ZM-1947-151

The thickest part of the frontal bone was the supraorbital torus, with the middle part over 11.0 mm (Figure 7.1). In both hemicrania, DC branches extended from the anterior edge of the frontal squama to the torus. Compared with the torus, the squama was thinner. The upper part of the squama showed thickness values ranging from 3.5 to 6.5 mm. The temporal lines, frontal crest, and anterior and posterior edges were the thickest (peaked at around 6.5 mm). The DCs of the upper squama appeared in these thickened areas and did not enter the lower squama, where the bone was compressed by the superior and middle frontal gyri and showed slight thinning. Inferior to the temporal lines, the lower part of the frontal bone showed a pair of extremely thin areas on both sides (<2.0 mm). The thinning on the right side was more evident than the right one. These areas of thinning were bypassed by the DCs and compressed by the inferior frontal gyrus.

Many frontal and parietal DC branches were around the bregma, which was the

intersection of a thickened cross-shaped area (5.5-6.5 mm) formed by the coronal suture, frontal crest, and sagittal suture. The thickening corresponded to the relief on the ectocranial surface. Most parietal DCs extended within the area between the two temporal lines (i.e., the upper parietal bone, 3.0-6.5 mm). There was almost no DCs manifested in the lower parietal bone (3.5-5.5 mm, except the asterional area and lambdoid suture), even though it was not thinner than the upper part. The scarce DCs in the lower parietal bone emerged in the thick asterional region (5.5-15.5 mm) and lambdoid suture (5.0-9.0 mm).

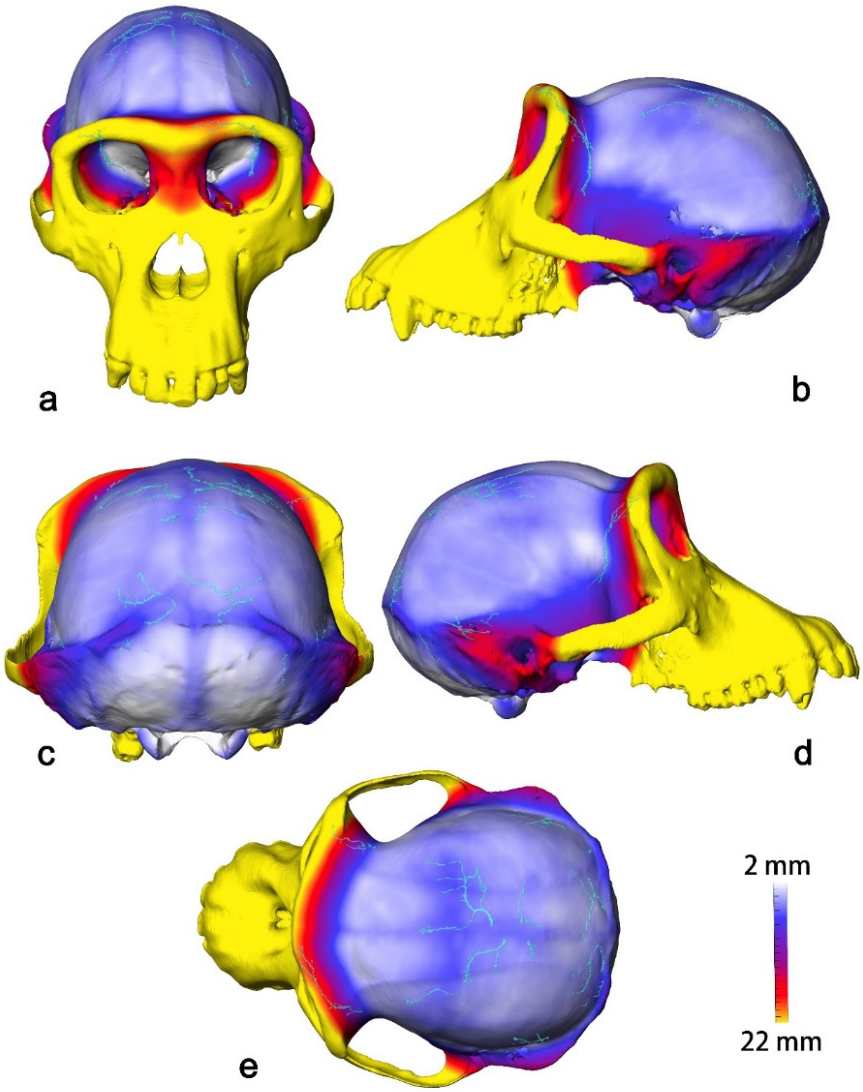

Figure 7.1 The CVT and DC distribution in the specimen 1947-151, shown in the anterior (a), lateral (b and d), posterior (c), and superior (e) views.

In the occipital bone, the area inferior to the lambdoid suture was generally thin. On both sides of the midline were extremely thin areas (<2.0 mm) compressed by the occipital gyri. The DCs did not appear in these thin areas and there were only few branches coursing along their edges. The midline itself was not very thin (4.0-5.5 mm). As many foramina (the inlets/outlets of DCs) were found in the external and internal surfaces along the midline, there should be DC branches located. However, the diploic structures there were very complex and the cavities were not very similar to vessels in shape. It was not feasible to judge which cavities ever house diploic veins nor to include them in the illustration.

ZM-1959-35

The supraorbital torus was generally thick, with the middle part over 10.0 mm (Figure 7.2). Some short and narrow DC branches emerged in the torus, and they derived from the main branches in the frontal squama. The anterior edge of the squama was thick (<8.0 mm) and housed the majority of the frontal DCs. In comparison, the rest of the squama was compressed by the pronounced frontal gyri, showing relatively lower thickness (3.5-6.0 mm) and scarce DCs. Especially, a pair of extremely thin areas (<2.0 mm) were found above the pterion and bypassed by the DCs. The thinning corresponded to the compression from the inferior frontal gyrus.

The bregmatic area was slightly thickened (around 5.5 mm), but there were no DCs. Most parietal DCs were inside or adjacent to the temporal lines and sagittal suture, which were three parallel belts (5.0-7.0 mm) thickened by the relieves on the ectocranial surface. The center of the lower parietal bone also showed evident thinning (<4.0 mm). No DCs appeared in this thin area, and no pronounced gyri were observed beneath this area of thinning. Still, the asterional regions on both sides were rather thick (7.5-15.0 mm) and housed a few narrow and short DCs.

The lambdoid suture was relatively thick (5.5-7.5 mm) and its lateral ends house a few

DCs. Except for the midline, the area inferior to the lambdoid suture was rather thin (<2.0 mm). The location of foramina on the internal and external surface indicated there were DCs in the midline (5.0-7.0 mm).

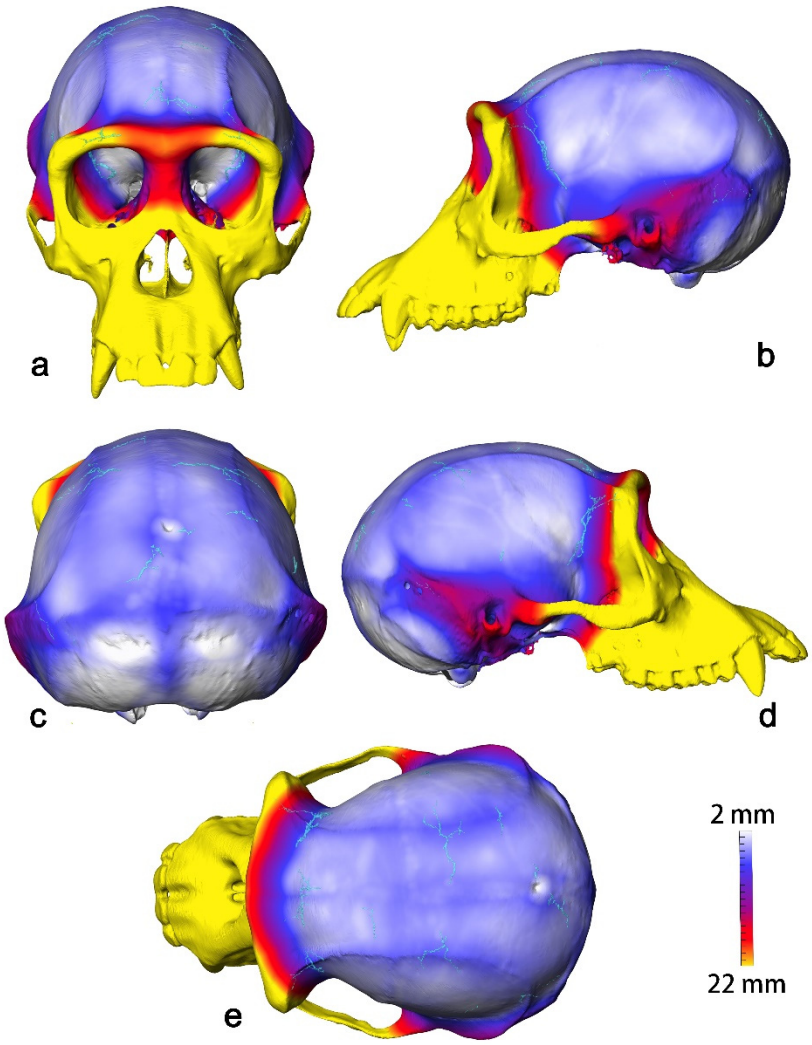

Figure 7.2 The CVT and DC distribution in the specimen 1959-35, shown in the anterior (a), lateral (b and d), posterior (c), and superior (e) views.

ZM-1974-72

The DC network in the specimen was much more developed than those in most chimpanzee specimens (Figure 7.3). Still, its cranial vault thickness was thinner than those of other specimens in this case study.

In the frontal bone, the supraorbital torus was generally thick, of which the middle part

was over 10.0 mm. The anterior edge of the frontal squama was also thick, with the thickness values ranging from 7.0 to 10.0 mm. In contrast, the other part of the frontal squama compressed by the superior and middle frontal gyri was much thinner (2.0-5.0 mm). Most frontal DCs were distributed in the area between the temporal lines and extended into the torus. Inferior to the left temporal line, an extremely thin area (< 2.0 mm) was manifested above the pterion and bypassed by the DCs. The thinning corresponded to the compression from the inferior frontal gyrus.

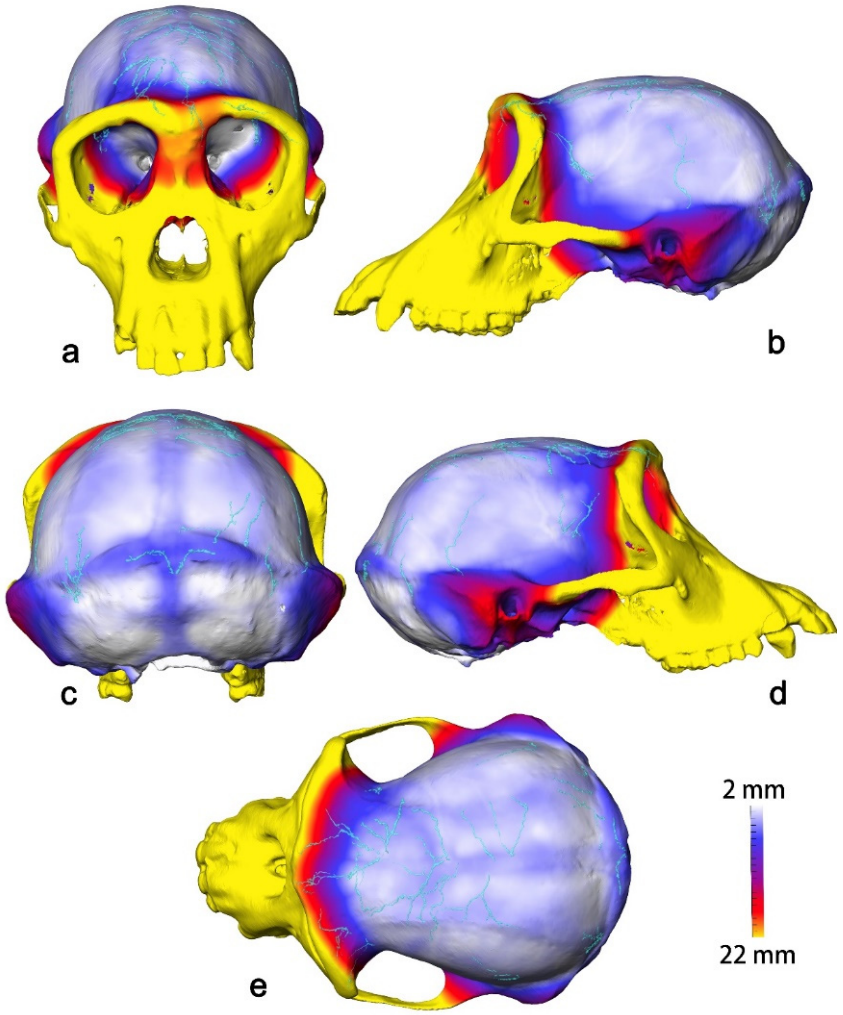

Figure 7.3 The CVT and DC distribution in the specimen 1974-72, shown in the anterior (a), lateral (b and d), posterior (c), and superior (e) views.

The parietal bone was similar to the posterior half of the frontal squama in thickness, but the DC network of the former was less developed than that of the latter. Most

parietal DCs were distributed in the area between the two temporal lines. The thickness of this area was thinner than 5.0 mm, with some extremely thin parts compressed by gyri thinner than 2.0 mm. No DCs appeared in these extremely thin parts, while the relatively thicker temporal lines and sagittal sutures did not house the richest DC branches. Also, adjacent and inferior to the temporal lines were a pair of extremely thin and belt-like areas on both sides (< 3.0 mm). The thinning was not attributed to the compression from the endocranial surface. Also, no DCs ran across these thin belts and extended from the upper parietal bone to the lower. The lower parietal bones on both sides were not very thin (around 4.5 mm) and they housed a pair of long DCs.

Most occipital DCs were distributed along the lambdoid suture (4.5-7.0 mm). Except for the midline, which was 4.5 to 7.0 mm in thickness, the area inferior to the lambdoid suture was compressed by the occipital gyri and was extremely thin (< 2.0 mm). The DC branches from the lambdoid suture extended inferiorly but stopped at the edge of this extremely thin area.

ZM-1982-02

The neurocranium of the specimen was slightly thicker than those of other specimens (Figure 7.4), but its DC network was not the most developed among the sample.

In the frontal bone, the supraorbital torus was the thickest, with the middle part over 9.0 mm. A pair of long and narrow DCs were located in the torus, coursing along the boundary between the torus and frontal squama. The frontal squama was much thinner than the torus, with a pair of areas with thinning (4.5-6.0 mm) lateral to the frontal crest, which was compressed by the superior and middle frontal gyri. The DCs in the torus gave off branches anteriorly but did not ramify posteriorly to enter these thin areas in the squama. Only outside these areas with thinning did the DCs in the upper frontal squama manifest themselves. Surrounding these thin areas, the frontal crest and temporal lines formed three parallel and thickened belts, but they did not house any

DCs. Inferior to the temporal lines, the DCs on the two sides bypassed the thin areas (3.5-5.5 mm), which were located close to the pterion and compressed by the inferior frontal gyrus.

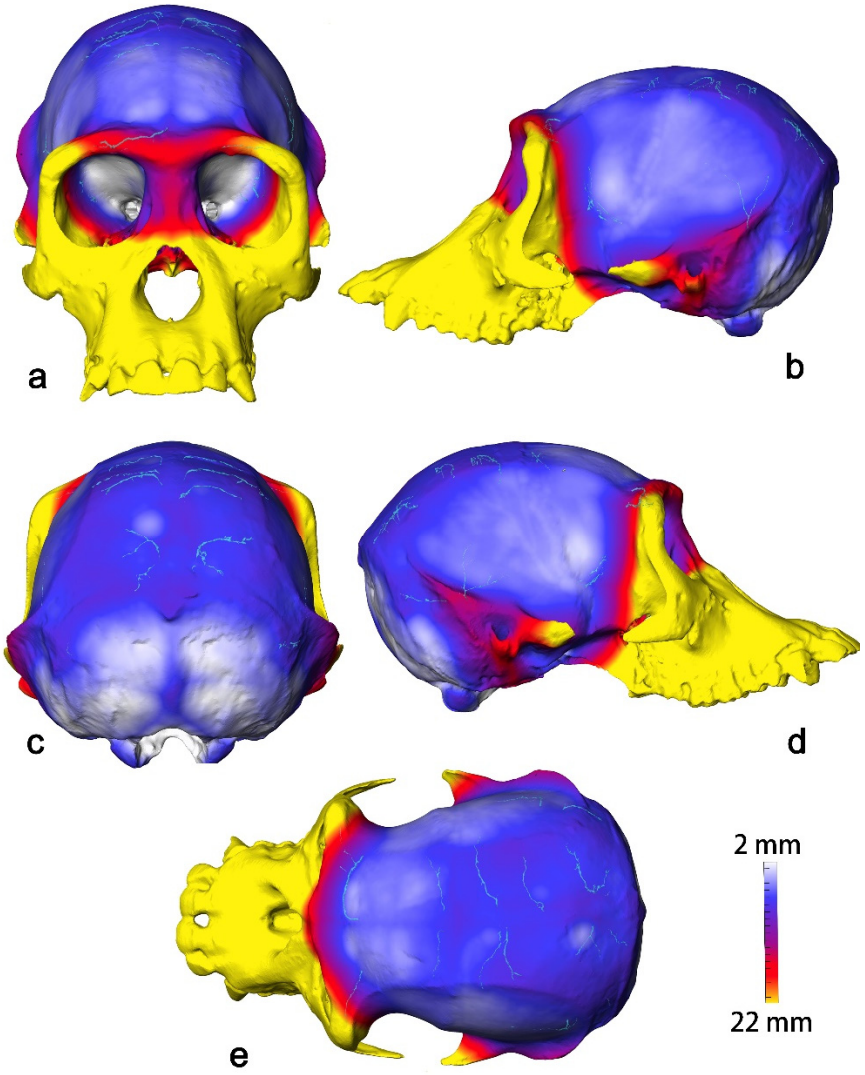

Figure 7.4 The CVT and DC distribution in the specimen 1982-02, shown in the anterior (a), lateral (b and d), posterior (c), and superior (e) views.

The frontal crest, sagittal suture and coronal suture formed a thickened cross-shaped area (7.5-9.0 mm), with the bregma as the intersection and the thickest point. Still, there was no parietal DCs reaching the bregma. Most parietal DCs were found in the upper half of the parietal bone (i.e., the area superior to the temporal lines, 5-9.5 mm), which was much thicker than the frontal squama. The distribution of the DCs in the upper parietal bone was almost even, despite the uneven distribution of the thickness. In

addition, a round-shaped thinning was also seen adjacent to the sagittal suture, which corresponded to a relief on the endocranial surface (possibly an arachnoid granulation). The parietal DCs touched the edge of this thin area without entering its center. Compared with the upper half of the parietal bone, the lower half (i.e., the area inferior to the temporal lines) was much thinner and housed fewer DCs. In the lower parietal bones, the DCs appeared in the thickened asterional regions (peaked at around 15 mm), while the rest part of the lower parietal bone showed no DCs and low thickness values (5.0-8.0 mm), though there was no pronounced compression from gyri.

In the occipital bone, the thickest point was the lambdoid (9.5 mm), but it showed no DCs. The lateral ends of the lambdoid suture were also thick (7.5-9.0 mm) and showed few short DCs. In contrast, the area inferior to the lambdoid suture was compressed by the occipital gyri and was much thinner, with the thinnest part below 2 mm. No DCs were manifested in these extremely thin areas. Still, the midline of the occipital bone was relatively thick (5.5-9.0 mm). Judging from the location of foramina, there should be DCs along the midline.

ZM-1987-004

The DC network of the specimen 1987-004 was much more developed than most chimpanzee specimens (Figure 7.5), but its cranial vault thickness in general was not the thickest among the sample.

In the frontal bone, a pair of DC branches coursed along the thick anterior edge (7.0-10.0 mm) of the frontal squama and extended into the thick supraorbital torus (>10.0 mm). In the center of the frontal bone, distributed on both sides of the thick frontal crest (6.0-7.0 mm) were several thin areas (<4.0 mm), which corresponded to the compression from the superior frontal gyrus and arachnoid granulations. The DCs in the upper frontal bone bypassed these thin areas and extended within thicker areas. In the lower part of the frontal bone, there were a pair of extremely thin areas (<2.0 mm)

close to the pterion, which were compressed by the inferior frontal gyrus. The DCs coursed along the edge of these extremely thin areas without entering their centers.

The general thickness of the upper parietal bones (4.0-7.0 mm) was close to that of the squama. Several DC branches were distributed close to the thick bregma (around 7.0 mm) and bypassed the relatively thinner areas (<4.5 mm) along the sagittal suture, which were corresponded to the compression from arachnoid granulations and gyri. The general thickness of the lower parietal bones was close to that of the upper part. Many long and complex DC branches were in the lower parietal bones. This was a rather rare trait in the chimpanzee sample, as most specimens did not house large branches in this part.

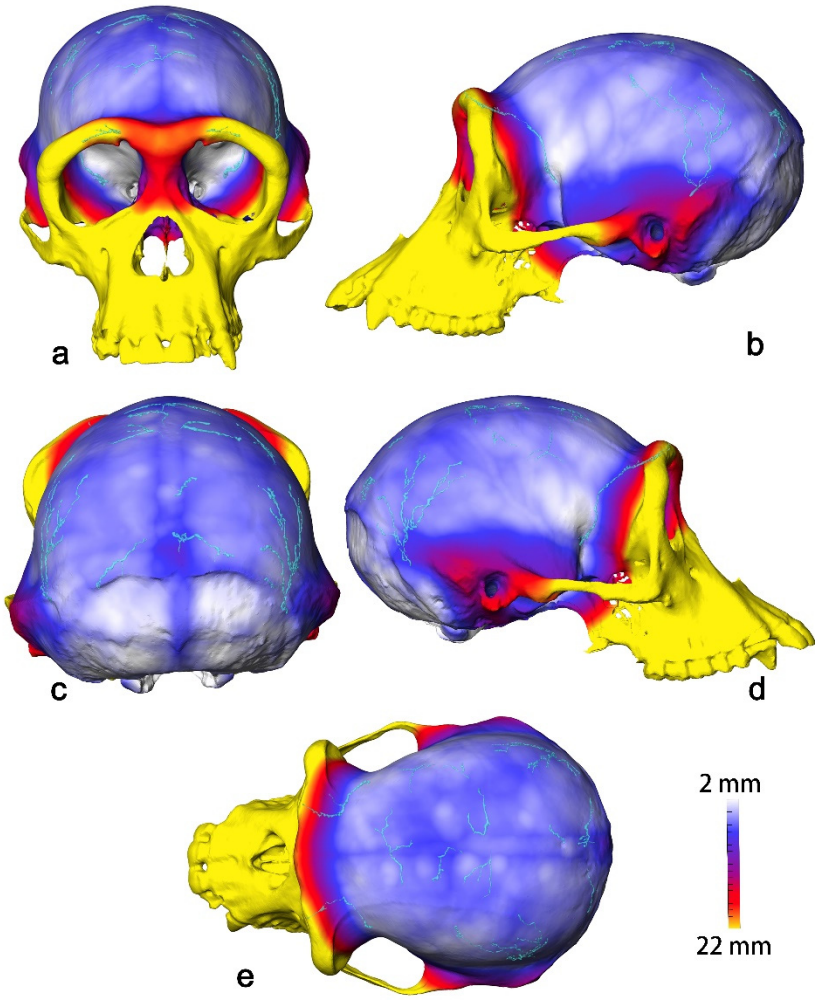

Figure 7.5 The CVT and DC distribution in the specimen 1987-004, shown in the anterior (a), lateral (b and d), posterior (c), and superior (e) views.

The lambdoid suture was slightly thickened (4.5-9.5 mm), and the lambdoid was the thickest point. Many DCs appeared along the upper edge of the lambdoid suture, but they did not enter the extremely thin areas (<2.0 mm) of the occipital bone, which were inferior to the suture and compressed by the occipital gyri. The midline of the occipital bone was relatively thick (5.5-7.5 mm), and foramina indicated there were DCs embedded in the midline.

7.1.2 Synthesis

All these chimpanzee specimens manifested very similar patterns of local thickening, even though their gross thicknesses were different. The supraorbital torus, bregmatic area, sagittal suture, temporal lines, asterional area, lambdoid suture, and the midline of the occipital bone were thickened. The thickening in these areas was mostly attributed to the relieves or superstructures on the ectocranial surface. As for the endocranial surface, the compression from gyri and arachnoid granulations corresponded to some areas with evident thinning (Figure 7.6). The superior frontal gyrus (and sometimes with the middle frontal gyrus) corresponded to the thinning along the midline of the frontal bone. The inferior frontal gyrus corresponded to the thinning between the temporal line and pterion. The occipital gyri corresponded to the thinning in the occipital bone. These areas with thinning consistently appeared in all these chimpanzee specimens. Besides, the arachnoid granulations in the parietal region suture sometimes corresponded to the thinning along the sagittal suture.

By comparing the CVT map and the DC distribution, it is clear that a thicker gross thickness of a cranium did not necessarily mean a more developed DC network. Conversely, the relatively more developed DC network appeared in the specimen (ZM-1974-72) with the thinnest global thickness among the five. Similarly, a thickened local area did not necessarily mean housing more and larger DC branches, but DCs clearly tended to bypass the areas with evident thinning.

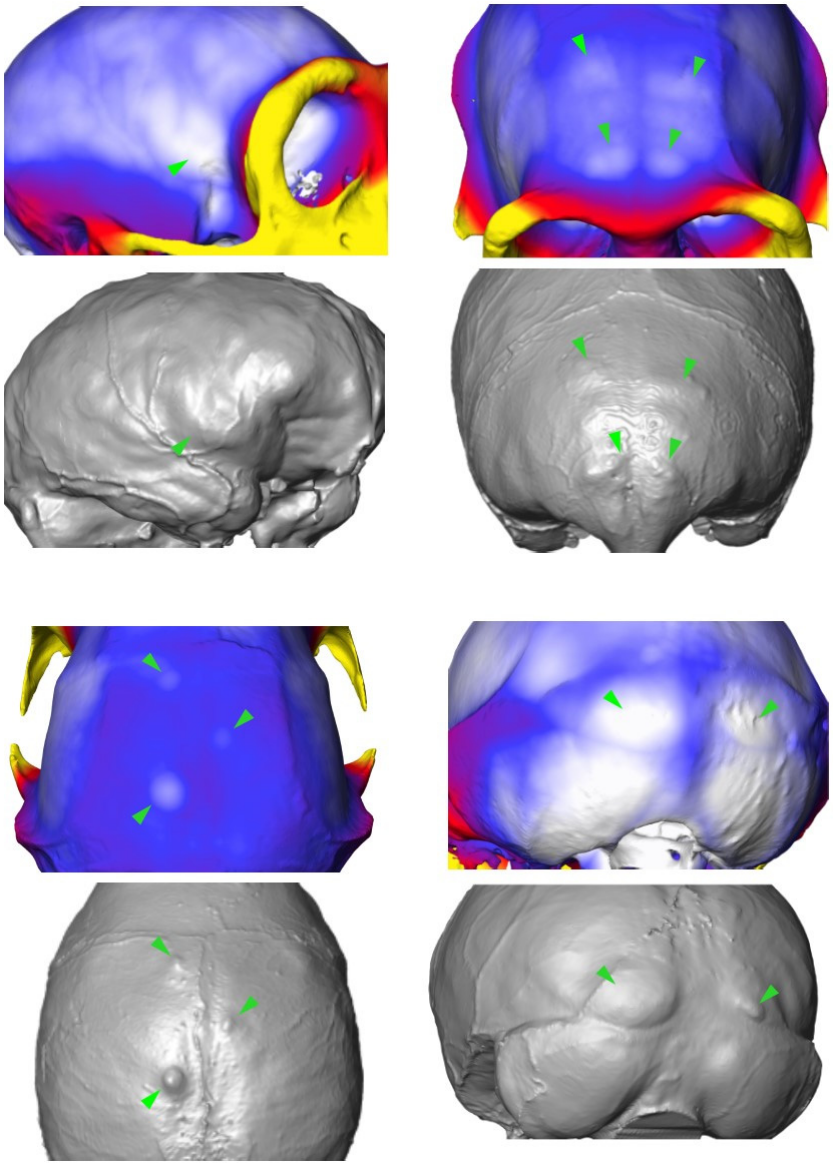

Figure 7.6 The areas of thinning (green arrows) and the corresponding gyri and arachnoid granulations on the endocranial surfaces

7.2 The spatial relationship between bone, brain, and diploic vessels in extant humans

7.2.1 The case study of extant human specimens

Overview

Five extant human crania were selected for in-depth case study and interindividual comparison. They were labelled as MNHN-HA-17425 (Russia), MNHN-HA-17434 (Russia), MNHN-HA-17461 (Romania), MNHN-HA-17498 (Moldova), and MNHN-HA-35026 (France). They were selected for the same criteria used for chimpanzees, as explained above.

MNHN-HA-17425

The supraorbital area of the frontal bone was thickened (>9.5 mm), housing many long and wide DC branches (Figure 7.7). Several branches among them extended towards the thick frontal crest (8.0-10.0 mm) but stopped at its edge. The areas between the frontal crest and temporal lines were compressed by the superior and middle frontal gyri and were much thinner, with the thinnest part on the left side (4.0-5.0 mm) bypassed by DCs. Areas of thinning (3.0-4.5 mm) could also be found inferior to the temporal lines on both sides, which were corresponded to the lateroinferior edge of the frontal squama. The left thinning was more evident than the right one. They were compressed by the inferior frontal gyrus and bypassed by DCs. In contrast with the thinning in the lower half of the frontal squama, the upper half was obviously thickened (peaked at 11.5 mm), with many large DC branches manifested. However, although the bregmatic area was slightly thickened (8.5-9.0 mm), no frontal DC branch extended into this area.

The parietal bones were relatively thinner than the frontal bones, but their DC complexity and amount were similar. The compression from the precentral gyrus and arachnoid granulations rendered the anterosuperior part of the bones (4.0-6.0 mm) much thinner than its surrounding areas and bypassed by DCs. Similarly, thinning

caused by the compression from the inferior parietal lobule and temporal gyri appeared in the temporal squama and lower parietal bone (< 4.5 mm). The extension of parietal DCs stopped when approaching these areas. In contrast, the thickened area of the parietal bones appeared along the sagittal and lambdoid sutures (6.0-10.0 mm), where many short DC branches extended inside. Still, most large parietal DCs were distributed outside this thickened area.

The thickness of the occipital bone was similar to that of the parietal bones, but fewer DCs were presented in the former. The long DC branches were located along the thick midline and superior nuchal line (7.5-14.5 mm). A few branches extended superiorly into the relatively thinner cerebral fossa (4.5-7.5 mm), which was compressed by the occipital gyri. Besides, no DCs extend inferiorly into the cerebellar fossa (2.0-7.5 mm), the thinnest part of the occipital bone.

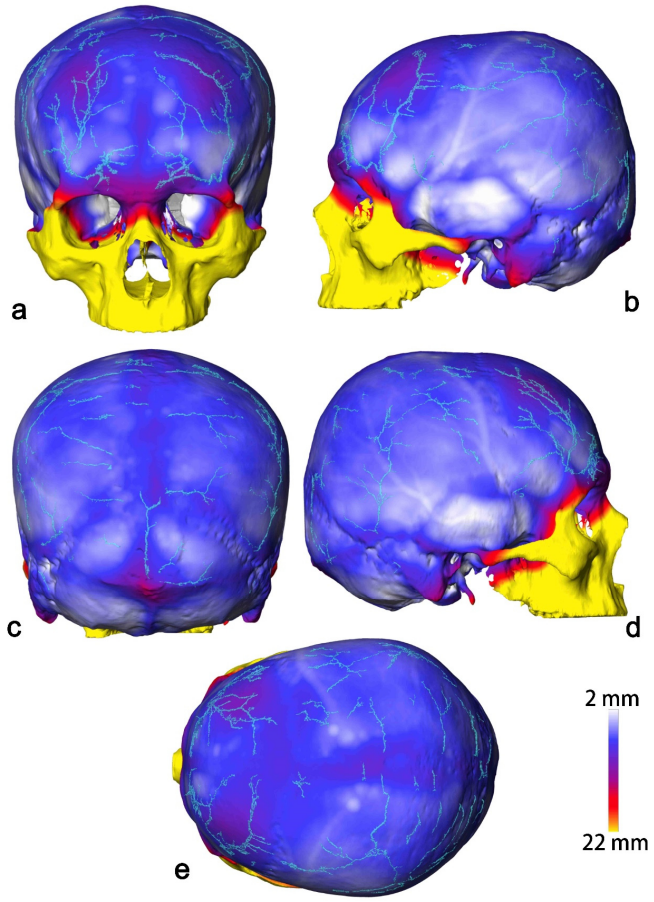

Figure 7.7 The CVT and DC distribution in the specimen MNHN-HA-17425, shown in the anterior (a), lateral (b and d), posterior (c), and superior (e) views.

The superior and anterior edges of the sphenoid greater wings were thickened (4.5-11.0 mm), where a few short DCs appeared. The thinnest parts of the greater wing were thinner than 2.0 mm, compressed by the inferior frontal and temporal gyri and bypassed by DCs. Adjacently, the majority of temporal squama was compressed by the temporal gyri and thinner than 2.0 mm, with no DCs appearing. The petromastoid parts of temporal bones were rather thick (5.5-15.0 mm), but only scarce and small DCs were distributed there.

MNHN-HA-17434

The supraorbital area (8.5-20.0 mm) was the thickest part of the frontal bone, but it housed few DC branches (Figure 7.8). The adjacent frontal crest was slightly thickened (7.0-9.5 mm), and it also housed no DCs. Most frontal DCs were distributed in the areas between the temporal line and frontal crest, where the thickness was almost evenly distributed (4.5-6.5 mm). Still, there were scattered small areas of thinning in this area compressed by arachnoid granulations or the superior frontal gyrus, with no DCs presented inside. Inferior to the temporal lines, areas of thinning (2.0-4.0 mm) on both sides were shown in the regions corresponded to the lateroinferior edge of frontal squama. The thinning on the left side was more evident than the one on the right side. These areas were also compressed by the endocranial surface (inferior frontal gyrus) and few DC branches course in these thin areas but bypassed the thinnest centre.

The parietal bones were comparable to the frontal squama in thickness and DC complexity. On the top, the anterosuperior part of the bones (2.0-6.0 mm, including the bregmatic area) had evident thinning compressed by the precentral gyrus and arachnoid granulations. No DCs extended into this thin area. In contrast, the parasagittal area posterior to this thinning was thickened (6.0-9.5 mm), with many DC branches extending inside. Still, most large parietal DCs were located outside this thickened area. These DCs ramified towards several directions but stopped before entering the thin

areas on both sides (<2.0 mm) close to the pterion, which was compressed by the stem of MMV.

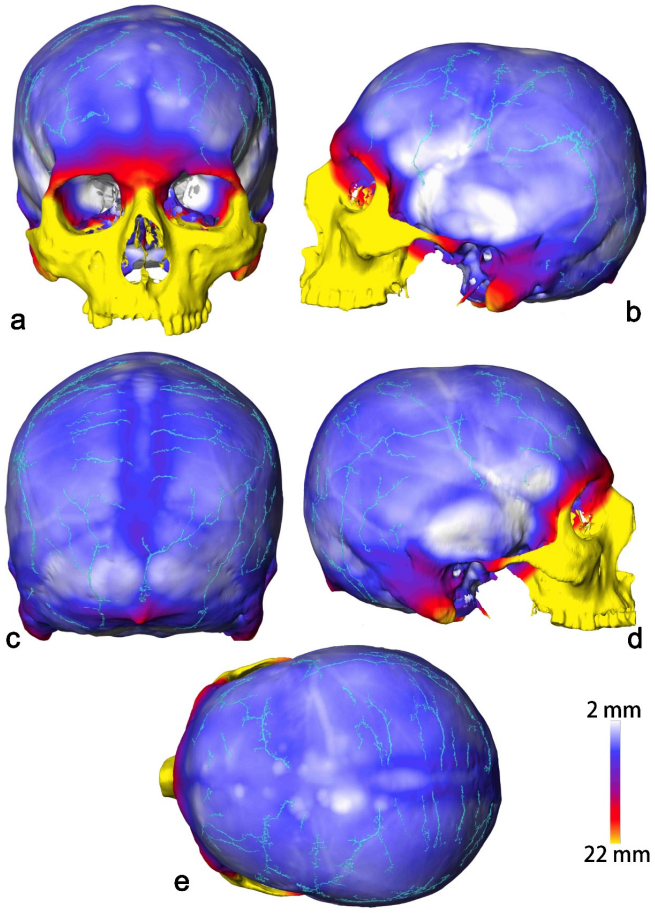

Figure 7.8 The CVT and DC distribution in the specimen MNHN-HA-17434, shown in the anterior (a), lateral (b and d), posterior (c), and superior (e) views.

The thickness of the occipital bone was similar to that of the frontal and parietal bone. Many large DC branches appeared in the occipital bone, and most of them were located in the thick midline and superior nuchal line (6.0-17.5 mm). These DCs also extended into the relatively thinner cerebral fossa (3.5-6.0 mm), which was compressed by the occipital gyri, but did not extend into the thinnest part of the fossa. Additionally, no DCs extended into the cerebellar fossa, where the thickness was generally below 3.0 mm.

The majority of the greater wings of sphenoid bone was extremely thin (<2.0 mm). It was compressed by the frontal and temporal gyri and bypassed by DCs. In contrast,

DCs appeared in the superior edges of the greater wings, which were relatively thicker (>4.5 mm). Additionally, no DCs appeared in the adjacent temporal squama, where the compression from the temporal gyri was corresponded to large areas of evident thinning (< 2.0 mm). And the DCs in the petromastoid part of the temporal bone were small and scarce, though the local thickness was over 9.0 mm.

MNHN-HA-17461

The thickest part of the frontal bone was the supraorbital area (6.0-11.5 mm), where rich DC branches were located (Figure 7.9). The thickness of the adjacent frontal crest was around 7.0 mm, housing no DCs. In comparison, the areas lateral to the frontal crest (i.e., the lower half of frontal squama) were relatively thinner (<7.0 mm), housing many long DC branches. Especially, the extremely thin area (2.5-3.0 mm) adjacent to the frontal crest was corresponded to an arachnoid granulation on the endocranial surface and it housed no DCs. A pair of extremely thin areas (< 2.0 mm) bypassed by DCs can also be found near the pterion, which were corresponded to the compression from the inferior frontal gyrus. The left thinning was more evident than the right one. The upper half of the frontal squama was thickened (peaked at around 7.5 mm), except for the bregmatic area (3.5-6.0 mm) with very slight thinning caused by compression from the arachnoid granulations. No DCs were manifested in the thin bregmatic area.

Compared with the frontal bone, the parietal bone was comparably thick. The degree of complexity and amount of parietal DC branches were similar to those of frontal DCs. On the top of the parietal bones, an evident thinning (2.0-4.5 mm) was presented along the anterior section of the sagittal suture and housed no DCs. This thin area was compressed by the precentral gyrus and many arachnoid granulations. Similarly, extremely thin areas (<2.5 mm) compressed by the inferior frontal gyrus, temporal gyri, and inferior parietal lobule could also be found along the lower coronal suture (close to the pterion) and squamous sutures. The extension of DCs stopped when approaching these thin areas. Additionally, the thickened areas of the parietal bone (6.0-9.5 mm)

were located lateral and adjacent to the posterior section of the sagittal suture. But they did not house the most nor largest DC branches.

The DCs in the occipital bone were fewer than those in the parietal and frontal bones. Most occipital DCs were distributed in the upper half of the bone (above the superior nuchal line), which was relatively thicker. In contrast, the lower half of the occipital bone was rather thin (around 2.0 mm), with no DCs manifested. The DCs in the upper part were mostly concentrated along the thick midline (6.5-11.0 mm). A few branches ran across the thinner cerebral fossa (4.5-6.5 mm, compressed by gyri) and arrived at the thick paralambdoid area (7.0-8.5 mm).

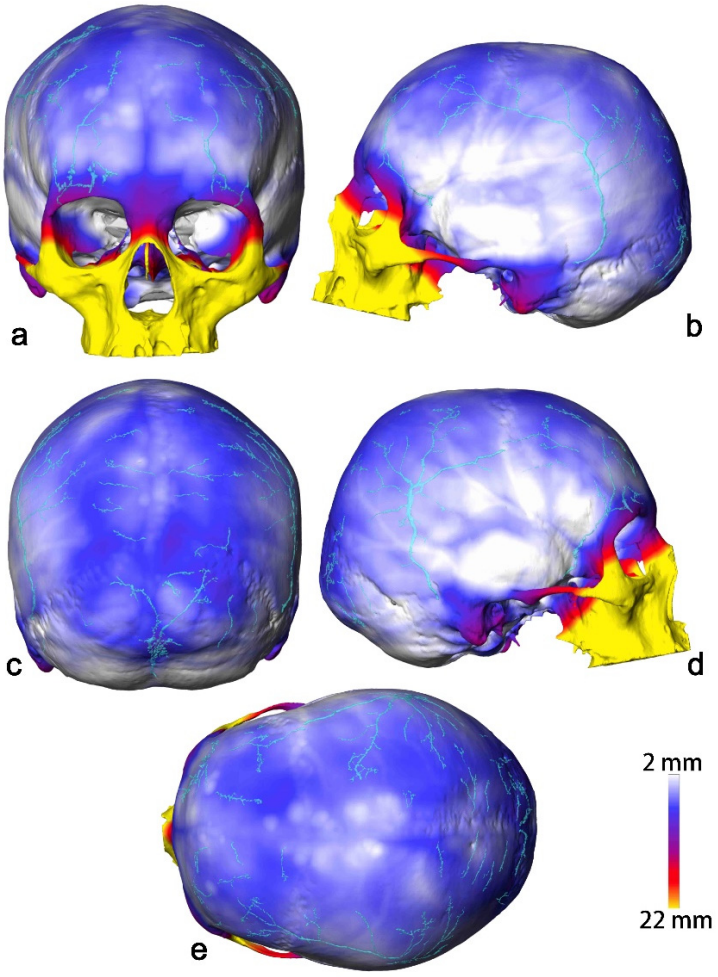

Figure 7.9 The CVT and DC distribution in the specimen MNHN-HA-17461, shown in the anterior (a), lateral (b and d), posterior (c), and superior (e) views.

The sphenoid greater wings were compressed by the inferior frontal gyrus and temporal gyri and showed evident thinning (<2.0 mm). DCs of the greater wings only appeared in the superior and anterior edges, where the thickness was over 4.0 mm. The adjacent temporal squama was compressed by the temporal gyri and generally thinner than 2.0 mm, while petromastoid parts of the temporal bones were thicker than 6.0 mm. No DCs appeared in the temporal squama, and only scarce and small DCs were in the petromastoid parts.

MNHN-HA-17498

The supraorbital area (7.0-12.0 mm) was the thickest part of the frontal bone, housing a pair of DC branches extended from the frontal squama (Figure 7.10). The frontal crest of frontal squama was also thickened (6.0-7.5 mm), but it did not house main DC branches. Only a few narrow branches extended from the lateral sides of the squama to the crest. Similarly, the bregmatic area was slightly thickened (6.0-7.0 mm) but with no DC manifested there. Most DC branches were located in the large area lateral to the frontal crest and anterior to the bregma, where the thickness value ranges between 2.0 to 6.5 mm. Besides, a pair of extremely thin areas (around 2.0 mm) were found close to the pterion. The left thinning was smaller than the right one. They corresponded to the pronounced inferior frontal gyrus and were obviously bypassed by DCs.

The parietal bones were comparable to the frontal squama in general thickness and their DC networks were also comparably developed. Many short DC branches arrived at the sagittal suture and its adjacent area (5.5-9.0 mm), which were the thickest part of the parietal bones. Still, most DCs were distributed outside the parasagittal area. The upper half of the parietal bone (4.0-7.5 mm, except the parasagittal area) was slightly thicker than the lower half (3.5-6.5 mm), but they did not differ obviously in the complexity and amount of DCs. Evident thinning could be found near the pterion on both sides (<2.0 mm), along the coronal suture on both sides (around 3.5 mm), and in the anterosuperior corner of the left parietal bone (3.0-4.0 mm). These areas of thinning

were caused by the compression from the precentral gyrus, inferior frontal gyrus, temporal gyri, and inferior parietal lobule. When reaching the edge of these thin areas, the extension of DC branches stopped.

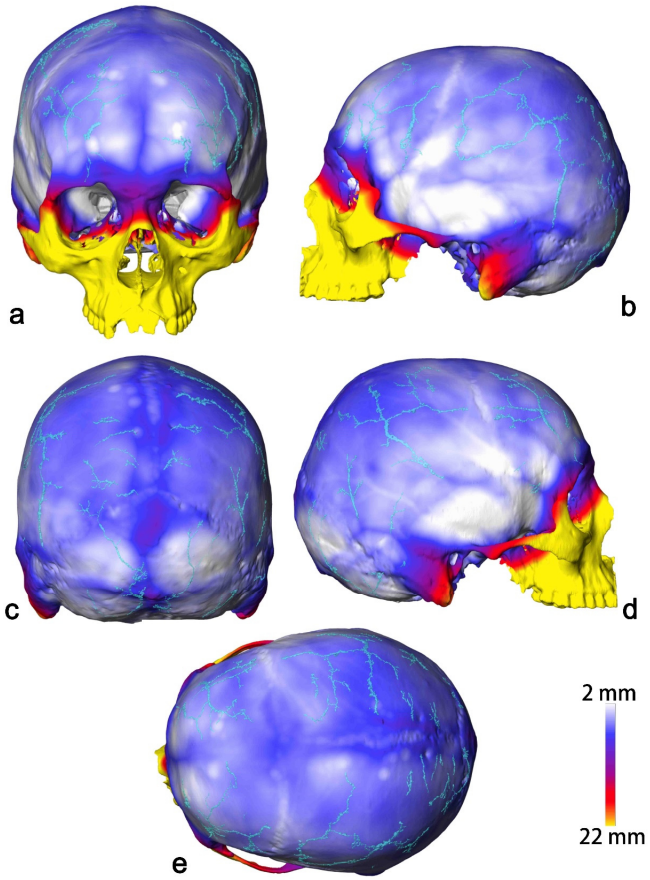

Figure 7.10 The CVT and DC distribution in the specimen MNHN-HA-17498, shown in the anterior (a), lateral (b and d), posterior (c), and superior (e) views.

The general thickness of the occipital bones was slightly thinner than those of the parietal and frontal bones. In comparison with the latter, fewer DC branches were found in the occipital bone. The occipital DCs were mainly distributed along the midline (6.0-10.5 mm), which was the thickest part of the bone. Several long but narrow branches extended from the midline to the thin cerebral fossa (2.0-6.0 mm), which was compressed by the occipital gyri. Still, the areas along these branches in the fossa were not extremely thin, with their thickness ranging from 3.0 to 6.0 mm.

The greater wings of the sphenoid bones were compressed by the inferior frontal gyrus

and temporal gyri and were generally thinner than 2.0 mm. Scarce DCs were distributed in the superior edge of the greater wings (around 4.0 mm). Adjacently, the temporal squamas were rather thin, with the areas compressed by the temporal gyri thinner than 2.0 mm. No DCs appear in the temporal squamas. The petromastoid parts of the temporal bones were generally thicker than 8.0 mm, while only a few small DCs were located there.

MNHN-HA-35026

The supraorbital area (7.5-15.5 mm) was the thickest in the frontal bone, housing a few DCs extending from the frontal squama (Figure 7.11). The frontal crest was very slightly thickened (5.5-7.5mm), with no DCs appearing. Large DC branches were located in a pair of thickened areas (5.5-9.0 mm) lateral to the frontal crest. When extending anteroinferiorly, these DC branches stopped at the edge of an extremely thin area (3.0-4.5 mm) located adjacent to the left side of the frontal crest, which was compressed by the superior frontal gyrus or arachnoid granulations. Also, when extending laterally, the DCs bypassed the extremely a pair of extremely thin areas (< 2.0 mm) below the temporal lines on both sides, which were compressed by the inferior frontal gyrus. The right thinning was larger than the left. The bregmatic area was thickened (peaked at around 8.0 mm), but no DCs were manifested there.

The parietal bones in general were slightly thinner than the frontal squama, and their DC networks were comparably developed. The parasagittal area adjacent and inferior to the bregmatic area was compressed by arachnoid granulations and precentral gyrus (and possibly postcentral gyrus), showing obvious thinning (< 2.0 mm). The extension of DCs stopped at the edge of this thin area. Also, lateral to the bregmatic area, the paracoronal area of parietal bones (< 4.5 mm) was compressed by the precentral gyrus and meningeal vessels. And the thinning caused by them interrupted the extension of scarce DCs in this area. Areas of thinning compressed by the temporal gyri and inferior parietal lobule appeared near the posterior half of the squamous sutures on both sides

(2.0-3.0 mm), where no DCs appeared. Besides, it was noticeable that the upper half of the parietal bones in general were slightly thicker than the lower half, and the former housed more and larger DCs.

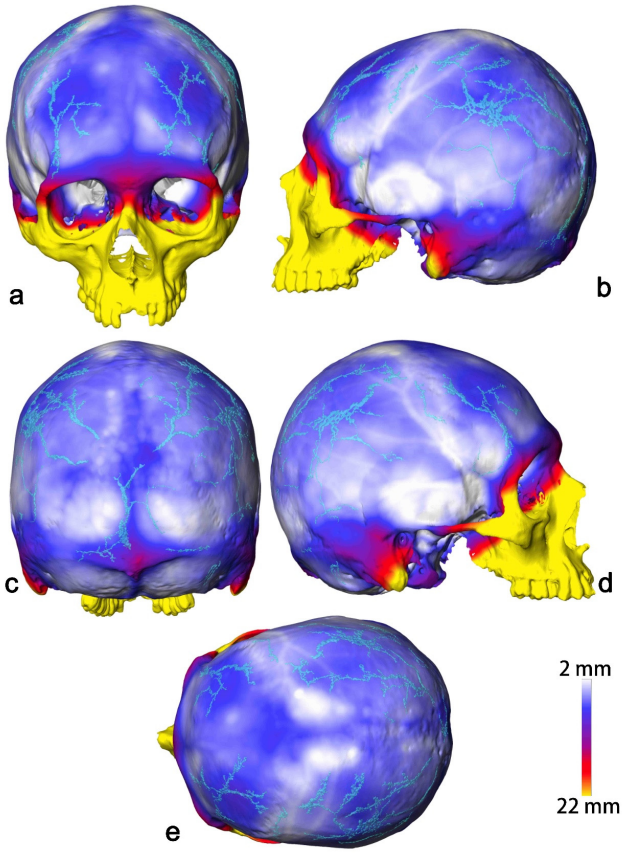

Figure 7.11. The CVT and DC distribution in the specimen MNHN-HA-35026, shown in the anterior (a), lateral (b and d), posterior (c), and superior (e) views.

The general thickness of the occipital bone was comparable to that of parietal bones, and was slightly thinner than the frontal. Many large DC branches were in the occipital bone. Most of them were distributed along the thick midline and superior nuchal line (5.0-15.0 mm). Some short branches extended into the relatively thinner cerebral fossa, which was compressed by the occipital gyri, but they course along the edge of the thinnest part (< 2.5 mm) without entering.

The sphenoid greater wings were compressed by the inferior frontal and temporal gyri, with the majority thinner than 2.0 mm. No DCs appear in these extremely thin areas,

and only a few were distributed in the superior edges (around 4.5 mm). In the adjacent temporal squama, the compression from the temporal gyri corresponded to the area of thinning (< 2.0 mm). The petromastoid parts of the temporal bones were over 8.5 mm. No DCs appear in the temporal bones.

7.2.2 Synthesis

The general thickness of extant human specimens was much thicker than that of chimpanzees. The thickest areas of extant human neurocranium did not house the most nor largest DC branches, and the areas with evident thinning were clearly bypassed by DCs (Figure 7.12).

The patterns of CVT variation were consistent among these extant human specimens. Across all extant human specimens, the thickest areas of the neurocrania were always the supraorbital area, the frontal crest, the asterional region, as well as the midline and superior nuchal line of the occipital bone. These thickened areas corresponded to the ridges and superstructures on the ecto-and endocranial surfaces.

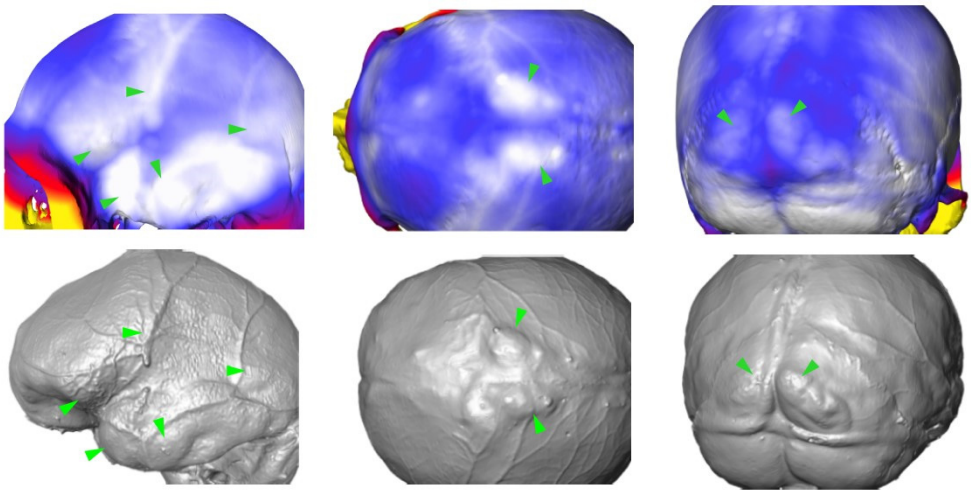

Figure 7.12 The areas of thinning correspond to gyri, vessels, and arachnoid granulations on the endocranial surface (green arrows). They also appear in the lower frontal squama, anterosuperior and inferior parietal bone, sphenoid greater wings, temporal squama, and cerebral fossa.

Areas of evident thinning were corresponded to the compression from brain gyri, arachnoid granulations, and meningeal vessels (Figure 7.12). In detail, a pair of extremely thin areas always appeared in the lateroinferior edge of the frontal squama (below the temporal line), which were usually asymmetric and compressed by the inferior frontal gyrus. The thinning in the greater wings of the sphenoid bone corresponded to the compression from the inferior frontal gyrus and temporal gyri. The thin temporal squama and inferior part of the parietal bone was corresponded to the compression from the temporal gyri and inferior parietal lobule. The anterosuperior part of the parietal bone was compressed by the precentral gyrus, meningeal vessels, and arachnoid granulations. The thin cerebral fossa was compressed by the occipital gyri.

7.3 The spatial relationship between bone, brain, and diploic vessels in hominin fossils

7.3.1 Middle Pleistocene hominins

Tighennif 4

This right parietal bone was very well preserved, with no evident taphonomical damages distorting the CVT. The thickest part was the asterional region (peaked at around 10.5 mm, Figure 7.13), while the center of the upper third of the bone was the second thickest (peaked at around 8.5 mm). Interestingly, the main branch of the DC network just ascended from the thickest region to the second thickest region. The bone surrounding the middle section of the main branch was slightly thickened (6.5-7.0 mm), which was corresponded to a sulcus on the endocast. The main branch also ramified towards several directions. It gave off a few narrow branches entering the center of the lower third of the bone, which was compressed by gyri and meningeal vessels and was much thinner than the asterional region. These branches stopped before entering the thinnest part of the lower third parietal bone (4.0-5.0 mm), which was located close to the pterion. In addition, thinning was also manifested in the superior edge of the bone (i.e., along the sagittal suture), which was corresponded to the pronounced gyri on the endocranial surface. The narrow branches extending superiorly bypassed these thin areas (4.5-5.5 mm).

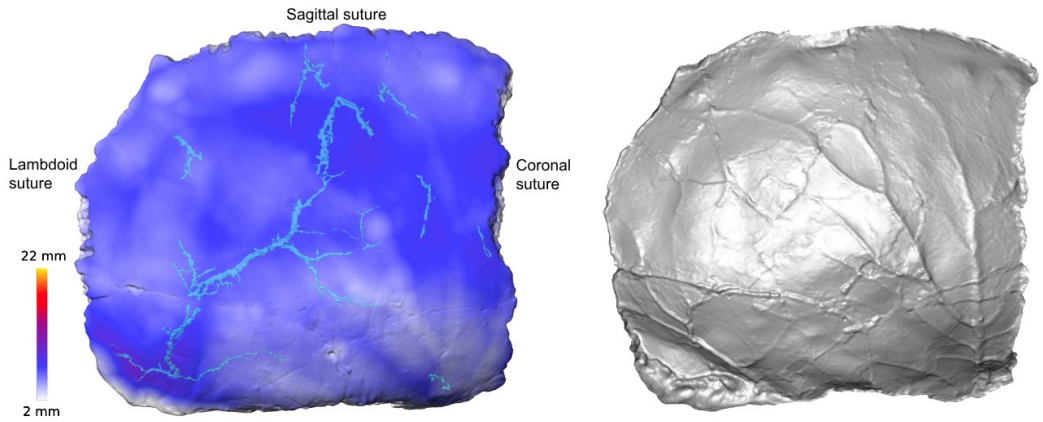

Figure 7.13 The CVT colormap, DC distribution, and endocranial surface of Tighennif 4.

LES 1

The frontal bone, left parietal bone, and left part of the occipital bone were relatively well preserved. Although taphonomic damages have changed the thickness values in limited areas, the majority of the preserved bones were not affected.

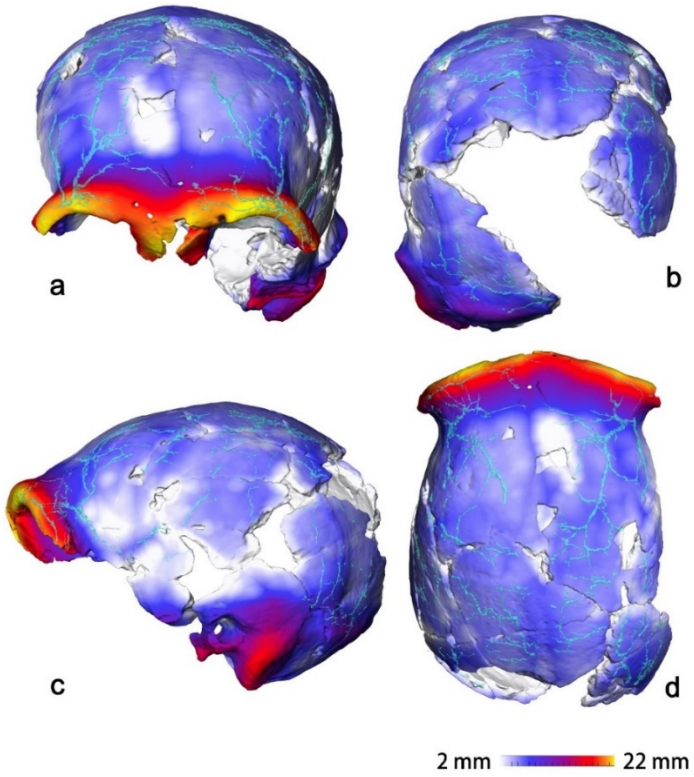

Figure 7.14 The CVT and DC distribution of the specimen LES 1, shown in the anterior, posterior, lateral, and superior views. For the lateral view, only the better-preserved side is presented.

In the frontal bone, the thickest part was the supraorbital ridge (>12.0 mm), where many long and narrow DC branches were found (Figure 7.14). In comparison, the relatively thinner frontal squama housed more and larger branches. The anterior edge (8.0-12.0 mm) and two temporal lines (5.5-8.5 mm) of the frontal squama were thickened, while the area semi-encircled by them in the squama was generally thinner than 5.5 mm (except the sagittal crest), which was compressed by the superior and middle frontal gyri. The DCs in the squama did not concentrate in the thick areas. Instead, the DCs extended from the thick anterior edge and temporal lines to the centre of the thinner area. The frontal crest was thickened (5.0-6.5 mm), but there was no DCs manifested.

This might result from the taphonomic damage. In addition, on the left side of the frontal bone, there was an extremely thinning (<2.0 mm) close to the pterion and bypassed by the DCs, which was compressed by the inferior frontal gyrus (Figure 7.15).

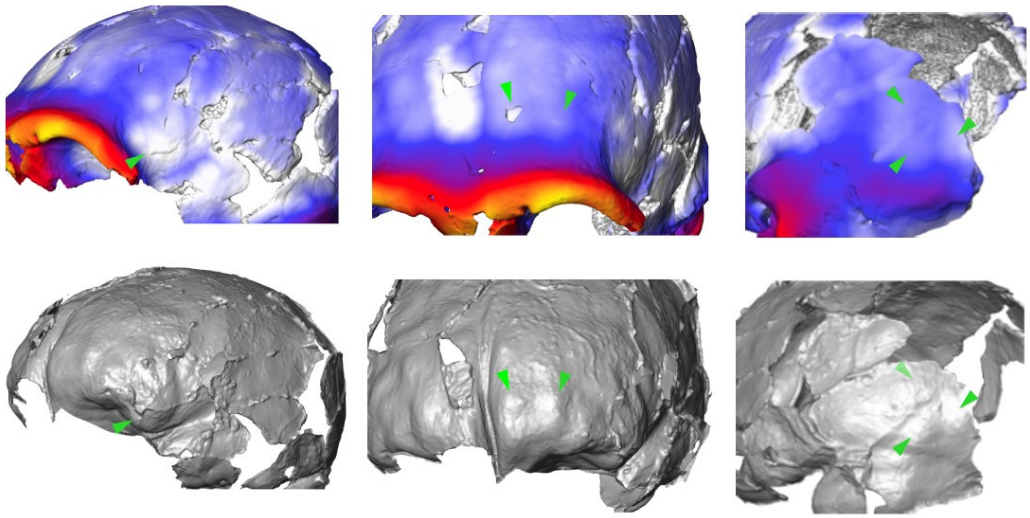

Figure 7.15 The areas of thinning (green arrows) and the corresponded gyri on the endocranial surfaces

In the parietal bones, the bregmatic area was damaged and its true thickness value was unknown. The thickness of the rest part of the parietal bones was comparable to that of the frontal squama. The sagittal suture of the parietal bones was slightly thickened (peaked at 7.0 mm), but there were only scarce and short DC branches. The majority of the parietal DC branches were almost evenly distributed in the bones (except the sagittal suture), despite the variable thickness—the asterional region (peaked at around 9.0 mm) and the centers of the parietal bones were thickened (peaked at around 7.5 mm), while the rest was between 5.0-6.5 mm.

In the occipital bone, the superior nuchal line was the thickest, standing between 8.0-12.0 mm. Still, the majority of the rest occipital network was not within this thickened line but was found in the relatively thinner area, which was between the belt and the lambdoid suture. This thinner area was slightly compressed by the occipital gyri.

7.3.2 Late Pleistocene hominins

Overview

Four *H. neanderthalensis* and four fossil *H. sapiens* specimens with generally well-preserved neurocranium were included in the comparison. An initial analysis of the CVT and DC distribution of these hominin fossils has been published in my paper (Hui & Balzeau, 2023a). Here, this current study reused the data, figures, descriptions, and conclusions from this published paper. Additionally, this current study provided new information about the interaction between endocranial morphology and CVT variation in each specimen.

La Quina H5

The neurocranium of La Quina H5 was generally thinner than those of other *H. neanderthalensis* specimens. Compared with them, La Quina H5 showed a lower density of DCs.

The thickest portion of the frontal bone was the supraorbital area (11.0-21.5 mm), through which a few narrow DCs traversed (Figure 7.16). The overall thickness of the frontal squama was relatively thin, with its thinnest sections located inferior to the temporal lines (<3.0 mm) and at the center of the frontal squama (excluding the frontal crest, 3.0-5.5 mm). These thinnest areas in the frontal bone were compressed by the superior, middle, and inferior frontal gyri and exhibited either no DCs or only isolated narrow ones. The majority of frontal DCs were concentrated in the lateral parts of the frontal squama (3.5-7.5 mm), where the thickness was slightly greater than in the thinnest regions.

The density of parietal DCs and thicknesses of the parietal bones resembled those of the frontal squama. The relatively thicker regions of the parietal bone included the parasagittal (4.5–6.5 mm), central (4.0–6.5 mm), and lower (3.5–7.0 mm) areas, where DCs were predominantly found. The areas of thinning (<4.0 mm) were observed in the

anterosuperior part of the parietal bone, which corresponded to the compression from the meningeal vessels and precentral gyrus. These thin areas lacked large DC branches, with the thinnest parts (around 2.0 mm) bypassed by DCs.

The thickness of the occipital bone was similar to that of the parietal bone but with fewer and smaller DCs. While no large branches ran along the thick midline (5.0–8.0 mm), most occipital DCs were distributed in the thick asterional region (4.0–7.0 mm) and the relatively thinner cerebral fossa (3.5–6.0 mm). The latter was compressed by the occipital gyri. The suprainiac fossa did not show evident thinning (excluding the taphonomically damaged area), with several DCs extending inside.

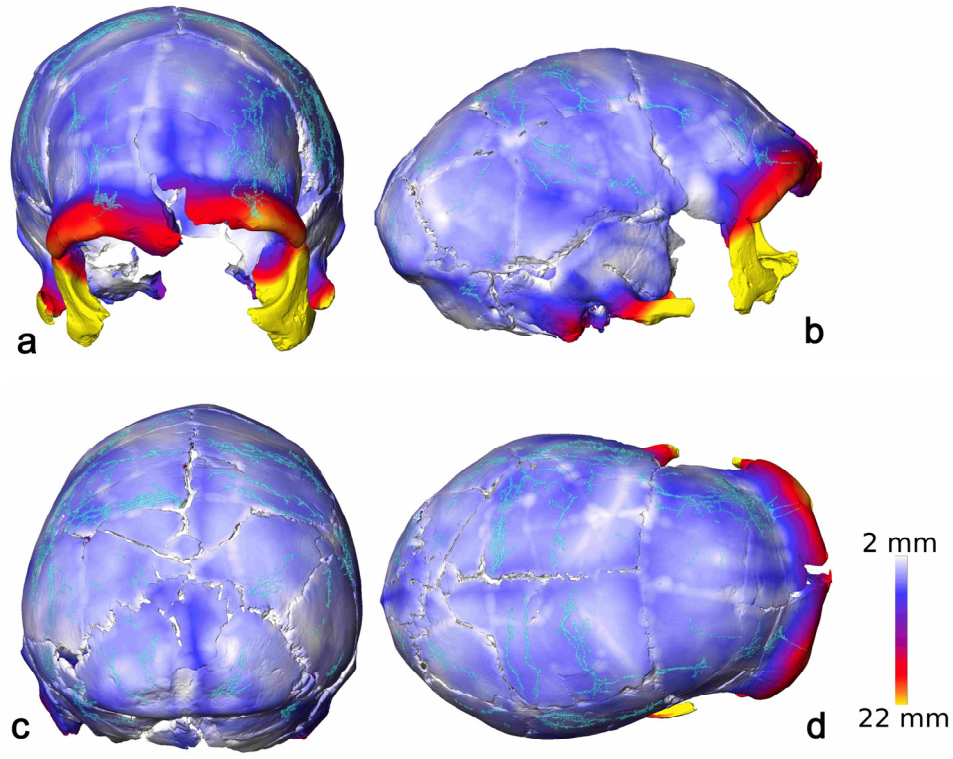

Figure 7.16 The CVT and DC distribution of La Quina H5. For the lateral view, the better-preserved side is present here. The figure is from Hui & Balzeau (2023a).

La Chapelle-aux-Saints 1

The neurocranium was generally thick, with dense DC branches. The thickest region of the frontal bone was the supraorbital area (>14.0 mm), which hosted a large amount of narrow DCs (Figure 7.17). Across the entire frontal squama, thickness ranged from 5.5

to 14.0 mm, marking it as one of the thickest areas within the entire neurocranium, housing an abundance of large DC branches. Thinner regions (<4.5 mm) of the frontal bone were situated below the temporal line. These thin areas were compressed by the inferior frontal gyrus and bypassed by DCs.

Comparably, the parietal bones had a thickness range close to that of the frontal squama and they housed a large and reticulated DC network. The thick regions within the parietal bones included the central area (7.5-9.5 mm), regions adjacent to the lambdoid (6.5-9.0 mm), and the area above the squamosal suture (6.0-9.5 mm), with all exhibiting rich DCs. Conversely, the thinnest portion of the parietal bone was in the anterosuperior region (<4.0 mm), characterized by scattered small DC branches. This thin area was compressed by the precentral gyrus and meningeal vessels.

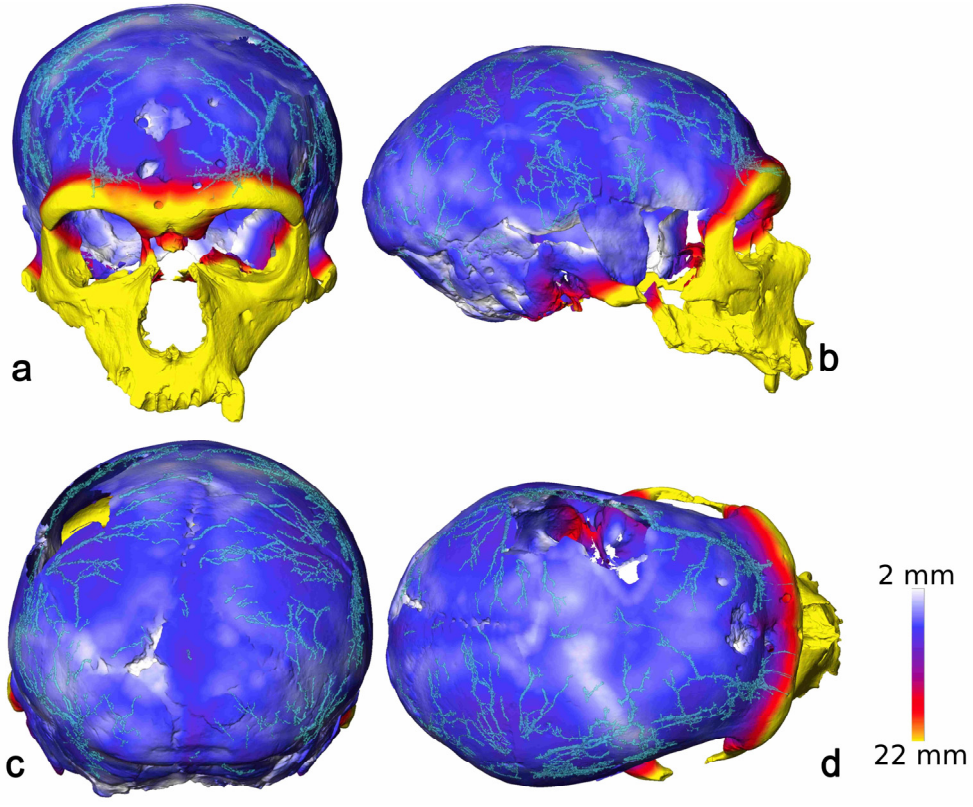

Figure 7.17 The CVT and DC distribution of La Chapelle-aux-Saints 1. For the lateral view, the better-preserved side is present here. The figure is from Hui & Balzeau (2023a).

Although the occipital bone was thick, it contained fewer DCs compared to the frontal

and parietal bones. Most occipital DCs were concentrated within the cerebral fossa (5.0-7.5 mm) and the asterional region (5.0-9.0 mm). The cerebral fossa was slightly compressed by the occipital gyri. Only a few narrow DCs dispersed along the midline (7.5-10.0 mm), which represented the thickest part of the occipital bone. Additionally, the suprainiac fossa did not manifest evident thinning, with several DC branches extending inside.

Spy 1

The neurocranium of the specimen was generally thick, with a large amount of DCs (Figure 7.18). The thickest region of the frontal bone, surpassing 14.0 mm, was the supraorbital area. But only scarce DCs extended into the supraorbital area. The thickness of the frontal squama ranged from 4.5 to 14.0 mm. The evident thinning between the temporal lines was caused by taphonomical erosion. The thinnest area (<4.5 mm) located below the temporal line on the right side was compressed by the inferior frontal gyrus and no DCs were present there.

The thickness of the parietal bones resembled that of the frontal squama, but the parietal DC network was larger and more complex. The thickness of parietal bones reached its peak in the central part of the bone (around 10.5 mm), though the DCs in this area were not the most abundant. The most developed DCs were found in the lower half of the parietal bones (5.5-7.5 mm). The anterosuperior part of the parietal bones (5.5-7.0 mm) housing scattered narrow DCs was compressed by meningeal vessels and precentral gyrus, and was slightly thinner than other areas in the parietal bones.

The thickness of the occipital bone was comparable to that of the parietal bones, yet it contained fewer and smaller DCs. Most DCs were present in the thickest region (9.5-11.5 mm) below the lambda, as well as in the cerebral fossa (6.5-9.5 mm) and the asterional region (7.0-10.5 mm). The cerebral fossa (including the suprainiac fossa) was compressed by the slightly pronounced occipital gyri, and it did not show evident

thinning.

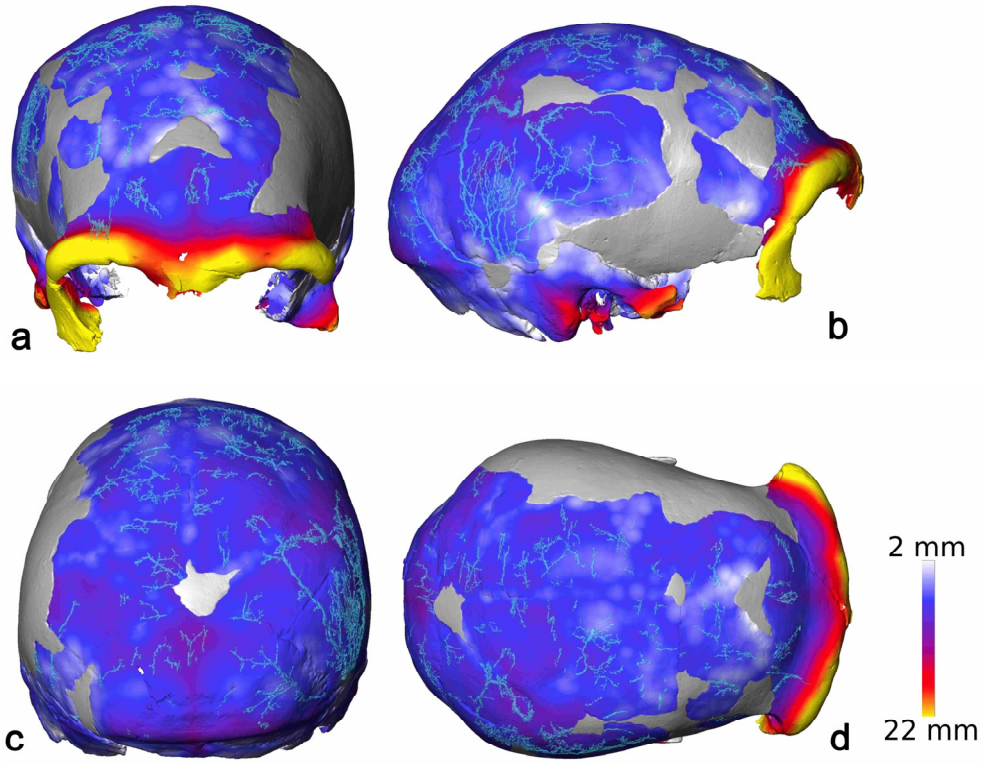

Figure 7.18 The CVT and DC distribution of Spy 1. The areas filled in with artificial materials were excluded from the analysis and colored in grey. For the lateral view, the better-preserved side is present here. The figure is from Hui & Balzeau (2023a).

Spy 10

The cranium was generally thick, presenting dense DC branches (Figure 7.19). The supraorbital area (>10.0 mm) was the thickest region of the frontal bone. However, only a few DCs were present in this area. The central portion of the frontal squama (4.5-5.5 mm) and the two sides of the temporal lines (4.0-6.0 mm) were notably thin, with scattered DCs observed. These areas of thinning were compressed by the frontal gyri. Conversely, other areas of the frontal squama were thicker (5.0-10.0 mm) and hosted the majority of large DC branches. An exception was the bregmatic area (6.5-8.0 mm), which was thick but in lack of DCs.

Compared with the frontal squama, the parietal bones exhibited a similar thickness and

a comparably dense DC network. The center (5.5-10.0 mm) and parasagittal area (5.0-9.5 mm) of the parietal bones were thick, housing most of the parietal DCs. The thickest points (peaked at around 10.0 mm) of the parietal bones on both sides were at the center, but DCs were not observable there due to taphonomic damage. The anterosuperior part of the parietal bones was compressed by the meningeal vessels and precentral gyrus, showing a relatively thinner thickness (3.0-5.0 mm) and scarce DCs. The inferoposterior part of the parietal bones, as well as the temporal squama, displayed a pair of large and belt-like areas (3.5-6.0 mm) with a relatively thinner thickness on both sides, which were compressed by the inferior parietal lobule and temporal gyri. The thinnest sections of the belt-like areas were located in the temporal squama and middle section of the lambdoid suture, where no DCs were present. The other part of the belts was not extremely thin, with many large DCs extending inside (especially inside the asterional region).

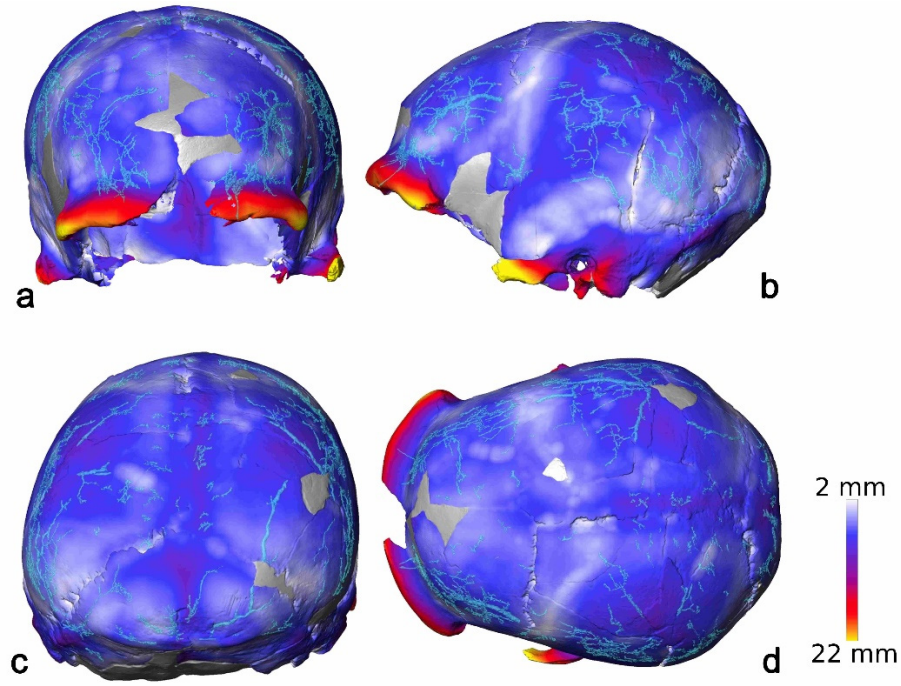

Figure 7.19 The CVT and DC distribution of Spy 10. The areas filled in with artificial materials were excluded from the analysis and colored in grey. For the lateral view, the better-preserved side is present here. The figure is from Hui & Balzeau (2023a).

The thickness of the occipital bone was similar to that of the parietal bones but with

fewer and smaller DCs. Occipital DCs were predominantly distributed in the thick midline (8.5-10.5 mm), the asterional region (6.5-10.0 mm), and the superior nuchal line (4.5-9.0 mm). Additionally, some DCs extended to the edge of the relatively thinner cerebral fossa (4.5–7.0 mm), which was compressed by the occipital gyri.

Cro-Magnon 1

Among the sample of fossil *H.sapiens*, Cro-Magnon 1 had the thickest neurocranium and the most dense DC network (Figure 7.20). The thickest region of the frontal bone was the supraorbital area, measuring over 14.5 mm and hosting a large number of narrow DC branches. The majority of the frontal DC network was located within the thickened area in the frontal squama and between the temporal lines. The upper half of this thickened area (5.0-15.5 mm) was slightly thicker than the lower half (7.5-12.5 mm), yet there was no notable increase in DC size and amount in the upper part. Several small areas with slight thinning appeared along the midline of the frontal squama, especially within the bregmatic area (<4.5 mm). These areas of thinning were compressed by the superior frontal gyrus, precentral gyrus, and arachnoid granulations. Large DC branches bypassed these relatively thinner areas, with only a few small branches extended to their edges. Similarly, inferior to the temporal lines were a pair of areas with evident thinning (2.0-5.0 mm), which were compressed by the inferior frontal gyrus and bypassed by DCs. Besides, a pathological region with thinning was located in the frontal squama. As the diploic layer has been damaged, it hindered the assessment of the presence of DCs. However, the surrounding DC branches did not tend to extend inside the pathological area.

The parietal bones and frontal squama were comparable in thickness, DC density, and complexity. The upper third of the parietal bones was the thickest portion (peaked at around 14.5 mm), though it did not house the most abundant DC branches. The anterosuperior part of the parietal bones (including the parietal part of the bregmatic area) was compressed by the meningeal vessels, precentral gyrus and postcentral gyrus.

It showed slight thinning, with the thinnest part on the left hemisphere bypassed by DCs. Similarly, the lower edge of the parietal bones and temporal squama were compressed by the inferior temporal lobule and temporal gyri, showing evident thinning (<4.5 mm). It is obvious that large DCs coursed along the edge of this area without entering, and no DCs appeared in the thinnest part (<2.0 mm).

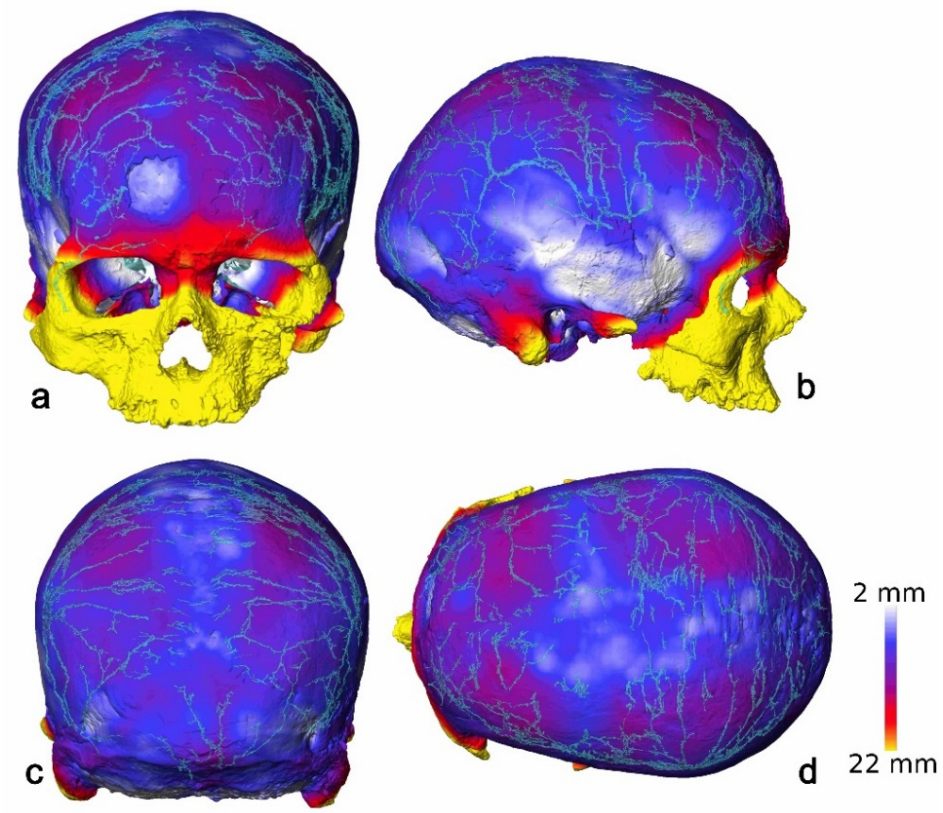

Figure 7.20 The CVT and DC distribution of Cro-Magnon 1. For the lateral view, the better-preserved side is present here. The figure is from Hui & Balzeau (2023a).

Comparatively, the occipital bone was thinner than the parietal and frontal bones, with a less developed DC network. Most occipital DCs were concentrated along the midline, the thickest area (7.5-13.5 mm) of the occipital bone. Additionally, some narrow DC branches were also present in the cerebral fossa, which was compressed by the occipital gyri and was relatively thinner (6.0-9.0 mm).

Cro-Magnon 2

The neurocranium of Cro-Magnon 2 was generally thinner than that of Cro-Magnon 1,

and the DC network of Cro-Magnon 2 presents lower degrees of density and complexity (Figure 7.21). The thickest areas of the frontal bone were the supraorbital area (9.0-14.0 mm) and frontal crest (9.5–11.5 mm), with a few branches extending inside. The frontal DC network was mainly situated in the middle and upper portions of the frontal squama. Especially, large DC branches circulated, but not extended inside, the thickened area of the frontal squama (7.5-11 mm). Notably, the bone was relatively thin on both sides of the temporal line—which was corresponded to the compression from the middle and inferior frontal gyri—while the temporal line itself measured between 5.0 and 8.5 mm in thickness. DCs coursed along and beneath the temporal line, bypassing the thinnest areas (<4.0 mm) on both sides.

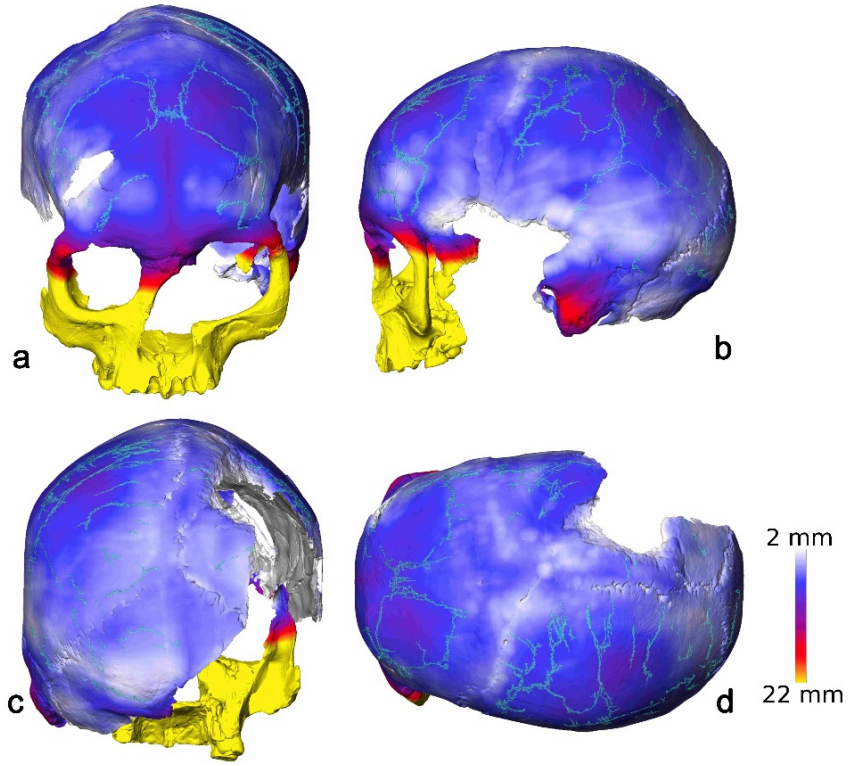

Figure 7.21 The CVT and DC distribution of Cro-Magnon 2. For the lateral view, the better-preserved side is present here. The figure is from Hui & Balzeau (2023a).

The parietal bones exhibited a similar thickness to the frontal squama and possessed a comparably developed DC network. Most parietal DCs were concentrated in the relatively thick upper part (6.0-10.0 mm), extending in the superoinferior direction but stopped as they approached the boundaries of the thin areas (3.0-6.0 mm), which were

located in the anterosuperior and lower parts of the parietal bones. The thinning in such areas were corresponded to the compression from the meningeal vessels, presental gyrus, inferior parietal lobule, and temporal gyri. The thickest areas of the parietal bones were located above the parietal eminence and reached a maximum of 10.0 mm, but they did not exhibit the most abundant DCs.

Occipital DCs were mostly confined in the relatively thick paralambdoid areas (5.5-7.0 mm) and the superior nuchal line (5.0-10.5 mm). Their extension ceased before entering the thinnest area (3.0-3.5 mm) located in the cerebral fossa, which was compressed by the occipital gyri.

Cro-Magnon 3

The neurocranium of Cro-Magnon 3 was slightly thinner than those of Cro-Magnon 1 and 2, and the DC network of Cro-Magnon 3 was comparable to that of Cro-Magnon 2 (Figure 7.22). The thickest section of the frontal bone was the supraorbital area, measuring between 11.0 and 17.0 mm, where only a few narrow DCs traversed. Adjacently, the lower edge of the frontal squama (5.0-7.0 mm) hosted abundant DC branches, and was notably thinner than the supraorbital ridge. Interestingly, the thickest areas (peaked at 10.0 mm) in the upper frontal squama did not house the most abundant DCs. The thinnest regions of the frontal bone, measuring below 3.0 mm, were located inferior to the temporal lines on both sides. They were compressed by the inferior frontal gyrus and bypassed by DC branches.

The two sides of the coronal suture showed different thicknesses, with the anterior side (located on the frontal bone, 4.0-6.5 mm) appearing thicker, while the posterior side (on the parietal bone, 3.0-5.5 mm) appeared thinner. Still, the both sides contained sparse DCs. The parietal bones in general were much thinner than the frontal bone, but the DCs of them were comparably developed. The upper part of the parietal bones (3.5-8.0 mm) was slightly thicker than the lower part (2.0-7.0 mm), and the upper part did not

house the most abundant DCs. The areas of evident thinning in the parietal bones were the anterosuperior (3.0-5.0 mm) and the lower edge of the bone (2.0-3.5 mm), which were compressed by the meningeal vessels, precentral gyrus, inferior parietal lobule, and temporal gyri. These areas were clearly bypassed by DCs.

In the preserved section of the occipital bone, the majority of DCs were concentrated along the midline (6.5-10.5 mm) and the superior nuchal line (5.5-9.0 mm), which were the thickest areas of the bone. The extension of DC branches ceased upon approaching the edge of thinner areas (3.5-4.5 mm) in the cerebral fossa compressed by the occipital gyri.

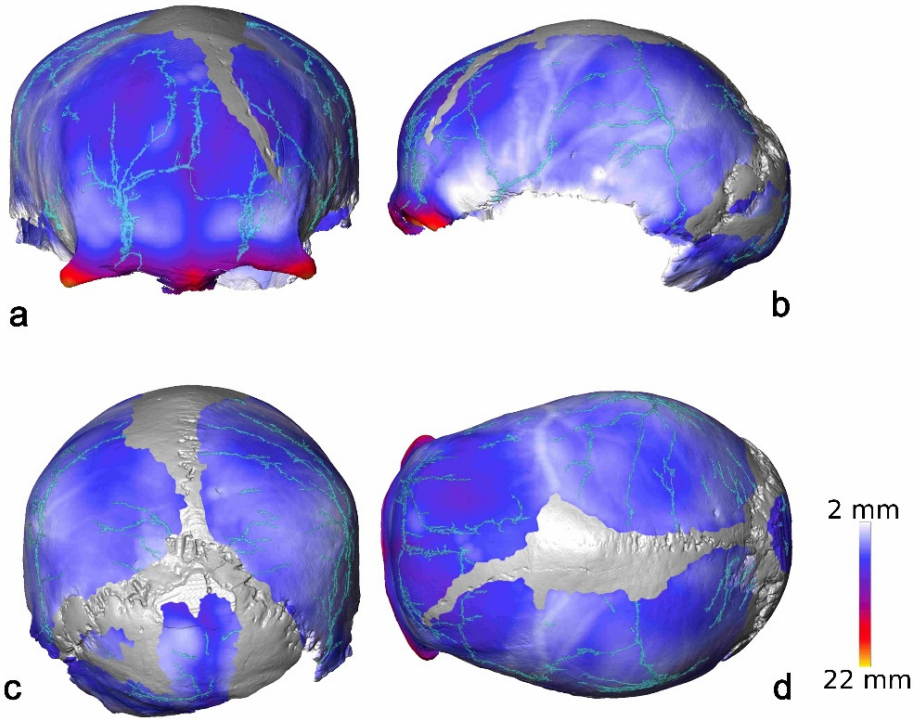

Figure 7.22 The CVT and DC distribution of Cro-Magnon 3. For the lateral view, the better-preserved side is present here. The figure is from Hui & Balzeau (2023a).

Abri Pataud 1

Abri Pataud 1 cranium had an overall thickness similar to that of Cro-Magnon 3 (Figure 7.23), with a comparably developed DC network. The thickest regions (9.0-13.0 mm) of the frontal bone were the supraorbital area and frontal crest, with no visible DCs.

The majority of frontal DCs did not appear in the thick center of the frontal squama (5.0-8.5 mm), and instead concentrated in the lateral parts on both sides, which were compressed by the superior and middle frontal gyri and were relatively thinner (4.0-7.0 mm). Moreover, the thinnest areas (<3.5 mm) were located inferior to the temporal lines on both sides. They were compressed by the inferior frontal gyrus and bypassed by DCs.

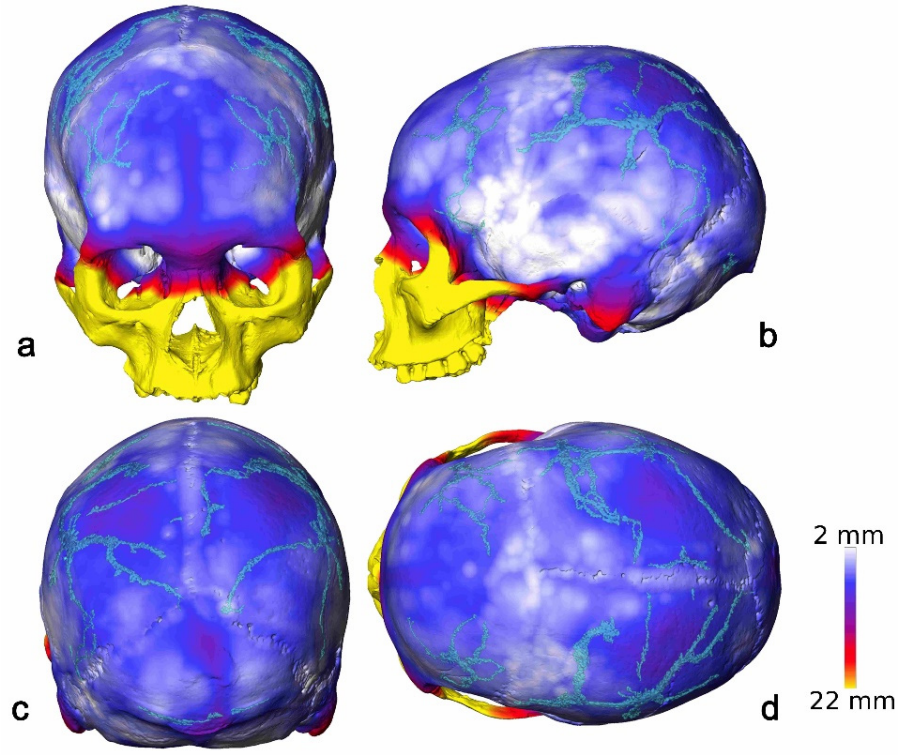

Figure 7.23 The CVT and DC distribution of Abri Pataud 1. For the lateral view, the better-preserved side is present here. The figure is from Hui & Balzeau (2023a).

The parietal bones generally exhibited higher thickness compared to the frontal squama. The sagittal suture (3.5-6.0 mm), as well as the anterior (<5.5 mm) and inferior (<4.0 mm) edges of the parietal bones, were the thinnest regions on the parietal bones. These areas of evident thinning were all connected and also extended into the temporal squama. DCs extended solely to the edges of these thin areas without entering. The thinning was corresponded to the compression from the meningeal vessels, superior sagittal sinus, precentral gyrus, postcentral gyrus, inferior parietal lobule, and temporal gyri. On the contrary, the thickest areas of the parietal bone, peaking at 10.5 mm, were positioned above the parietal eminence on both sides. However, they did not host the

most abundant DCs.

The thickness of the occipital bone was comparable to that of the parietal bone. Nevertheless, only a few DCs were visible in the occipital bone. Occipital DCs were mainly distributed along the thick superior nuchal line and possibly along the midline, which were the thickest area (6.0-12.5 mm) of the bone, In comparison, the cerebral fossa (4.0-6.0 mm) compressed by the occipital gyri was much thinner and devoided of DCs.

7.3.3 Synthesis

Similar to extant specimens, the results of hominin fossils showed that the thickest areas of neurocranium did not house the most nor largest DC branches, and the areas with evident thinning were clearly bypassed by DCs. Still, unlike the extant chimpanzee sample whereby the most developed DC network appeared in the thinnest specimen, hominin fossil specimens with higher global thicknesses tended to display larger and denser DCs.

The specimens of fossil *H. sapiens*, *H. neanderthalensis*, and *H. naledi* had some similarities in their CVT patterns (Figure 7.24), which were also shared with extant human specimens. The areas of evident thickening always appeared in the supraorbital area, frontal crest, asterional region, and superior nuchal line. For fossil *H. sapiens* and *H. neanderthalensis*, the midline of the occipital bone was also thickened. These areas of thickening corresponded to the superstructures or ridges of bones present on the ectocranial and endocranial surfaces.

Furthermore, in these three taxa, the areas with evident thinning always appeared in the lateroinferior edge of the frontal squama (below the temporal line). This corresponded to the compression from the inferior frontal gyrus. For the specimens of fossil *H. sapiens* and *H. neanderthalensis*, the anterosuperior part of the parietal bone also showed thinning, which was compressed by the meningeal vessels, precentral gyrus,

and sometimes the postcentral gyrus. In contrast, the anterosuperior parietal bone of Tighennif 4 was thickened. Besides, this area in the *H. naledi* specimen was not well-preserved, and thus the situation was unclear.

Like in extant humans, the inferior parietal bone of fossil *H. sapiens* specimens always showed evident thinning and was compressed by the inferior parietal lobule and temporal gyri. In addition, except for Cro-Magnon 1, the compression from the occipital gyri of all fossil *H. sapiens* specimens was involved in the evident thinning in the cerebral fossa. In contrast, in the sample of *H. neanderthalensis* (except for Spy 10), the compression from these brain structures did not lead to evident thinning in the corresponding areas nor the lack of DCs.

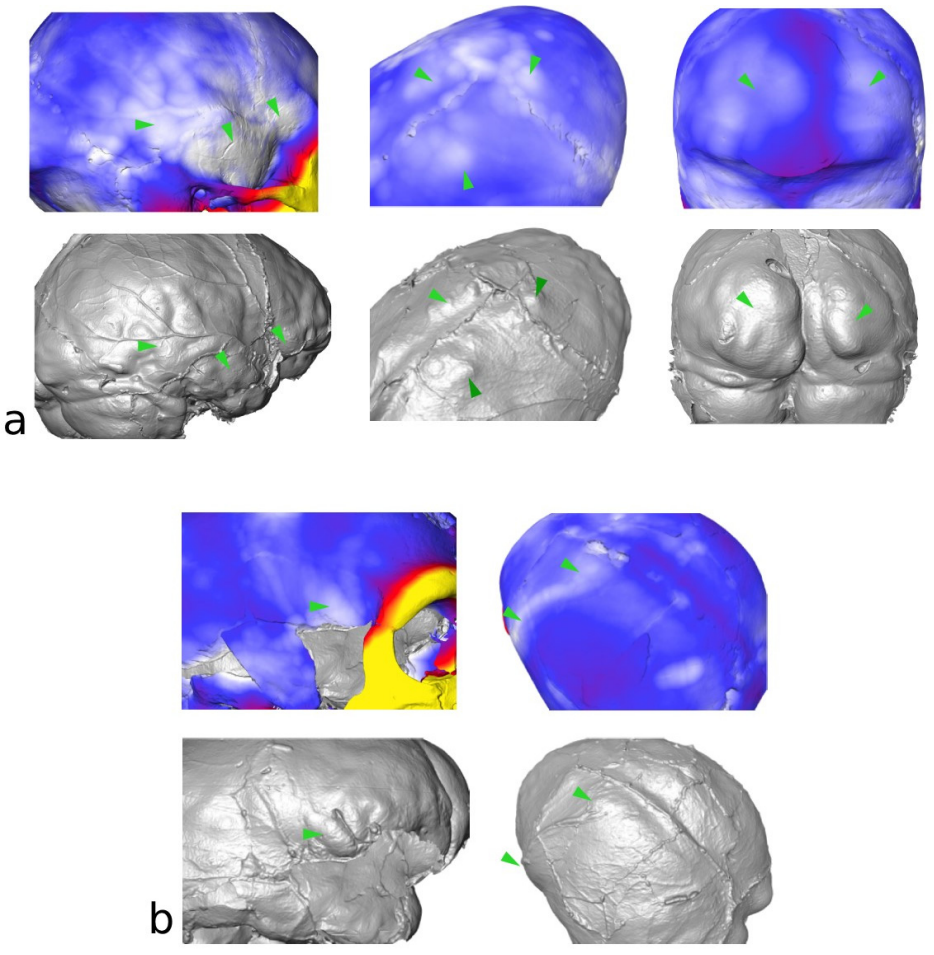

Figure 7.24 The areas of thinning (green arrows) and the corresponded gyri on the endocranial surfaces in fossil *H. sapiens* (a) and *H. neanderthalensis* (b).

Finally, the suprainiac fossa, as a unique trait of *H. neanderthalensis*, was worth noticing. This fossa located in the central occipital bone was not obviously thinner than its surrounding areas in the CVT maps, and it did not show a reduction in the thickness in the external table. However, the thickness of its diploic layer was largely reduced (Figure 7.25). Along the midline of the suprainiac fossa, the reduction in diploic thickness was compensated by the increase brought by the thick internal occipital protuberance. This prevented the diploic layer along the midline from being rather thin. In comparison, the diploic layer of the suprainiac fossa distant from the midline reduced to about 1.0-2.0 mm in thickness. Nevertheless, this thickness was still larger than many DC diameters, which means the diploic layer had enough space allowing the passage of DCs. In the sample of *H. neanderthalensis*, the DCs in the suprainiac fossa were commonly found.

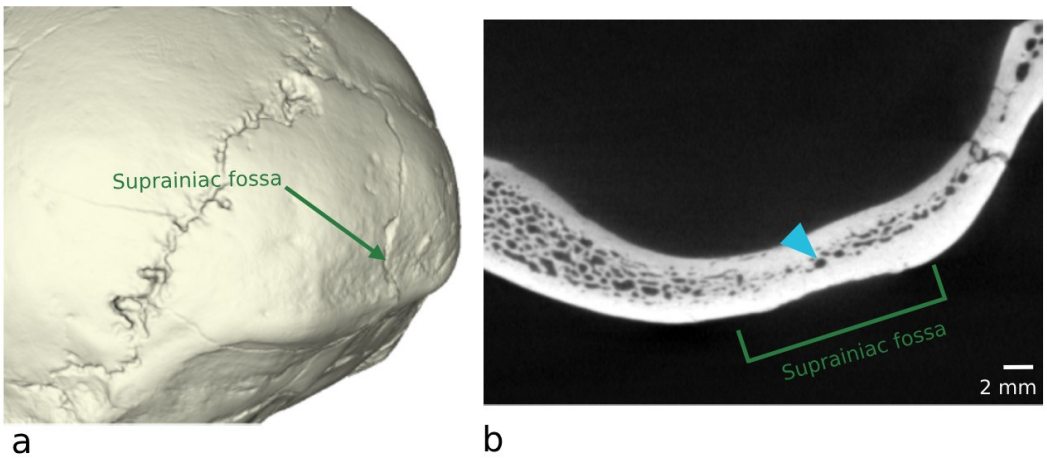

Figure 7.25 The suprainiac fossa (a) of *H. neanderthalensis* and its internal structures (b), whereby the diploic is thin but it allows the passage of DC (marked by a blue arrow).

8. Discussion

8.1 Verification and correction of classical descriptions

The sheltered location of the diploic venous system brings difficulties to traditional anatomical dissection. Studies relying on traditional methods could hardly reveal the whole picture of the diploic venous system. Moreover, the number of empirical studies concerning DVs is rather small. The descriptions of DVs first published in the 1820s are continually used in most anatomical books and anthropological studies nowadays, without any major revisions or adequate verifications. For this reason, the current knowledge about DVs possibly contains errors or ignorance.

Following the descriptions made by Breschet (1829), as shown in Figure 8.1, most previous studies stated that the DVs are distributed in the frontal, parietal, and occipital bones (García-González et al., 2009; Hershkovitz et al., 1999; Lachkar et al., 2019; Lang, 1983; Schünke et al., 2016). However, a latest study noticed that the DVs in the skull base may also appear in other cranial bones besides those mentioned above (Tsutsumi et al., 2019), though they did not detail in which exact bone these DVs are embedded. Here, the result of this current study shows that DCs, the bony shells of DVs, frequently appear in the sphenoid and temporal bones in extant humans. These DVs in the sphenoid and temporal bones have a similar function in blood circulation to those in the frontal, parietal, and occipital bones, communicating with the dural sinus, meningeal vessels and other vascular networks. Still, these sphenoid and temporal DCs are relatively short and narrow, compared with other DCs, and they are usually hidden in the thick and hard section of the bones. This may explain why previous studies based on traditional dissection or projectional radiography did not notice the existence of them.

Furthermore, as shown in this study, DCs also appear in the nasal bones and zygomatic bones in some rare cases among fossil hominins and extant *P. troglodytes*. These DCs are extended from the frontal bone. As located in the nasal and zygomatic bones, these

DCs are not connected with the meningeal vessels nor the dural sinus, which means their function in blood circulation is different from those in the neurocranium. Still, no such DCs appear in the nasal or zygomatic bones in the sample of extant humans in this study, and there is no such report in previous studies.

Nevertheless, it is true that the majority of the diploic venous system is housed in the frontal, parietal, and occipital bones. The classical description following Breschet (1829) classified the DVs in these bones into four sections: frontal DVs, anterior temporal DVs (ATDV), posterior temporal DVs (PTDV), and occipital DVs. Each section is described as a small network formed by at least one main branch and many secondary branches originated from it. The ATDV and PTDV are considered located in the anterior and posterior parts of the neurocranium respectively.

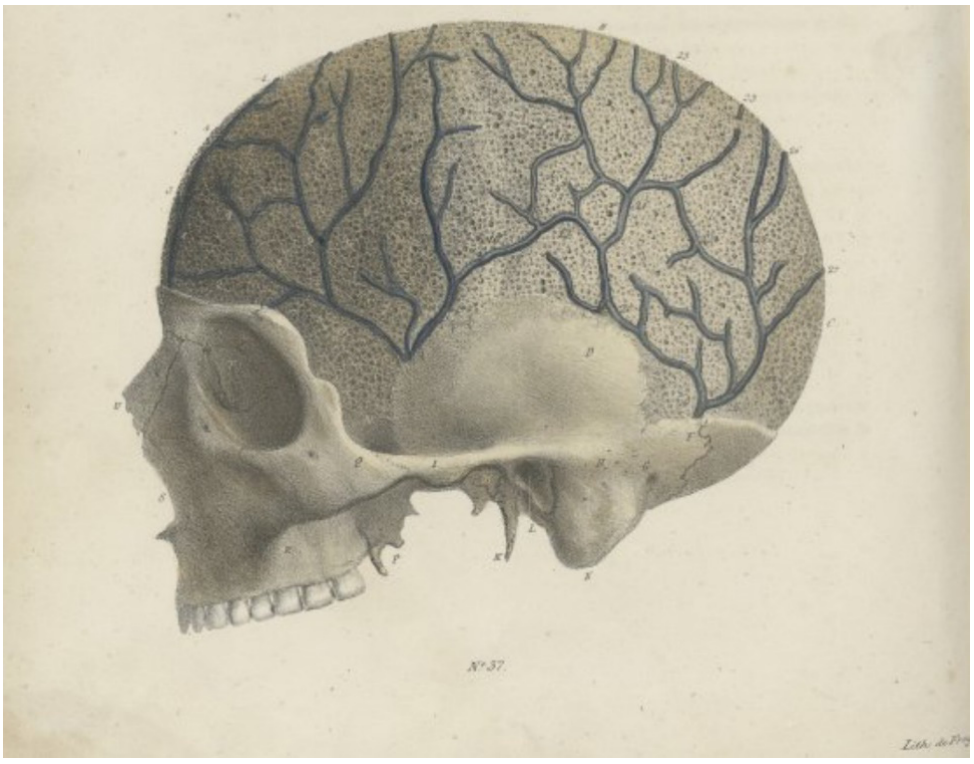

Figure 8.1 The first illustration of diploic venous network in history published by Breschet (1829). The photocopy is provided by Bibliothèque interuniversitaire de santé (Paris).

Although this classification has been widely applied in many anatomical books

(Lachkar et al., 2019; Lang, 1983; Schünke et al., 2016; Warwick & Williams, 1973), many problems of it have been exposed in this current study. First, the ATDV and PTDV do not always appear in the sample of extant humans. Second, when ATDV and PTDV both appear in a cranium, they may fuse together and make it difficult to distinguish them. Finally, there are always some short and independent branches scattered in the parietal bone, which are not connected to the main branches or their secondary branches. These independent branches can be hardly classified as part of ATDV or PTDV networks. Considering all these limits, this classification established in the early 19th century is more or less impractical. Instead, a more feasible classification is to simply classify the DVs according to the bones housing them (e.g., frontal DVs, parietal DVs, etc.). Additionally, different from the depictions in some anatomical books (Breschet, 1829; Schünke et al., 2016; Warwick & Williams, 1973), the DVs in each bone may not always anastomose with those in other bones, as revealed in this study. In other words, the diploic venous system is a group of several independent large networks and many scattered and independent short branches.

Hershkovitz et al. (1999) also noticed the impracticality of the categories 'ATDV' and 'PTDV' in the traditional classification, and they instead named the DV after their host bones. Furthermore, as mentioned in the 'Methods' chapter, they classified the variable distribution patterns of parietal DVs into six types (spider, bonsai, coronal, etc.). This classification established by Hershkovitz et al. (1999) has been applied in a few studies recently (Eisová et al., 2022; García-González et al., 2009). Here, the results of this study find all these types of distribution patterns manifested in the sample of extant humans and even most Late Pleistocene hominins, which confirms the effectiveness of these types. Nevertheless, the distribution patterns of parietal DVs in around one-third of extant human specimens are not similar to any type in this classification. This means the classification system cannot fully reflect all the variations in the distribution patterns. Further studies are required to investigate larger populations, in order to build a new classification system documenting more variations.

Hershkovitz et al. (1999) further indicated that the distribution pattern could determine whether the DVs anastomose with the meningeal vessels, transverse sinus, and extracranial vessels. For instance, the parietal DVs in the spider type were reported to connect with the transverse sinus while those in the coronal type did not show such connections (Hershkovitz et al., 1999). However, this study shows that the distribution pattern of DVs is not concerned with anastomosis between vascular networks. No matter how the distribution pattern varies, the DVs in extant humans are consistently connected to the meningeal vessels, transverse sinus, and extracranial vessels.

8.2 Technical notes

Technical and methodological difficulties are always obstacles hindering the studies of the diploic venous system. Specifically, there are three major challenges we have to face—How can we see the diploic venous system? How to digitally reconstruct the diploic venous system? How to quantitatively measure the diploic venous system?

For the first challenge, traditional anatomical studies rely on invasive dissections to expose the diploe (Breschet, 1829; García-González et al., 2009; Lachkar et al., 2019). This method is definitely not applicable to fossils. Another drawback is that when removing the out table of cranial bones, the orifices linking DVs with extracranial vessels are also removed. That way, we lose important information about their drainage pathways. Clinical non-invasive imaging methods, such as clinical CT, can avoid damaging cranial bones, but neither can they reveal the whole picture of diploic venous system. This is because the resolution of clinical CT scanning is usually above 1 mm (Ford & Decker, 2016; Guggenbuhl et al., 2008; Treece et al., 2010), while the diameters of many DVs are smaller than this level. In this respect, the results of this current study demonstrate the application value of high-resolution Micro-CT scanning. Its resolution is high enough for detecting microscopic DCs, enabling this study to find unexplored structures and drainage pathways. For fossils, a high resolution is beneficial in distinguishing taphonomic structures and biological structures. For this reason, it is necessary to promote the use of Micro-CT in this field.

However, applying non-invasive methods induces another challenge. They generate raw data in 2D format, which requires 3D reconstruction. Although there are several semi-automatic applications facilitating the segmentation, it remains unavoidable to manually identify DCs. Especially, taphonomic damages and alterations change the gray values of diploic structures in fossil specimens. This causes a complex situation beyond the capabilities of the current semi-automatic algorithms used in the field of anatomy and paleoanthropology, and thus we have to turn to manual segmentation.

Consequently, the 3D reconstruction process remains laborious and impedes the expansion of sample size. Future works are expected to develop advanced algorithms automating the identification of DCs and taphonomic structures.

When the diploic venous system is finally reconstructed, the next challenge emerging in front of us would be the quantification of its morphological information. This current study is largely based on qualitative analyses, which are enough to accomplish its objectives and answer the critical questions concerning anatomy and evolution. What is more, because the field of diploic venous system studies currently remains in its infancy stage, the new information brought by these qualitative analyses can make a considerable contribution to our knowledge. However, as our understanding of the diploic venous system deepens, it is foreseeable that more complex questions may emerge in this field in near future, which necessitates the access to richer information. That time, the limited amount of information provided by qualitative analyses may no longer be adequate, and thus we must induce more quantitative analyses.

Some have developed several methods quantifying the morphology of DVs, including rating intensity levels and measuring absolute lengths and absolute volumes (Eisová et al., 2022; Hershkovitz et al., 1999; Rangel de Lázaro et al., 2016, 2020). This current study has shown the reliability and broad applicability of rating diploic venous networks with an intensity level scale. However, this method only generates ordinal data, which are relatively less informative. In this respect, the fractal analysis tested in this study can provide richer and more detailed information about vascular complexity. In addition, measurements of the absolute size of DVs are applicable to complete specimens, but they are problematic for incomplete fossils. In the latter situation, it is worth considering using the relative volume index, which can help us correct the bias brought by preservation statuses. As shown in this study, it corrects the previous understanding based on absolute DC volume data from incomplete fossils, clarifying that a small and simple DV system is not a feature of *H. neanderthalensis*.

8.3 Evolutionary trajectory and taxonomic significance

8.3.1 General evolutionary trend

Studies on the diploic venous system were mainly conducted in the field of clinical medicine, and thus they focused on extant human populations. Only a few studies in the last few decades examined the diploic venous system in great apes and fossil hominins, suggesting that great apes and *H. neanderthalensis* had less developed DVs than those in *H. sapiens* (Hershkovitz et al., 1999; Rangel de Lázaro et al., 2016). However, constrained by small sample sizes and a lack of high-definition imaging methods, these results may not be able to reflect the whole picture in each taxon. The evidence is far from sufficient to map the evolution trajectory and determine the taxonomic significance of the diploic venous system.

Many issues are thus left: Do the DVs get more developed with the course of human evolution? Does the intensity of DVs peak in *H. sapiens*? Can we use DVs as a signal in taxonomic studies estimating the classification of fossil specimens? The new findings present in this study could engage in the discussion.

The diploic venous system in the samples of fossil hominins and extant humans is generally much more developed than that of extant chimpanzees and gorillas. This is in accordance with the findings from the previous study (Hershkovitz et al., 1999). If a less developed diploic venous system is widely shared by great apes, chimpanzee-human and gorilla-human common ancestors may likewise possess this trait. In other words, a less developed system is a primitive trait, while a developed system is a derived trait. This is further supported by previous studies showing that most mammals have small or even absent frontal DVs (Miller et al., 1979; Thewissen, 1989).

The cranium StW 53 is the oldest fossil in this study with a highly developed diploic venous system. The taxonomic status of this fossil is controversial. While some assigned it to *H. habilis* or *H. gautengensis* (Curnoe, 2010; Curnoe & Tobias, 2006;

Hughes & Tobias, 1977), some argued it was a member of *A. africanus* (Clarke, 2008; Ferguson, 1989; Williams et al., 2012). If the latter is confirmed, it means a highly developed diploic venous system has emerged in *Australopithecus* and it is possibly a symplesiomorphy for *Homo*. Further studies need to include more *Australopithecus* specimens to test this hypothesis, but it would be a difficult task, as well-preserved crania of *Australopithecus* are rather rare.

In any case, the information from the fossil StW 53 confirms that a highly developed diploic venous system has emerged since, at the latest, the Early Pleistocene. After that, the diploic venous system remained highly developed in all specimens from the Middle and Late Pleistocene (except those not well preserved). Different from previous knowledge, this study with high-definition imaging methods reveals that *H. sapiens* do not house a more developed diploic venous system when compared with the sample of other *Homo* species. This indicates the diploic venous system in the genus *Homo* did not continually evolve to become more developed with the course of human evolution. The intensity of DVs does not peak in *H. sapiens*.

Interestingly, it seems that the high variability of diploic venous system never reduced during human evolution. It has long been noticed that the diploic venous system is like a 'fingerprint' and can be used in forensic medicine, for its morphology in each individual is different (Hershkovitz et al., 1999; Píšová et al., 2017). In this study, except for those species with a single individual specimen, the diploic venous systems of all species show high intraspecies variations. Usually, a high variability of a biological structure signifies a low selection pressure. However, the situation of the diploic venous system is not that simple. The variability of diploic venous system is mainly reflected in its details in distribution, including the exact position of each branch and its ramifications, curvature of pathways, angle of extension, etc. These factors cannot determine the physiological functions and thus may face a low selection pressure. Furthermore, unlike most vessels coursing in the gaps between complex layers of

muscles, vessels, skin, and other soft tissue, the diploic and emissary venous systems are the only two vascular networks inside the diploe. Considering the emissary vessels only pierce through the diploe and occupy a minor portion of space, the diploe can provide enough space for the DVs to extend freely and form diverse patterns, without the necessity of making way for other vessels. On the other hand, the size, degree of complexity, and drainage pattern of the diploic venous system are critical to its physiological functions. These aspects face relatively higher selection pressure and show lower variability in each species.

8.3.2 Detailed differences between taxa

Although the diploic venous system in great apes is generally simple and small, its DC drainage pattern shown in this study has already possessed functions similar to those in hominins. The system can communicate and bridge many layers of vascular networks (e.g., extracranial vessels, dural sinuses, etc.) and function as collateral pathways for them. Still, constrained by size and number of branches, the DVs in apes drain smaller areas and transmit smaller amounts of drainage when compared with those in hominins.

Interestingly, the sphenoid DVs in chimpanzees are even more developed than those in extant humans. Most chimpanzee specimens house sphenoid DVs bridging the ethmoid sinuses and cavernous/intercavernous sinus (and basilar plexus in some rare cases), which forms a shortcut for the drainage flow in the skull base. In one-fourth of chimpanzee specimens, the DVs in the greater wings can function as a stem of meningeal vessels. These features of the sphenoid DVs in chimpanzees can accelerate the drainage flow in the skull base. In comparison, the sphenoid DVs in extant humans are usually shorter and smaller, with no such functions, while those in fossil hominins are unclear due to preservation constraints.

For hominins, their diploic venous systems are comparably developed, and the differences between taxa can be detected in drainage patterns. First, the consistent

connection between the frontal sinus and DVs in chimpanzees and extinct hominin species becomes inconsistent in *H. sapiens*. Second, this study and previous reports all noticed that the parietal foramina are usually present in pairs along the sagittal suture in *H. sapiens* (Al-Shuaili et al., 2024; De Souza Ferreira et al., 2021; Falk, 1990). In comparison, the parietal foramina and their connection with DVs are frequently absent in chimpanzees, and almost always absent in *H. neanderthalensis*, which is also noticed by previous studies (De Stefano & Hauser, 1992; Manzi et al., 2000). The rarity of parietal foramen is reasonable to be taken as a feature of *H. neanderthalensis*. Finally, the most noticeable difference between taxa is in the asterional region. Although the drainage pattern of this region is diverse in extant humans, the parietal DVs always reach this area and drain directly into the trunk of the transverse-sigmoid sinus. This feature was noticed by several previous inspections (García-González et al., 2009; Tsutsumi et al., 2013; Tubbs et al., 2016), and is confirmed in this current study. Likewise, the anastomosis between the transverse-sigmoid sinus and parietal DVs appears in around 90 % of chimpanzee specimens and almost all Middle Pleistocene hominin specimens with well-preserved asterional regions, as well as in fossil *H. sapiens* from the Late Pleistocene. In contrast, the parietal DVs of all *H. neanderthalensis* specimens do not directly anastomose with the transverse-sigmoid sinus, and they instead drain into some other sinuses (especially the petrosquamous sinus) in the asterional region. The high incidence of the isolation between transverse-sigmoid sinus and parietal DVs is a feature of *H. neanderthalensis*, distinguishing it from other taxa.

Still, the isolation does not uniquely appear in *H. neanderthalensis*, but also appears in around 5% of extant chimpanzee specimens and in Hexian *H. erectus*. Thus, it is reasonable to hypothesise that this trait may have emerged since the chimpanzee-human common ancestor, and its occurrence kept very low in most descendants but had a dramatic increase in the lineage of *H. neanderthalensis*. Additionally, we cannot exclude the possibility that the trait might emerge independently in the lineage leading

to chimpanzees and the lineage leading to *H. neanderthalensis*, and the existence of the trait in Hexian indicates an affinity with the recent ancestor of *H. neanderthalensis*. This would be a surprising scenario, but it is more or less reasonable considering that the inner ear structures of Hexian are close to those of *H. neanderthalensis* (Wu et al., 2014), and that many Asian specimens from the late Middle Pleistocene share potential morphological affinities with *H. neanderthalensis* (Li et al., 2017; Wu et al., 2014; Wu & Bruner, 2016).

Having discussed the differences between species, we may turn to the utility of the diploic venous system in taxonomy. In other words, can the DVs help us judge the taxonomic classification of a fossil? First, the degree of complexity and size of DVs can distinguish great apes from hominins, but they cannot distinguish between hominin species. Thus, this element may not be of use in classifying hominin fossils. Similarly, the drainage pattern of sphenoid DVs can distinguish chimpanzees from *H. sapiens*, but its variation among extinct hominin species is unknown. We need further data on the skull base of fossil hominins to verify the potential utility of sphenoid DVs. Besides, the isolation between the frontal sinus and frontal DVs is a unique trait found only in *H. sapiens*. When this trait appears, it may help us identify *H. sapiens* fossils. Also, the parietal foramen is rather rare in *H. neanderthalensis* but prevalent in *H. sapiens*. This feature may be useful in distinguishing the fossils of the two taxa. Finally, the isolation between the transverse-sigmoid sinus and parietal DVs is a characteristic of *H. neanderthalensis* and is rare in other species. This could be especially useful in identifying the affinities with *H. neanderthalensis* in fossil specimens.

From these, it is reasonable to acknowledge the potential of DVs in taxonomic studies. They are especially useful in distinguishing great apes from hominins and identifying *H. sapiens* and *H. neanderthalensis* fossils. This is interesting because many important fossils have controversial affinities with the two taxa (Hublin et al., 2017; Li et al., 2017; Wu & Bruner, 2016), which are necessary to be verified with new evidence. When the

information from the external surface is not enough to classify a fossil specimen, resorting to DVs and other internal structures would be meaningful. Moreover, sometimes when the external surface has been seriously damaged, the diploe may remain well preserved as it is protected by the compact layers of bones. The hidden position of DVs hindering traditional anatomical studies, in this case, can be converted into a benefit for taxonomic studies. Absolutely, the precondition is applying high-resolution imaging methods which are able to construct a complete drainage pattern.

8.4 The interaction between vessels, bones, and brain

8.4.1 The relationship of diploic vessels with other vessels and sinuses

The fundamental functions of the diploic venous system are bridging extracranial and intracranial vascular networks and paranasal sinuses, as well as playing the role of their collateral drainage pathways. As these vessels and sinuses evolved in terms of morphology and drainage patterns, it is reasonable to hypothesise that the DVs might have accordingly made adaptations during the course of human evolution. Thus, it would be interesting to compare the evolutionary trajectories of DVs and other structures, and to examine to what extent they are matched.

First, the superior sagittal sinus, which is the stem of the dural sinus network, is consistently anastomosed with the DVs. The anastomosis can be found in all extant and fossil specimens in this study. A previous study reported that the anastomosis appeared in extant tree shrews (Thewissen, 1989), a so-called 'living fossil' morphologically close to ancestral primates (Ni & Qiu, 2012). This means the connection between DVs and superior sagittal sinus is possibly a symplesiomorphy of primates enduring to date. It also indicates that the role of DVs in superior sagittal sinus drainage is so critical that no mutations isolating them could be preserved during natural selection. When the superior sagittal sinus, as the stem of the dural sinus network, has blocks in its drainage pathway, which may be caused by meningiomas or thrombosis (Thron et al., 1986; Yamashiro et al., 2021), the DVs could function as collateral drainage pathways. Besides, recent studies noticed that the DVs might connect to the arachnoid granulations located on the wall of the superior sagittal sinus, which means the DVs are involved in not only blood circulation but also cerebrospinal circulation (Tsutsumi et al., 2014, 2015). However, it is not clear whether the size of superior sagittal sinus ever evolved in the hominid lineage, as there are no comparisons between living great apes and humans, while the imprints on dry skulls cannot reflect the exact size of sinuses. For this reason, it is unknown whether the high degree of development of hominin DVs is an adaptation to the evolutionary change of the superior sagittal sinus.

When the drainage of superior sagittal sinus courses into the posterior fossa of the cranium, it exits the head mainly by two routes, as shown in Figure 8.2: 1) enter the transverse-sigmoid sinus and then exit the head by draining into the jugular vein (JV); 2) enter the occipital and marginal sinus (OMS) and then exit the heads through the vertebral venous plexus (VVP). Both routes are connected to the DVs, and interestingly, the connections are related to the evolution of bipedalism. In detail, many studies have documented that the drainage from superior sagittal sinus primarily goes through the JV route when an individual is lying down or practicing quadrupedal locomotion (Batson, 1944; Epstein et al., 1970; Falk, 1990; Falk & Conroy, 1983). They also noticed that if the individual changes into an upright posture with the head held up, most of the drainage originally chosen JV route would need to exit the brain through the VVP, which is related to hydrostatic pressure and viscosity of venous blood. Because apes do not frequently take upright postures, the volume of drainage flow taking the VVP route is small and can be transported fluently, even though the size of OMS is small. In contrast, bipedal locomotion is more frequent and lasting in hominins. This brings hominins a large amount of drainage flow that needs to be transported to the VVP, but the small OMS cannot handle the large flow on its own. Especially, the occipital sinus is the smallest among dural sinuses in extant humans (Tubbs et al., 2011). To compensate for the small size of OMS and its limited ability to transport blood, many emissary vessels transport drainage from the superior sagittal sinus and transverse-sigmoid sinus to those extracranial vessels (e.g., occipital vein) leading to the VVP, without going through the OMS (Falk, 1990).

Here, this current study finds a similar function in occipital DVs (Figure 8.2). In chimpanzees, the occipital DVs are always anastomosed with the superior sagittal sinus and frequently anastomosed with the transverse-sigmoid sinus, transporting venous drainage to extracranial vessels leading to the VVP. In hominin fossils and extant human specimens, this pathway also appears and is more developed than those in chimpanzees, as human occipital DVs have larger sizes and more branches. This allows

transporting a larger amount of blood flow to the VVP and thus facilitating the drainage in the posterior fossa. Accordingly, the highly developed occipital DVs in hominins are geared to the derived dural sinus drainage pattern induced by bipedalism. Moreover, occipital DVs may play a more important role in draining dural venous blood compared to emissary vessels, considering the size of the former is much larger.

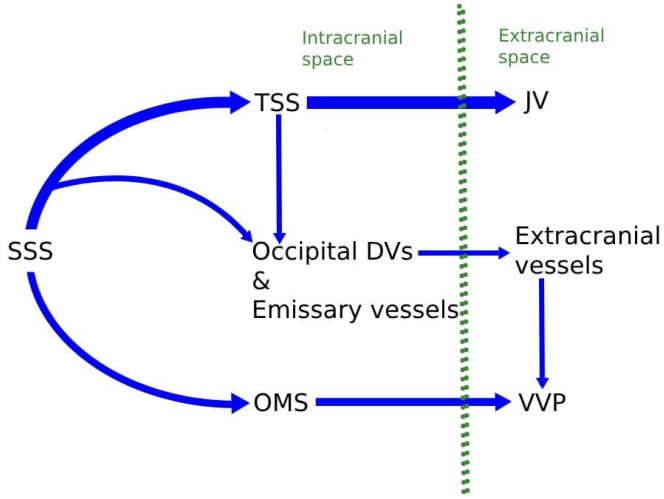

Figure 8.2 The schematic dural sinus drainage in the posterior fossa of hominids. With help from the occipital DVs, dural venous drainage can leave the TSS-JV route and join the VVP. (SSS, superior sagittal sinus; TSS, transverse-sigmoid sinus; JV, jugular vein; DVs, diploic vessels; OMS, occipital and marginal sinuses; VVP, vertebral venous plexus)

In addition to anastomosing with the occipital DVs, the transverse-sigmoid sinus almost always anastomoses with the parietal DVs. As mentioned above, the exceptions in hominins are *H. neanderthalensis* specimens and Hexian *H. erectus* specimen. These fossil specimens share a common feature—the asterion is higher than the transverse-sigmoid sinus. In other words, their transverse-sigmoid sinus is inferior to the lower edge of the parietal bone. In comparison, the asterion in other hominin fossils and extant humans is usually at the same level as the transverse-sigmoid sinus. In a few cases, the asterion is inferior to the transverse-sigmoid sinus. In extremely rare cases, the asterion is at the upper edge of transverse-sigmoid sinus. These findings are consistent with previous studies among extant human populations (Muche, 2021; Mwachaka et al., 2010). From this, the isolation between the transverse-sigmoid sinus and parietal DVs

in hominins is associated with the relatively low position of transverse-sigmoid sinus (Figure 8.3). As for chimpanzees, there are also a few cases showing the isolation, but it is not associated with the spatial location of the transverse-sigmoid sinus. Instead, it is because the DVs are rather scarce in these chimpanzee cases, and there are no parietal DVs distributed adjacent to the transverse-sigmoid sinus in the asterional region.

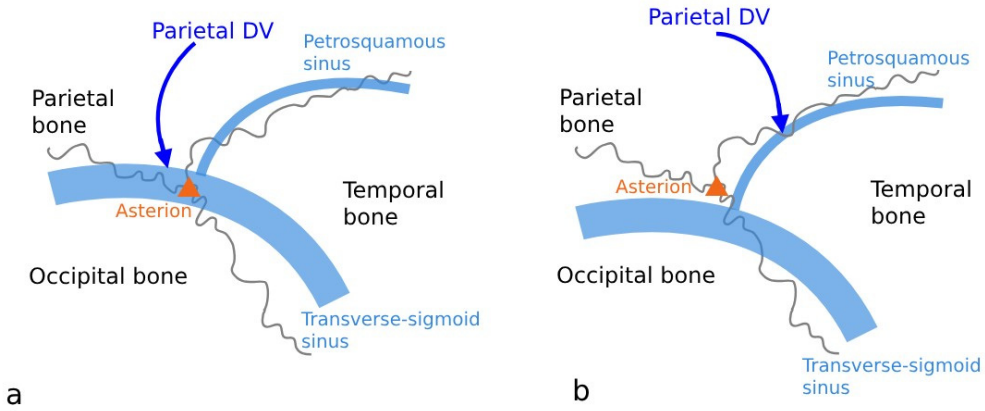

Figure 8.3 The spatial relation between transverse-sigmoid sinus, asterion, and parietal DVs. In most hominids (a), the parietal DV and transverse-sigmoid sinus are directly connected, while they are isolated in *H. neanderthalensis* and Hexian *H. erectus* (b).

Like the dural sinuses, the meningeal vascular network as a whole has consistent connections with the diploic venous system in all specimens in this study. The connection seems to be a plesiomorphy and never disappears during human evolution. Still, the evolutionary trajectory of the meningeal vascular network in general does not match that of DVs. The meningeal vessels of chimpanzees, as present in this current study and documented in previous studies (Bruner & Sherkat, 2008; Marcozzi, 1942), are highly reticulated like those of extant humans. However, the DVs of chimpanzees in this current study are much less developed than humans. Among fossil hominins, *H. erectus* and *H. neanderthalensis* were reported to have a reduction in the meningeal vessels (Bruner et al., 2006; Schwartz et al., 2002a), but their DVs remained highly developed. Furthermore, along with the course of human evolution, the anterior part of the MMV (in the frontal and anterior parietal) saw an increase in development, while

the posterior part (in the posterior and occipital) saw a decrease (Bruner & Sherkat, 2008; Schwartz et al., 2002a). Such a tendency is not manifested in the diploic venous system.

Finally, as for the paranasal sinuses, their evolving drainage patterns and morphology seem to have influenced their connections with the DVs. The connections between the frontal sinus and DVs are constant in extant chimpanzees and all extinct hominin species in this study. As documented in previous studies, these species all have large sizes of frontal sinuses (Balzeau et al., 2022). A large frontal sinus may generate a large amount of drainage flow requiring the involvement of the DVs in transportation, which makes the connection with DVs necessary. On the other hand, *H. sapiens* have a highly variable frontal sinus size (Balzeau et al., 2021, 2022). The frontal sinus is relatively small in some extant human populations and many *H. sapiens* fossils (including Cro-Magnon 2, 3, and Abri Pataud 1). The drainage of a small frontal sinus may not need the involvement of DVs. This may explain the inconsistent connection between the frontal sinus and DVs in this species.

The frontal sinus is fused with the ethmoid sinus in chimpanzees. The mucus from the frontal sinus first courses into the middle ethmoid sinus, before entering the nasal cavity (House et al., 1966). Likewise, the blood drainage from the frontal sinus may also enter the ethmoid sinus. This is because their mucus membrane (where vessels are embedded) are fused and the blood may descend to the ethmoid sinus for gravity. This possible pathway may increase the volume of drainage flow inside the ethmoid sinus and may require support from the DVs. In *H. sapiens*, the mucus drainage from the frontal sinus does not enter the middle ethmoid sinus (Daniels et al., 2003; Kountakis et al., 2016; Lang, 1983). Their ethmoid sinuses are composed of several independent small cells, which are not fused with the frontal sinus and thus may not receive the blood from the frontal sinus. The difference in drainage pathway may explain why chimpanzee DVs are frequently connected with the ethmoid sinus and link it to the

cavernous/intercavernous sinus and basilar plexus through a shortcut, while *H. sapiens* have no such feature.

8.4.2 The relationship between diploic vessels and encephalization

Brain evolution is one of the most attractive issues in the field of evolutionary biology. High intelligence is a distinguishing feature of humans and the basis of human activities. As an energy-consuming organ, the human brain receives 15-20% of the blood output from the heart (C.-Y. Xing et al., 2017), though the weight of the brain only accounts for around 2% of body weight (Dekaban & Sadowsky, 1978). If there are no effective vascular networks managing such a large amount of blood flow, it is hard to imagine how the brain can function normally. Therefore, it is widely accepted that the brain has co-evolved with the vascular networks (Falk, 1990; Kunz & Iliadis, 2007; Lieberman, 2011; Saban, 1995).

A frequently discussed issue in this field is whether encephalization is associated with the intensity of head vascular networks. For instance, Saban (1995) argued that the complexity of hominin meningeal vessels increased along with the increase of brain volume, though his argument has been challenged by many empirical findings (Bruner & Sherkat, 2008; Schwartz et al., 2002a). Similarly, based on the comparison between extant chimpanzees and humans, which was provided by Hershkovitz et al.(1999), Kunz & Iliadis (2007) concluded that the intensity of DVs correlated with brain size.

It is natural to come to such a conclusion if we only consider the comparison between chimpanzees and extant humans, in which the small-brained chimpanzees indeed show much simpler diploic venous networks. However, after this current study adding extinct hominins to the comparison, the hypothesised correlation of DVs with encephalization trend in hominids turns out to be problematic. StW 53 cranium (as a specimen of *A. africanus* or *H. habilis*) has a brain volume smaller than 480 cc (Ferguson, 1989). *H. naledi* (LES 1 specimen) has a brain volume of 610 cc (Berger et al., 2015; Hawks et

al., 2017). Their brain sizes are very close to the average level of extant chimpanzees and gorillas, which stands at 400 cc and 469 cc respectively (Aiello & Dean, 1990), but their DVs are much more complex and denser than those of chimpanzees and gorillas. Furthermore, although the average brain volume of *H. sapiens* is about 1.3 times larger than the *H. erectus* average level (Rightmire, 2013), and more than 2 times larger than those of StW 53 and LES 1, they all share a similar degree of intensity. The DC volume indices of StW 53 and LES 1 are even higher than many *H. sapiens* specimens. From this, it is reasonable to argue that the brain size of a hominid species does not determine how developed its DC would be.

Still, an interesting phenomenon is that larger-brained individuals within the sample of *H. sapiens* and *H. neanderthalensis* indeed tend to show higher DC volume indices. As this possible correlation is found in a sample of less than 15 individuals, we should not exclude the possibility of bias induced by the small sample size. What is more, some larger-brained individuals (e.g., La Chapelle-aux-Saints 1 and Spy 10) possess relatively thicker crania. As shown in this study, the general thickness of hominins may affect DC intensity. The relatively higher DC volume indices of these individuals may result from their cranial thickness rather than large brains.

8.4.3 The relationship of diploic vessels with brain shape and bone thickness

Apart from the hypothesized influence from encephalization, the relationship of brain shape with head vascular networks is another key issue frequently discussed (Bruner & Sherkat, 2008; Píšová et al., 2017; Rangel de Lázaro et al., 2016). A previous study argued that the enlarged parietal lobe of *H. sapiens* makes parietal vascular networks the most developed among all neurocranial vessels (Rangel de Lázaro et al., 2016). However, in this current study, the frontal and parietal DVs are usually comparably developed in *H. sapiens*. There is no such hypothesized association found between lobe size and DV intensity in other species. In other words, the enlargement of a brain lobe may not necessarily increase the intensity of its adjacent DVs.

Nevertheless, this current study reveals that the brain shape may affect bone thickness and thus indirectly influence the distribution of DVs and their communications with other vessels. The cranial bones are the space where DVs are housed. A thicker bone may provide a larger space for the extension of DVs, allowing them to develop wider diameters and more complex ramifications. Also, a thicker bone may contain more tissues, requiring support from an intense vascular system in terms of metabolism and ontogeny. For the same reason, a thinner bone may contain smaller and simpler DVs, or may even make DVs completely absent. In this respect, Rangel de Lázaro et al. (2020) recently noticed a possible 'threshold' effect in the development of DVs—when the bone thickness of a local area is lower than a certain threshold value, the DVs in extant humans would not develop.

This current study has a similar finding among the sample of hominids. In the areas with evident thinning, DVs are scarce or absent. When the thickness falls below the threshold value, the DVs are completely absent. Additionally, this current study further points out the threshold value is variable among individuals and related to overall cranial thickness. For example, DVs in the thick Cro-Magnon 1 cranium do not appear in areas thinner than 4.5 mm. But in the case of Cro-Magnon 3, which has a thinner overall thickness, the threshold value is around 3.5 mm.

The cranial vault thickness (CVT) pattern is jointly determined by the ectocranial and endocranial surfaces (Balzeau, 2013), whereby brain shape plays an important role. In detail, the reliefs or superstructures on the ectocranial surface, like the supraorbital ridge and mastoid process, can increase bone thickness. As for the endocranial surface, some reliefs like the frontal crest may increase thickness, while the compression from the endocast (including gyri, vessels, or arachnoid granulations) may decrease thickness (Anzelmo et al., 2015). When an area has no reliefs on both surfaces and is strongly compressed by the endocast, the area may display evident thinning, which leads to the

lack of DVs in such areas.

As revealed in this study, a common location of evident thinning shared by chimpanzees and hominins is in the lateroinferior part of the frontal bone, below the temporal line. Although the results of chimpanzees and extant humans come from the case study with a limited sample size, the specimens of each species manifest a highly consistent pattern. The thin area is intracranially compressed by the inferior frontal gyrus (IFG, Figure 8.4), and there is no relief on the ectocranial surface. Surrounding DVs bypass this thin area and only course along its edges. Interestingly, many studies have noticed that the IFG of *Pan* is smaller than those of fossil hominins and extant humans (Aiello & Dean, 1990; Balzeau et al., 2014; Beaudet et al., 2021; Holloway, 1972). This current study comes to the same conclusion after comparing chimpanzees, extant humans, and well-preserved hominin fossils included in the bone thickness analysis. And compared with chimpanzees, this area of evident thinning corresponded to the IFG is larger in hominins, which also means a larger area that DVs need to bypass. The IFG is well-known for its involvement in language processing, inhibition, and attentional control (Hampshire et al., 2010; Ishkhanyan et al., 2020; Liakakis et al., 2011). The difference in cognition (especially language comprehension) between chimpanzees and hominins may explain their diverged IFG morphology. Additionally, the IFG on the two hemispheres are sometimes asymmetric in chimpanzees and is usually asymmetric in hominins (Balzeau et al., 2014; Schenker et al., 2010), with the dominant side being larger. In this current study, the thin area corresponding to the IFG is also sometimes asymmetric in chimpanzees and always asymmetric in extant humans. However, the differences are marginal between the two sides.

In agreement with a previous study (Balzeau, 2013), this current study notices an area of evident thinning in the anterosuperior parietal bone shared by *H. neanderthalensis* and *H. sapiens*. DVs are scarce or absent in this thin area, which impacts the connection between DVs and the anterior branch of MMVs. The thinning corresponds to the

compression from the precentral gyrus (PG). In addition, the compression from arachnoid granulations and meningeal vessels also contributes to decreasing bone thickness in such areas. The size and thickness of this area with evident thinning is variable among *H. neanderthalensis* and *H. sapiens* specimens of this study, and it seems associated with global CVT. Individuals with a thick global CVT, like Cro-Magnon 1, tend to have a relatively small area of thinning in the anterosuperior parietal bone, with scarce DVs distributed there. Individuals with a thinner global CVT, like La Quina H5 and other *H. sapiens* specimens, show a larger area of thinning with lower thickness, and there are no DVs inside the area. In other words, the strong compression from a pronounced PG may not always largely reduce the local thickness to the threshold level and eliminate DVs.

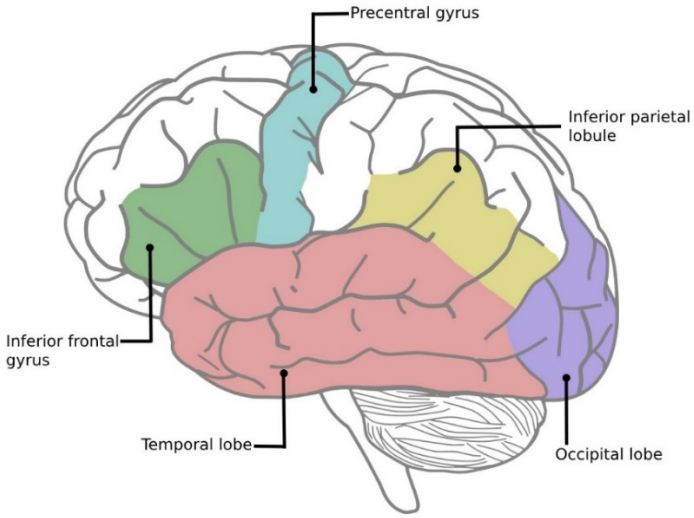

Figure 8.4 The locations of the inferior frontal gyrus, precentral gyrus, inferior parietal lobule, temporal lobe, and occipital lobe.

Interestingly, some *H. heidelbergensis* (e.g., Kabwe 1) and Asian *H. erectus* (e.g., Nagwi 1) individuals also display thinning in the anterosuperior parietal bone corresponding to pronounced PG, as reported in previous studies (Balzeau, 2013; Balzeau et al., 2017), but the thinning in these fossils is less prominent than that in *H. neanderthalensis* and *H. sapiens*. This is possibly because these *H. erectus* and *H. heidelbergensis* crania have a relatively thick global CVT with ectocranial reliefs (e.g.,

bregmatic eminence or parasagittal keel) thickening the anterosuperior parietal bone, and thus the compression from PG can hardly lead to evident thinning. Still, due to taphonomic damages, it is unknown whether their slight thinning can affect the distribution of DVs.

Another evident thinning in the parietal bone appears in its inferior part. It consistently appears in extant and fossil *H. sapiens* in this study, and it has been documented in many studies on extant populations (Eisová et al., 2016; Jung et al., 2003; Marsh, 2013). DVs in the lower half parietal bone have to bypass this thin area, and their connections with the posterior branch of MMVs are also affected. The thinning corresponds to the pronounced inferior parietal lobule and temporal gyri in *H. sapiens*. In contrast, the inferior parietal lobule produces less pronounced reliefs on the endocasts of chimpanzees and other hominins. This may explain why the thinning usually does not appear in the inferior parietal bones in these species.

Finally, the compression from the occipital lobe is prevalent in the hominid sample of this study, but the thinning effect caused by the compression shows interspecies variations. In chimpanzees, the compression corresponds to the extremely thin cerebral fossa, where occipital DVs do not extend inside. Similarly, in extant humans and most fossil *H. sapiens*, evident thinning is displayed inside the cerebral fossa, but it is thicker than that in chimpanzees. The extension of *H. sapiens* DVs stops at the edge of the thin area. In comparison, *H. naledi* and *H. neanderthalensis* show a slight thinning in the cerebral fossa, and so is Kabwe 1 cranium as previously reported (Balzeau et al., 2017), with no obvious impact on the distribution of DVs. The difference between species is possibly not a consequence of the evolving morphology of the occipital lobe, considering that the occipital lobe of *H. neanderthalensis* is larger and more posteriorly projecting than that of *H. sapiens* (Balzeau et al., 2012, 2017; Kochiyama et al., 2018). Instead, it is possibly because the occipital bone of chimpanzees and *H. sapiens* is generally thinner than that of *H. naledi*, *H. neanderthalensis*, and Kabwe 1. Even if

depressions of equal absolute thickness appear on the endocranial surfaces of the two groups, proportionally, the thinner group would experience a greater loss in thickness. Furthermore, unlike *H. neanderthalensis* and Kabwe 1, chimpanzees and *H. sapiens* have less prominent or no superstructures on the ectocranial surface, which can hardly compensate for the compression from the endocranial surface. In addition, although the suprainiac fossa in *H. neanderthalensis* decreases diploic thickness (Balzeau & Rougier, 2010), it does not produce evident thinning nor affect DVs.

8.4.4 Brain thermoregulation

During the course of human brain evolution, the increase in brain size led to a corresponding increase in heat production. The larger the brain, the more heat is generated through the metabolic process. However, human brains are intolerant to high temperatures. Even a one-centigrade increase is enough to cause neurological deterioration (Bertolizio et al., 2011). Falk (1990) hypothesised that a heat management system was crucial to human brain evolution, and a large brain must be equipped with an effective heat management system. Many studies have revealed such a system in non-primate mammals (e.g., horses and sheep), in which the cool venous blood from the nasal area courses into the neurocranium to control the brain temperature (Cabanac, 1986; Jessen, 2001). The mechanism of brain heat management in humans is so far unclear. Some hypothesised that the diploic and emissary vessels might have played an important role in cooling brains (Cabanac & Brinnel, 1985; Falk, 1990; Kunz & Iliadis, 2007). It is because sweat evaporation cools down extracranial blood, and the diploic and emissary vessels can drain that cool blood intracranially.

The thermoregulatory function has been a core issue among the studies of the diploic venous system. Here, in this current study, the diploic venous system indeed manifests numerous connections with extracranial vessels. Also, it has numerous connections with intracranial vessels. These connections can facilitate the drainage of cool blood. Furthermore, as the DVs are widespread in the neurocranium, they can deliver cool blood to many areas of the brain. From this, we see the anatomical features of the diploic

venous system pave the way for cooling brains. A DV may be more effective than an emissary vessel in heat management, considering the former allows a larger drainage volume and a larger delivery area. Nevertheless, this evidence does not indicate that DVs play a critical role in brain heat management, nor can it demonstrate the evolution of DVs resulted from adapting to the progressively increasing thermoregulatory demands.

Conversely, some evidence emerges on the opposite side. Although large-brained hominin species (e.g., *H. sapiens* and *H. neanderthalensis*) have higher thermoregulatory demands than small-brained species (e.g., *H. naledi* and *H. erectus*), they share a comparably developed diploic venous system. Moreover, as StW 53 and LES 1 are close to great apes in terms of brain size, they may share a similar level of thermoregulatory demands, but the diploic venous systems of chimpanzees and gorillas are much less developed than these two fossil specimens. Therefore, a highly developed diploic venous system should not be considered as an adaptation to thermoregulatory demands.

In addition, the distribution of DVs in some local areas is in conflict with thermoregulatory demands. Based on brain size and shape, the main factors determining thermal distribution, many studies have reconstructed the maps of brain thermal loads in *H. sapiens* and *H. neanderthalensis* (Bruner et al., 2011, 2012, 2014). These two populations with similar brain sizes show different thermal load patterns, as they have different brain shapes (Figure 8.5). Still, both of them present high thermal loads in the anterosuperior parts of the parietal lobe. Juskys et al.(2022) also noticed that these areas had a high metabolic demand, as many large cortical veins were concentrated there. As we mentioned above, the metabolic process generates heat. If the distribution of DVs is an adaptation to thermal loads, there should be more DVs found in the corresponding areas. Conversely, this study finds a lack of DVs in such areas, which is attributed to the bone thinning caused by compression from the endocranial surface. Obviously, the

thermoregulatory function of DVs is undermined in such areas.

What is more, these reconstructed thermal maps indicated the superior part of the parietal lobe in *H. neanderthalensis* possesses a higher thermal load than that of *H. sapiens* (Bruner et al., 2011, 2012, 2014). If the DVs are an essential cooling system as hypothesized, *H. neanderthalensis* would be thus more likely to possess the parietal foramina, which is a large and important orifice where the DVs drain cool venous blood from the scalp to thermoregulate the parietal lobe. However, the parietal foramen frequently appears in *H. sapiens* while it is rare in *H. neanderthalensis*.

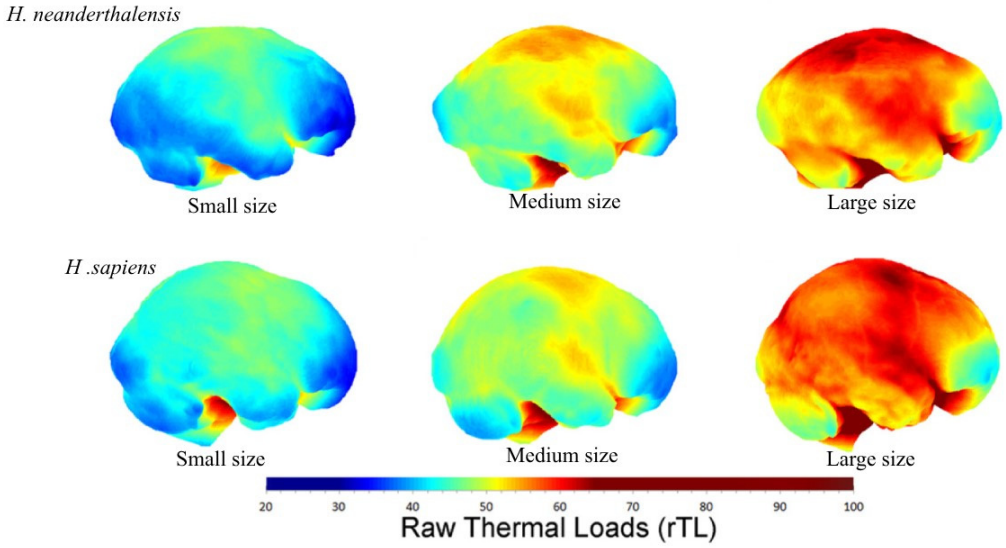

Figure 8.5 The thermal loads map of three *H. neanderthalensis* crania and three *H. sapiens* crania of variable sizes reconstructed and published by Bruner et al. (2014).

Additionally, the outflow route of the parietal DVs in *H. neanderthalensis* specimens is not likely a thermoregulatory adaptation. The parietal DVs in La Chapelle-aux-Saints 1 and La Quina H5 drain into the petrosquamous sinus (PSQS), a sinus coursing along the lateral surface of the temporal lobe. In other words, the parietal DVs and PSQS form a bridge for heat exchange between the parietal and temporal lobes. According to the distribution patterns of thermal loads (Bruner et al., 2011, 2012, 2014), the parietal lobe releases more heat than the temporal lobe does. As a result, the pathway of the vessels may transfer heat to the temporal lobe. In this particular case, the DVs may function as

a heating system, rather than a cooling system.

Finally, craniotomy is common in clinical medicine, in which the DVs are frequently damaged (García-González et al., 2009; Tsutsumi et al., 2013). However, so far there is no report about thermoregulatory problems after such surgery operations.

9. Conclusion and perspectives

This study debuts the diploic venous systems of hominin fossils, many of which are critical in human fossil records and their DVs were never before seen. This study is also the first comprehensive comparison of diploic venous systems between great apes, fossil hominins, and extant humans. Based on detailed descriptions and comparisons, this study preliminarily maps the general evolutionary trajectory of the diploic venous system in hominins. *Homo* has much more developed DVs than chimpanzees and gorillas. But the DVs did not gradually become more developed during the evolution of *Homo*. Instead, a highly developed diploic venous system is a trait emerging in *Australopithecus* or early *Homo* from Early Pleistocene, and the trait was never reduced among Middle and Late Pleistocene hominins. The evolution of DV intensity and relative size did not follow the trend of encephalization in *Homo*, as small-brained hominins share comparably developed DVs with large-brained hominins.

By exploring the characteristics of each hominid taxa, this study evaluates the taxonomic values of the diploic venous system. The diploic venous system of chimpanzees, though less developed, is not a simpler and smaller version of the human system. The chimpanzee diploic venous system is featured with highly connective sphenoid DVs, which can serve as a stem of meningeal vessels and as a shortcut between the paranasal sinuses and middle & posterior cranial fossae. As for hominin species, they share large similarities in the drainage pathways. Differences among them emerge in the drainage patterns surrounding the frontal sinus, parietal foramen, and asterion. Especially, the connection patterns between DVs and dural sinuses in the asterional area can be used to distinguish *H. neanderthalensis* affinities. These findings evidence the potential of the diploic venous system in taxonomic and phylogenetic discussions.

Although encephalization is unlikely to be a driving force behind the evolution of the diploic venous system in hominins, the influence from brain shape is clearly revealed

in this study. A spatial interaction between endocranial shape, cranial bone thickness, and DVs is found in chimpanzees, extant humans, and Middle & Late Pleistocene hominins. The areas with evident thinning in the neurocranium frequently correspond to the compression from the endocranial surface, especially the compression from pronounced brain gyri and arachnoid granulations. DVs tend to bypass these thin areas, and thus their connections with other vascular networks are also affected in such areas. Furthermore, hominids show interspecies variations in brain shapes, which contributes to the taxonomical differences in cranial vault thickness pattern and distribution of DVs.

In agreement with previous studies (Cabanac & Brinnel, 1985; Falk, 1990), this study suggests that DVs potentially contribute to brain thermoregulation by facilitating the exchange between extracranial and intracranial blood. However, the drainage pathways of many DVs are unlikely to be adaptations to brain thermal demands. The evidence in this study does not support a key role of the diploic venous system in brain thermoregulation and evolution.

In addition to the interaction with the brain, there is a possible co-evolution between DVs and their connected paranasal sinuses, extracranial vessels, and intracranial vessels. The featured sphenoid DVs of chimpanzees are possibly an adaptation to their distinct paranasal sinuses. The highly variable frontal sinus in *H. sapiens* may explain its inconsistent connection with frontal DVs. The distinct location of the transverse-sigmoid sinus in *H. neanderthalensis* corresponds to their distinct drainage pattern in the asterional region. The highly developed occipital diploic venous network in hominins is possibly an adaptation to the high demand of draining venous blood extracranially to the vertebrate venous plexus, which is induced by bipedalism.

In conclusion, this pioneering study contributes to our understanding of the anatomy and evolution of the diploic venous system, and it also sheds light on the relationship in human evolutionary history between the brain, cranial bones, and vascular networks.

As a large proportion of this study is based on qualitative analysis, it is expected to see more quantitative data in the following studies providing richer information. Especially, the fractal analysis and relative volume analysis tested in this study have manifested their application values. Also, considering the three layers of the cranial bone are not equally thick, future research is expected to investigate the spatial interaction between DVs and each layer. Finally, based on this current study, future research should investigate more non-human primates and fossil species from the Late Pliocene and Early Pleistocene. This will further complete the map of the evolutionary trajectory of DVs in hominids.

References

Adachi, B. (1928). *Das Arteriensystem der Japaner*. Kaiserlich-Japanischen Universitat zu Kyoto.

Aiello, L., & Dean, C. (1990). *An introduction to human evolutionary anatomy*. Academic Press.

Albessard-Ball, L. (2018). *Co-variation morphologique du crâne et de l'endocrâne au cours de l'évolution du genre* Homo [Ph.D. Dissertation]. Muséum national d'Histoire naturelle.

Al-Shuaili, A., Al-Ajmi, E., Mogali, S. R., Al-Qasmi, S., Al-Mufargi, Y., Kariyattil, R., & Sirasanagandla, S. R. (2024). Computed-tomography evaluation of parietal foramen topography in adults: A retrospective analysis. *Surgical and Radiologic Anatomy*. https://doi.org/10.1007/s00276-023-03284-8

Alvernia, J. E., Fraser, K., & Lanzino, G. (2006). The Occipital Artery: Amicroanatomical Study. *Operative Neurosurgery*, *58*(suppl_1), ONS-114-ONS-122. https://doi.org/10.1227/01.NEU.0000193519.00443.34

Anzelmo, M., Ventrice, F., Barbeito-Andrés, J., Pucciarelli, H. M., & Sardi, M. L. (2015). Ontogenetic changes in cranial vault thickness in a modern sample of *Homo sapiens*. *American Journal of Human Biology*, *27*(4), 475–485. https://doi.org/10.1002/ajhb.22673

Balzeau, A. (2013). Thickened cranial vault and parasagittal keeling: Correlated traits and autapomorphies of *Homo erectus*? *Journal of Human Evolution*, *64*(6), 631–644. https://doi.org/10.1016/j.jhevol.2013.02.005

Balzeau, A., Albessard-Ball, L., Kubicka, A. M., Filippo, A., Beaudet, A., Santos, E., Bienvenu, T., Arsuaga, J.-L., Bartsiokas, A., Berger, L., Bermúdez de Castro, J. M., Brunet, M., Carlson, K. J., Daura, J., Gorgoulis, V. G., Grine, F. E., Harvati, K., Hawks, J., Herries, A., … Buck, L. T. (2022). Frontal sinuses and human evolution. *Science Advances*, *8*(42), eabp9767.

https://doi.org/10.1126/sciadv.abp9767

Balzeau, A., Albessard-Ball, L., Kubicka, A. M., Noûs, C., & T. Buck, L. (2021). Frontal sinus variation in extant species of the genera *Pan*, *Gorilla* and *Homo*. *Bulletins et Mémoires de La Société d'anthropologie de Paris*, *33*(2). https://doi.org/10.4000/bmsap.7840

Balzeau, A., Buck, L. T., Albessard, L., Becam, G., Grimaud-Hervé, D., Rae, T. C., & Stringer, C. B. (2017). The Internal Cranial Anatomy of the Middle Pleistocene Broken Hill 1 Cranium. *PaleoAnthropology*, 107–138. https://doi.org/doi:10.4207/PA.2017.ART107

Balzeau, A., & Charlier, P. (2016). What do cranial bones of LB1 tell us about *Homo floresiensis*? *Journal of Human Evolution*, *93*, 12–24. https://doi.org/10.1016/j.jhevol.2015.12.008

Balzeau, A., Gilissen, E., Holloway, R. L., Prima, S., & Grimaud-Hervé, D. (2014). Variations in size, shape and asymmetries of the third frontal convolution in hominids: Paleoneurological implications for hominin evolution and the origin of language. *Journal of Human Evolution*, *76*, 116–128. https://doi.org/10.1016/j.jhevol.2014.06.006

Balzeau, A., Grimaud-Hervé, D., Détroit, F., Holloway, R. L., Combès, B., & Prima, S. (2013). First description of the Cro-Magnon 1 endocast and study of brain variation and evolution in anatomically modern *Homo sapiens*. *Bulletins et Mémoires de La Société d'anthropologie de Paris*, *25*(1–2), 1–18. https://doi.org/10.1007/s13219-012-0069-z

Balzeau, A., Holloway, R. L., & Grimaud-Hervé, D. (2012). Variations and asymmetries in regional brain surface in the genus *Homo*. *Journal of Human Evolution*, *62*(6), 696–706. https://doi.org/10.1016/j.jhevol.2012.03.007

Balzeau, A., & Pagano, A. (2022). The cranial base and related internal anatomical features in *Homo neanderthalensis* and *Homo sapiens*. *The Anatomical Record*, *305*(8), 2030–2037.

https://doi.org/10.1002/ar.24854

Balzeau, A., & Rougier, H. (2010). Is the suprainiac fossa a Neandertal autapomorphy? A complementary external and internal investigation. *Journal of Human Evolution*, *58*(1), 1–22. https://doi.org/10.1016/j.jhevol.2009.05.016

Bartsiokas, A., & Day, M. H. (1993). Electron probe energy dispersive X-ray microanalysis (EDXA) in the investigation of fossil bone: The case of Java man. *Proceedings of the Royal Society of London. Series B: Biological Sciences*, *252*(1334), 115–123. https://doi.org/10.1098/rspb.1993.0054

Batson, O. V. (1944). Anatomical problems concerned in the study of cerebral blood flow. *Federation Proceedings*, *3*, 139–144.

Beaudet, A., Francesco d'Errico, Backwell, L., Wadley, L., Zipfel, B., de la Peña, P., & Reyes-Centeno, H. (2022). A reappraisal of the Border Cave 1 cranium (KwaZulu-Natal, South Africa). *Quaternary Science Reviews*, *282*, 107452. https://doi.org/10.1016/j.quascirev.2022.107452

Beaudet, A., Holloway, R., & Benazzi, S. (2021). A comparative study of the endocasts of OH 5 and SK 1585: Implications for the paleoneurology of eastern and southern African Paranthropus. *Journal of Human Evolution*, *156*, 103010. https://doi.org/10.1016/j.jhevol.2021.103010

Berger, L. R., & Hawks, J. (2023). Revisiting the age of the Florisbad hominin material. *HOMO*, 102793. https://doi.org/10.1127/homo/2023/1541

Berger, L. R., Hawks, J., De Ruiter, D. J., Churchill, S. E., Schmid, P., Delezene, L. K., Kivell, T. L., Garvin, H. M., Williams, S. A., DeSilva, J. M., Skinner, M. M., Musiba, C. M., Cameron, N., Holliday, T. W., Harcourt-Smith, W., Ackermann, R. R., Bastir, M., Bogin, B., Bolter,

D., … Zipfel, B. (2015). *Homo naledi*, a new species of the genus *Homo* from the Dinaledi Chamber, South Africa. *eLife*, *4*, e09560. https://doi.org/10.7554/eLife.09560

Bermúdez De Castro, J.-M., Martinón-Torres, M., Gómez-Robles, A., Prado, L., & Sarmiento, S. (2007). Comparative analysis of the Gran Dolina-TD6 (Spain) and Tighennif (Algeria) hominin mandibles. *Bulletins et Mémoires de La Société d'anthropologie de Paris*, *19*(3–4), 149–167. https://doi.org/10.4000/bmsap.4623

Bertolizio, G., Mason, L., & Bissonnette, B. (2011). Brain temperature: Heat production, elimination and clinical relevance. *Pediatric Anesthesia*, *21*(4), 347–358. https://doi.org/10.1111/j.1460-9592.2011.03542.x

Betts, J. G., Desaix, P., Johnson, E., Korol, O., Kruse, D., Poe, B., Wise, J. A., Womble, M., & Young, K. A. (2022). *Anatomy and physiology, 2e* (2e ed.). OpenStax ; Rice University.

Boman, F., Froment, A., & Charlier, P. (2016). Variations in the thickness of the cranial vault in a deformed skull from Pre-Hispanic Ancón (Peru). *Bulletins et Mémoires de La Société d'Anthropologie de Paris*, *28*(3–4), 221–225. https://doi.org/10.1007/s13219-016-0160-y

Bonasia, S., Smajda, S., Ciccio, G., & Robert, T. (2020). Middle Meningeal Artery: Anatomy and Variations. *American Journal of Neuroradiology*, *41*(10), 1777–1785. https://doi.org/10.3174/ajnr.A6739

Boyer, D. M., & Harrington, A. R. (2018). Scaling of bony canals for encephalic vessels in euarchontans: Implications for the role of the vertebral artery and brain metabolism. *Journal of Human Evolution*, *114*, 85–101. https://doi.org/10.1016/j.jhevol.2017.09.003

Braga, J. (1995). Emissary canals in the Hominoidea and their phylogenetic significance. *Folia Primatologica*, *65*(3), 144–153. https://doi.org/10.1159/000156880

Braga, J., & Boesch, C. (1997). Further data about venous channels in South African Plio-Pleistocene hominids. *Journal of Human Evolution*, *33*(4), 423–447. https://doi.org/10.1006/jhev.1997.0135

Brengelmann, G. L. (1990). Brain cooling via emissary veins: Fact or fancy? *Behavioral and Brain Sciences*, *13*(2), 349–350. https://doi.org/10.1017/S0140525X00079036

Breschet, G. (1829). *Recherches anatomiques, physiologiques et pathologiques sur le système veineux*. Villeret.

Brown, M., & Lowe, D. G. (2007). Automatic panoramic image stitching using invariant features. *International Journal of Computer Vision*, *74*(1), 59–73. https://doi.org/10.1007/s11263-006-0002-3

Bruner, E., De la Cuétara, J. M., Masters, M., Amano, H., & Ogihara, N. (2014). Functional craniology and brain evolution: From paleontology to biomedicine. *Frontiers in Neuroanatomy*, *8*. https://doi.org/10.3389/fnana.2014.00019

Bruner, E., De La Cuétara, J. M., & Musso, F. (2012). Quantifying patterns of endocranial heat distribution: Brain geometry and thermoregulation. *American Journal of Human Biology*, *24*(6), 753–762. https://doi.org/10.1002/ajhb.22312

Bruner, E., & Eisova, S. (2024). Vascular microforamina and endocranial surface: Normal variation and distribution in adult humans. *The Anatomical Record*. https://doi.org/10.1002/ar.25426

Bruner, E., & Lombard, M. (2020). The skull from Florisbad: A paleoneurological report. *Journal of Anthropological Sciences*, *98*, 89–97. https://doi.org/10.4436/JASS.98014

Bruner, E., Mantini, S., Musso, F., De La Cuétara, J. M., Ripani, M., & Sherkat, S. (2011). The evolution of the meningeal vascular system in the human genus: From brain shape to

thermoregulation. *American Journal of Human Biology*, *23*(1), 35–43. https://doi.org/10.1002/ajhb.21123

Bruner, E., Mantini, S., Perna, A., Maffei, C., & Manzi, G. (2006). Fractal dimension of the middle meningeal vessels: Variation and evolution in *Homo erectus*, Neanderthals, and modern humans. *European Journal of Morphology*, *42*(4/5), 217–224. https://doi.org/10.1080/09243860600746833

Bruner, E., & Sherkat, S. (2008). The middle meningeal artery: From clinics to fossils. *Child's Nervous System*, *24*(11), 1289–1298. https://doi.org/10.1007/s00381-008-0685-6

Buck, L. T., & Stringer, C. B. (2014). *Homo heidelbergensis*. *Current Biology*, *24*(6), R214–R215. https://doi.org/10.1016/j.cub.2013.12.048

Butler, H. (1957). The development of certain human dural venous sinuses. *Journal of Anatomy*, *91*(4), 510–526.

Cabanac, M. (1986). Keeping a cool head. *Physiology*, *1*(2), 41. https://doi.org/10.1152/physiologyonline.1986.1.2.41

Cabanac, M., & Brinnel, H. (1985). Blood flow in the emissary veins of the human head during hyperthermia. *European Journal of Applied Physiology and Occupational Physiology*, *54*(2), 172–176. https://doi.org/10.1007/BF02335925

Casanova, R., Cavalcante, D., Grotting, J. C., Vasconez, L. O., & Psillakis, J. M. (1986). Anatomic basis for vascularized outer-table calvarial bone flaps. *Plastic and Reconstructive Surgery*, *78*(3), 300–308.

Cave, A. J. E. (1994). Note on the venous drainage of the gorilla (*Gorilla gorilla*) diploe. *Journal of Zoology*, *233*(1), 37–43. https://doi.org/10.1111/j.1469-7998.1994.tb05260.x

Cave, A. J., & Haines, R. W. (1940). The paranasal sinuses of the anthropoid apes. *Journal of Anatomy*, *74*(Pt 4), 493–523.

Chell, J. (1991). Anatomical note The squamoso-petrous sinus: A fetal remnant. *Journal of Anatomy*, *175*, 269–271.

Cheng, Y., & Haorah, J. (2019). How does the brain remove its waste metabolites from within? *International Journal of Physiology, Pathophysiology and Pharmacology*, *11*(6), 238–249.

Cheung, N., & McNab, A. A. (2003). Venous anatomy of the orbit. *Investigative Opthalmology & Visual Science*, *44*(3), 988. https://doi.org/10.1167/iovs.02-0865

Chmielewski, P., Skrzat, J., & Walocha, J. (2013). Clinical importance of the middle meningeal artery. *Folia Medica Cracoviensia*, *LIII*(1), 41–46.

Chrcanovic, B. R., Abreu, M. H. N. G., & Custódio, A. L. N. (2011). A morphometric analysis of supraorbital and infraorbital foramina relative to surgical landmarks. *Surgical and Radiologic Anatomy*, *33*(4), 329–335. https://doi.org/10.1007/s00276-010-0698-1

Clarke, R. J. (2008). Latest information on Sterkfontein's *Australopithecus* skeleton and a new look at *Australopithecus*. *South African Journal of Science*, *104*(11/12). https://doi.org/10.1590/S0038-23532008000600015

Cong, L., Phothong, W., Lee, S.-H., Wanitphakdeedecha, R., Koh, I., Tansatit, T., & Kim, H.-J. (2017). Topographic analysis of the supratrochlear artery and the supraorbital artery: Implication for improving the safety of forehead augmentation. *Plastic & Reconstructive Surgery*, *139*(3), 620e–627e. https://doi.org/10.1097/PRS.0000000000003060

Cotofana, S., Steinke, H., Schlattau, A., Schlager, M., Sykes, J. M., Roth, M. Z., Gaggl, A., Giunta, R. E., Gotkin, R. H., & Schenck, T. L. (2017). The anatomy of the facial vein: Implications

for plastic, reconstructive, and aesthetic procedures. *Plastic & Reconstructive Surgery*, *139*(6), 1346–1353. https://doi.org/10.1097/PRS.0000000000003382

Coyle, P., & Heistad, D. D. (1991). Development of collaterals in the cerebral circulation. *Journal of Vascular Research*, *28*(1–3), 183–189. https://doi.org/10.1159/000158860

Cui, Y., & Wu, X. (2015). A geometric morphometric study of a Middle Pleistocene cranium from Hexian, China. *Journal of Human Evolution*, *88*, 54–69. https://doi.org/10.1016/j.jhevol.2015.08.001

Curnoe, D. (2010). A review of early *Homo* in southern Africa focusing on cranial, mandibular and dental remains, with the description of a new species (*Homo gautengensis* sp. Nov.). *HOMO*, *61*(3), 151–177. https://doi.org/10.1016/j.jchb.2010.04.002

Curnoe, D., & Brink, J. (2010). Evidence of pathological conditions in the Florisbad cranium. *Journal of Human Evolution*, *59*(5), 504–513. https://doi.org/10.1016/j.jhevol.2010.06.003

Curnoe, D., & Tobias, P. V. (2006). Description, new reconstruction, comparative anatomy, and classification of the Sterkfontein Stw 53 cranium, with discussions about the taxonomy of other southern African early *Homo* remains. *Journal of Human Evolution*, *50*(1), 36–77. https://doi.org/10.1016/j.jhevol.2005.07.008

Daniels, D. L., Mafee, M. F., Smith, M. M., Smith, T. L., Naidich, T. P., Brown, W. D., Bolger, W. E., Mark, L. P., Ulmer, J. L., Hacein-Bey, L., & Strottmann, J. M. (2003). The frontal sinus drainage pathway and related structures. *American Journal of Neuroradiology*, *24*(8), 1618–1627.

Davison, S. P., & Kaplan, K. A. (2005). The deep temporal vein: An alternative recipient vessel in microsurgical head and neck reconstruction. *Plastic and Reconstructive Surgery*, *116*(4),

1181–1182. https://doi.org/10.1097/01.prs.0000183302.24571.fc

de Ruiter, D. J., Laird, M. F., Elliott, M., Schmid, P., Brophy, J., Hawks, J., & Berger, L. R. (2019). *Homo naledi* cranial remains from the Lesedi chamber of the rising star cave system, South Africa. *Journal of Human Evolution*, *132*, 1–14. https://doi.org/10.1016/j.jhevol.2019.03.019

De Souza Ferreira, M. R., Galvão, A. P. O., De Queiroz Lima, P. T. M. B., De Queiroz Lima, A. M. B., Magalhães, C. P., & Valença, M. M. (2021). The parietal foramen anatomy: Studies using dry skulls, cadaver and in vivo MRI. *Surgical and Radiologic Anatomy*, *43*(7), 1159–1168. https://doi.org/10.1007/s00276-020-02650-0

De Stefano, G. F., & Hauser, G. (1992). Epigenetic traits of the Circeo I skull. In *The Circeo I Neandertal Skull, Studies and Documentation* (pp. 273–300). Instituto Poligrafico e Zecca Dello Stato.

Dekaban, A. S., & Sadowsky, D. (1978). Changes in brain weights during the span of human life: Relation of brain weights to body heights and body weights. *Annals of Neurology*, *4*(4), 345–356. https://doi.org/10.1002/ana.410040410

Delgove, L., Lebeau, J., Raphaël, B., & Champetier, J. (1991). Drainage of the scalp by the superficial temporal vein: Surgical implications. *Surgical and Radiologic Anatomy*, *13*(4), 277–282. https://doi.org/10.1007/BF01627758

Devièse, T., Abrams, G., Hajdinjak, M., Pirson, S., Modica, K. D., Toussaint, M., Fischer, V., Comeskey, D., Spindler, L., Meyer, M., Semal, P., & Higham, T. (2021). Reevaluating the timing of Neanderthal disappearance in Northwest Europe. *Proceedings of the National Academy of Sciences of the United States of America*, *118*(12), e2022466118.

Di Ieva, A. (Ed.). (2016). *The fractal geometry of the brain*. Springer.

Dirks, P. H., Roberts, E. M., Hilbert-Wolf, H., Kramers, J. D., Hawks, J., Dosseto, A., Duval, M., Elliott, M., Evans, M., Grün, R., Hellstrom, J., Herries, A. I., Joannes-Boyau, R., Makhubela, T. V., Placzek, C. J., Robbins, J., Spandler, C., Wiersma, J., Woodhead, J., & Berger, L. R. (2017). The age of *Homo naledi* and associated sediments in the Rising Star Cave, South Africa. *eLife*, *6*, e24231. https://doi.org/10.7554/eLife.24231

Domander, R., Felder, A. A., & Doube, M. (2021). BoneJ2—Refactoring established research software. *Wellcome Open Research*, *6*, 37. https://doi.org/10.12688/wellcomeopenres.16619.1

Douka, K., Chiotti, L., Nespoulet, R., & Higham, T. (2020). A refined chronology for the Gravettian sequence of Abri Pataud. *Journal of Human Evolution*, *141*, 102730. https://doi.org/10.1016/j.jhevol.2019.102730

Duncan, I. C. (2003). Arachnoid granulations—Anatomy and imaging. *South African Journal of Radiology*, *7*(4), 5–10.

Durband, A. C., Kidder, J. H., & Jantz, R. L. (2005). A multivariate examination of the Hexian calvaria. *Anthropological Science*, *113*(2), 147–154. https://doi.org/10.1537/ase.040303

Edizer, M., Beden, U., & Icten, N. (2009). Morphological parameters of the periorbital arterial arcades and potential clinical significance based on anatomical identification. *Journal of Craniofacial Surgery*, *20*(1), 209–214. https://doi.org/10.1097/SCS.0b013e318191cf9f

Eisová, S., Rangel De Lázaro, G., Píšová, H., Pereira-Pedro, S., & Bruner, E. (2016). Parietal bone thickness and vascular diameters in adult modern humans: A survey on cranial remains. *The Anatomical Record*, *299*(7), 888–896. https://doi.org/10.1002/ar.23348

Eisová, S., Velemínský, P., Velemínská, J., & Bruner, E. (2022). Diploic vein morphology in normal and craniosynostotic adult human skulls. *Journal of Morphology*, *283*(10), 1318–1336. https://doi.org/10.1002/jmor.21505

Ellis, H., & Mahadevan, V. (2014). The surgical anatomy of the scalp. *Surgery (Oxford)*, *32*, e1–e5. https://doi.org/10.1016/j.mpsur.2013.04.024

Epstein, H. M., Linde, H. W., Crompton, A. R., Cine, I. S., & Eckenholf, J. J. E. (1970). The vertebral venous plexus as a major cerebral venous outflow tract. *Anesthesiology*, *32*(4), 332–340. https://doi.org/10.1097/00000542-197004000-00007

Erdogmus, S., & Govsa, F. (2007). Anatomy of the supraorbital region and the evaluation of it for the reconstruction of facial defects. *Journal of Craniofacial Surgery*, *18*(1), 104–112. https://doi.org/10.1097/01.scs.0000246498.39194.20

Falk, D. (1986). Evolution of cranial blood drainage in hominids: Enlarged occipital/marginal sinuses and emissary foramina. *American Journal of Physical Anthropology*, *70*(3), 311–324. https://doi.org/10.1002/ajpa.1330700306

Falk, D. (1990). Brain evolution in *Homo:* The "radiator" theory. *Behavioral and Brain Sciences*, *13*(2), 333–344. https://doi.org/10.1017/S0140525X00078973

Falk, D. (1993). Meningeal arterial patterns in great apes: Implications for hominid vascular evolution. *American Journal of Physical Anthropology*, *92*(1), 81–97. https://doi.org/10.1002/ajpa.1330920107

Falk, D., & Conroy, G. C. (1983). The cranial venous sinus system in *Australopithecus afarensis*. *Nature*, *306*(5945), 779–781. https://doi.org/10.1038/306779a0

Fedorov, A., Beichel, R., Kalpathy-Cramer, J., Finet, J., Fillion-Robin, J.-C., Pujol, S., Bauer, C.,

Jennings, D., Fennessy, F., Sonka, M., Buatti, J., Aylward, S., Miller, J. V., Pieper, S., & Kikinis, R. (2012). 3D Slicer as an image computing platform for the Quantitative Imaging Network. *Magnetic Resonance Imaging*, *30*(9), 1323–1341. https://doi.org/10.1016/j.mri.2012.05.001

Feibel, C. S., Brown, F. H., & McDougall, I. (1989). Stratigraphic context of fossil hominids from the Omo group deposits: Northern Turkana Basin, Kenya and Ethiopia. *American Journal of Physical Anthropology*, *78*(4), 595–622. https://doi.org/10.1002/ajpa.1330780412

Ferguson, W. W. (1989). Reappraisal of the taxonomic status of the cranium Stw 53 from the Plio/Pleistocene of Sterkfontein, in South Africa. *Primates*, *30*(1), 103–109. https://doi.org/10.1007/BF02381216

Ford, J. M., & Decker, S. J. (2016). Computed tomography slice thickness and its effects on three-dimensional reconstruction of anatomical structures. *Journal of Forensic Radiology and Imaging*, *4*, 43–46. https://doi.org/10.1016/j.jofri.2015.10.004

Frouin, M., Lahaye, C., Valladas, H., Higham, T., Debénath, A., Delagnes, A., & Mercier, N. (2017). Dating the Middle Paleolithic deposits of La Quina Amont (Charente, France) using luminescence methods. *Journal of Human Evolution*, *109*, 30–45. https://doi.org/10.1016/j.jhevol.2017.05.002

García-González, U., Cavalcanti, D. D., Agrawal, A., Gonzalez, L. F., Wallace, R. C., Spetzler, R. F., & Preul, M. C. (2009). The diploic venous system: Surgical anatomy and neurosurgical implications. *Neurosurgical Focus*, *27*(5), E2. https://doi.org/10.3171/2009.8.FOCUS09169

Gausas, R. E. (2004). Advances in applied anatomy of the eyelid and orbit: *Current Opinion in*

Ophthalmology, *15*(5), 422–425. https://doi.org/10.1097/01.icu.0000139303.24272.8d

Geraads, D. (2016). Pleistocene Carnivora (Mammalia) from Tighennif (Ternifine), Algeria. *Geobios*, *49*(6), 445–458. https://doi.org/10.1016/j.geobios.2016.09.001

Geraads, D., Hublin, J.-J., Jaeger, J.-J., Tong, H., Sen, S., & Toubeau, P. (1986). The Pleistocene hominid site of Ternifine, Algeria: New results on the environment, age, and human industries. *Quaternary Research*, *25*(3), 380–386. https://doi.org/10.1016/0033-5894(86)90008-6

Godinho, R. M., & O'Higgins, P. (2017). Virtual Reconstruction of Cranial Remains: The *H. Heidelbergensis*, Kabwe 1 Fossil. In *Human Remains: Another Dimension* (pp. 135–147). Elsevier. https://doi.org/10.1016/B978-0-12-804602-9.00011-4

Godinho, R. M., & O'Higgins, P. (2018). The biomechanical significance of the frontal sinus in Kabwe 1 (*Homo heidelbergensis*). *Journal of Human Evolution*, *114*, 141–153. https://doi.org/10.1016/j.jhevol.2017.10.007

Gómez Díaz, O. J., & Cruz Sánchez, M. D. (2016). Anatomical and clinical study of the posterior auricular artery angiosome: In search of a rescue tool for ear reconstruction. *Plastic and Reconstructive Surgery - Global Open*, *4*(12), e1165. https://doi.org/10.1097/GOX.0000000000001165

Gray, H. (1918). *Anatomy of the human body*. Lea & Febiger.

Grine, F. E., Jungers, W. L., & Schultz, J. (1996). Phenetic affinities among early *Homo* crania from East and South Africa. *Journal of Human Evolution*, *30*(3), 189–225. https://doi.org/10.1006/jhev.1996.0019

Grün, R., Brink, J. S., Spooner, N. A., Taylor, L., Stringer, C. B., Franciscus, R. G., & Murray, A. S.

(1996). Direct dating of Florisbad hominid. *Nature*, *382*(6591), 500–501. https://doi.org/10.1038/382500a0

Grün, R., Pike, A., McDermott, F., Eggins, S., Mortimer, G., Aubert, M., Kinsley, L., Joannes-Boyau, R., Rumsey, M., Denys, C., Brink, J., Clark, T., & Stringer, C. (2020). Dating the skull from Broken Hill, Zambia, and its position in human evolution. *Nature*, *580*(7803), 372–375. https://doi.org/10.1038/s41586-020-2165-4

Grün, R., & Stringer, C. B. (1991). Electron spin resonance dating and the evolution of modern humans. *Archaeometry*, *33*(2), 153–199. https://doi.org/10.1111/j.1475-4754.1991.tb00696.x

Guérin, G., Aldeias, V., Baumgarten, F., Goldberg, P., Gómez-Olivencia, A., Lahaye, C., Madelaine, S., Maureille, B., Philippe, A., Sandgathe, D., Talamo, S., Thomsen, K., Turq, A., & Balzeau, A. (2023). A third Neanderthal individual from La Ferrassie dated to the end of the Middle Palaeolithic. *PaleoAnthropology*, 98-118 Pages. https://doi.org/10.48738/2023.ISS1.811

Guggenbuhl, P., Chappard, D., Garreau, M., Bansard, J.-Y., Chales, G., & Rolland, Y. (2008). Reproducibility of CT-based bone texture parameters of cancellous calf bone samples: Influence of slice thickness. *European Journal of Radiology*, *67*(3), 514–520. https://doi.org/10.1016/j.ejrad.2007.08.003

Guo, Y., Chen, H., Chen, X., & Yu, J. (2019). Clinical importance of the occipital artery in vascular lesions: A review of the literature. *The Neuroradiology Journal*, *32*(5), 366–375. https://doi.org/10.1177/1971400919857245

Hampshire, A., Chamberlain, S. R., Monti, M. M., Duncan, J., & Owen, A. M. (2010). The role of

the right inferior frontal gyrus: Inhibition and attentional control. *NeuroImage*, *50*(3), 1313–1319. https://doi.org/10.1016/j.neuroimage.2009.12.109

Hawks, J., Elliott, M., Schmid, P., Churchill, S. E., Ruiter, D. J. D., Roberts, E. M., Hilbert-Wolf, H., Garvin, H. M., Williams, S. A., Delezene, L. K., Feuerriegel, E. M., Randolph-Quinney, P., Kivell, T. L., Laird, M. F., Tawane, G., DeSilva, J. M., Bailey, S. E., Brophy, J. K., Meyer, M. R., … Berger, L. R. (2017). New fossil remains of *Homo naledi* from the Lesedi Chamber, South Africa. *eLife*, *6*, e24232. https://doi.org/10.7554/eLife.24232

Hayreh, S. S. (2006). Orbital vascular anatomy. *Eye*, *20*(10), 1130–1144. https://doi.org/10.1038/sj.eye.6702377

Hedjoudje, A., Piveteau, A., Gonzalez-Campo, C., Moghekar, A., Gailloud, P., & San Millán, D. (2019). The occipital emissary vein: A possible marker for pseudotumor cerebri. *American Journal of Neuroradiology*, *40*(6), 973–978. https://doi.org/10.3174/ajnr.A6061

Heim, Jean-Louis. (1976). *Les Hommes Fossiles de La Ferrassie, Tomo I*. Masson.

Henry-Gambier, D. (2002). Les fossiles de Cro-Magnon (Les Eyzies-de-Tayac, Dordogne): Nouvelles données sur leur position chronologique et leur attribution culturelle. *Bulletins et mémoires de la société d'anthropologie de Paris*, *14*(1–2). https://doi.org/10.4000/bmsap.459

Herries, A. I. R., & Shaw, J. (2011). Palaeomagnetic analysis of the Sterkfontein palaeocave deposits: Implications for the age of the hominin fossils and stone tool industries. *Journal of Human Evolution*, *60*(5), 523–539. https://doi.org/10.1016/j.jhevol.2010.09.001

Hershkovitz, I., Greenwald, C., Rothschild, B. M., Latimer, B., Dutour, O., Jellema, L. M., Wish-Baratz, S., Pap, I., & Leonetti, G. (1999). The elusive diploic veins: Anthropological and

anatomical perspective. *American Journal of Physical Anthropology*, *108*(3), 345–358. https://doi.org/10.1002/(SICI)1096-8644(199903)108:3<345::AID-AJPA9>3.0.CO;2-S

Holloway, R. L. (1972). Australopithecine Endocasts, Brain Evolution in the Hominoidea, and a Model of Hominid Evolution. In R. Tuttle (Ed.), *The Functional and Evolutionary Biology of Primates* (1st ed., pp. 185–203). Routledge. https://doi.org/10.4324/9781315132129-8

House, E. L., Pansky, B., Jacobs, M. S., & Wagner, B. M. (1966). Gross structure of the ear, nasal cavity and paranasal sinuses of the chimpanzee. *The Anatomical Record*, *155*(1), 77–88. https://doi.org/10.1002/ar.1091550109

Hublin, J.-J. (2001). Northwestern African Middle Pleistocene hominids and their bearing on the emergence of *Homo sapiens*. In *Human Roots: Africa and Asia in the Middle Pleistocene* (pp. 99–121). Western Academic and Specialist Press.

Hublin, J.-J., Ben-Ncer, A., Bailey, S. E., Freidline, S. E., Neubauer, S., Skinner, M. M., Bergmann, I., Le Cabec, A., Benazzi, S., Harvati, K., & Gunz, P. (2017). New fossils from Jebel Irhoud, Morocco and the pan-African origin of *Homo sapiens*. *Nature*, *546*(7657), 289–292. https://doi.org/10.1038/nature22336

Hughes, A. R., & Tobias, P. V. (1977). A fossil skull probably of the genus *Homo* from Sterkfontein, Transvaal. *Nature*, *265*(5592), 310–312. https://doi.org/10.1038/265310a0

Hui, J., & Balzeau, A. (2023a). Investigating the relationship between cranial bone thickness and diploic channels: A first comparison between fossil *Homo sapiens* and *Homo neanderthalensis*. *The Anatomical Record*, ar.25360. https://doi.org/10.1002/ar.25360

Hui, J., & Balzeau, A. (2023b). The diploic venous system in *Homo neanderthalensis* and fossil *Homo sapiens*: A study using high-resolution computed tomography. *American Journal of*

Biological Anthropology, ajpa.24843. https://doi.org/10.1002/ajpa.24843

Imanishi, N., Nakajima, H., Minabe, T., Chang, H., & Aiso, S. (2002). Venous drainage architecture of the temporal and parietal regions: Anatomy of the superficial temporal artery and vein. *Plastic and Reconstructive Surgery*, *109*(7), 2197–2203. https://doi.org/10.1097/00006534-200206000-00003

Ishkhanyan, B., Michel Lange, V., Boye, K., Mogensen, J., Karabanov, A., Hartwigsen, G., & Siebner, H. R. (2020). Anterior and posterior left inferior frontal gyrus contribute to the implementation of grammatical determiners during language production. *Frontiers in Psychology*, *11*, 685. https://doi.org/10.3389/fpsyg.2020.00685

Jain, R. K. (1988). Determinants of tumor blood flow: A review. *Cancer Research*, *48*(10), 2641–2658.

Jelev, L., & Malinova, L. (2020). Occipital emissary foramina in human skulls: Review of literature and proposal of a classification scheme of the occipital venous anastomoses in the posterior cranial fossa. *Anatomy*, *14*(1), 11–15. https://doi.org/10.2399/ana.20.002

Jessen, C. (2001). Selective brain cooling in mammals and birds. *The Japanese Journal of Physiology*, *51*(3), 291–301. https://doi.org/10.2170/jjphysiol.51.291

Jung, Y.-S., Kim, H.-J., Choi, S.-W., Kang, J.-W., & Cha, I.-H. (2003). Regional thickness of parietal bone in Korean adults. *International Journal of Oral and Maxillofacial Surgery*, *32*(6), 638–641. https://doi.org/10.1054/ijom.2002.0415

Juskys, R., Rocka, S., & Suchomlinov, A. (2022). Anatomical variations of superior sagittal sinus and tributary bridging veins: A cadaveric study. *Cureus*. https://doi.org/10.7759/cureus.21979

Kato, N., & Outi, H. (1962). Relation of the supraorbital nerve and vessels to the notch and foramen of the supraorbital margin. *Okajimas Folia Anatomica Japonica*, *38*(5), 411–424. https://doi.org/10.2535/ofaj1936.38.5_411

Keser, N., Avci, E., Soylemez, B., Karatas, D., & Baskaya, M. K. (2018). Occipital artery and its segments in vertebral artery revascularization surgery: A microsurgical anatomic study. *World Neurosurgery*, *112*, e534–e539. https://doi.org/10.1016/j.wneu.2018.01.073

Kilgour, F. G. (1961). William Harvey and his contributions. *Circulation*, *23*(2), 286–296. https://doi.org/10.1161/01.CIR.23.2.286

Kimbel, W. H., White, T. D., & Johanson, D. C. (1984). Cranial morphology of *Australopithecus afarensis*: A comparative study based on a composite reconstruction of the adult skull. *American Journal of Physical Anthropology*, *64*(4), 337–388. https://doi.org/10.1002/ajpa.1330640403

Kılıç, T., & Akakın, A. (2007). Anatomy of Cerebral Veins and Sinuses. In V. Caso, G. Agnelli, & M. Paciaroni (Eds.), *Frontiers of Neurology and Neuroscience* (Vol. 23, pp. 4–15). KARGER. https://doi.org/10.1159/000111256

Kobayashi, K., Suzuki, M., Ueda, F., & Matsui, O. (2006). Anatomical study of the occipital sinus using contrast-enhanced magnetic resonance venography. *Neuroradiology*, *48*(6), 373–379. https://doi.org/10.1007/s00234-006-0087-y

Kochiyama, T., Ogihara, N., Tanabe, H. C., Kondo, O., Amano, H., Hasegawa, K., Suzuki, H., Ponce De León, M. S., Zollikofer, C. P. E., Bastir, M., Stringer, C., Sadato, N., & Akazawa, T. (2018). Reconstructing the Neanderthal brain using computational anatomy. *Scientific Reports*, *8*(1), 6296. https://doi.org/10.1038/s41598-018-24331-0

Kountakis, S. E., Senior, B. A., & Draf, W. (Eds.). (2016). *The Frontal Sinus*. Springer Berlin Heidelberg. https://doi.org/10.1007/978-3-662-48523-1

Kubo, D. (2022). Internal carotid supply to the parietal meninges: A comparative study based on cranio-orbital vascular traces in modern humans and Indonesian *Homo erectus*. *Anthropological Science*, *130*(2), 107–119. https://doi.org/10.1537/ase.211223

Kunz, A. R., & Iliadis, C. (2007). Hominid evolution of the arteriovenous system through the cranial base and its relevance for craniosynostosis. *Child's Nervous System*, *23*(12), 1367–1377. https://doi.org/10.1007/s00381-007-0468-5

L. Hilgen, S., Pop, E., Adhityatama, S., A. Veldkamp, T., W.K. Berghuis, H., Sutisna, I., Yurnaldi, D., Dupont-Nivet, G., Reimann, T., Nowaczyk, N., F. Kuiper, K., Krijgsman, W., B. Vonhof, H., Ekowati, D. R., Alink, G., Ni Luh Gde Dyah Mega Hafsari, Drespriputra, O., Verpoorte, A., Bos, R., … Joordens, J. C. A. (2023). Revised age and stratigraphy of the classic *Homo erectus* -bearing succession at Trinil (Java, Indonesia). *Quaternary Science Reviews*, *301*, 107908. https://doi.org/10.1016/j.quascirev.2022.107908

Lachkar, S., Dols, M.-M., Ishak, B., Iwanaga, J., & Tubbs, R. S. (2019). The diploic veins: A comprehensive review with clinical applications. *Cureus*, *11*(4), e4422. https://doi.org/10.7759/cureus.4422

Lang, J. (1983). *Clinical anatomy of the head*. Springer Berlin Heidelberg. https://doi.org/10.1007/978-3-642-68242-1

Leach, J. L., Jones, B. V., Tomsick, T. A., Stewart, C. A., & Balko, M. G. (1996). Normal appearance of arachnoid granulations on contrast-enhanced CT and MR of the brain: Differentiation from dural sinus disease. *American Journal of Neuroradiology*, *17*(8), 1523–1532.

Lee, H.-J., Choi, Y.-J., Lee, K.-W., & Kim, H.-J. (2018). Positional patterns among the auriculotemporal nerve, superficial temporal artery, and superficial temporal vein for use in decompression treatments for migraine. *Scientific Reports*, *8*(1), 16539. https://doi.org/10.1038/s41598-018-34765-1

Lee, K.-L., Choi, Y.-J., Gil, Y.-C., Hu, K.-S., Tansatit, T., & Kim, H.-J. (2019). Locational relationship between the lateral border of the frontalis muscle and the superior temporal line. *Plastic & Reconstructive Surgery*, *143*(2), 293e–298e. https://doi.org/10.1097/PRS.0000000000005202

L'Engle Williams, F., Schmidt, C. W., Henry, A. G., Discamps, E., Droke, J. L., Becam, G., & De Lumley, M.-A. (2022). The Ice Age diet of the La Quina 5 Neandertal of southwest France. *L'Anthropologie*, *126*(4), 103056. https://doi.org/10.1016/j.anthro.2022.103056

Li, Z.-Y., Wu, X., Zhou, L.-P., Liu, W., Gao, X., Nian, X.-M., & Trinkaus, E. (2017). Late Pleistocene archaic human crania from Xuchang, China. *Science*, *355*(6328), 969–972. https://doi.org/10.1126/science.aal2482

Liakakis, G., Nickel, J., & Seitz, R. J. (2011). Diversity of the inferior frontal gyrus—A meta-analysis of neuroimaging studies. *Behavioural Brain Research*, *225*(1), 341–347. https://doi.org/10.1016/j.bbr.2011.06.022

Liao, Z.-F., Cong, L.-Y., Hong, W.-J., Luo, C.-E., & Luo, S.-K. (2022). Three-dimensional computed tomographic study of the supratrochlear artery and supraorbital artery to determine arterial variations and their relationship. *Dermatologic Surgery*, *48*(2), 225–231. https://doi.org/10.1097/DSS.0000000000003347

Lieberman, D. (2011). *The evolution of the human head*. Belknap Press of Harvard University Press.

Liu, W., Athreya, S., Xing, S., & Wu, X. (2022). Hominin evolution and diversity: A comparison of earlier-Middle and later-Middle Pleistocene hominin fossil variation in China. *Philosophical Transactions of the Royal Society B: Biological Sciences*, *377*(1847), 20210040. https://doi.org/10.1098/rstb.2021.0040

Liu, W., Martinón-Torres, M., Kaifu, Y., Wu, X., Kono, R. T., Chang, C., Wei, P., Xing, S., Huang, W., & Bermúdez De Castro, J. M. (2017). A mandible from the Middle Pleistocene Hexian site and its significance in relation to the variability of Asian *Homo erectus*. *American Journal of Physical Anthropology*, *162*(4), 715–731. https://doi.org/10.1002/ajpa.23162

Louis, R. G., Loukas, M., Wartmann, C. T., Tubbs, R. S., Apaydin, N., Gupta, A. A., Spentzouris, G., & Ysique, J. R. (2009). Clinical anatomy of the mastoid and occipital emissary veins in a large series. *Surgical and Radiologic Anatomy*, *31*(2), 139. https://doi.org/10.1007/s00276-008-0423-5

Mandelbrot, B. B. (1982). *The fractal geometry of nature*. Freeman.

Manzi, G., Gracia, A., & Arsuaga, J.-L. (2000). Cranial discrete traits in the Middle Pleistocene humans from Sima de los Huesos (Sierra de Atapuerca, Spain). Does hypostosis represent any increase in “ontogenetic stress” along the Neanderthal lineage? *Journal of Human Evolution*, *38*(3), 425–446. https://doi.org/10.1006/jhev.1999.0362

Marano, S. R., Fischer, D. W., Gaines, C., & Sonntag, V. K. H. (1985). Anatomical study of the superficial temporal artery. *Neurosurgery*, *16*(6), 786–790. https://doi.org/10.1227/00006123-198506000-00008

Marcozzi, V. (1942). L’arteria meningea media negli uomini recenti, nel Sinantropo e nelle rcimmie. *Riv Antropol*, *34*, 407–436.

Marsh, H. E. (2013). *Beyond thick versus thin: Mapping cranial vault thickness patterns in recent* Homo sapiens [Doctor of Philosophy, University of Iowa]. https://doi.org/10.17077/etd.hbxcmbbg

Marsot-Dupuch, K., Gayet-Delacroix, M., Elmaleh-Berges, M., Bonneville, F., & Lasjaunias, P. (2001). *The Petrosquamosal Sinus: CT and MR Findings of a Rare Emissary Vein*. 8.

Masters, B. R. (2004). Fractal analysis of the vascular tree in the human retina. *Annual Review of Biomedical Engineering*, *6*(1), 427–452. https://doi.org/10.1146/annurev.bioeng.6.040803.140100

McKinnon, V. E., Riaz, S., Stubbs, E., McRae, M. H., & McRae, M. C. (2022). Identification of the anatomy of the deep temporal vein using computed tomography imaging: A retrospective cross-sectional review of patient imaging. *Microsurgery*, *42*(8), 757–765. https://doi.org/10.1002/micr.30956

Millard, A. R. (2008). A critique of the chronometric evidence for hominid fossils: I. Africa and the Near East 500–50ka. *Journal of Human Evolution*, *54*(6), 848–874. https://doi.org/10.1016/j.jhevol.2007.11.002

Miller, M. E., Evans, H. E., & Christensen, G. C. (1979). *Miller's Anatomy of the Dog* (4th ed.). Saunders.

Motomura, H., Muraoka, M., & Nose, K. (2003). Eyebrow reconstruction with intermediate hair from the hairline of the forehead on the pedicled temporoparietal fascial flap. *Annals of Plastic Surgery*, *51*(3), 314–318. https://doi.org/10.1097/01.SAP.0000054246.96906.F7

Movius, H. (1969). The abri of Cro-Magnon, Les Eyzies (Dordogne) and the probable age of the contained burials on the basis of the evidence of the nearby abri Pataud. *Anuario de*

Estudios Atlánticos, *15*, 323–344.

Muche, A. (2021). Morphometry of asterion and its proximity to dural venous sinuses in Northwest Ethiopian adult skulls. *Journal of Craniofacial Surgery*, *32*(3), 1171–1173. https://doi.org/10.1097/SCS.0000000000007364

Mwachaka, P. M., Hassanali, J., & Odula, P. O. (2010). Anatomic position of the asterion in Kenyans for posterolateral surgical approaches to cranial cavity. *Clinical Anatomy*, *23*(1), 30–33. https://doi.org/10.1002/ca.20888

Ni, X., & Qiu, Z. (2012). Tupaiine tree shrews (Scandentia, Mammalia) from the Yuanmou *Lufengpithecus* locality of Yunnan, China. *Swiss Journal of Palaeontology*, *131*(1), 51–60. https://doi.org/10.1007/s13358-011-0029-0

Ostrowski, P., Bonczar, M., Plutecki, D., Kwiecińska, M., Rams, D., Dziedzic, M., Piątek-Koziej, K., Przybycien, W., Sporek, M., Walocha, J., & Koziej, M. (2023). The occipital artery: A meta-analysis of its anatomy with clinical correlations. *Anatomical Science International*, *98*(1), 12–21. https://doi.org/10.1007/s12565-022-00693-4

Patchana, T., Zampella, B., Berry, J. A., Lawandy, S., & Sweiss, R. B. (2019). Superior sagittal sinus: A review of the history, surgical considerations, and pathology. *Cureus*. https://doi.org/10.7759/cureus.4597

Pekcevik, Y., & Pekcevik, R. (2013). Why should we report posterior fossa emissary veins? *Diagnostic and Interventional Radiology*. https://doi.org/10.5152/dir.2013.13203

Peña-Melián, A., Rosas, A., García-Tabernero, A., Bastir, M., & De La Rasilla, M. (2011). Paleoneurology of two new Neandertal occipitals from El Sidrón (Asturias, Spain) in the context of *Homo* endocranial evolution. *The Anatomical Record*, *294*(8), 1370–1381.

https://doi.org/10.1002/ar.21427

Pinar, Y. A., & Govsa, F. (2006). Anatomy of the superficial temporal artery and its branches: Its importance for surgery. *Surgical and Radiologic Anatomy*, *28*(3), 248–253. https://doi.org/10.1007/s00276-006-0094-z

Píšová, H., Rangel de Lázaro, G., Velemínský, P., & Bruner, E. (2017). Craniovascular traits in anthropology and evolution: From bones to vessels. *Journal of Anthropological Sciences*, *95*, 35–65. https://doi.org/10.4436/JASS.95003

Pop, E., Hilgen, S., Adhityatama, S., Berghuis, H., Veldkamp, T., Vonhof, H., Sutisna, I., Alink, G., Noerwidi, S., Roebroeks, W., & Joordens, J. (2023). Reconstructing the provenance of the hominin fossils from Trinil (Java, Indonesia) through an integrated analysis of the historical and recent excavations. *Journal of Human Evolution*, *176*, 103312. https://doi.org/10.1016/j.jhevol.2022.103312

Prakash, R., Prabhu, L. V., Kumar, J., Nayak, V., & Singh, G. (2006). Variations of jugular veins: Phylogenic correlation and clinical implications. *Southern Medical Journal*, *99*(10), 1146–1148. https://doi.org/10.1097/01.smj.0000240708.08972.c0

Prat, S. (2002). Anatomical study of the skull of the Kenyan specimen KNM-ER 1805: A re-evaluation of its taxonomic allocation? *Comptes Rendus Palevol*, *1*(1), 27–33. https://doi.org/10.1016/S1631-0683(02)00001-5

Rangel de Lázaro, G., de la Cuétara, J. M., Píšová, H., Lorenzo, C., & Bruner, E. (2016). Diploic vessels and computed tomography: Segmentation and comparison in modern humans and fossil hominids. *American Journal of Physical Anthropology*, *159*(2), 313–324. https://doi.org/10.1002/ajpa.22878

Rangel de Lázaro, G., Eisová, S., Píšová, H., & Bruner, E. (2018). The Endocranial Vascular System: Tracing Vessels. In E. Bruner, N. Ogihara, & H. C. Tanabe (Eds.), *Digital Endocasts* (pp. 71–91). Springer Japan. https://doi.org/10.1007/978-4-431-56582-6_6

Rangel de Lázaro, G., Neubauer, S., Gunz, P., & Bruner, E. (2020). Ontogenetic changes of diploic channels in modern humans. *American Journal of Physical Anthropology*, *173*(1), 96–111. https://doi.org/10.1002/ajpa.24085

Rao, Y., Ballal, V., Murlimanju, B., Pai, M., Tonse, M., & Krishnamurthy, A. (2018). Undivided retromandibular vein leading to the absence of external jugular vein. *Journal of Morphological Sciences*, *35*(04), 225–228. https://doi.org/10.1055/s-0038-1675760

Rightmire, G. P. (1978). Florisbad and human population succession in Southern Africa. *American Journal of Physical Anthropology*, *48*(4), 475–486. https://doi.org/10.1002/ajpa.1330480406

Rightmire, G. P. (1990). *Evolution of* Homo erectus. Cambridge University Press.

Rightmire, G. P. (1993). Variation among early *Homo* crania from Olduvai Gorge and the Koobi Fora region. *American Journal of Physical Anthropology*, *90*(1), 1–33. https://doi.org/10.1002/ajpa.1330900102

Rightmire, G. P. (2013). *Homo erectus* and Middle Pleistocene hominins: Brain size, skull form, and species recognition. *Journal of Human Evolution*, *65*(3), 223–252. https://doi.org/10.1016/j.jhevol.2013.04.008

Robbins, J. L., Dirks, P. H. G. M., Roberts, E. M., Kramers, J. D., Makhubela, T. V., Hilbert-Wolf, H. L., Elliott, M., Wiersma, J. P., Placzek, C. J., Evans, M., & Berger, L. R. (2021). Providing context to the *Homo naledi* fossils: Constraints from flowstones on the age of

sediment deposits in Rising Star Cave, South Africa. *Chemical Geology*, *567*, 120108. https://doi.org/10.1016/j.chemgeo.2021.120108

Rosas, A., Peña-Melián, A., García-Tabernero, A., Bastir, M., & De La Rasilla, M. (2014). Temporal lobe sulcal pattern and the bony impressions in the middle cranial fossa: The case of the El Sidrón (Spain) Neandertal sample. *The Anatomical Record*, *297*(12), 2331–2341. https://doi.org/10.1002/ar.22957

Rosas, A., Peña-Melián, A., García-Tabernero, A., Bastir, M., De La Rasilla, M., & Fortea, J. (2008). Endocranial occipito-temporal anatomy of SD-1219 from the Neandertal El Sidrón site (Asturias, Spain). *The Anatomical Record*, *291*(5), 502–512. https://doi.org/10.1002/ar.20684

Roth, G., & Dicke, U. (2012). Evolution of the brain and intelligence in primates. In *Progress in Brain Research* (Vol. 195, pp. 413–430). Elsevier. https://doi.org/10.1016/B978-0-444-53860-4.00020-9

Ruız, D. S. M., Fasel, J. H. D., Rufenacht, D. A., & Gailloud, P. (2004). *The sphenoparietal sinus of Breschet: Does it exist? An anatomic study*.

Saban, R. (1995). Image of the human fossil brain: Endocranial casts and meningeal vessels in young and adult subjects. In *Origins of the human brain* (pp. 11–39). Oxford University Press.

Samadian, M., Nazparvar, B., Haddadian, K., Rezaei, O., & Khormaee, F. (2011). The anatomical relation between the superior sagittal sinus and the sagittal suture with surgical considerations. *Clinical Neurology and Neurosurgery*, *113*(2), 89–91. https://doi.org/10.1016/j.clineuro.2010.09.006

San Millán Ruíz, D., Gailloud, P., Yilmaz, H., Perren, F., Rathgeb, J.-P., Rüfenacht, D. A., & Fasel, J. H. D. (2006). The petrosquamosal sinus in humans. *Journal of Anatomy*, *209*(6), 711–720. https://doi.org/10.1111/j.1469-7580.2006.00652.x

Sant'Anna, M. A. F., Luciano, L. L., Chaves, P. H. S., Santos, L. A. D., Moreira, R. G., Peixoto, R., Barcellos, R., Reis, G. A., Pereira, C. U., & Rabelo, N. N. (2021). Anatomy of the Middle Meningeal Artery. *Arquivos Brasileiros de Neurocirurgia: Brazilian Neurosurgery*, *40*(04), e339–e348. https://doi.org/10.1055/s-0041-1733863

Schenker, N. M., Hopkins, W. D., Spocter, M. A., Garrison, A. R., Stimpson, C. D., Erwin, J. M., Hof, P. R., & Sherwood, C. C. (2010). Broca's Area Homologue in Chimpanzees (*Pan troglodytes*): Probabilistic Mapping, Asymmetry, and Comparison to Humans. *Cerebral Cortex*, *20*(3), 730–742. https://doi.org/10.1093/cercor/bhp138

Schmidt, R. F., & Thews, G. (Eds.). (1989). *Human Physiology*. Springer Berlin Heidelberg. https://doi.org/10.1007/978-3-642-73831-9

Schneider, C. A., Rasband, W. S., & Eliceiri, K. W. (2012). NIH Image to ImageJ: 25 years of image analysis. *Nature Methods*, *9*(7), 671–675. https://doi.org/10.1038/nmeth.2089

Schunk, H., & Maruyama, Y. (1960). Two vascular grooves of the external table of the skull which simulate fractures. *Acta Radiologica*, *54*(3), 186–194. https://doi.org/10.3109/00016926009172539

Schünke, M., Schulte, E., Schumacher, U., & Vitte, É. (2016). *Tête, cou et neuro-anatomie*. De Boeck supérieur.

Schwartz, J. H., Tattersall, I., & Holloway, R. L. (Eds.). (2002a). *The human fossil record, brain endocasts—The paleoneurological evidence* (Vol. 3). Wiley-Liss.

Schwartz, J. H., Tattersall, I., & Holloway, R. L. (Eds.). (2002b). *The human fossil record: Volume one* (Vol. 1). Wiley-Liss.

Schwartz, J. H., Tattersall, I., & Holloway, R. L. (Eds.). (2002c). *The human fossil record: Volume two* (Vol. 2). Wiley-Liss.

Seker, A., Martins, C., & Rhoton, A. L. (2010). Meningeal Anatomy. In *Meningiomas* (pp. 11–51). Elsevier. https://doi.org/10.1016/B978-1-4160-5654-6.00002-7

Semal, P., Rougier, H., Crevecoeur, I., Jungels, C., Flas, D., Hauzeur, A., Maureille, B., Germonpré, M., Bocherens, H., Pirson, S., Cammaert, L., De Clerck, N., Hambucken, A., Higham, T., Toussaint, M., & van der Plicht, J. (2009). New data on the late Neandertals: Direct dating of the Belgian Spy fossils. *American Journal of Physical Anthropology*, *138*(4), 421–428. https://doi.org/10.1002/ajpa.20954

Shen, G., Tu, H., Xiao, D., Qiu, L., Feng, Y., & Zhao, J. (2014). Age of Maba hominin site in southern China: Evidence from U-series dating of Southern Branch Cave. *Quaternary Geochronology*, *23*, 56–62. https://doi.org/10.1016/j.quageo.2014.06.004

Shin, H. S., Choi, D. S., Baek, H. J., Choi, H. C., Choi, H. Y., Park, M. J., Kim, J. E., Han, J. Y., & Park, S. (2017). The oblique occipital sinus: Anatomical study using bone subtraction 3D CT venography. *Surgical and Radiologic Anatomy*, *39*(6), 619–628. https://doi.org/10.1007/s00276-016-1767-x

Singh, M., Nagashima, M., & Inoue, Y. (2004). Anatomical variations of occipital bone impressions for dural venous sinuses around the torcular Herophili, with special reference to the consideration of clinical significance. *Surgical and Radiologic Anatomy*, *26*(6), 480–487. https://doi.org/10.1007/s00276-004-0269-4

Smith, G. E. (1907). A new typographical survey of the human cerebral cortex. *Journal of Anatomy and Physiology*, *41*, 237–254.

Stringer, C. (2003). Out of Ethiopia. *Nature*, *423*(6941), 693–695. https://doi.org/10.1038/423692a

Tatlisumak, E., Ovali, G. Y., Asirdizer, M., Aslan, A., Ozyurt, B., Bayindir, P., & Tarhan, S. (2008). CT study on morphometry of frontal sinus. *Clinical Anatomy*, *21*(4), 287–293. https://doi.org/10.1002/ca.20617

Thewissen, J. G. M. (1989). Mammalian frontal diploic vein and the human foramen caecum. *The Anatomical Record*, *223*(2), 242–244. https://doi.org/10.1002/ar.1092230217

Thron, A., Wessel, K., Linden, D., Schroth, G., & Dichgans, J. (1986). Superior sagittal sinus thrombosis: Neuroradiological evaluation and clinical findings. *Journal of Neurology*, *233*(5), 283–288. https://doi.org/10.1007/BF00314160

Treece, G. M., Gee, A. H., Mayhew, P. M., & Poole, K. E. S. (2010). High resolution cortical bone thickness measurement from clinical CT data. *Medical Image Analysis*, *14*(3), 276–290. https://doi.org/10.1016/j.media.2010.01.003

Trinkaus, E. (2009). The human tibia from Broken Hill, Kabwe, Zambia. *PaleoAnthropology*, *2009*, 145–165.

Tsutsumi, S., Nakamura, M., Tabuchi, T., Yasumoto, Y., & Ito, M. (2013). Calvarial diploic venous channels: An anatomic study using high-resolution magnetic resonance imaging. *Surgical and Radiologic Anatomy*, *35*(10), 935–941. https://doi.org/10.1007/s00276-013-1123-3

Tsutsumi, S., Ogino, I., Miyajima, M., Ito, M., Arai, H., & Yasumoto, Y. (2015). Cerebrospinal fluid drainage through the diploic and spinal epidural veins. *Journal of Anatomy*, *227*(3), 297–301. https://doi.org/10.1111/joa.12349

Tsutsumi, S., Ogino, I., Miyajima, M., Nakamura, M., Yasumoto, Y., Arai, H., & Ito, M. (2014). Cranial arachnoid protrusions and contiguous diploic veins in CSF drainage. *American Journal of Neuroradiology*, *35*(9), 1735–1739. https://doi.org/10.3174/ajnr.A4007

Tsutsumi, S., Ono, H., Ishii, H., & Yasumoto, Y. (2019). Diploic veins of the cranial base: An anatomical study using magnetic resonance imaging. *Surgical and Radiologic Anatomy*, *41*(9), 1029–1036. https://doi.org/10.1007/s00276-019-02283-y

Tsutsumi, S., Sugiyama, N., Ueno, H., & Ishii, H. (2022). Does diploic venous flow drain extracranially in the pterional area? A magnetic resonance imaging study. *Surgical Neurology International*, *13*, 425. https://doi.org/10.25259/SNI_760_2022

Tubbs, R. S., Bosmia, A. N., Shoja, M. M., Loukas, M., Curé, J. K., & Cohen-Gadol, A. A. (2011). The oblique occipital sinus: A review of anatomy and imaging characteristics. *Surgical and Radiologic Anatomy*, *33*(9), 747–749. https://doi.org/10.1007/s00276-011-0831-9

Tubbs, R. S., Salter, E. G., Wellons, J. C., Blount, J. P., & Oakes, W. J. (2007). The sphenoparietal sinus. *Operative Neurosurgery*, *60*(2), 9–12. https://doi.org/10.1227/01.NEU.0000249241.35731.C6

Tubbs, R. S., Shoja, M. M., & Loukas, M. (Eds.). (2016). *Bergman's Comprehensive Encyclopedia of Human Anatomic Variation* (1st ed.). Wiley. https://doi.org/10.1002/9781118430309

Uddin, M. A., Haq, T. U., & Rafique, M. Z. (2006). *Cerebral venous system anatomy*. *56*(11), 516–519.

Upton, M. L., & Weller, R. O. (1985). The morphology of cerebrospinal fluid drainage pathways in human arachnoid granulations. *Journal of Neurosurgery*, *63*(6), 867–875. https://doi.org/10.3171/jns.1985.63.6.0867

Warwick, R., & Williams, P. L. (1973). *Gray's Anatomy* (35th edition). W. S. Saunders Company.

Williams, F. L., Schroeder, L., & Ackermann, R. R. (2012). The mid-face of lower Pleistocene hominins and its bearing on the attribution of SK 847 and StW 53. *HOMO*, *63*(4), 245–257. https://doi.org/10.1016/j.jchb.2012.05.005

Woo, J., & Pen, R. (1959). Fossil human skull of early paleoanthropic stage found at Mapa, Shao-quan, Kwangtung Province. *Vertebrata Palasiatica*, *3*(4), 176–182.

Wood, B. (1992). Origin and evolution of the genus *Homo*. *Nature*, *355*(6363), 783–790. https://doi.org/10.1038/355783a0

Woodward, A. S. (1921). A new cave man from Rhodesia, South Africa. *Nature*, *108*, 371–372.

Wu, X. (1988). Comparative study of early *Homo Sapiens* from China and Europe. *Acta Anthropologica Sinica*, *7*(4), 287–293.

Wu, X., & Bruner, E. (2016). The endocranial anatomy of Maba 1. *American Journal of Physical Anthropology*, *160*(4), 633–643. https://doi.org/10.1002/ajpa.22974

Wu, X., Crevecoeur, I., Liu, W., Xing, S., & Trinkaus, E. (2014). Temporal labyrinths of eastern Eurasian Pleistocene humans. *Proceedings of the National Academy of Sciences*, *111*(29), 10509–10513. https://doi.org/10.1073/pnas.1410735111

Wu, X., Schepartz, L. A., Liu, W., & Trinkaus, E. (2011). Antemortem trauma and survival in the late Middle Pleistocene human cranium from Maba, South China. *Proceedings of the National Academy of Sciences*, *108*(49), 19558–19562. https://doi.org/10.1073/pnas.1117113108

Xing, C.-Y., Tarumi, T., Liu, J., Zhang, Y., Turner, M., Riley, J., Tinajero, C. D., Yuan, L.-J., & Zhang, R. (2017). Distribution of cardiac output to the brain across the adult lifespan.

Journal of Cerebral Blood Flow & Metabolism, *37*(8), 2848–2856. https://doi.org/10.1177/0271678X16676826

Xing, S., Martinón-Torres, M., Bermúdez De Castro, J. M., Zhang, Y., Fan, X., Zheng, L., Huang, W., & Liu, W. (2014). Middle Pleistocene hominin teeth from Longtan Cave, Hexian, China. *PLoS ONE*, *9*(12), e114265. https://doi.org/10.1371/journal.pone.0114265

Yamashiro, K., Muto, J., Wakako, A., Murayama, K., Kojima, D., Omi, T., Adachi, K., Hasegawa, M., & Hirose, Y. (2021). Diploic veins as collateral venous pathways in patients with dural venous sinus invasion by meningiomas. *Acta Neurochirurgica*, *163*(6), 1687–1696. https://doi.org/10.1007/s00701-021-04777-4

Yuan, S., Chen, T., & Gao, S. (1986). Uranium series chronological sequence of some palaeolithic sites in South China. *Acta Anthropologica Sinica*, *5*(2), 179–190.

Zhang, J., & Stringer, M. D. (2010). Ophthalmic and facial veins are not valveless. *Clinical & Experimental Ophthalmology*, *38*(5), 502–510. https://doi.org/10.1111/j.1442-9071.2010.02325.x

Zhang, Y., & Li, Z. (2023). Investigating the internal structure of the suprainiac fossa in Xuchang 2. *Journal of Human Evolution*, *184*, 103440. https://doi.org/10.1016/j.jhevol.2023.103440

Zhao, P., Wang, Z., Xian, J., Yan, F., & Liu, Z. (2014). Persistent petrosquamosal sinus in adults: Qualitative imaging evaluation on high-resolution CT venography. *Acta Radiologica*, *55*(2), 225–230. https://doi.org/10.1177/0284185113498534

Zhou, Y.-H., Chen, C.-L., Luo, C.-E., Wang, H.-B., & Luo, S.-K. (2023). Deep temporal artery anatomy: Implications for improving the safety of deep temporal injections. *Aesthetic Plastic Surgery*, *47*(5), 2045–2050. https://doi.org/10.1007/s00266-023-03341-y

Zümre, Ö., Salbacak, A., Çiçekcibaşi, A. E., Tuncer, I., & Seker, M. (2005). Investigation of the bifurcation level of the common carotid artery and variations of the branches of the external carotid artery in human fetuses. *Annals of Anatomy - Anatomischer Anzeiger*, *187*(4), 361–369. https://doi.org/10.1016/j.aanat.2005.03.007